

**STUDIES ON STRUCTURAL BEHAVIOUR OF BIAXIAL  
VOIDED SLAB UNDER FLEXURE AND PUNCHING SHEAR**

*A THESIS*

*submitted by*

**SAGADEVAN R**

*for the award of the degree*

*of*

**DOCTOR OF PHILOSOPHY**



**STRUCTURAL ENGINEERING LABORATORY  
DEPARTMENT OF CIVIL ENGINEERING  
INDIAN INSTITUTE OF TECHNOLOGY MADRAS**

**FEBRUARY 2020**



## THESIS CERTIFICATE

This is to certify that the thesis entitled **Studies on Structural Behaviour of Biaxial Voided Slab under Flexure and Punching Shear**, submitted by **Sagadevan R** to the Indian Institute of Technology Madras, for the award of the degree of **Doctor of Philosophy** is a bonafide record of research work carried out by him under my supervision. The contents of this thesis, in full or in parts, have not been submitted to any other Institute or University for the award of any degree or diploma.

Place: Chennai

Date: 28 February, 2020

**Prof. B. Nageswara Rao**

Research Guide

Dept. of Civil Engineering

IIT Madras, 600036



## **DECLARATION BY THE RESEARCH SCHOLAR**

This is to declare that the thesis entitled “**Studies on Structural Behaviour of Biaxial Voided Slab under Flexure and Punching Shear**” submitted by me to the Indian Institute of Technology Madras, Chennai for the award of degree of **Doctor of Philosophy** is a bonafide record of research work carried out by me under the supervision of **Prof. B. Nageswara Rao**, Department of Civil Engineering. The contents of the thesis have not been submitted and will not be submitted to any other Institute or University for the award of any degree or diploma.

Place: Chennai  
Date: 28 February, 2020

**Sagadevan R**  
Research Scholar  
Dept. of Civil Engineering  
IIT Madras, 600036

Forwarded

**Prof. B. Nageswara Rao**  
Research Guide  
Dept. of Civil Engineering  
IIT Madras, 600036



## ACKNOWLEDGEMENTS

I express my sincere gratitude to my research guide Prof. B. Nageswara Rao, Department of Civil Engineering, IIT Madras, for his guidance, support and constant motivation. I also thank him for providing me the computational facilities. My sincere thanks to the doctoral committee members, Prof. P. Alagusundaramoorthy, and Prof. Amlan Kumar Sengupta, Department of Civil Engineering and Prof. C. Lakshmana Rao, Department of Applied Mechanics for their valuable suggestions and comments.

I thank Prof. Manu Santhanam, Head of the Civil Engineering Department for all the administrative support. I also thankful to Prof. A. Meher Prasad, Prof. K. Ramamurthy, and Prof. S. R. Gandhi, Former Head of the Civil Engineering Department for all the administrative support. I am also thankful to the Dean and Deputy Registrar, Academic Research and the administrative staff for their help.

I also express my sincere thanks to Dr. Alagappan Ponnalagu, Prof. Arul Jayachandran S., Dr. Arun Menon, Prof. Appa Rao G., Prof. Devdas Menon, Dr. Lakshmi Priya, Prof. Murty C. V. R., Dr. Phanisri Pradeep Pratapa, Prof. Raghu Kanth S. T. G., Dr. Rupen Goswami, Prof. Saravanan U., and Prof. Satish Kumar S. R., Structural Engineering Laboratory, and Prof. G. R. Dodagoudar, Geotechnical Engineering Laboratory for providing review comments and inputs which helped a lot in enhancing the quality of the project.

I am grateful to present and former Technical and administrative staff members (Rajkumar T., Ashok M., Jainudeen Y., Krishnan B., Satish Kumar, Balamurugan G., Murali R., Anandharaj T., Anbalagan, Ashok Kumar, Balamurugan A., Charles, Chellapriya, David, Devaraj, Gajendran, Jani, Lingam, Logesh K., Madhan K., Meerasri R., Mohamed Gnaiyar K. M., Padmanaban, Pefamalla Alluraiah, Praveen Kumar P., Rajendran, Rajkumar, Ramadass A., Revathi S., Santhanam, Sathyamoorthy, Sudhakar, Vijaya Banu, Vincent, and Watsan) of Structural Engineering Laboratory, for their enormous support in casting and testing of my specimens. I am also thankful to the Technical and administrative staff members of HoD Office, DCF, and MPCEM Laboratory, Department of Civil Engineering. My sincere thanks to Housekeeping staff members Adilakshmi, Pappu, and Victoria Rani.

I thank my dear friends and fellow students for their understanding, timely support and encouragement to sustain my energy levels in overcoming numerous obstacles during the Ph.D. Program. Also, I extend my thanks to all other persons, who helped me directly or indirectly.

I am grateful to my friends (Abishek A., Inigo B. S., Pradeep L., and Ravi Sankar C. N.), because of whom I am pursuing my higher studies. I feel that *“nothing is impossible for a person who has such great friends in life”*.

I express my deep gratitude to my family: my grandparents, parents, sister, brother and wife for their kind understanding, many a sacrifice, wishes and everlasting prayers, without which it would not have been possible for me to complete this work.

**Sagadevan R**



## ABSTRACT

**KEYWORDS:** *biaxial voided slab, flexure, yield line analysis, tensile membrane action, reinforcement orientation effect, flexural stiffness, punching shear, effect of voids, effective area.*

Reinforced concrete (RC) slab systems are common structural element in any building. *Biaxial voided slab* is an innovative slab system which results in a self-weight reduction of up to 50% in comparison with solid slabs, without any significant change in its flexural capacity. However, the presence of voids leads to reduction in effective concrete area, thereby a reduction in flexural stiffness and shear capacity. In addition, the presence of voids alters the location of the critical failure section under punching shear. Hence, the design procedure for the biaxial voided slab needs to be formulated for wide application of the same in the construction industry. In this study such guidelines are developed for the biaxial voided slabs subjected to flexure and concentrated load (punching shear). The influence of tensile membrane action and reinforcement orientation on the ultimate flexural capacity is found to be significant in RC solid slab. The question of whether such beneficial effect of enhancement in capacity of RC voided slab, is yet to be explored. This would help to determine the ultimate capacity of such slabs with reasonable accuracy. In this study, based on the experimental results of current study and the data reported in the literature such investigation is carried out and analytical formulations are developed. It is found that the conventional yield line analysis is applicable for the biaxial voided slab as well.

The estimation of the punching shear capacity is significantly influenced by the voids (shape and location). In this study, in addition to the current experimental investigation, the data available in the literature are also included to understand the structural behaviour of biaxial voided slabs under punching shear. The estimation of punching shear capacity of biaxial voided slab by existing provisions for solid slabs in standards (ACI 318, EN 1992-1-1 and IS 456) does not lead to satisfactory results. Hence, an effective area method is proposed to predict the punching shear capacity of biaxial voided slab. Further, a parametric study (numerical investigation) to determine the effect of void shape on the structural behaviour of biaxial voided slabs is carried out.

This page is intentionally left blank.

## TABLE OF CONTENTS

Title	Page No.
<b>Acknowledgements</b>	i
<b>Abstract</b>	iii
<b>Table of Contents</b>	v
<b>List of Tables</b>	xi
<b>List of Figures</b>	xiii
<b>Abbreviations</b>	xxi
<b>Notations</b>	xxiii
<b>Chapter 1 Introduction</b>	
1.1 Floor Slab System – Overview	1
1.2 Voided Slab	3
1.3 Need for the Present Study	5
1.4 Objectives	6
1.5 Scope	7
1.6 Methodology	7
1.7 Organisation of the Thesis	8
<b>Chapter 2 Voided Slab Systems – Literature Review</b>	
2.1 Overview	11
2.2 Voided Slab	11
2.3 Flexure	12
2.3.1 One-way Flexure	12
2.3.1.1 Loading Type	12
2.3.2 Two-way Flexure	13
2.3.2.1 Loading Type	13
2.3.2.2 Tensile Membrane Action	15
2.3.3 Effect of Reinforcement Orientation	16
2.3.3.1 One-Way RC Slabs	18
2.3.3.2 Two-Way RC Slabs	19
2.4 Shear and Punching Shear	20
2.4.1 Shear (One-way)	20

	<b>Title</b>	<b>Page No.</b>
2.4.2	Punching Shear (Two-way)	20
2.4.2.1	Test Setup	21
2.4.2.2	Prediction of Punching Shear Capacity of Biaxial Voided Slab	23
2.5	Summary	25

### **Chapter 3 Behaviour of Voided Slabs in Flexure**

3.1	Overview	27
3.2	Experimental Study	27
3.2.1	Details of Void Formers	27
3.2.1.1	Sphere Void Former	27
3.2.1.2	Cuboid Void Former	28
	(i) Tests on Cuboid Void Former	29
3.2.2	Details of Test Specimens	31
3.2.2.1	Material Properties	38
3.2.2.2	Fabrication of Steel Mould	39
3.2.2.3	Casting of Specimens	40
3.2.3	Test Set-up and Instrumentation	43
3.2.3.1	One-way Flexure	43
	(i) Test Set-up	43
	(ii) Instrumentation	45
	(iii) Testing Procedure	45
3.2.3.2	Two-way Flexure: Phase I (Load up to 1000 kN)	45
	(i) Test Set-up	45
	(ii) Instrumentation	47
	(iii) Testing Procedure	49
3.2.3.3	Two-way Flexure: Phase I (Load up to Ultimate Failure)	50
3.2.3.4	Two-way Flexure: Phase II	50
	(i) Test Set-up	50
	(ii) Instrumentation	50
	(iii) Testing Procedure	51
3.2.4	Fabrication of Loading and Support Frame	53

	<b>Title</b>	<b>Page No.</b>
	3.2.4.1 Erected Test Set-up	54
	3.2.6 Results and Discussion	56
	3.2.6.1 One-way Flexure	56
	(i) Load Deflection Behaviour	56
	(ii) Crack Pattern	60
	(iii) Load Carrying Capacity	61
	(iv) Strain of Bottom Reinforcement	62
	(v) Strain of Concrete Surface along Depth of Slab	62
	3.2.6.2 Two-way Flexure	63
	(i) Load Deflection Behaviour	63
	(ii) Crack Pattern	69
	(iii) Load Carrying Capacity	72
	(iv) Strain of Bottom Reinforcement	72
3.3	Analytical Study	74
	3.3.1 One-way Flexure	74
	3.3.1.1 Load Carrying Capacity	74
	3.3.1.2 Moment Capacity of Slab Section	76
	(i) IS 456:2000	77
	(ii) ACI 318-19	78
	3.3.1.3 Flexural Stiffness	78
	3.3.2 Two-way Flexure	82
	3.3.2.1 Load Carrying Capacity	82
	3.3.2.2 Tensile Membrane Action in Slabs	88
	3.3.2.3 Effect of Reinforcement Orientation	89
3.4	Summary	91
<b>Chapter 4 Behaviour of Voided Slabs in Punching Shear</b>		
4.1	Overview	93
4.2	Experimental Study	93
	4.2.1 Details of Void Formers	93
	4.2.2 Details of Test Specimens	93
	4.2.2.1 Material Properties	100

	<b>Title</b>	<b>Page No.</b>
	4.2.2.2 Casting of Specimens	101
	4.2.3 Test Set-up and Instrumentation	103
	4.2.3.1 Punching Shear: Phase I	103
	(i) Test Set-up	104
	(ii) Instrumentation	105
	(iii) Testing Procedure	106
	4.2.3.2 Punching Shear: Phase II	108
	(i) Test Set-up	108
	(ii) Instrumentation	109
	(iii) Testing Procedure	109
	4.2.4 Results and Discussion	110
	4.2.4.1 Load Deflection Behaviour	110
	4.2.4.2 Crack Pattern	118
	4.2.4.3 Load Carrying Capacity	124
	4.2.4.4 Strain of Bottom Reinforcement	124
4.3	Analytical Study	126
	4.3.1 Punching Shear Capacity Prediction of Solid Slabs by Various Standards	126
	4.3.1.1 ACI 318	126
	4.3.1.2 EN 1992-1-1	127
	4.3.1.3 IS 456	128
	4.3.2 Experimental Test Data and Prediction of Punching Shear Capacity	128
	4.3.2.1 Prediction of Capacity by Various Standards	132
	4.3.2.2 Prediction of Capacity by Effective Concrete Area	132
	4.3.3 Prediction of Punching Shear Capacity by Critical Shear Crack Theory	141
4.4	Summary	145
<b>Chapter 5 Finite Element Analysis</b>		
5.1	Overview	147
5.2	Materials' Properties	147
	5.2.1 Mechanical Properties of Concrete	147

	<b>Title</b>	<b>Page No.</b>
	5.2.1.1 Compression	147
	5.2.1.2 Tension	148
	5.2.1.3 Tension Softening	148
	5.2.1.4 Tension Cut-off	149
	5.2.1.5 Shear Retention Factor	149
	5.2.1.6 Material Model	150
	(i) Mohr–Coulomb Plasticity Model	150
	(ii) Total Strain based Crack Model	150
	5.2.1.7 Element	150
	5.2.2 Mechanical Properties of Reinforcement	151
	5.2.2.1 Uniaxial Stress-Strain	151
	5.2.2.2 Element	151
5.3	Finite Element Model – Effect of Void Shape	152
	5.3.1 Shape of Void Formers	152
	5.3.2 Simulation of Voided Slab	152
	5.3.2.1 Punching Shear	152
	5.3.2.2 Two-way Flexure	157
	5.3.3 Results and Discussion	160
	5.3.3.1 Punching Shear	160
	5.3.3.2 Two-way Flexure	162
5.4	Finite Element Model – Based on Current Experimental Study	163
	5.4.1 One-way Flexure	163
	5.4.2 Two-way Flexure	168
	5.4.3 Shear (One-way)	172
	5.4.4 Punching Shear (Two-way)	175
5.5	Summary	178
<b>Chapter 6 Summary and Conclusions</b>		
6.1	Summary	179
6.2	Observations and Conclusions	180
	6.2.1 One-way Flexure	181
	6.2.2 Two-way Flexure	181

	<b>Title</b>	<b>Page No.</b>
	6.2.3 Punching Shear	182
	6.2.4 Numerical (Parametric) Study	183
6.3	Scope for Further Research	183
	<b>References</b>	185
	<b>List of Papers Submitted on the Basis of This Thesis</b>	191
	<b>Curriculum Vitae</b>	193
	<b>Doctoral Committee</b>	195



## LIST OF TABLES

<b>Table</b>	<b>Page No.</b>
Table 4.1 – Details of Punching Shear Test Specimens	100
Table 4.2 – Mechanical Properties of Reinforcement	100
Table 4.3 – Punching Shear Capacity of Test Specimens	124
Table 4.4 – Details and Experimental Results of Voided Slab Specimens of Various Researchers	129
Table 4.5 – Punching shear capacity of voided slabs calculated by various standards without considering the voids	134
Table 4.6 – Punching shear capacity of voided slabs calculated by various standards with effective concrete area	137
Table 4.7 – Details and Experimental Results of Voided Slab Specimens of Various Researchers	142
Table 5.1 – Materials’ Properties	157
Table 5.2 – Biaxial Voided Slab Specimen Details	157
Table 5.3 – Properties of Concrete	164
Table 5.4 – Numerical Results: One-way Flexure	168
Table 5.5 – Comparison of Results: One-way Flexure	168
Table 5.6 – Comparison of Ultimate Load: Two-way Flexure	171
Table 5.7 – Numerical Results: One-way Shear	175

This page is intentionally left blank.

## LIST OF FIGURES

<b>Figure</b>	<b>Page No.</b>
Figure 1.1 – Wall-supported Slab Systems	1
Figure 1.2 – Beam-supported Slab Systems	2
Figure 1.3 – Ribbed Slab Systems	2
Figure 1.4 – Flat Plate System	3
Figure 1.5 – Flat Slab System	3
Figure 1.6 – Cross Section of One-way Voided Slab with Hollow Tiles	3
Figure 1.7 – Cross Section of One-way Voided Slab with Hollow Core	4
Figure 1.8 – Two-way Voided Slab with Plastic Void Formers	4
Figure 1.9 – Components of Two-way Voided Slab and Typical Cross-section	4
Figure 1.10 – Concept of Voided Slab	5
Figure 1.11 – Specimen Configurations and Type of Loading Pattern	7
Figure 2.1 – Loading Configurations of Four-Point Bending Test	13
Figure 2.2 – Loading Configurations Adopted by Various Researchers	14
Figure 2.3 – Development of Membrane Forces in Laterally Unrestrained Slab	15
Figure 2.4 – Square Yield Criterion and Rotation of Axis	17
Figure 2.5 – A Square Slab Supported on Beams Subjected to 16-Point Load	17
Figure 2.6 – Schematic Arrangement of Reinforcement with Fracture Line (One-Way)	19
Figure 2.7 – Schematic Arrangement of Reinforcement with Fracture Lines (Two-Way – Square Slab)	19
Figure 2.8 – Schematic Arrangement of Reinforcement with Fracture Lines (Two-Way – Rectangular Slab)	19
Figure 2.9 – Type-I Test Setup	21
Figure 2.10 – Three-Dimensional View of Type-I Test Setup	22
Figure 2.11 – Photograph of Type-II Test Setup	22
Figure 2.12 – Effective Concrete Area	23
Figure 2.13 – Assumed Critical Sections in Voided Slabs	24
Figure 3.1 – Single Unit of Sphere Void Formers	28
Figure 3.2 – Single Unit of Cuboid Void Former and Lateral Spacer	28
Figure 3.3 – Setup for Test of Cuboid Void Former	29

<b>Figure</b>	<b>Page No.</b>
Figure 3.4 – Tested Specimens	30
Figure 3.5 – Details of Test Specimen OF-S180V	32
Figure 3.6 – Details of Test Specimen OF-CV (1 – 3)	33
Figure 3.7 – Details of Test Specimen TF-Solid	34
Figure 3.8 – Details of Test Specimen TF-S90V	35
Figure 3.9 – Details of Test Specimen TF-S180V	36
Figure 3.10 – Details of Test Specimens TF-CV (1 – 3)	37
Figure 3.11 – Idealised Stress versus Strain Behaviour of Reinforcements	38
Figure 3.12 – Fabrication of Steel Mould in Progress	39
Figure 3.13 – Typical Reinforcement Mesh	40
Figure 3.14 – Strain Gauges Fixed on Reinforcements	40
Figure 3.15 – One-way Flexural Test Specimens OF-S180V and OF-CV	40
Figure 3.16 – Two-way Flexural Test Specimen TF-Solid	41
Figure 3.17 – Two-way Flexural Test Specimen TF-S90V	41
Figure 3.18 – Two-way Flexural Test Specimen TF-CV	42
Figure 3.19 – Concreting in Progress	42
Figure 3.20 – Schematic Test Set-up (Four-point Bending)	43
Figure 3.21 – Instrumentation of Test Specimen (Four-point Bending)	44
Figure 3.22 – Schematic Test Set-up (Sixteen-point Bending) – Phase I: Load up to 1000 kN	46
Figure 3.23 – Position of Sixteen-point (Patch) Load	47
Figure 3.24 – Instrumentation of Test Specimen (Sixteen-point Bending) – Phase I	48
Figure 3.25 – Schematic Test Set-up (Sixteen-point Bending) – Phase I: Load up to Ultimate	49
Figure 3.26 – Schematic Test Set-up (Sixteen-point Bending) – Phase II	51
Figure 3.27 – Instrumentation of Test Specimen (Sixteen-point Bending) – Phase II	52
Figure 3.28 – Loading and Support Frame	53
Figure 3.29 – Ono-way Flexural Test Set-up	54
Figure 3.30 – Two-way Flexural Test Set-up: Phase I (Load up to 1000 kN)	55
Figure 3.31 – Two-way Flexural Test Set-up: Phase I (Load up to Ultimate)	55

<b>Figure</b>	<b>Page No.</b>
Figure 3.32 – Two-way Flexural Test Set-up: Phase II	56
Figure 3.33 – Load versus Deflection Behaviour of Specimen OF-S180V	57
Figure 3.34 – Load versus Deflection Behaviour of Specimen OF-CV-1	57
Figure 3.35 – Load versus Deflection Behaviour of Specimen OF-CV-2	58
Figure 3.36 – Load versus Deflection Behaviour of Specimen OF-CV-3	58
Figure 3.37 – Load versus Mid-span Deflection of Sphere Voided Specimen	59
Figure 3.38 – Load versus Mid-span Deflection of Cuboid Voided Specimens	59
Figure 3.39 – Observed Crack Pattern of Slab Specimen OF-S180V	60
Figure 3.40 – Observed Crack Pattern of Slab Specimen OF-CV-1	60
Figure 3.41 – Observed Crack Pattern of Slab Specimen OF-CV-2	61
Figure 3.42 – Observed Crack Pattern of Slab Specimen OF-CV-3	61
Figure 3.43 – Load versus Reinforcement Strain: One-way Flexure	63
Figure 3.44 – Load versus Concrete Surface Strain along Depth of Slab	63
Figure 3.45 – Load versus Mid-span Deflection of Specimens TF-Solid and TF-S90V	64
Figure 3.46 – Load versus Mid-span Deflection of Specimen TF-S180V	65
Figure 3.47 – Load versus Mid-span Deflection of Specimens TF-CV-2 and TF-CV-3	65
Figure 3.48 – Load versus Deflection of Specimen TF-CV-1	66
Figure 3.49 – Load versus Lateral Displacement of Specimen TF-CV-1	66
Figure 3.50 – Load versus Deflection of Specimen TF-CV-2	67
Figure 3.51 – Load versus Lateral Displacement of Specimen TF-CV-2	67
Figure 3.52 – Load versus Deflection of Specimen TF-CV-3	68
Figure 3.53 – Load versus Lateral Displacement of Specimen TF-CV-3	68
Figure 3.54 – Observed Typical Crack Pattern	69
Figure 3.55 – Observed Crack Pattern of Slab Specimen TF-Solid	69
Figure 3.56 – Observed Crack Pattern of Slab Specimen TF-S180V	70
Figure 3.57 – Observed Crack Pattern of Slab Specimen TF-CV-1	70
Figure 3.58 – Observed Crack Pattern of Slab Specimen TF-CV-2	71
Figure 3.59 – Observed Crack Pattern of Slab Specimen TF-CV-3	71
Figure 3.60 – Load versus Reinforcement Strain: Two-way Flexure	73
Figure 3.61 – Assumed Yield Line Pattern and Failure Mode: One-way Flexure	75

<b>Figure</b>	<b>Page No.</b>
Figure 3.62 – Strain and Stress Distribution in a Slab Section	76
Figure 3.63 – Stress versus Strain Behaviour of Concrete (IS 456)	77
Figure 3.64 – Stress versus Strain Behaviour of Concrete (ACI 318)	78
Figure 3.65 – Voided Slab Sections used to Calculate Moment of Inertia	80
Figure 3.66 – Assumed Yield Line Pattern with Deformation Contour: 16-point Load	84
Figure 3.67 – Assumed Yield Line Pattern with Deformation Contour: 12-point Load	85
Figure 3.68 – Assumed Yield Line Pattern with Deformation Contour: UDL	85
Figure 3.69 – Moment Capacity of a Yield Line and Application of Equilibrium of Slab Parts	86
Figure 4.1 – Details of Test Specimen S	94
Figure 4.2 – Details of Test Specimen V1	95
Figure 4.3 – Details of Test Specimen V2	96
Figure 4.4 – Details of Test Specimen V3	97
Figure 4.5 – Details of Test Specimen V4	98
Figure 4.6 – Details of Test Specimen V5 – V7	99
Figure 4.7 – Idealised Stress versus Strain Behaviour of Reinforcements	101
Figure 4.8 – Punching Shear Test Specimen V1	102
Figure 4.9 – Punching Shear Test Specimen V3	102
Figure 4.10 – Punching Shear Test Specimen V5	103
Figure 4.11 – Typical Punching Shear Test Specimen after Cast	103
Figure 4.12 – Schematic Test Set-up (Punching Shear) – Phase I	104
Figure 4.13 – Punching Shear Test Set-up: Phase I	106
Figure 4.14 – Position of Point Load (Column)	106
Figure 4.15 – Instrumentation of Test Specimen (Punching Shear Test) – Phase I	107
Figure 4.16 – Schematic Test Set-up (Punching Shear) – Phase II	108
Figure 4.17 – Punching Shear Test Set-up: Phase II	109
Figure 4.18 – Load versus Mid-span Deflection of Specimens S, V1 and V2	111
Figure 4.19 – Load versus Mid-span Deflection of Specimens V3 and V4	112
Figure 4.20 – Load versus Mid-span Deflection of Specimens V5, V6 and V7	113
Figure 4.21 – Load versus Deflection of Specimens S	114

<b>Figure</b>	<b>Page No.</b>
Figure 4.22 – Load versus Deflection of Specimens V1	114
Figure 4.23 – Load versus Deflection of Specimens V2	115
Figure 4.24 – Load versus Deflection of Specimens V3	115
Figure 4.25 – Load versus Deflection of Specimens V4	116
Figure 4.26 – Load versus Deflection of Specimens V5	116
Figure 4.27 – Load versus Deflection of Specimens V6	117
Figure 4.28 – Load versus Deflection of Specimens V7	117
Figure 4.29 – Observed Crack Pattern of Slab Specimen S	118
Figure 4.30 – Observed Crack Pattern of Slab Specimen V1	119
Figure 4.31 – Observed Crack Pattern of Slab Specimen V2	119
Figure 4.32 – Observed Crack Pattern of Slab Specimen V3	120
Figure 4.33 – Observed Crack Pattern of Slab Specimen V4	120
Figure 4.34 – Observed Crack Pattern of Slab Specimen V5	121
Figure 4.35 – Observed Crack Pattern of Slab Specimen V6	122
Figure 4.36 – Observed Crack Pattern of Slab Specimen V7	123
Figure 4.37 – Load versus Reinforcement Strain	125
Figure 4.38 – Critical section for punching shear as per (a) ACI 318 and IS 456, (b) EN 1992-1-1	126
Figure 4.39 – Typical critical sections based on void locations for (a) ACI 318 and IS 456, (b) EN 1992-1-1	133
Figure 4.40 – Comparison of punching shear capacity of voided slab specimens	140
Figure 4.41 – Normalised Load versus Rotation (Current Study)	144
Figure 4.42 – Failure Criterion: Punching Shear Strength as Function of Width of Critical Shear Crack	144
Figure 4.43 – Comparison of punching shear capacity of voided slab specimens obtained from experiments and Critical Shear Crack Theory	145
Figure 5.1 – Concrete Behaviour Considered in Finite Element Analysis (a) Compression and (b) Tension	148
Figure 5.2 – Tension Cut-off: Linear	149
Figure 5.3 – TE12L Element	150
Figure 5.4 – Stress-Strain Behaviour of Reinforcement	151

<b>Figure</b>	<b>Page No.</b>
Figure 5.5 – Reinforcement: Embedded Line Element in Solid (TE12L) Element	151
Figure 5.6 – Different Void Former Shapes considered in Numerical Study	152
Figure 5.7 – Typical Specimen Details: Punching Shear	153
Figure 5.8 – Punching Shear Test Set-up	154
Figure 5.9 – Finite Element Model of Biaxial Sphere Voided Slab	154
Figure 5.10 – Slab Model with Mesh and Boundary Conditions	155
Figure 5.11 – Slab Model with Mesh showing the Sphere Voids	155
Figure 5.12 – Slab Model with Mesh showing the Cuboid Voids	156
Figure 5.13 – Slab Model with Mesh showing the Ellipsoid Voids	156
Figure 5.14 – Typical Specimen Details: Two-way Flexure	158
Figure 5.15 – Slab Model with Mesh and Boundary Conditions (Two-way Flexure)	159
Figure 5.16 – Slab Model with Mesh showing the Sphere Voids (Two-way Flexure)	159
Figure 5.17 – Load versus Mid-span Deflection (Numerical Simulation – Punching Shear)	160
Figure 5.18 – Deformed Configuration (Punching Shear – Sphere Voided Slab)	161
Figure 5.19 – Deflection Contour (Punching Shear – Sphere Voided Slab)	161
Figure 5.20 – Load versus Mid-span Deflection (Numerical Simulation – Two-way Flexure)	162
Figure 5.21 – Typical Deflection Contour (Two-way Flexure – Sphere Voided Slab)	162
Figure 5.22 – Model of Slab Specimen (OF-CV)	164
Figure 5.23 – Finite Element Model with Mesh	165
Figure 5.24 – Deformed Shape with Deflection Contour of Voided Slab	165
Figure 5.25 – Stress Contour of Voided Slab prior to Initial Crack (One-quarter of Slab)	166
Figure 5.26 – Load versus Mid-span Deflection Behaviour (One-way Flexure)	166
Figure 5.27 – Load versus Reinforcement Strain of Specimen OF-CV-1	167
Figure 5.28 – Observed Crack Pattern of Slab Specimen OF-CV-1 (Front Elevation)	167



<b>Figure</b>	<b>Page No.</b>
Figure 5.29 – Model of Slab Specimen (TF-CV)	169
Figure 5.30 – Finite Element Model with Mesh (Two-way Flexure)	170
Figure 5.31 – Deflection Contour at 800 kN (Two-way Flexure)	170
Figure 5.32 – Load versus Mid-span Deflection Behaviour (Two-way Flexure)	171
Figure 5.33 – Model of Slab Specimen (OF-CV)	172
Figure 5.34 – Finite Element Model with Mesh (One-way Shear)	173
Figure 5.35 – Deflection Contour at 140 kN (One-way Shear)	174
Figure 5.36 – Configuration of Nodes before and after Shear Failure	174
Figure 5.37 – Load versus Deflection Behaviour (One-way Shear)	175
Figure 5.38 – Model of Slab Specimen (Punching Shear)	176
Figure 5.39 – Finite Element Model with Mesh (Punching Shear)	177
Figure 5.40 – Typical Deflection Contour (Punching Shear)	177
Figure 5.41 – Load versus Mid-span Deflection Behaviour (Punching Flexure)	178

This page is intentionally left blank.

## ABBREVIATIONS

ACI	– American Concrete Institute
COV	– Coefficient of Variation
CSCT	– Critical Shear Crack Theory
CV	– Cuboid Void
DIANA	– Displacement Analyser
EN	– European Standard
FE	– Finite Element
FEA	– Finite Element Analysis
FEM	– Finite Element Method
ID	– Identification
IS	– Indian Standard
ISMB	– Indian Standard Medium Weight Beam
LVDT	– Linear Variable Differential Transformer
NA	– Neutral Axis
OF	– One-way Flexure
RC	– Reinforced Concrete
SD	– Standard Deviation
SG	– Strain Gauge
S180V	– 180 mm dia. Sphere Void
S90V	– 90 mm dia. Sphere Void
TF	– Two-way Flexure
TM	– Tensile Membrane
UDL	– Uniformly Distributed Load
UK	– United Kingdom
YLA	– Yield Line Analysis
kg	– kilo gram
kN	– kilo Newton
N	– Newton
mm	– millimetre
m	– meter
sec	– second

This page is intentionally left blank.

## NOTATIONS

$A_{st}$	– area of reinforcement
$A_{st,b}$	– area of bottom reinforcement
$A_{st,t}$	– area of top reinforcement
$a_0, a_1, a_2, a_3$	– constants
$b$	– parameter defining the magnitude of membrane force
$b_c$	– breadth of compression face
$b_w$	– breadth of web
$b_0$	– perimeter of critical section
$C$	– force in concrete per unit length of slab
$C_y$	– location of centre of gravity from base
$c$	– cohesion
$c_1$ & $c_2$	– constants
$D$	– overall depth of slab
$d, d_e$	– effective depth to bottom reinforcement (effective depth of the slab)
$d_{e,n}$	– effective depth of the slab
$d'$	– effective depth to top reinforcement
$D_{\text{secant}}^{\text{II}}$	– shear stiffness (secant)
$d_k$	– width of void intersecting the control perimeter
$d_r$	– diameter of control perimeter
$d_v$	– width of void overlapping the critical section
$E$	– elastic modulus of material
$E_c$	– elastic modulus of concrete (Young's modulus)
$E_s$	– elastic modulus of reinforcement
$e$	– enhancement factor (tensile membrane action)
$e_b$	– enhancement factor due to bending action
$e_m$	– enhancement factor due to membrane forces
$f_c$	– stress in concrete (compressive)
$f_{ck}$	– concrete cube compressive strength;
$f_{cm}$	– mean compressive strength of concrete cubes
$f_{cm}'$	– mean compressive strength of concrete cylinders
$f_{cr}$	– modulus of rupture of concrete

$f_n$	– stress in concrete (theoretical)
$f_o$	– enhancement factor (effect of reinforcement orientation)
$f_{st,b}$	– stress in bottom reinforcement
$f_{st,t}$	– stress in top reinforcement
$f_t$	– stress in concrete (tensile)
$f_u$	– ultimate stress of reinforcement
$f_y$	– yield stress of reinforcement
$G$	– shear modulus
$G_f$	– fracture energy
$g_0$	– parameter to fix the depth of compressive stress block
$h_v$	– height of void overlapping the critical section
$I$	– moment of inertia
$I_{eff}$	– effective moment of inertia of section
$I_{g,Solid}$	– uncracked moment of inertia of solid slab section
$I_{g,V}$	– uncracked moment of inertia of voided slab section
$I_{gr}$	– moment of inertia of gross-section about the centroidal axis (ignoring reinforcement)
$I_r$	– moment of inertia of cracked section
$I_{r,Solid}$	– cracked moment of inertia of solid slab section
$I_{r,V}$	– cracked moment of inertia of voided slab section
$K_s$	– flexural secant stiffness corresponds to $P_s$
$K_y$	– flexural secant stiffness corresponds to $P_y$
$k_1$	– concrete compressive strength factor
$k_2$	– factor for depth of equivalent compressive stress (rectangular) in concrete
$k_3$	– factor to account for size effect and conversion of cube strength to cylinder strength
$l$	– overall length of slab
$l_e$	– effective length of slab
$l_r$	– length to be deducted from the critical section located at a distance $d/2$ from the column face
$M$	– maximum moment under service load
$M_{AB}$	– moment developed by the externally applied load about support AB
$M_n$	– bending moment per unit length of slab in $n$ -direction

$M_r$	– cracking moment
$M_t$	– bending moment per unit length of slab in $t$ -direction
$M_x$	– bending moment per unit length of slab in $x$ -direction
$M_y$	– bending moment per unit length of slab in $y$ -direction
$m$	– ultimate moment capacity per unit length of slab (yield)
$m'$	– negative ultimate moment capacity per unit length of slab (yield)
$m_{DL}$	– in-plane moment per unit length of slab due to self-weight
$m_x$	– ultimate moment capacity per unit length of slab in $x$ -direction
$m_y$	– ultimate moment capacity per unit length of slab in $y$ -direction
$m_\theta$	– ultimate moment capacity per unit length of the yield line
$n$	– number of voids in a section
$P$	– experimental load (line load in four-point bending test)
$P_n$	– theoretical ultimate load of solid slab based on YLM
$P_r$	– load corresponds to first crack
$P_s$	– load corresponds to limiting deflection (50% of $P_u$ )
$P_u$	– observed maximum load in experiment
$P_{u, Solid-Num}$	– ultimate load of solid slab (numerical)
$P_{u, Void-exp}$	– ultimate load of voided slab (experimental)
$P_{u, Void-Num}$	– ultimate load of voided slab (numerical)
$P_y$	– load corresponding to yielding of reinforcement
$T_b$	– force in bottom reinforcement
$T_t$	– force in top reinforcement
$u_i$	– local translation of an element
$u_{xyz}$	– global translation of an element
$V_c$	– punching shear capacity of slab
$W_{DL}$	– self-weight of slab (dead load)
$W_n$	– theoretical ultimate load (UDL) of solid slab based on YLM
$W_{n1}$	– theoretical ultimate load (UDL) of solid slab based on YLM and membrane action
$W_{n2}$	– theoretical ultimate load (UDL) of solid slab based on YLM including the effects of tensile membrane action and reinforcement orientation
$W_s$	– equivalent UDL of $P_s$
$W_u$	– equivalent UDL of $P_u$ without considering self-weight of slab

$W_{u1}$	– equivalent UDL of $P_u$ inclusive of self-weight of slab
$w$	– deflection of yield line
$x$	– depth of neutral axis
$\bar{x}$	– depth of resultant compressive force in concrete
$x_u$	– neutral axis depth at ultimate
$y_t$	– distance from centroidal axis of gross section to extreme fibre in tension (ignoring reinforcement)
$z$	– lever arm distance
$\alpha_s$	– constant
$\beta$	– shear retention factor
$\delta$	– theoretical maximum mid-span deflection
$\delta_c$	– mid-span deflection of slab
$\delta_r$	– mid-span deflection of slab corresponds to $P_r$
$\delta_s$	– mid-span deflection of slab corresponds to $P_s$
$\delta_u$	– mid-span deflection of slab corresponds to $P_u$
$\delta_y$	– mid-span deflection of slab corresponds to $P_y$
$\varepsilon$	– strain
$\varepsilon_c$	– strain in concrete
$\varepsilon_P$	– strain in concrete corresponding to $f_c$
$\varepsilon_{st}$	– strain in reinforcement
$\varepsilon_{st,b}$	– strain in bottom reinforcement
$\varepsilon_{st,t}$	– strain in top reinforcement
$\varepsilon_t$	– strain in concrete corresponding to $f_t$
$\varepsilon_u$	– ultimate strain
$\varepsilon_y$	– yield strain
$\varepsilon_0$	– strain in concrete at maximum stress
$\theta$	– angle measured at the centre of the column between the two points along the perimeter of the void overlapping the critical section
$\theta_u$	– rotation angle along the yield line
$\theta_x$	– inclination of yield line with respect to the $x$ -direction
$\theta'$	– inclination of $n$ -direction with respect to the $x$ -direction
$\nu$	– Poisson's ratio
$\xi, \eta, \zeta$	– local axis of element



$\rho$	– mass density
$\sigma_1$	– major principal stress
$\sigma_2$	– minor principal stress
$\sigma_{XX}$	– Cauchy stress
$\varphi$	– friction angle
$\mu$	– $m_x/m_y$
$\emptyset$	– diameter

This page is intentionally left blank.

# CHAPTER 1

## INTRODUCTION

### 1.1 Floor Slab System – Overview

In general, slabs are two-dimensional flat horizontal structural members, being used to transfer mainly gravitational loads such as dead loads and imposed loads. In addition, slab systems are acting as a horizontal diaphragm for a structural building, which helps to transfer the lateral loads (usually developed by wind loads and earthquakes) effectively to vertical members such as columns, structural walls, etc. The slab systems are mainly classified as one- and two-way slabs based on its structural behaviour. If the slab predominantly bends (deflects) in one direction, then it is known as a one-way slab (Figure 1.1a). Similarly, if the slab bends in two directions (longitudinal and transverse), then it is known as a two-way slab (Figure 1.1b). The various types of conventional slab systems are wall-supported, beam-supported, grid beam-supported, ribbed, flat plate, and flat slab (Pillai and Menon, 2012).

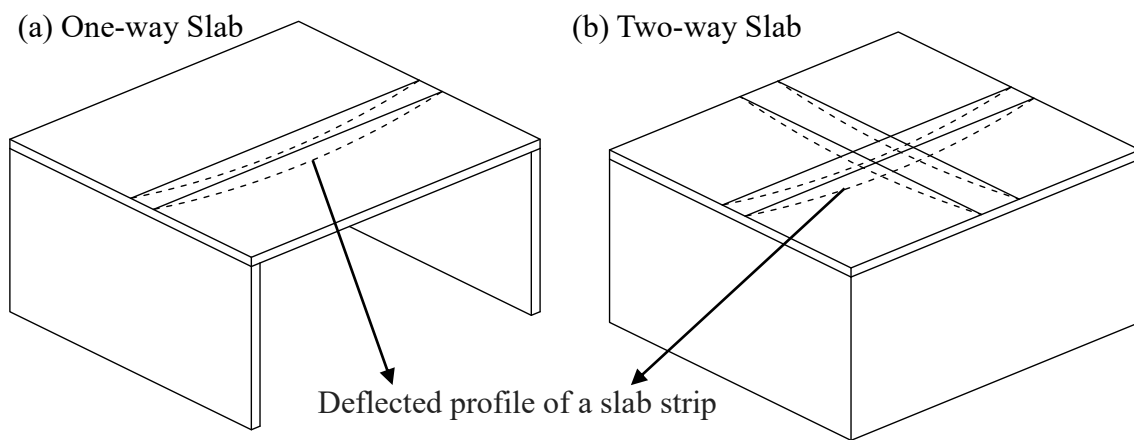


Figure 1.1 – Wall-supported Slab Systems

The beam-supported slabs are the slab system which is supported on the beams; it is classified as one-way, two-way, and grid floor system. The photographs shown in Figure 1.2 are typical examples of beam-supported slabs. Ribbed slab system is a type of grid floor, in which the slender beams used to be provided closely and thin slab as a topping. Based on the rib orientation, it is further classified as one-way (Figure 1.3a) and two-way (waffle - Figure 1.3b) ribbed slab system. In flat plate system (Figure 1.4), the thin slab is directly supported on the columns, while in the flat slab system (Figure 1.5), the slab is stiffened using drop

panels/column capitals near the columns. All these slab systems have many advantages by means of fulfilling structural and architectural requirements. However, its heavy self-weight leads to an increase in the size of other structural members such as beam, column, and foundation. The size of structural members directly affecting the quantity of material consumption and cost.



(a) One-way Slab

Structural Engineering Lab, IIT Madras



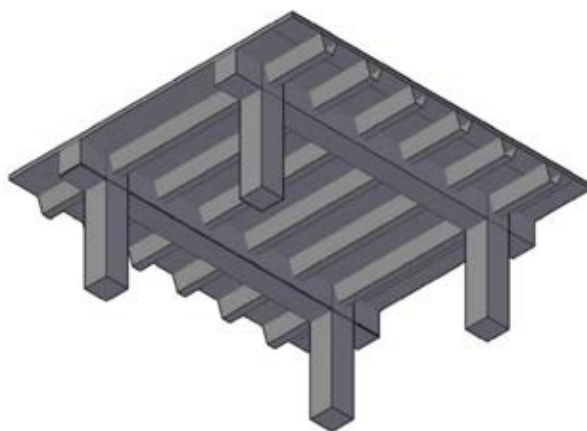
(b) Two-way Slab

Nilgiri, IIT Madras



(c) Grid Floor – Central Library, IIT Madras

Figure 1.2 – Beam-supported Slab Systems



(a) One-way Slab



(b) Two-way Slab (Waffle Slab)

Durga Peeli Amman Temple, IIT Madras

Figure 1.3 – Ribbed Slab Systems

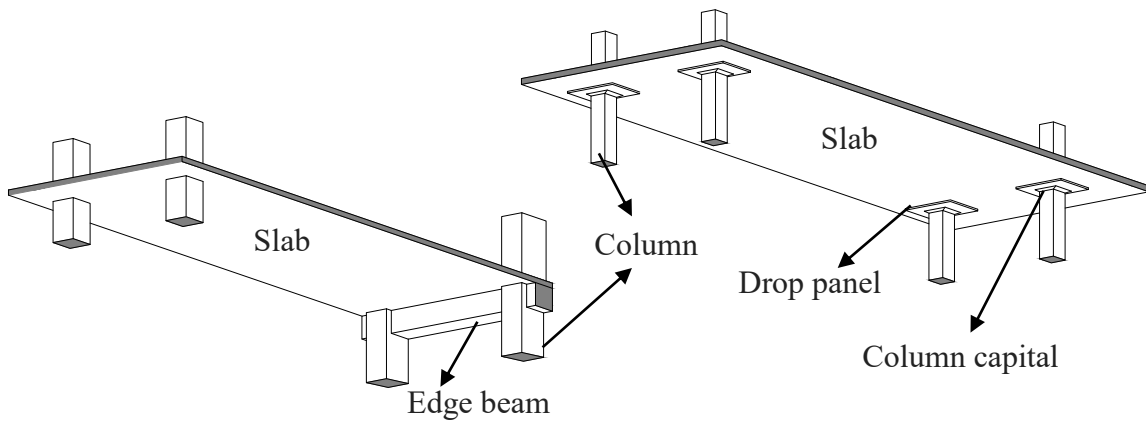


Figure 1.4 – Flat Plate System

Figure 1.5 – Flat Slab System

### 1.2 Voided Slab

Generally, the self-weight of the conventional slab systems explained in Section 1.1 are much higher than that of the imposed loads acting on it. In order to overcome this one-way voided slabs (Figure 1.6) were introduced by Hatt in 1907 at Purdue University, Indiana, by means of hollow tiles (Mota, 2013).

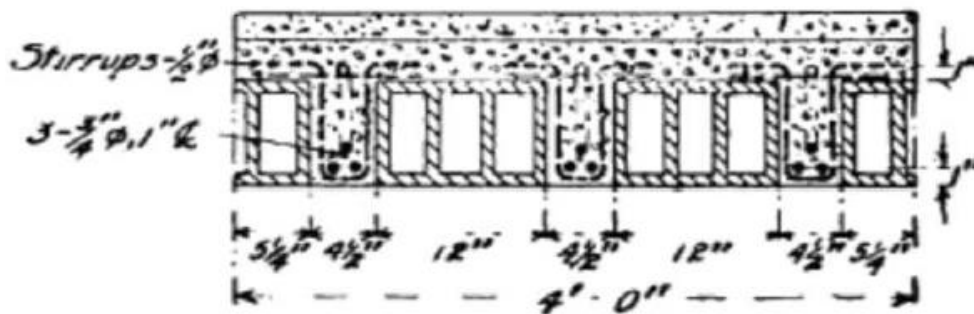


Figure 1.6 – Cross Section of One-way Voided Slab with Hollow Tiles (Source: Mota, 2013)

In 1914, hollow cores (void formers) made of metal and tar paper were used to create voids in the slabs (Figure 1.7). Studies showed that the structural behaviour of one-way hollow core slabs in orthogonal directions was observed to vary significantly. In 1997, Cobiax, Germany developed a lightweight, environmentally effective two-way hollow slab by using plastic void formers, as shown in Figure 1.8. In the two-way hollow core slabs (biaxial voided slab), the void former units usually placed with equal spacing in both lateral and longitudinal directions. The void formers used to be placed between the top and bottom reinforcement gauge. Typical cross-section of the biaxial voided slab with its components is shown in Figure 1.9. The voids

usually placed where the stress in concrete is minimum, generally on the tension side. Typical conceptual strain and stress variation in a section of the slab are shown in Figure 1.10.

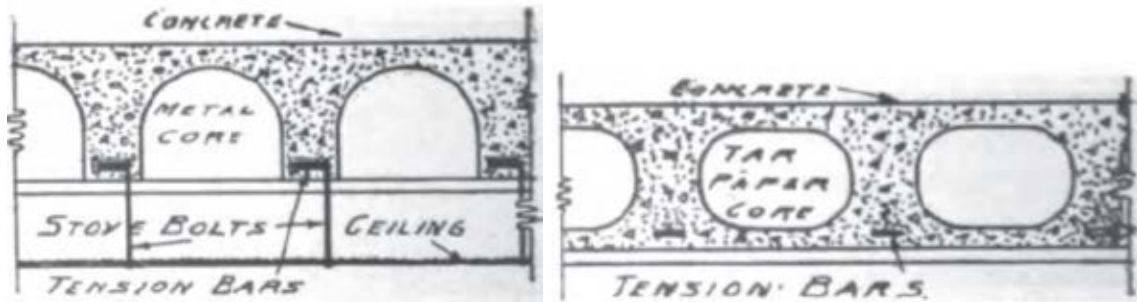


Figure 1.7 – Cross Section of One-way Voided Slab with Hollow Core (Source: Mota, 2013)



Figure 1.8 – Two-way Voided Slab with Plastic Void Formers (Source: www.cobias.com)

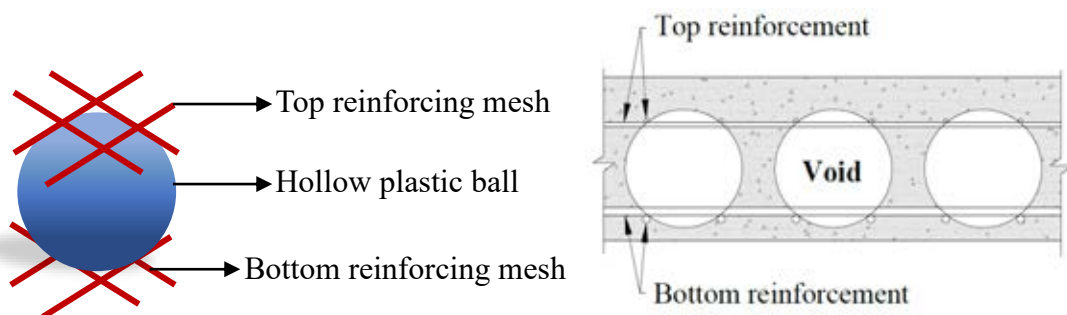


Figure 1.9 – Components of Two-way Voided Slab and Typical Cross-section

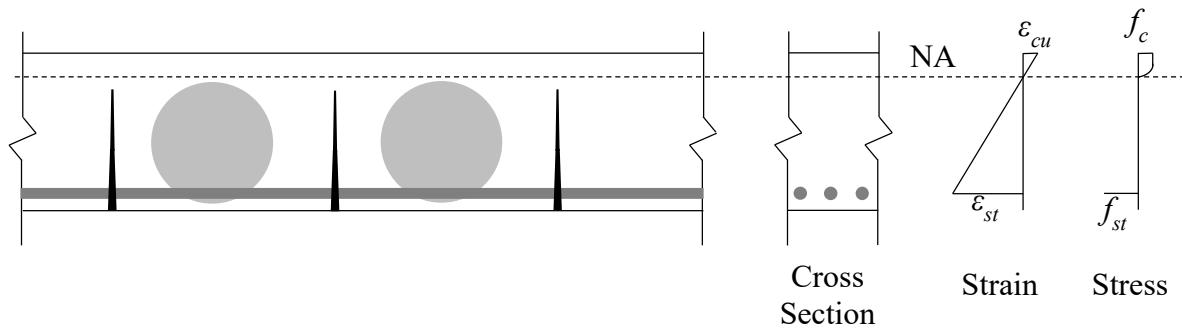


Figure 1.10 – Concept of Voided Slab

The voids lead to a reduction in self-weight up to 50% in comparison with conventional reinforced concrete solid slab without any significant change in its structural performance under flexure (Björnson, 2003 and Harding, 2004). The voided slab reduces the size and reinforcement requirement about 15% of other structural elements such as beam, column and footing. The overall result is the voided slab renders a significant cost saving of about 10% of total construction cost. The voided slab system is one of the Green Design techniques as 1 kg of recycled plastic replaces 100 kg of concrete and it reduces carbon emission from transportation and equipment. Further, the voided slab system is leads to energy efficiency buildings by means of thermal performance.

### 1.3 Need for the Present Study

The biaxial voided slabs are produced with various shapes of plastic void formers such as sphere, cylinder, donut, cuboid, and hexahedron with rounded edges. The shape, position, and volume of voids affect the structural performance of voided slab system significantly under various types of loads. In particular, the initial flexural stiffness of voided slab reduces due to the reduction in the cross-sectional area of concrete. Similarly, the one-way and two-way (punching) shear capacity of the voided slab is observed to be significantly affected by the voids. As the voided slabs are usually adopted as a flat slab system, the punching shear resistance plays a major role in fixing the dimensions of structural elements. In addition, the deflection should be within permissible limit under service load.

The key observations from the literature review (Chapter 2) are summarised below.

- The shape and volume of voids affect the initial flexural stiffness.
- In addition to the shape and volume of voids, the location of the void from the column face significantly affects the punching shear capacity of the voided slab.

In addition, the following inferences are drawn.

- Whether the analysis and design guidelines developed for the (flexure and punching shear) conventional solid slab is applicable for the voided slab as well.
- What will be the optimum location of voids from the column face to obtain maximum punching shear capacity?
- The effect of tensile membrane action at large deflection on the flexural behaviour of the biaxial voided slab needs to be investigated.
- The orientation of reinforcement also plays a significant role in enhancing flexural load carrying capacity of solid slab. Such beneficial load enhancing effect in biaxial voided slab needs to be studied.

#### **1.4 Objectives**

Based on the above inferences, the following objectives of this thesis have been defined:

- To understand the behaviour and predict the collapse load and collapse mechanism of the biaxial voided slab with simple supports subject to one-way and two-way bending, by carrying out analytical and experimental studies.
- To verify the application of the effect of tensile membrane action at large deflection and orientation of reinforcement along with yield line analysis to predict the collapse load of biaxial voided slab subject to two-way bending.
- To understand the behaviour and predict the collapse load of biaxial voided slab subject to concentrated load (punching shear) at the centre of the square slab, by carrying out analytical and experimental studies.
- To understand the influence of void location from the face of a column on the punching shear capacity of the biaxial voided slab, by carrying out an analytical study.
- To understand the influence of void shape on the structural behaviour of the biaxial voided slab with uniformly distributed load and concentrated load, by carrying out a numerical (parametric) study.



## 1.5 Scope

The scope of the present study is given below.

- The experimental studies on the solid and biaxial voided slab specimens are limited to the specimen configurations shown in Figure 1.11, which are based on the loading pattern.
- The experimental studies on the biaxial voided slab specimens are limited to the sphere (fabricated) and cuboid without shape edges (commercially available) void formers.
- The experimental studies on the solid and biaxial voided slab specimens are limited to the monotonic load and specimens are provided with simple supports.
- The numerical studies are carried out in commercial finite element software Displacement Analyser (DIANA) versions 9.4.4 and 10.2 for parametric study and comparison with current experimental study, respectively.

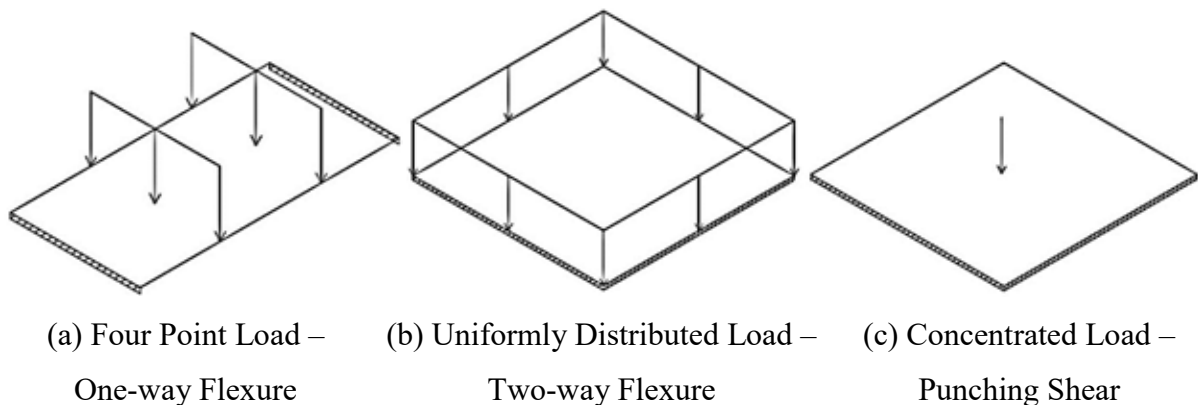


Figure 1.11 – Specimen Configurations and Type of Loading Pattern

## 1.6 Methodology

- Literature survey on voided slab systems and various experimental test setup associated with one-way and two-way flexure and punching shear.
- Experimental studies on the biaxial voided slab under one-way and two-way flexure are carried out. The flexural capacity of the biaxial voided slab is predicted by yield line analysis considering the effect of tensile membrane action at large deflection and orientation of reinforcement. Validated the same using experimental results of the current study and reported in the literature.
- Experimental study on the biaxial voided slab under concentrated load (punching shear) is carried out. The applicability of conventional methods for solid slabs in the design

standards, such as ACI 318 (2014), EN 1992-1-1 (2004) and IS 456 (2000) to predict the punching shear capacity of the voided slab is examined. For the same, the experimental results of the current study and reported in the literature are considered.

- Numerical studies on the biaxial voided slab subject to uniformly distributed load (two-way flexure) and concentrated load (punching shear) are conducted to understand the effect of void shape on the structural behaviour. Also, the numerical results are compared with the experimental results of the current study.
- Finally, guidelines to design and analysis the biaxial voided slab for one-way and two-way flexure and punching shear are developed.

### **1.7 Organisation of the Thesis**

This chapter introduces the thesis with an overview of existing slab systems and voided slab systems, objectives, scope and methodology of the study. An outline of the following chapters is summarised below.

Chapter 2 describes the detailed literature on voided slab system, structural behaviour of voided slabs subjected to various loading configuration, analysis of slabs based on yield line method along with tensile membrane action and influence of reinforcement orientation on the ultimate flexural capacity of the slab. Also, various experimental test setup associated with one-way and two-way flexure and punching shear is discussed.

Chapter 3 explains the complete experimental and analytical studies on the biaxial voided slabs under one-way and two-way flexure. Prediction of one-way flexural behaviour of biaxial voided slab based on the yield line analysis is explained. In addition, estimation and validation of two-way flexural ultimate capacity by including the effect of tensile membrane action and orientation of reinforcement with experimental results of the current study and available in the literature are carried out.

Similarly, Chapter 4 explains the complete experimental and analytical studies on the biaxial voided slabs subjected to concentrated load (punching shear). The punching shear capacity is predicted by guidelines given for solid slab in various standards. Modified equations were proposed to predict the punching shear capacity of the biaxial voided slab.

Chapter 5 covers the parametric study conducted to understand the influence of void shape on the structural behaviour of the biaxial voided slab. Also, the numerical results of the biaxial cuboid voided slab are compared with the experimental results of the current study. Also, the results of the numerical studies which carried out to understand the biaxial cuboid voided slab subject to one-way and two-way flexure and one-way and two-way (punching) shear are given.

Finally, Chapter 6 summarises the observations and conclusions of the current study and scope for future works.

This page is intentionally left blank.

## CHAPTER 2

### VOIDED SLAB SYSTEMS – LITERATURE REVIEW

#### 2.1 Overview

In this chapter, the studies carried out in the past on the slabs, subjected to various loading conditions are summarised. This chapter broadly divided as flexure and shear & punching shear based on structural behaviour. The different experimental test setup adopted by researchers are summarised. In addition, the studies carried out to quantify the effect of tensile membrane action on the ultimate flexural strength of slab is explained in detail with the background theories associated with it.

#### 2.2 Voided Slab

Initially, in 1914, one-way voided slabs are developed to reduce the self-weight. The void in the slab was created in the longitudinal direction of the slab using hollow tiles, metal, tar paper, sonotube, slag block and foam (Mota, 2013). The one-way voided slab systems showed a significant difference in load-carrying capacity in orthogonal directions, and it is more suitable for floor slabs spanning in one direction alone. In order to overcome this shortcoming, ribbed slab systems such as joist and waffle slabs were developed. Later in 1997, Cobiax developed lightweight, environmentally effective hollow body system. Followed by that in 2001, U-Boot, a modular prefabricated element used in building construction in order to decrease the transportation costs and in 2003, Airdeck (biaxial voided slab) concept was adopted in the construction field. Biaxial voided slab is reinforced concrete slab with plastic void formers usually made of shapes such as spherical, donut, and cuboid placed in between reinforcing mesh at top and bottom (BubbleDeck Technology, 2008; Chung et al., 2010; Churakov, 2014; Cobiax Technologies, 2010; Daliform Group, 2012; Ezhilan, 2011; Ibrahim et al., 2013a; Kim et al., 2011; Kim, 2011; Taskin and Peker, 2014; Valivonis et al., 2014). It leads to a reduction in self-weight up to 50 % in comparison with conventional reinforced concrete solid slab without any significant change in its structural performance (Björnson, 2003; Harding, 2004). Such reduction in self-weight decreases the demand induced in other structural elements (*such as column and foundation*), resulting in lesser consumption of materials such as reinforcement and concrete up to a total of 15 % (Daliform Group, 2012).

## **2.3 Flexure**

### **2.3.1 One-way Flexure**

The one-way flexural capacity of the voided slab was evaluated using different shapes of void formers conducting various experimental or analytical and numerical studies. These studies evidenced that biaxial voided slabs show similar strength and slightly lower stiffness compared to that of solid slab having equal depth (BubbleDeck Technology, 2008; Cobiax Technologies, 2010; Daliform Group, 2012; Ibrahim et al., 2013b; Kim et al., 2011; Valivonis et al., 2014). Few studies showed that:

- The ultimate flexural capacity of sphere voided slab is same as that of solid slab. The bending stiffness of this voided slab gets reduced by 13 % in comparison with the solid slab. But, overall, the concrete requirement is reduced by 44 % (BubbleDeck Technology, 2008).
- In slab with rectangular polystyrene void forms, the initial and secant stiffness were influenced by volume ratio of polystyrene void forms (Kim, 2011).
- The donut type hollow sphere voided slab shows almost similar or larger flexural capacity than solid slabs; the presence of a hole in this void also has some effect on slab capacity. The strength and material properties of the donut type void highly affect the flexural strength of the voided slab (Kim et al., 2011).
- The flexural strength of spherical voided slab is the same as that of solid slab having equal depth, and its flexural stiffness is 80 – 90 % of the solid slab (Midkiff, 2013).

Similarly, one-way flexural behaviour of a unidirectional voided slab which was strengthened with fibre reinforced polymer and overlay techniques system were investigated by conducting experiments and numerical studies. It showed that strength and displacement ductility are dependent on the strengthening techniques (Kankeri et al., 2018).

#### **2.3.1.1 Loading Type**

Researchers have adopted four-point loading configurations to study the one-way flexural behaviour of RC solid and voided slabs. Based on the required shear span to depth ratio researchers fixed the loading positions. Typical schematic diagrams of the four-point bending test are shown in Figure 2.1, which were adopted by Kim (2011).

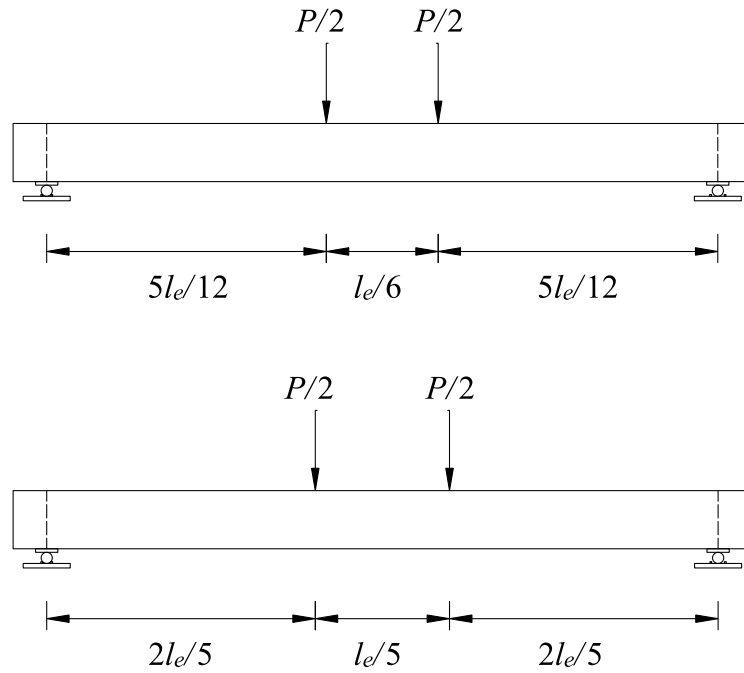


Figure 2.1 – Loading Configurations of Four-Point Bending Test

### 2.3.2 Two-way Flexure

The two-way flexural behaviour of voided RC slab system was also studied similarly by previous researchers (Chung et al., 2018b; Ibrahim et al., 2013b). The capacity of voided slabs constructed using the spherical void former is 89 – 100% of the ultimate load of RC solid slab with equal depth and shows marginal stiffness reduction (Ibrahim et al., 2013b). On the other hand, RC slabs constructed using donut-type void former showed 25% lower in the flexural secant stiffness when compared to that of an RC solid slab of the same dimensions and reinforcement. However, the flexural capacity remains the same (Chung et al., 2018b).

#### 2.3.2.1 Loading Type

Researchers have adopted various loading configurations to study the two-way flexural behaviour of RC square solid and voided slabs. Application of single-point load at the centre of the slab (Figure 2.2a) often results in premature localised punching shear failure (Matešan et al., 2012). The punching shear failure was avoided by adopting five-point load (Figure 2.2b) in small-scale specimens (Ibrahim et al., 2013a, b) and twelve-point load (Figure 2.2c) in full-scale specimens (Chung et al. 2018b). However, the load was concentrated at the central region alone, not equally distributed throughout the slab surface. Loading configurations adopted by various researchers were not able to capture the uniformly distributed load (UDL) conditions. For example, the slab subjected to UDL and slab subjected to twelve-point load (equivalent to

62.5% of UDL) results in the same deflection. Taylor et al. (1966) and Bijily (2017) adopted the sixteen-point load (Figure 2.2d), which is equivalent to 89% of UDL.

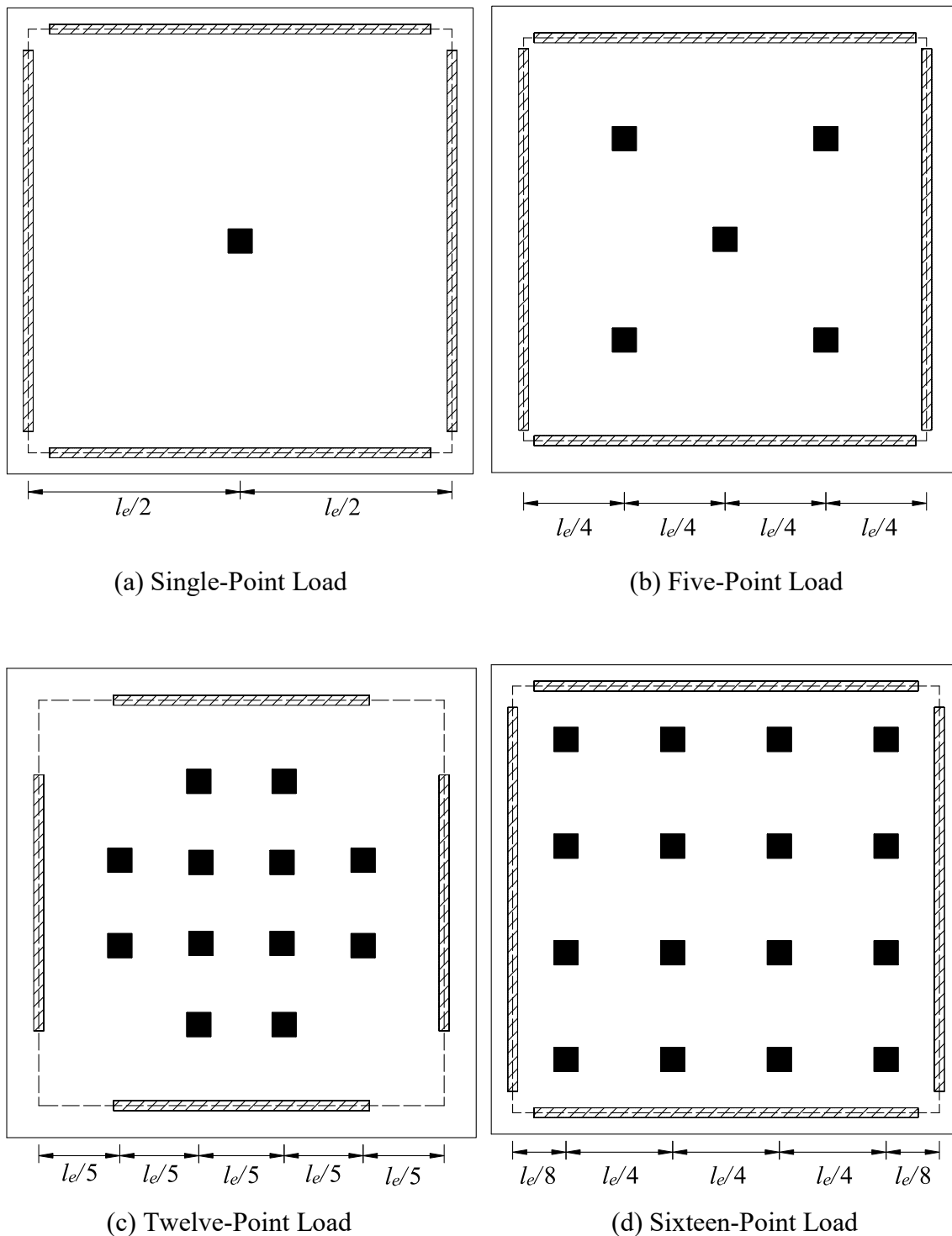


Figure 2.2 – Loading Configurations Adopted by Various Researchers



### 2.3.2.2 Tensile Membrane Action

In addition to the loading type effect on the structural behaviour of slabs, in the early 1960s, research on the effect of tensile membrane action was initiated in the analysis and design of lightly RC slabs with large deflections. Researchers found that the effect of tensile membrane action is significant in enhancing the capacity of slab considerably as compared to the capacity estimated by conventional flexural theory (Bailey, 2001; Bailey, Toh, and Chan, 2008; Brotchie and Holley, 1971; Burgess, 2017; Eyre, 1997; Herraiz and Vogel, 2016; Matešan et al., 2012; Taylor, 1965; Taylor et al., 1966; Wood, 1961). These works focused on the conventional RC solid slab with various shapes, aspect ratios, reinforcement details, and yield line pattern and crack formation at the ultimate stage. The question of whether such beneficial effect of enhancement of capacity due to tensile membrane action at the ultimate stage exists in an RC voided slab is yet to be explored. This would help to determine the ultimate capacity of such slabs with reasonable accuracy.

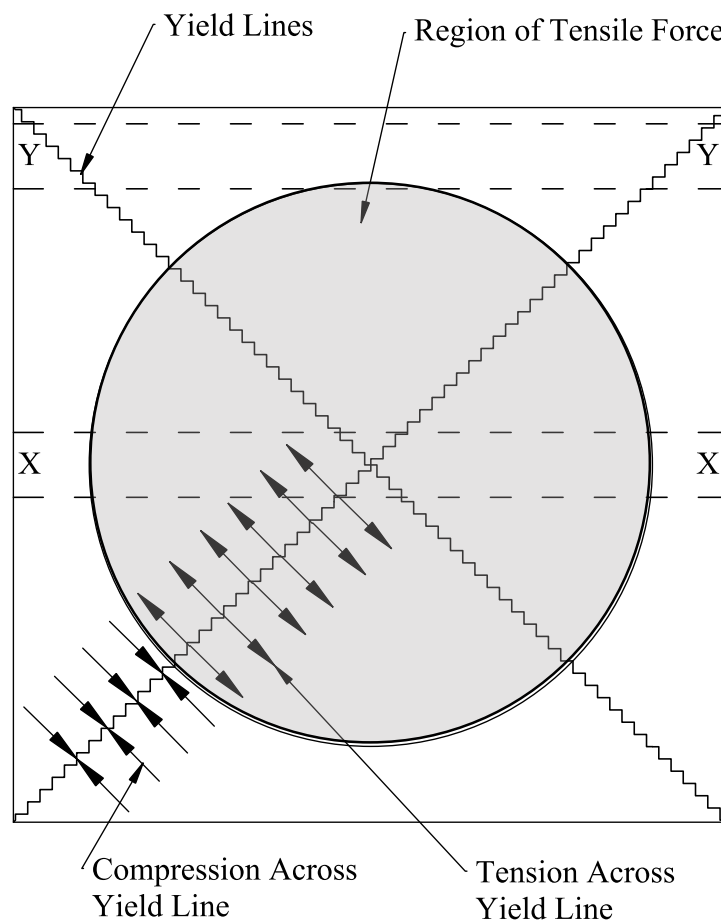


Figure 2.3 – Development of Membrane Forces in Laterally Unrestrained Slab (Bailey, 2001)

In a two-way (laterally unrestrained slab) slab which is supported vertically around its edges (Figure 2.3), the deflection profile of the middle strip (denoted as XX) and the edge strip (denoted as YY) will differ significantly as the slab ends offer resistance. The interaction between the strips resulting in the development of membrane forces. *“Therefore the load-carrying capacity of an unrestrained slab at large displacements comprises tensile membrane action in the centre and an increase in yield moment in the areas where in-plane compressive stresses occur. This type of behaviour is typically termed tensile membrane action.”* (Bailey, 2001). A theoretical approach to estimate the effect of tensile membrane action was developed by various researchers (Hayes, 1968; Kemp, 1967; Sawczuk and Winnicki, 1965; Taylor et al., 1966 and Wood, 1961). The shortcomings of these approaches can be found in (Bailey, 2001). Bailey (2001) proposed analytical equations to estimate the enhancement in load carrying capacity by assuming that rigid-plastic behaviour will cause the crack to form across the short span. The enhancement is due to in-plane tensile stresses developing at the centre of the slab and the increase in yield moment in the outer regions of the slab, where compressive stresses occur (Figure 2.3). Section 3.3.2.2 summarises the key parameters related to the estimate of the enhancement in load carrying capacity due to tensile membrane action.

### **2.3.3 Effect of Reinforcement Orientation**

In general, it is assumed that the yield moment ( $m$ ) given by the orthogonal direction reinforcements are independent of each other. For the RC slab reinforced in  $x$  and  $y$  directions, this can be described by the *square yield criterion*, which is represented in Figure 2.4. The RC slab is said to be yielding when the bending moment  $M_x$  in  $x$ -direction or  $M_y$  in  $y$ -direction reaches yield moment,  $\pm m$ , subjected to the condition that reinforcement at top and bottom of the slab is the same. If the reinforcement at the top of the slab is lesser than that of the bottom of the slab, then the negative yield moment reduces, say  $m'$ , which is denoted by a dashed line in Figure 2.4. The point A in Figure 2.4 represents the centre of a square slab where fracture lines meet (Figure 2.5b). Points B, C, and D in Figure 2.4 represent the corner of a square slab where the fracture lines meet orthogonally (Figure 2.5a). The points B, C, and D are typical representations of the cases where negative yield moment, equal to zero, lesser than positive yield moment and equal to positive yield moment, respectively.

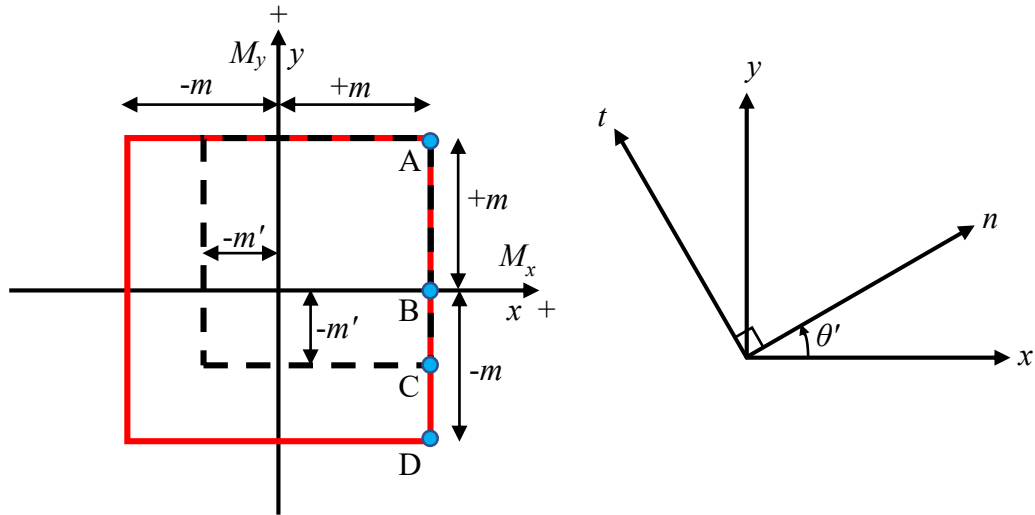
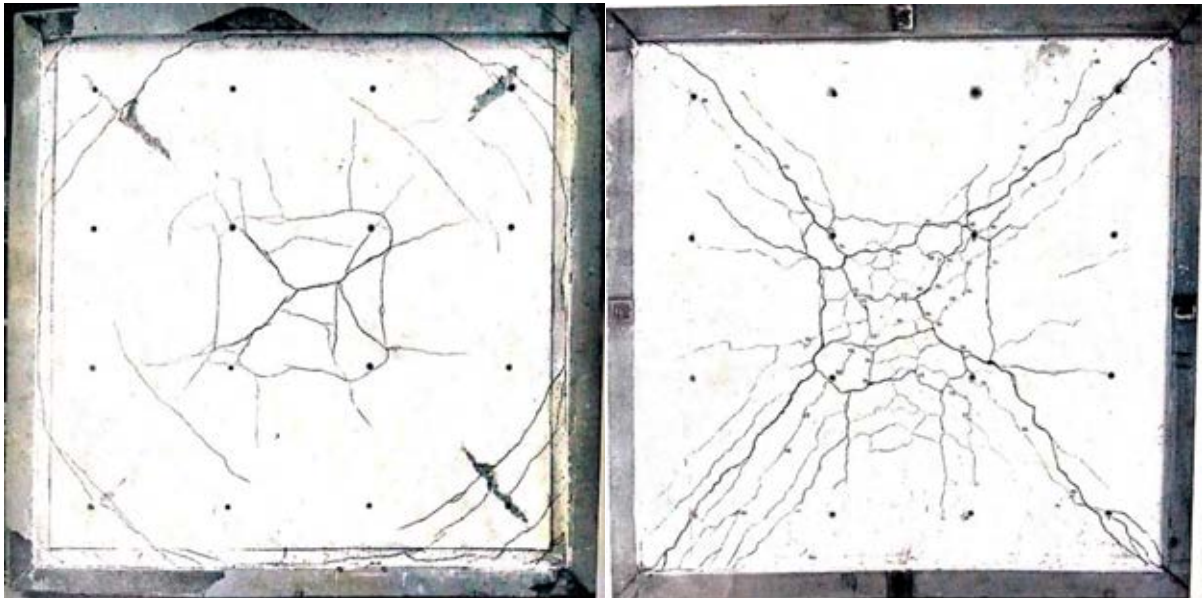


Figure 2.4 – Square Yield Criterion and Rotation of Axis



(a) Top Side of Slab

(b) Bottom Side of Slab

Figure 2.5 – A Square Slab Supported on Beams Subjected to 16-Point Load (Wood, 1961)

Point 'A' indicates a condition of no twist and equal moment in all the directions, while point C indicates a condition of the considerable twisting moment which is equal to the yield moment. The moment in any other axes  $n$  and  $t$  at right angles (Figure 2.4) can be estimated by rotating the axes or diagram. If a fracture line is not in line with the reinforcement axes  $x$  and  $y$ , both reinforcement must yield and with this background, the moment in axes  $n$  and  $t$  can be estimated by Eq. 2.1 and Eq. 2.2, respectively.

$$M_n = M_x \cos^2 \theta' + M_y \sin^2 \theta' \quad \text{Eq. 2.1}$$

$$M_t = M_x \sin^2 \theta' + M_y \cos^2 \theta' \quad \text{Eq. 2.2}$$

At the yield stage,  $M_x = m$  and  $M_y = m$ . After substituting the values of  $M_x$  and  $M_y$  in Eq. 1a and 1b, the moment in axes  $n$  and  $t$  become as  $M_n = m$  and  $M_t = m$ . However, this is applicable only to point 'A' (centre of the slab) where the uniform moment is present in all the directions. In other locations, the moment changes in magnitude on the fracture line and also the direction of the moment changes near the corner, i.e.,  $M_n = m$  and  $M_t < m$ , where  $M_n$  is a principle moment. This results in  $M_x < m$  and  $M_y < m$ . This phenomenon points out that to achieve a lower bound solution, the moment should be varied along fracture lines. Further, the fracture moment is likely to exceed  $m$ , if the reinforcement in  $x$  and  $y$  directions is compelled to yield along a diagonal fracture line. Thus, the use of square yield criterion seems to be conservative. The enhancement is about 15 %, and it was found through experiments by various researchers (Hedley, n.d.; Wood, 1961). The details of the experiments are summarised below.

### 2.3.3.1 One-Way RC Slabs

Experiments were carried out at Building Research Station, UK, on one-way RC slabs to study the effect of reinforcement orientation on the ultimate capacity (Wood, 1961). The details of the experiments and results are summarised in this section. Slab specimens with the reinforcement (i) parallel to slab edges (Figure 2.6a), (ii) at  $22.5^\circ$  and  $67.5^\circ$  to the slab edges (Figure 2.6b), and (iii) at  $\pm 45^\circ$  to the slab edges (Figure 2.6c) were tested. The study found that the specimen with reinforcement placed at an angle of  $45^\circ$  with respect to slab edges, showed 16 % higher load carrying capacity as compared to the specimen with reinforcement parallel to slab edges. The fracture line (in zigzag pattern) is shown in Figure 2.6.

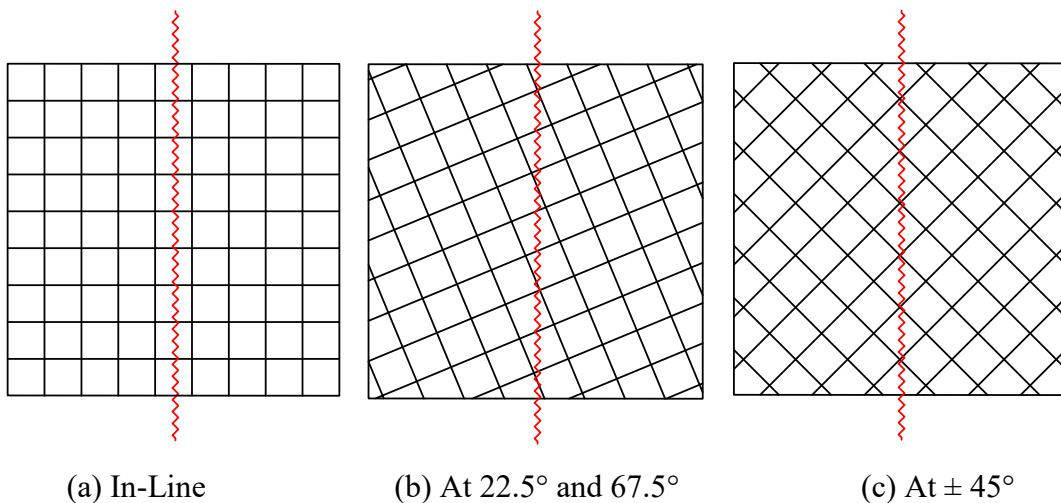
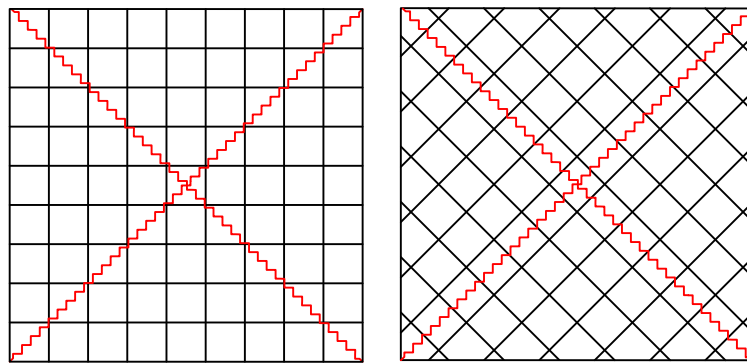


Figure 2.6 – Schematic Arrangement of Reinforcement with Fracture Line (One-Way)

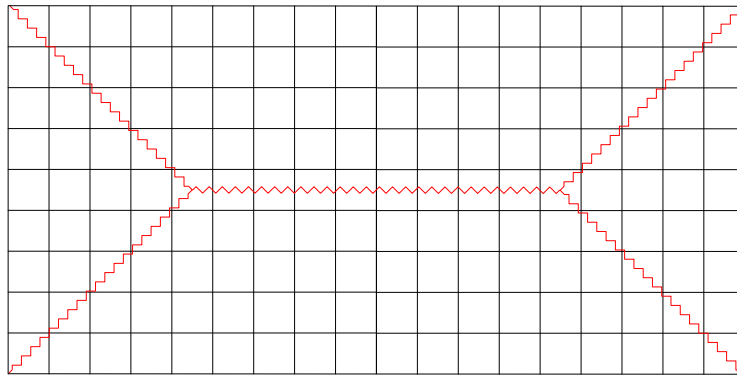
### 2.3.3.2 Two-Way RC Slabs



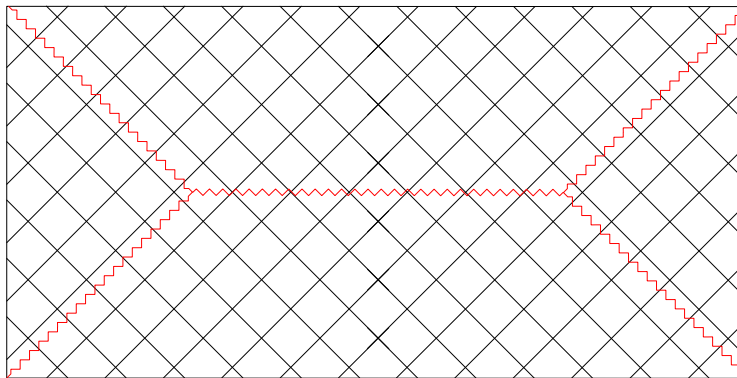
(a) In-Line

(b) At  $\pm 45^\circ$

Figure 2.7 – Schematic Arrangement of Reinforcement with Fracture Lines  
(Two-Way – Square Slab)



(a) In-Line



(b) At  $\pm 45^\circ$

Figure 2.8 – Schematic Arrangement of Reinforcement with Fracture Lines  
(Two-Way – Rectangular Slab)

Experiments were carried out at Atomic Weapons Research Establishment, Foulness, UK, on two-way RC slabs to study the effect of reinforcement orientation on the ultimate capacity (Hedley, n.d.). The details of the experiments and results are summarised in this section. Slab specimens with the reinforcement (i) parallel to slab edges (Figure 2.7a), and (ii) at  $\pm 45^\circ$  to the slab edges (Figure 2.7b) were tested. The study found that the specimen with reinforcement placed at an angle of  $45^\circ$  with respect to slab edges showed 15 % lesser load-carrying capacity as compared to the specimen with reinforcement parallel to slab edges. The fracture line (in zigzag pattern) is shown in Figure 2.7 and Figure 2.8. The enhancement of capacity due to reinforcement orientation may not be significant in rectangular slabs as a part of fracture line aligns parallel to the reinforcement. Typical examples of slab specimens with the reinforcement (i) parallel to slab edges (Figure 2.8a), and (ii) at  $\pm 45^\circ$  to the slab edges (Figure 2.8b) clearly illustrate the same.

## **2.4 Shear and Punching Shear**

### **2.4.1 Shear (One-way)**

Even though the ultimate flexural capacity of biaxial voided slab remains same as that of a solid slab, a considerable reduction in the shear capacity of the voided slab is reported. One-way shear capacity of the biaxial hollow slab with rounded box and donut type hollow void formers showed 40 % and 27 % reduction in comparison with that of the solid slab, respectively (Chung et al., 2011b).

### **2.4.2 Punching Shear (Two-way)**

Similarly, the reduction in punching shear capacity (two-way shear) was studied by researchers with various shape of void formers (BubbleDeck Technology, 2008; Chung et al., 2011a; Chung et al., 2018a; Han and Lee, 2014; Held and Pfeffer, 2002; Oukaili and Husain, 2017; Valivonis et al., 2017a, b) and reported that it decreases up to 40 % in comparison with conventional RC solid slab (BubbleDeck Technology, 2008). The reduction in punching shear capacity of cylinder voided slab with 10 % volume void ratio was observed to up 30 % in comparison with reference solid slab (Wang et al., 2008). The punching shear capacity of slab with donut type void shape was 87 % of that of solid slab, and the critical failure section was observed to be in the range of 0.5 ~ 2.5 times of effective depth of slab ( $d$ ) from face of the column which depends on the number of void formers in that section (Chung et al., 2011a, 2018a). The slab specimens with cylinder shape voids carried 50 – 70 % of the punching shear

capacity of the solid slab (Han and Lee, 2014). The reduction of punching shear capacity of the slab with sphere shape void was about 4.41 – 18 % and 14.7 – 29.4 % for slabs with voids at sections located at  $2d$  and  $d$  from face of the column, respectively (Oukaili and Husain, 2017). Further, in the same study, it was observed that the perimeter of the critical failure section in voided slabs was 4.2 – 41.7 % higher than that of solid slabs. The punching shear capacity of the specimens with plastic units of box type voids (hexahedron with rounded edges) and solid cross-shaped parts was 43 % and 18 % lower than that of the specimens without voids (Valivonis et al. 2017a, b). These studies explore that the punching shear capacity of the voided slab is highly dependent on the shape and location (from the face of the column) of voids.

### 2.4.2.1 Test Setup

Researchers have adopted two different loading configurations to study the structural behaviour of solid and voided slabs subject to concentrated load (punching shear). In the Type-I test setup, the load is applied from the bottom (vertically upward) of the column which cast monolithically with the slab. In case of Type-II test setup, the load is applied from the top (vertically downward) of the column. The Type-I test setup is difficult to arrange as the slab specimen used to be supported at eight locations radially. The photograph and schematic diagram of the test setup (Type-I) adopted by Held and Pfeffer (2002) is shown in Figure 2.9. The three-dimensional view of Type-I test setup is shown in Figure 2.10 for clarity.

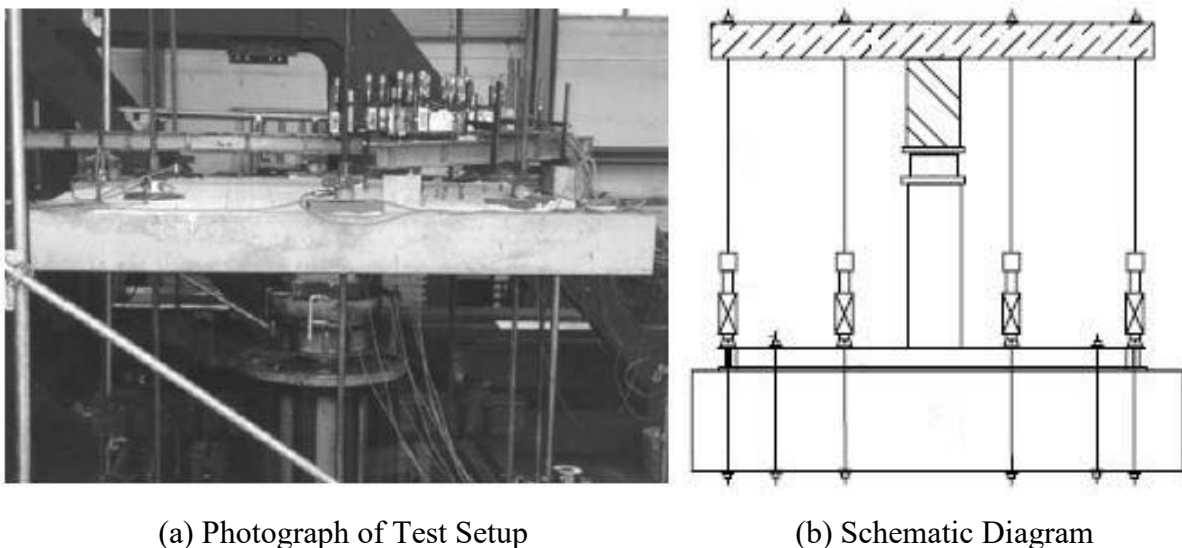


Figure 2.9 – Type-I Test Setup (Held and Pfeffer, 2002)

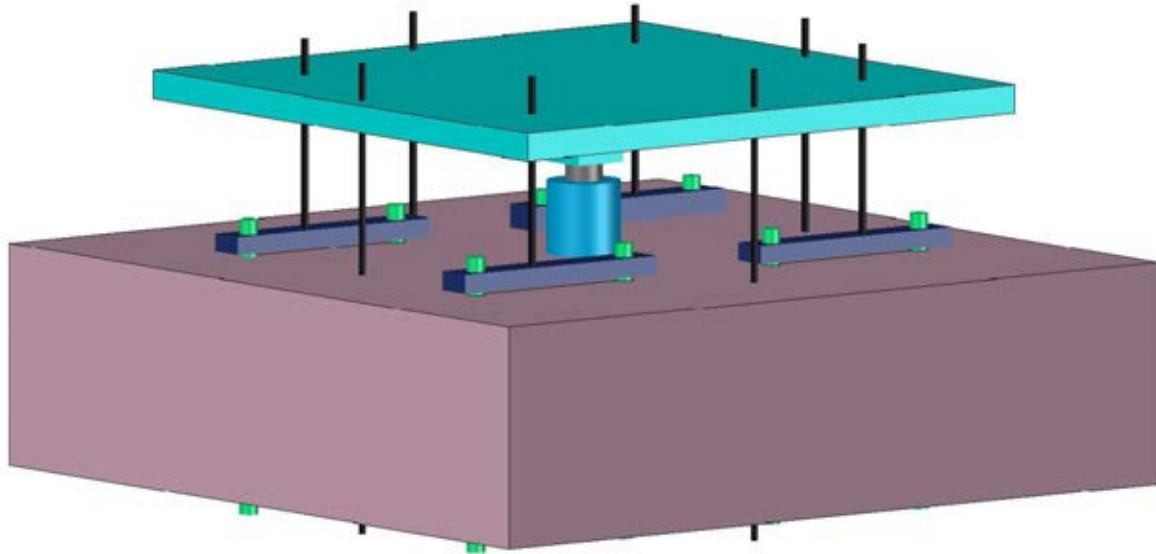


Figure 2.10 – Three-Dimensional View of Type-I Test Setup



Figure 2.11 – Photograph of Type-II Test Setup (Valivonis et al., 2017a)

The Type-II test setup can be easily erected as the slab specimen usually supported at its all edges with rigid members. In addition, casting of specimens with column at top of slab is simple in comparison with the specimen with column at bottom of the slab. The photograph of the test setup (Type-II) adopted by Valivonis et al. (2017a) is shown in Figure 2.11.



### 2.4.2.2 Prediction of Punching Shear Capacity of Biaxial Voided Slab

The past studies explore that the punching shear capacity of the voided slab is highly dependent on the shape and location (from the face of the column) of voids. Held and Pfeffer (2002) proposed an analytical equation (Eq. 2.3) to estimate the effective area of concrete ( $A_e$ ) available at critical perimeter located at a distance half of effective depth ( $d_e/2$ ) from the face of column (Figure 2.12). If there is no void intersects the control perimeter, the design guidelines of a solid slab for punching can be applied to the biaxial hollow slab without modification. However, past studies showed that the location of voids significantly affecting the critical perimeter, thus punching shear capacity of the biaxial voided slab.

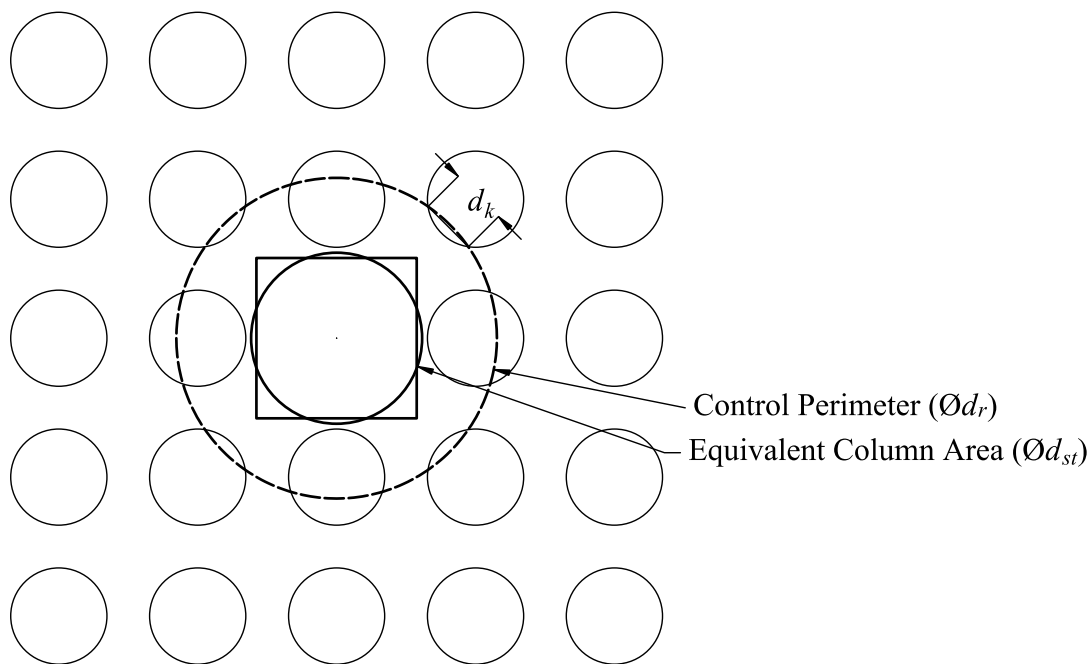


Figure 2.12 – Effective Concrete Area

$$A_e = \pi d_r d_e - \sum \frac{\pi d_k^2}{4} \quad \text{Eq. 2.3}$$

where,  $d_r$  is diameter of control perimeter, and  $d_k$  is the width of void intersecting the control perimeter.

Han and Lee (2014), proposed empirical equations (Eq. 2.4, Eq. 2.5, and Eq. 2.6) to predict the punching shear capacity of the voided slab with cylindrical voids ( $V_c$ ) based on the experimental results and guidelines available for the solid slab in the ACI 318 (2011).

$$V_C = 0.33\sqrt{f_c'}(b_0d - \sum d_v h_v) \quad \text{Eq. 2.4}$$

$$V_C = 0.33\sqrt{f_c'}\left(2\pi d_r d - \sum 2\pi d_r \frac{\theta}{360} h_v\right) \quad \text{Eq. 2.5}$$

$$V_C = 0.33\sqrt{f_c'}(b_0d - \sum l_r h_v) \quad \text{Eq. 2.6}$$

where,  $b_0$  is perimeter of critical section located at  $d/2$  distance from column face,  $d$  is effective depth of slab,  $d_v$  and  $h_v$  are the width and height of voids overlapping the critical section (Figure 2.13a),  $d_r$  is the diameter of control perimeter,  $\theta$  is the angle (in degrees) measured at the centre of the column between the two points along the perimeter of the void overlapping the critical section (Figure 2.13b), and  $l_r$  is the length to be deducted from the critical section located at a distance  $d/2$  from the column face (Figure 2.13c).

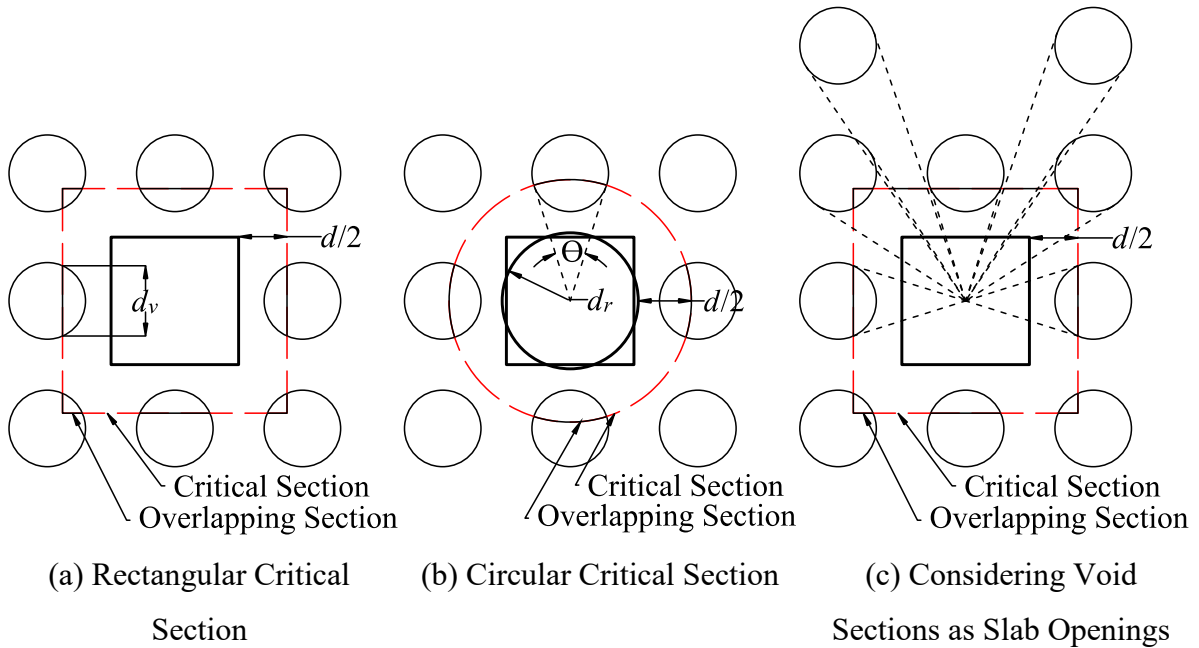


Figure 2.13 – Assumed Critical Sections in Voided Slabs

Chung et al. (2018a), proposed an empirical equation (Eq. 2.7) to predict the punching shear capacity of the biaxial voided slab ( $V_c$ ) based on the reported experimental results and guidelines available for the solid slab in the ACI 318 (2011).

$$V_C = 0.083\left(2 + 50\alpha_s\left(\frac{d}{b_0}\right)^3\right)\sqrt{f_{ck}}(b_0d - \sum A_v) \quad \text{Eq. 2.7}$$

where,  $\alpha_s$  is 40 for interior columns, 30 for edge columns, and 20 for corner columns,  $d$  is effective depth of slab,  $b_0$  is perimeter of critical section located at  $d/2$  distance from column face,  $f_{ck}$  is compressive strength of concrete cube, and  $A_v$  is area of void at control perimeter.

All these equations (Eq. 2.3 – Eq. 2.7) are based on the fixed control perimeter located at a distance of  $d_e/2$ ; it may overestimate the punching shear capacity of slabs with voids located just away from the control perimeter. In addition, Eq. 2.6 will underestimate (may lead to zero also) the punching shear capacity of slabs as the voids usually placed all over the slab.

## **2.5 Summary**

This chapter summaries the various studies carried out in the past on the biaxial voided slab subjected to one-way and two-way flexure and one-way and two-way (punching shear). The summary of the studies carried out to quantify the effect of tensile membrane action on the ultimate flexural strength of slab is given. The influence of reinforcement orientation on the ultimate flexural capacity of the slab is explained with background theory and reported experimental results. The outcome of various experimental study related to the test setup is briefly described. In particular, the importance of the number of loading points on the two-way flexural behaviour is explained. The available methods/equations to predict the punching shear capacity of biaxial voided slabs are summarised in details with its demerits.

This page is intentionally left blank.

## CHAPTER 3

### BEHAVIOUR OF VOIDED SLABS IN FLEXURE

#### 3.1 Overview

This chapter explains the experiments that are carried out to study the structural behaviour of biaxial voided slab subject to one-way and two-way flexure. Under the heading of the experimental study (Section 3.2), the details of void formers, test specimens, test set-up, instrumentation, loading procedure and observed test results are summarised. Similarly, in Section 3.3, the detailed procedure to obtain the flexural stiffness, load corresponding to the first crack, yielding of reinforcement, and the ultimate stage are explained. In addition, the influence of tensile membrane action and reinforcement orientation on the ultimate load-carrying capacity are explained with the test results of the current study and reported in the literature.

#### 3.2 Experimental Study

In this section, the details of the void formers, specimen details, materials' properties, test set-up, instrumentation, test procedure and experimental observations & results are explained.

##### 3.2.1 Details of Void Formers

Void formers of sphere and cuboid, manufactured from recycled polypropylene were used to cast the voided slab specimens. The specifications of the void formers are summarised below.

##### 3.2.1.1 Sphere Void Former

The sphere void formers are spherical hollow plastic balls of wall thickness 3 mm of two different outer diameters, 90 mm and 180 mm. The top and bottom reinforcement mesh used to keep the void former in position with 20 mm clear cover at the bottom. The diameter of the void formers is arrived such that the clear cover to the void at the top will be 40 mm and 50 mm for slabs with 90 mm and 180 mm sphere void, respectively. The sphere void former was placed such that the centre to centre spacing in longitudinal and transverse directions is 160 mm (113 mm in diagonal) and 210 mm for 90 mm and 180 mm diameter void formers, respectively. The spacing between voids was arrived to achieve  $\approx 20\%$  and  $\approx 30\%$  weight

reduction for slabs with 90 mm and 180 mm sphere void, respectively. The dimensions of the sphere void formers with its photographs are shown in Figure 3.1.



Figure 3.1 – Single Unit of Sphere Void Formers

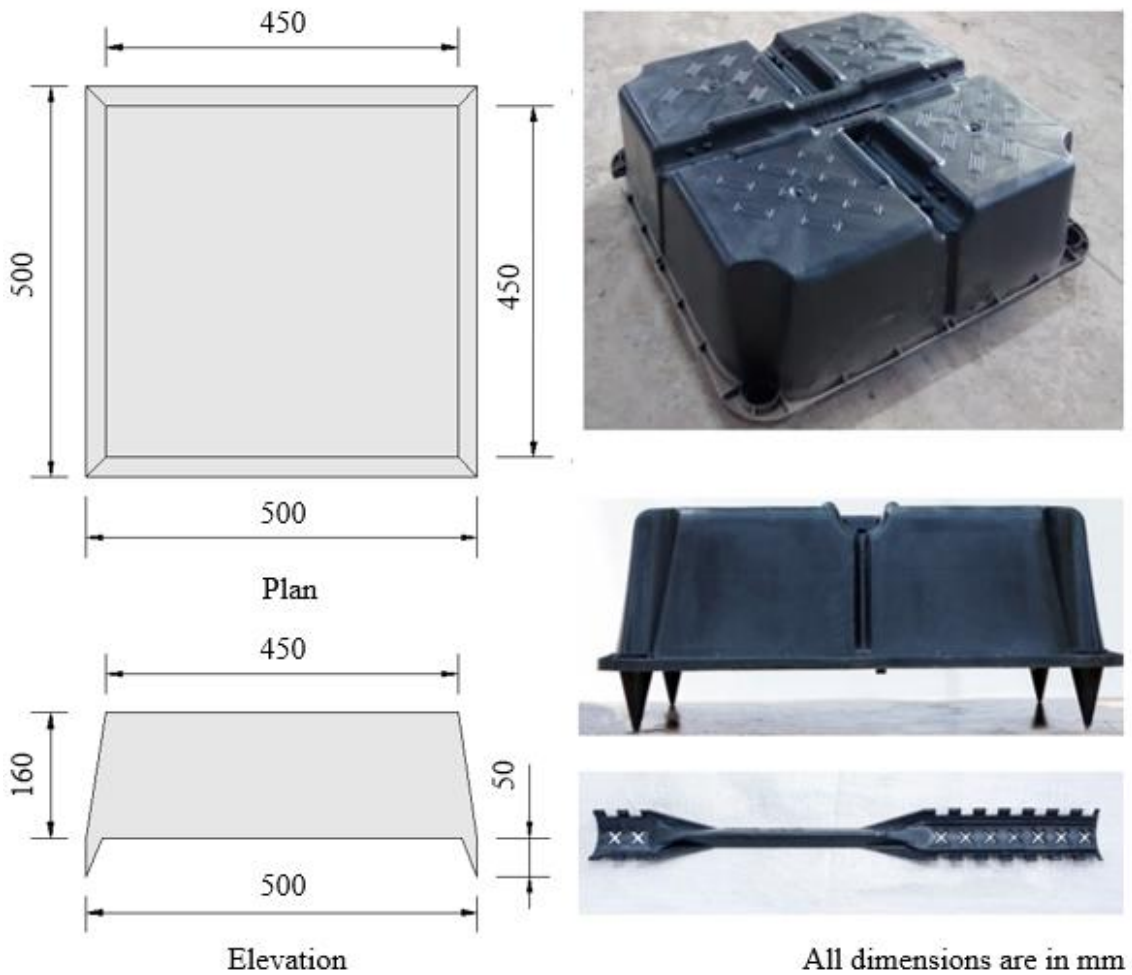


Figure 3.2 – Single Unit of Cuboid Void Former and Lateral Spacer

### 3.2.1.2 Cuboid Void Former

The commercially available cuboid void former (Figure 3.2) was used in the present study, which does not have any sharp edges. The average plan dimension of the void is 475 mm ×

475 mm. To hold this void former at the centre of the slab, elevator feet of 50 mm is provided at its bottom face of four corners. Similarly, it is separated in lateral direction using lateral spacers such that the void formers are placed at 600 mm centre to centre. Its depth and clear cover (at top and bottom) are 160 mm and 50 mm, respectively. The spacing between voids is arrived to achieve  $\approx 40\%$  weight reduction. The void former contains stiffeners at inner sides of the flange and web, which helps to resist the weight of concrete without any significant change in its shape. The load resisting capacity of the cuboid void former is obtained based on the experiments. The details of the same are explained below.

### **(i) Tests on Cuboid Void Former**

The cuboid void former is tested to know the load-carrying capacity when it is loaded at the centre and a corner. The photograph of test set-up is shown in Figure 3.3. Three specimens were tested for each category of loading. The loading plate of size 70 mm  $\times$  70 mm was used. The test results showed that the cuboid void former can carry the load of 200 kg and 174 kg when it is loaded at the centre and a corner, respectively. The tested specimens are shown in Figure 3.4.



Figure 3.3 – Set-up for Test of Cuboid Void Former



(a) Specimens Loaded at Centre



(b) Specimens Loaded at a Corner

Figure 3.4 – Tested Specimens



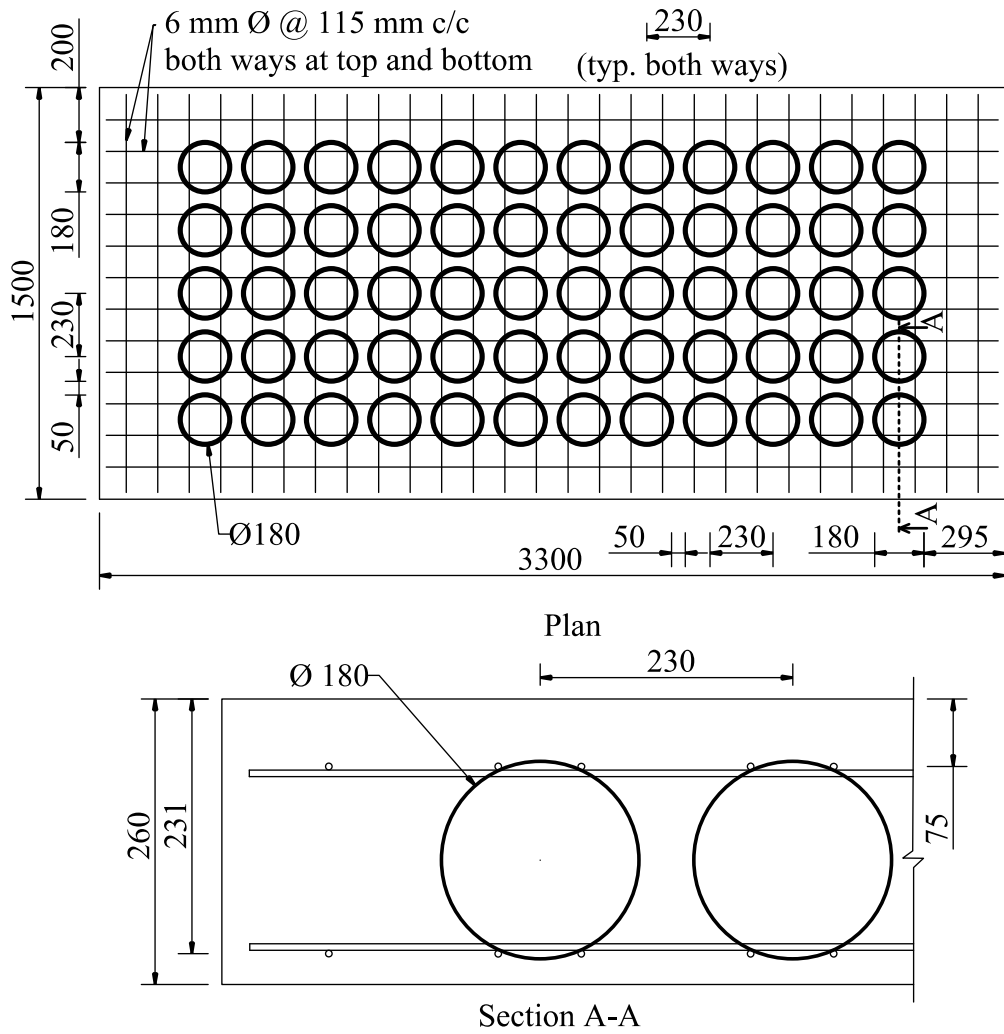
### 3.2.2 Details of Test Specimens

In total, ten full-scale specimens were tested under flexure. In which four were tested under one-way flexure and six were tested under two-way flexure. The overall plan dimensions of one-way and two-way test specimens were 3300 mm × 1500 mm and 3300 mm × 3300 mm, respectively. The detailed specifications about test specimens such as dimensions, cross-section and reinforcement details are summarised in Table 3.1. The minimum reinforcement requirement specified in IS 456: 2000 is provided based on the gross area of the slab specimens. The reinforcement was arranged as top and bottom mesh in longitudinal and transverse directions, such that the voids can be placed between the reinforcement gauges. The detailed arrangement of reinforcement and void formers are shown in Figure 3.5 – Figure 3.10. For all type of voided slab, reference solid slab specimens were not cast and tested as the maximum lifting capacity of available crane facility is 5 ton.

Table 3.1 – Details of Flexural Test Specimens

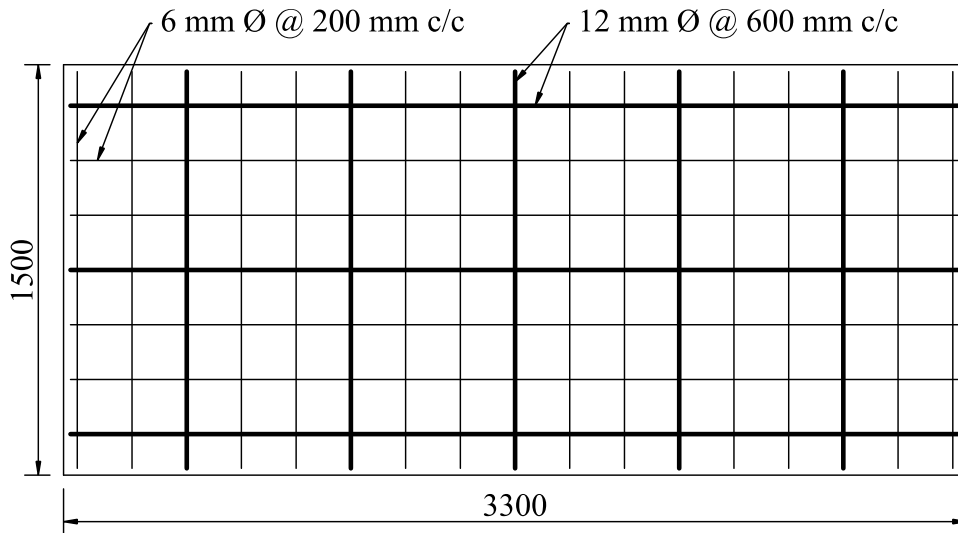
Specimen	Void details	Dimension (mm)	$A_{st}$ (mm <sup>2</sup> /m)		$f_{cm}$ (N/mm <sup>2</sup> )
			Top	Bottom	
OF-S180V	Ø 180 mm Sphere	3300 × 1500 × 260	226	226	25.7
OF-CV-1					24.8
OF-CV-2	Cuboid	3300 × 1500 × 260	132	301	24.8
OF-CV-3					24.8
TF-Solid	–				31.2
TF-S90V	Ø 90 mm Sphere	3300 × 3300 × 150	343	343	31.0
TF-S180V	Ø 180 mm Sphere	3300 × 3300 × 250	257	257	29.4
TF-CV-1					24.3
TF-CV-2	Cuboid	3300 × 3300 × 260	146	274	26.1
TF-CV-3					24.4

Note: OF – One-way Flexure; TF – Two-way Flexure; S180V – 180 mm dia. Sphere Void; S90V – 90 mm dia. Sphere Void; CV – Cuboid Void.

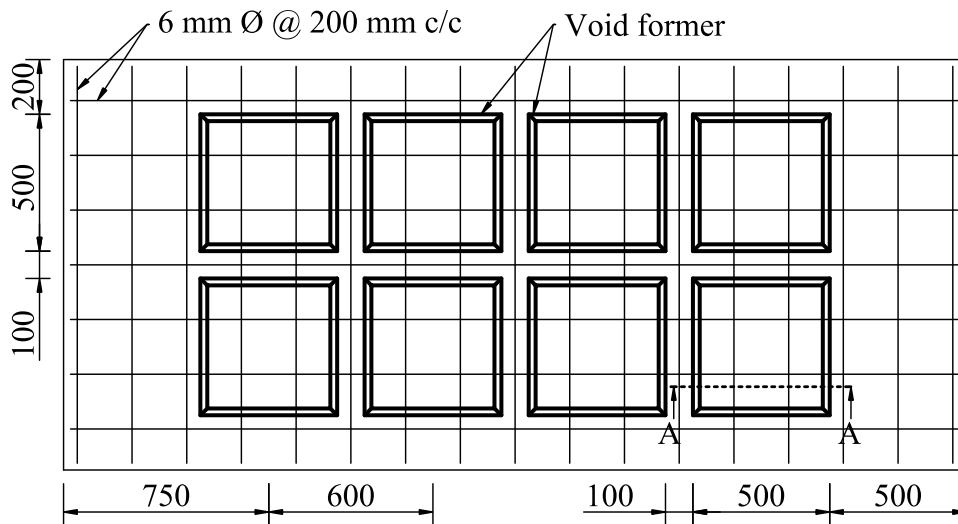


All dimensions are in mm

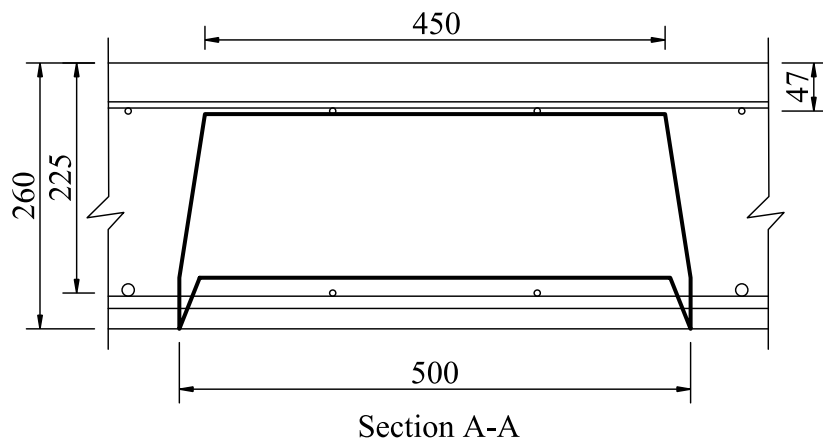
Figure 3.5 – Details of Test Specimen OF-S180V



Plan - Bottom reinforcement

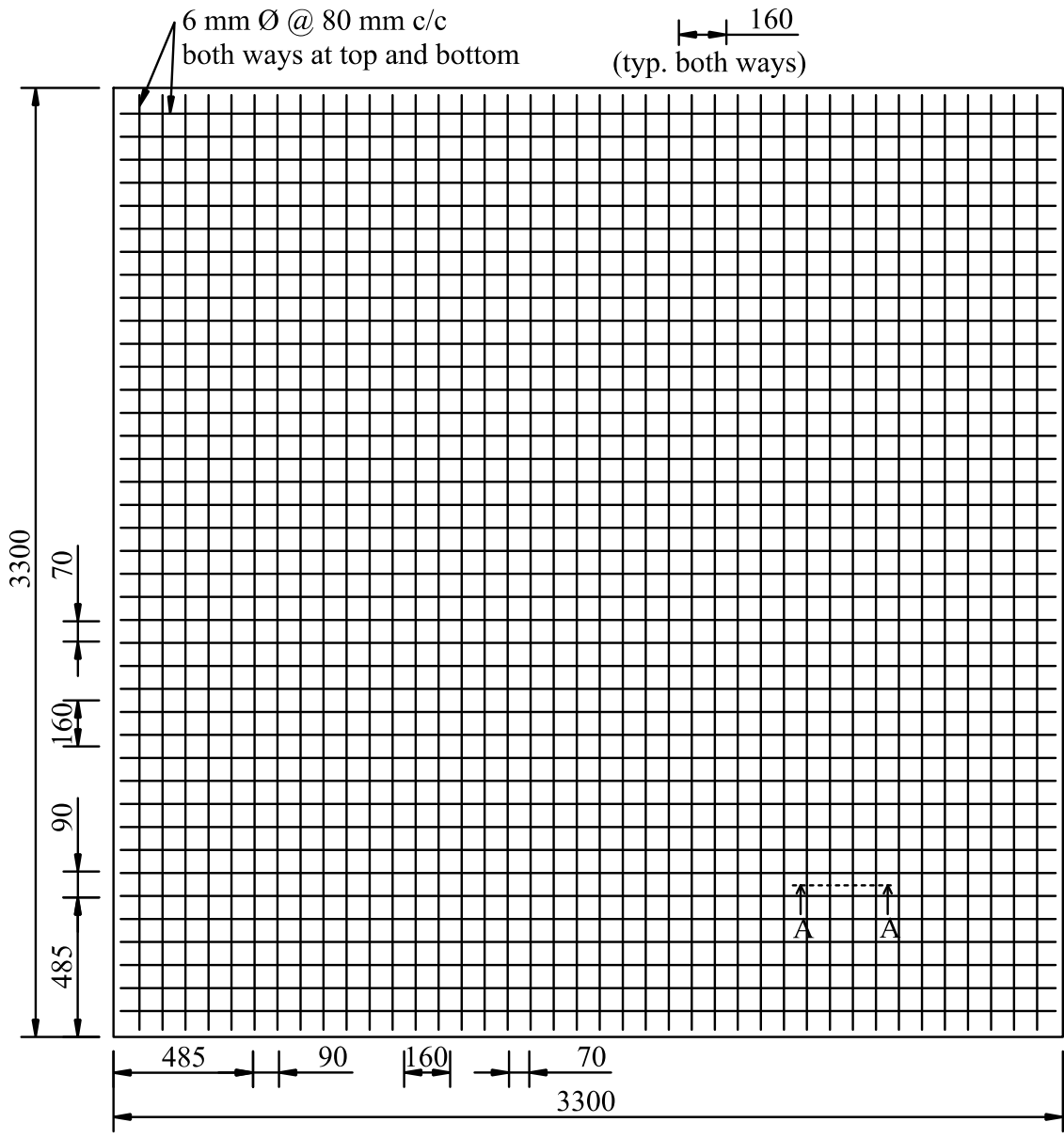


Plan - Top reinforcement

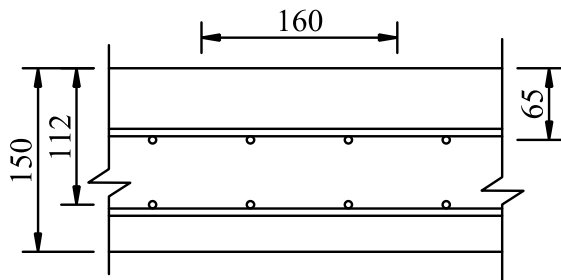


All dimensions are in mm

Figure 3.6 – Details of Test Specimen OF-CV (1 – 3)



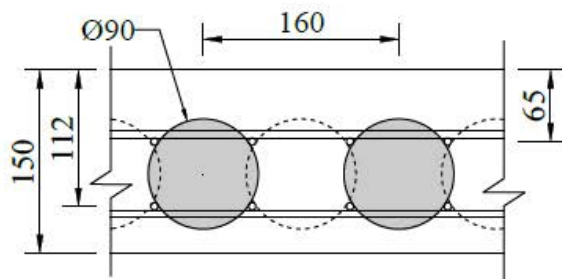
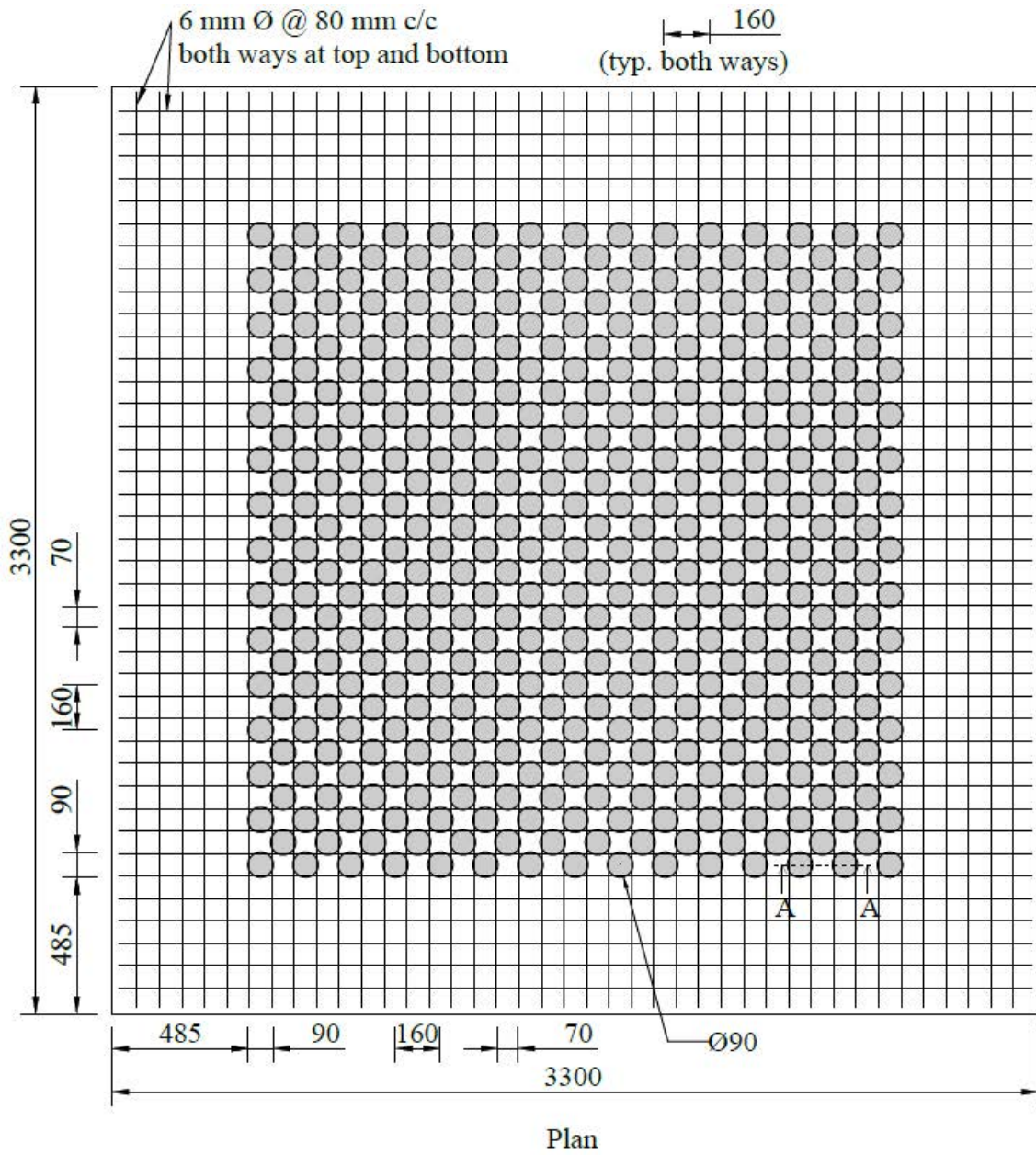
Plan



Section A-A

All dimensions are in mm

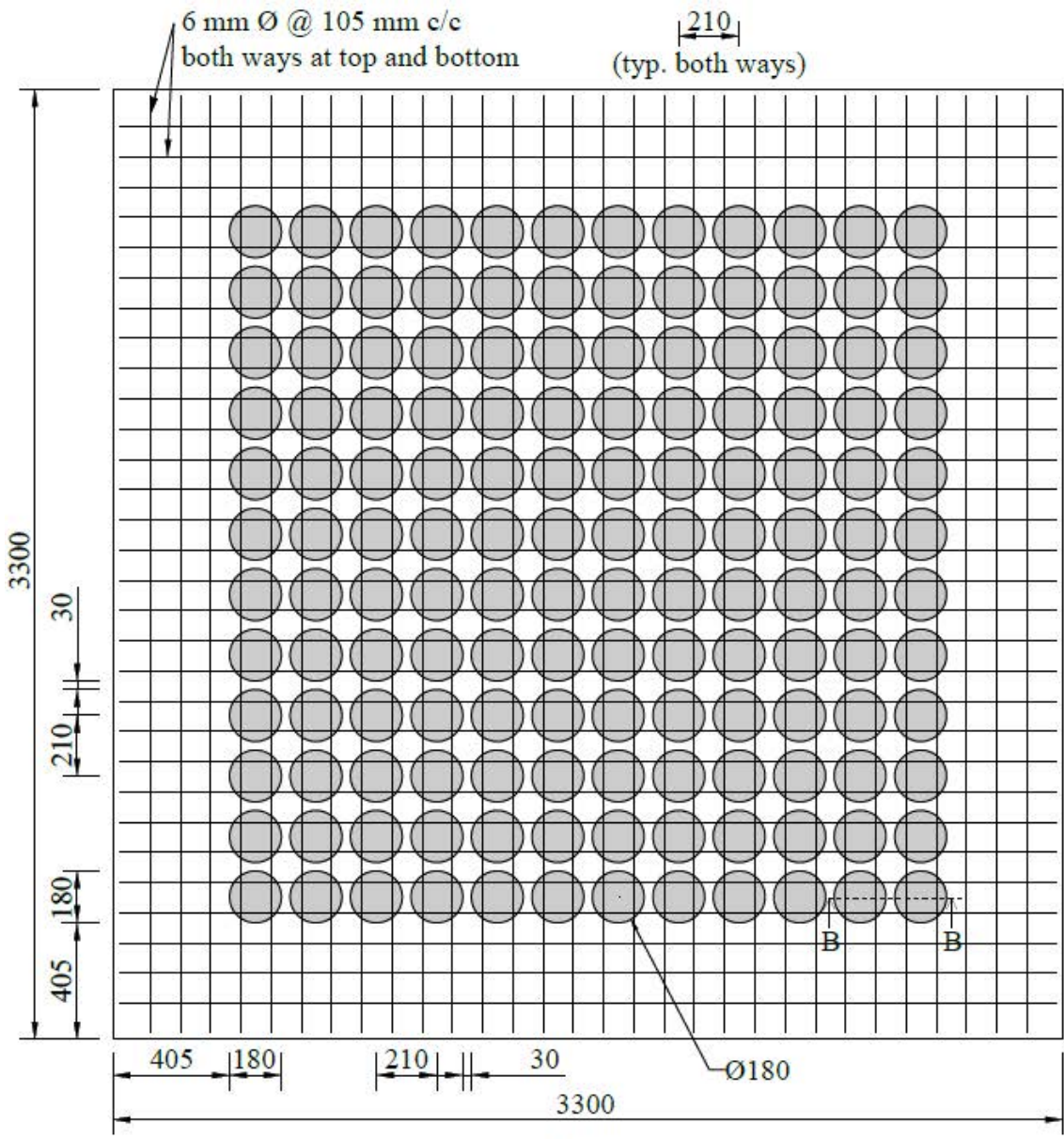
Figure 3.7 – Details of Test Specimen TF-Solid



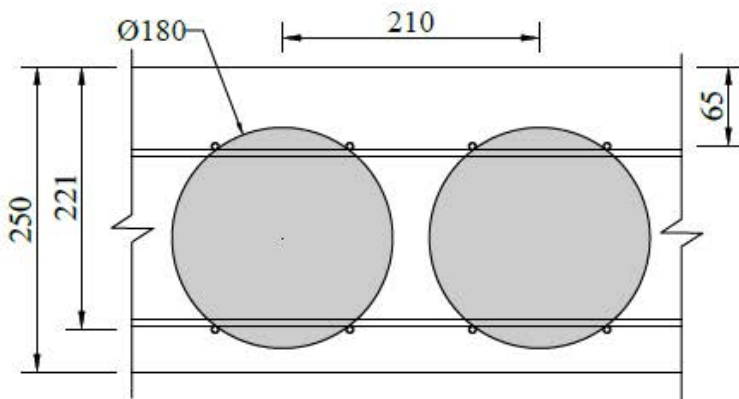
Section A-A

All dimensions are in mm

Figure 3.8 – Details of Test Specimen TF-S90V



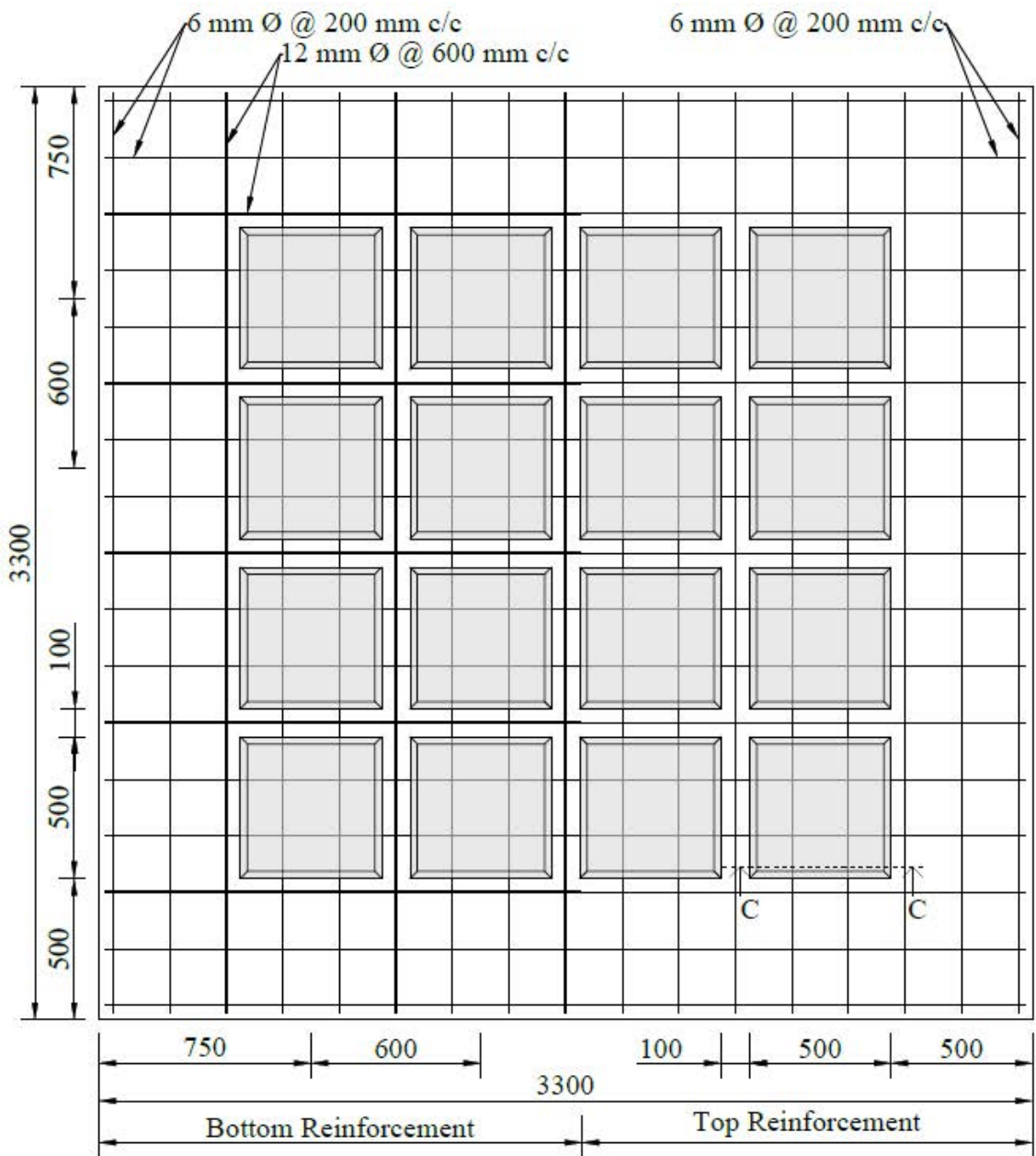
Plan



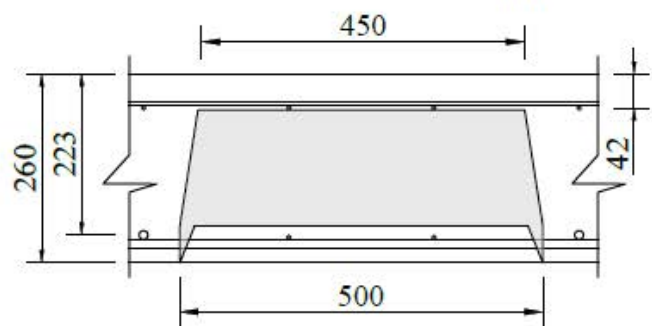
Section B-B

All dimensions are in mm

Figure 3.9 – Details of Test Specimen TF-S180V



Plan



Section C-C

All dimensions are in mm

Figure 3.10 – Details of Test Specimens TF-CV (1 – 3)

### 3.2.2.1 Material Properties

The specimens were cast using concrete, with mix proportion of 1 : 2.25 : 4.5 (cement : fine aggregate : coarse aggregate) with a water-cement ratio of 0.55. Cube specimens were cast with a size of 150 mm and cured under similar exposure condition as that of slab specimens. The compression test on cubes was carried out simultaneously with the flexure test on the companion slab specimen. The observed mean compressive strength for each test specimen is summarised in Table 3.1. The nominal yield strength of the selected reinforcement of size 6 mm and 12 mm diameter was 500 N/mm<sup>2</sup>, conforming to IS 1786 (2008). Tensile tests of reinforcement were conducted as per IS 1608 (Part 1) 2018, and the properties are summarised in Table 3.2. The idealised stress-strain behaviour of the reinforcements is shown in Figure 3.11.

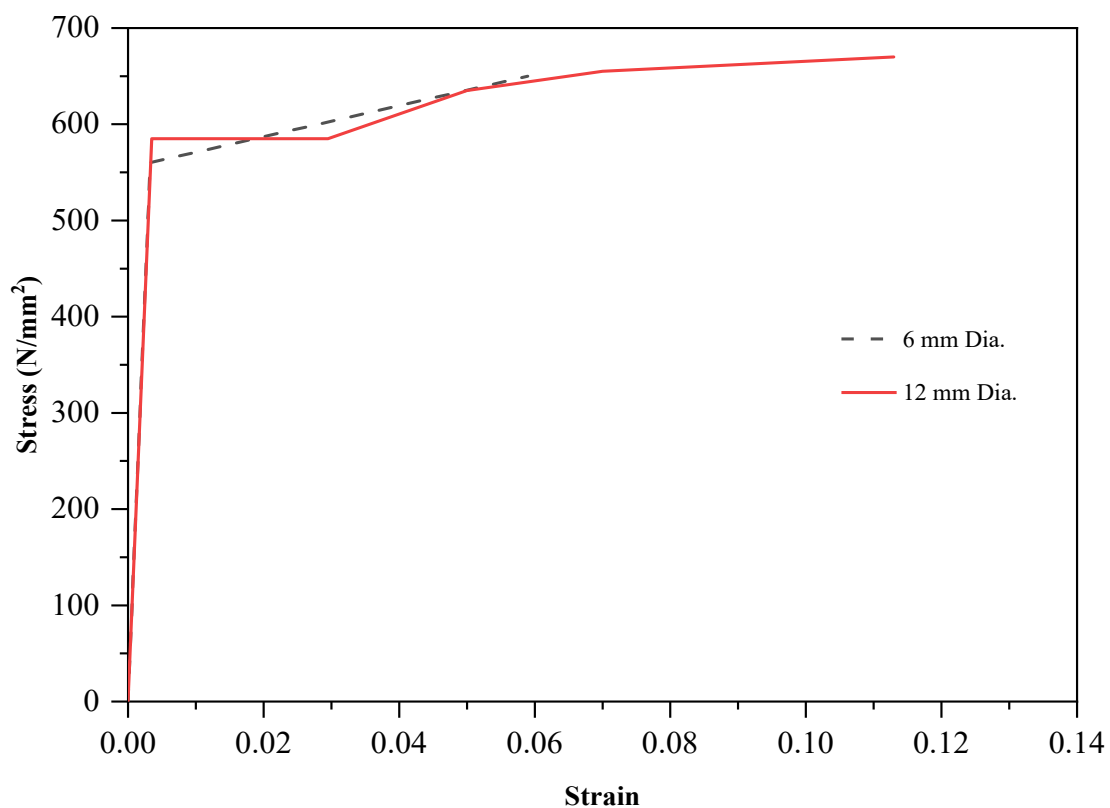


Figure 3.11 – Idealised Stress versus Strain Behaviour of Reinforcements

Table 3.2 – Mechanical Properties of Reinforcement

Reinforcement diameter (mm)	Strength (N/mm <sup>2</sup> )			Strain (%)	
	Nominal	Yield	Ultimate	Yield	Ultimate
6	500	560	650	0.33	5.91
12	500	585	670	0.35	10.84



### 3.2.2.2 Fabrication of Steel Mould

Specimens were cast by using steel mould made of channel sections as side shuttering and plywood sheets as a base. Figure 3.12 shows photographs of various stages of the fabrication of steel mould.



Figure 3.12 – Fabrication of Steel Mould in Progress

### 3.2.2.3 Casting of Specimens

Reinforcement gauge was prepared as per the details summarised Table 3.1 and Figure 3.5 – Figure 3.10. Various stages of specimens casting are shown in Figure 3.13 – Figure 3.19.



Figure 3.13 – Typical Reinforcement Mesh

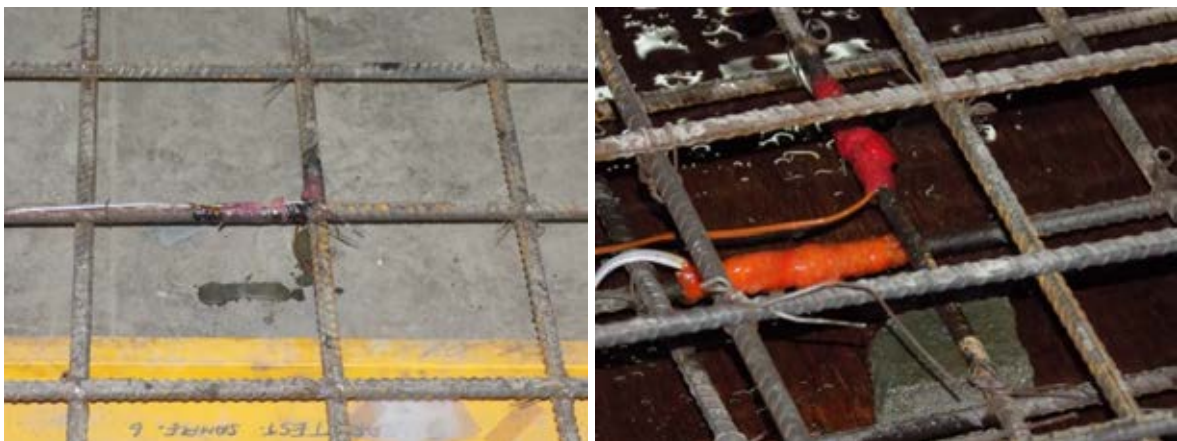


Figure 3.14 – Strain Gauges Fixed on Reinforcements



Figure 3.15 – One-way Flexural Test Specimens OF-S180V and OF-CV



Figure 3.16 – Two-way Flexural Test Specimen TF-Solid



Figure 3.17 – Two-way Flexural Test Specimen TF-S90V



Figure 3.18 – Two-way Flexural Test Specimen TF-CV



Figure 3.19 – Concreting in Progress

### 3.2.3 Test Set-up and Instrumentation

#### 3.2.3.1 One-way Flexure

##### (i) Test Set-up

Four-point bending test was conducted to study one-way flexural behaviour of the voided slab. Figure 3.20 shows the schematic test set-up. Load (line load) was applied through steel plate of size 1500 mm × 80 mm × 16 mm as patch load to avoid localised pre-mature shear failure (Figure 3.21a). Two 500 kN capacity pseudo-dynamic hydraulic actuators were used to apply the load. The slab specimens were supported by a hinge at one end and roller at the other end at their edges, which is located 150 mm from specimen edges along short span directions by a line-type reaction hinge of length 1500 mm.

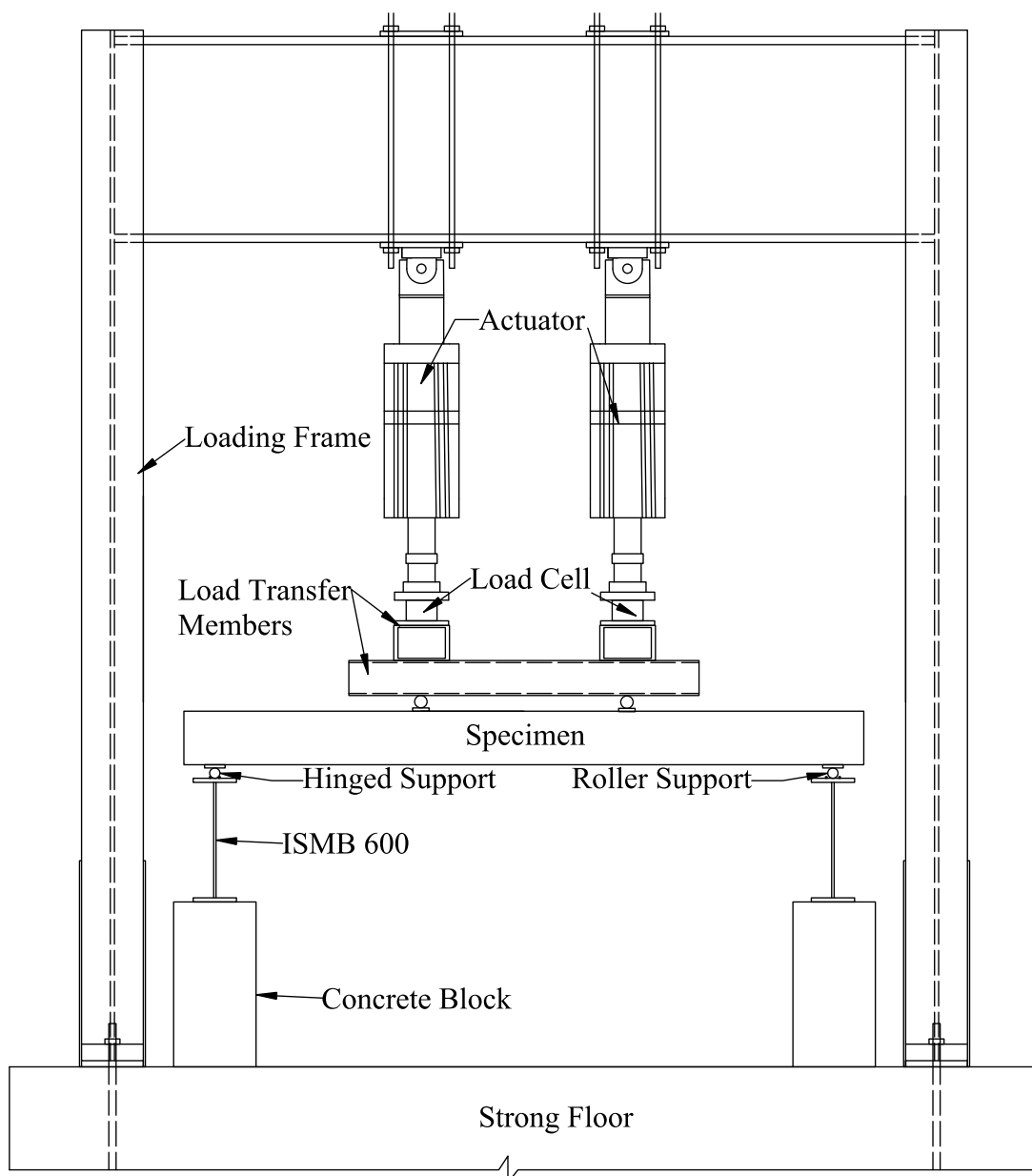
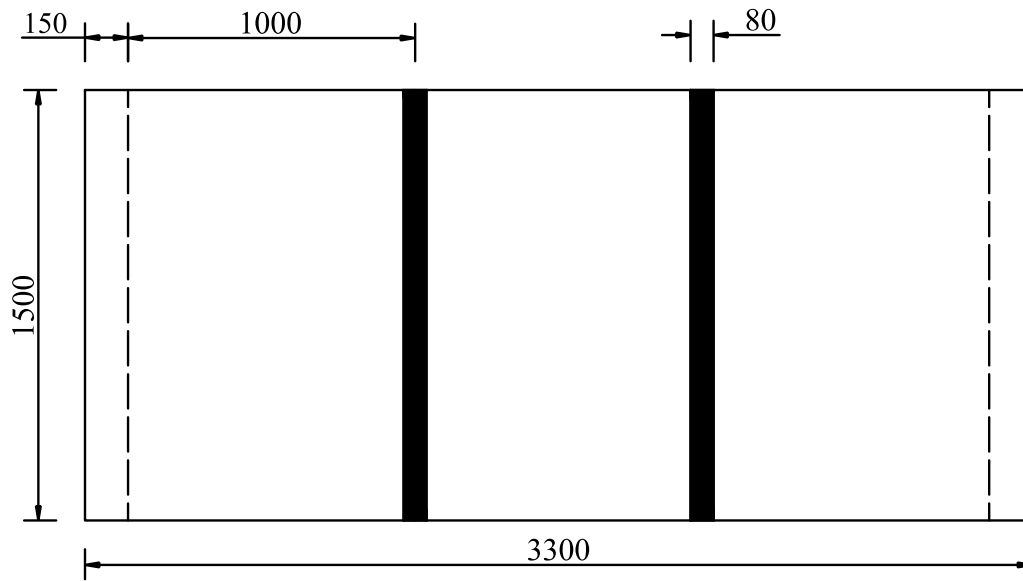
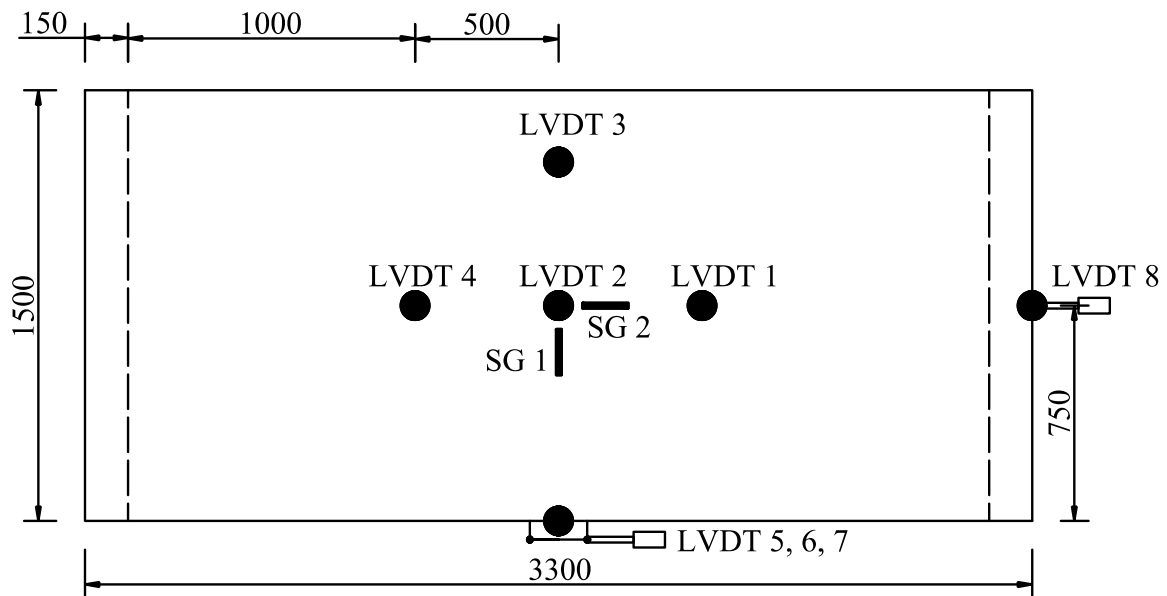


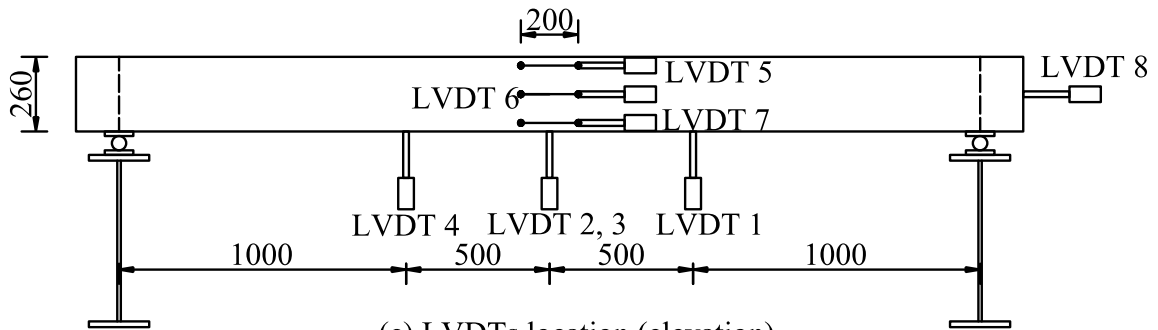
Figure 3.20 – Schematic Test Set-up (Four-point Bending)



(a) Load position



(b) LVDTs and strain gauge location (plan)



(c) LVDTs location (elevation)

All dimensions are in mm

Figure 3.21 – Instrumentation of Test Specimen (Four-point Bending)

## **(ii) Instrumentation**

Applied loads, deflections, and strain in reinforcements & concrete surface were measured through appropriate instruments. Load-cells with a capacity of 1000 kN were used to measure the applied loads. Four linear variable differential transformers (LVDTs) with a measurement range of  $\pm 100$  mm were used to measure the deflections at mid-span and under the point of application of loads. The concrete surface strain along the depth of slab were measured at the front face of the slab in elevation using three LVDTs with a measurement range of  $\pm 20$  mm. Figure 3.21(b) and (c) show the schematic arrangement of LVDTs. Strain in the bottom reinforcements located at the centre of slab specimens was measured by strain gauges with 10 mm gauge length. Strain gauges were provided in the longitudinal and transverse direction of bottom reinforcements, as shown Figure 3.21(b). A data acquisition system was used to obtain real-time experimental data which has the facility to record the load, deflection, and strain simultaneously.

## **(iii) Testing Procedure**

Displacement controlled monotonic tests were performed with two pseudo-dynamic hydraulic actuators. Equal load distribution across each actuator was ensured by synchronising the actuators and operating with a single master control system. The rate of loading was 0.05 mm/sec. To ensure the safety of measuring and loading devices, the tests were terminated immediately after hearing the fractured sound of bottom reinforcements.

### **3.2.3.2 Two-way Flexure: Phase I (Load up to 1000 kN)**

In Phase I of the two-way flexural test, sphere voided slab specimens (TF-S90V and TF-S180V) along with reference solid slab specimen (TF-Solid) were tested.

#### **(i) Test Set-up**

A sixteen-point load test was conducted to study the two-way flexural behaviour of the slab. Figure 3.22 shows the schematic test set-up. To avoid localised pre-mature punching shear failure, the point load was applied through steel plate of size 170 mm  $\times$  170 mm  $\times$  12 mm as patch load as shown in Figure 3.23. A pseudo-dynamic hydraulic actuator of 1000 kN capacity was used to apply the load. The load was transferred through hot rolled steel sections to the slab specimens. The steel sections were supported on the rollers at its ends to enable free rotation along with specimen deformation. Discontinuity of supports at corners minimises the

experimental errors such as stress concentration and generation of fixed end moment etc. (Chung et al., 2018b). This is achieved by employing a line-type reaction hinge of length 2800 mm as support on each of the four sides of the slab. The support was located at a distance of 150 mm from specimen edges.

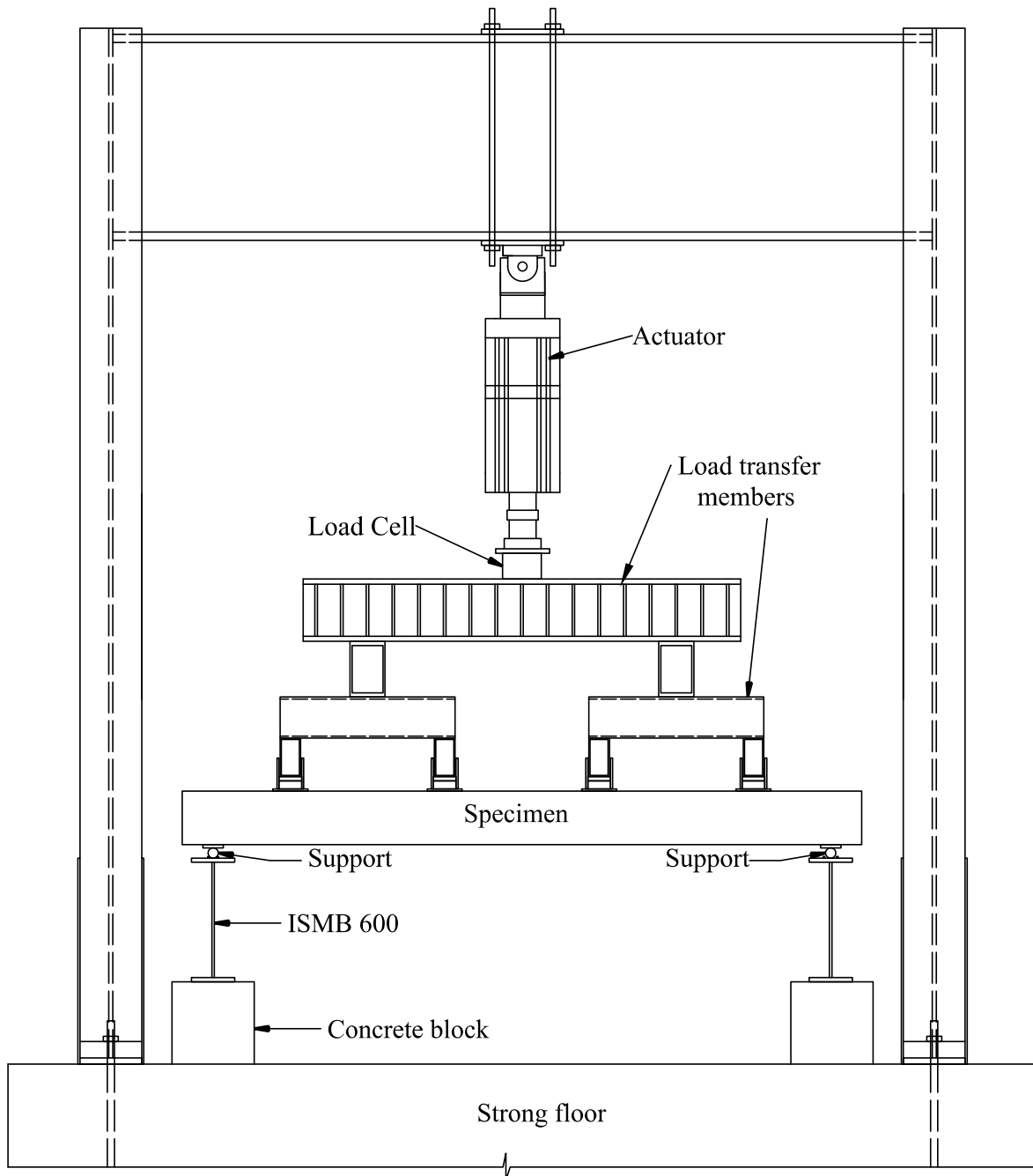
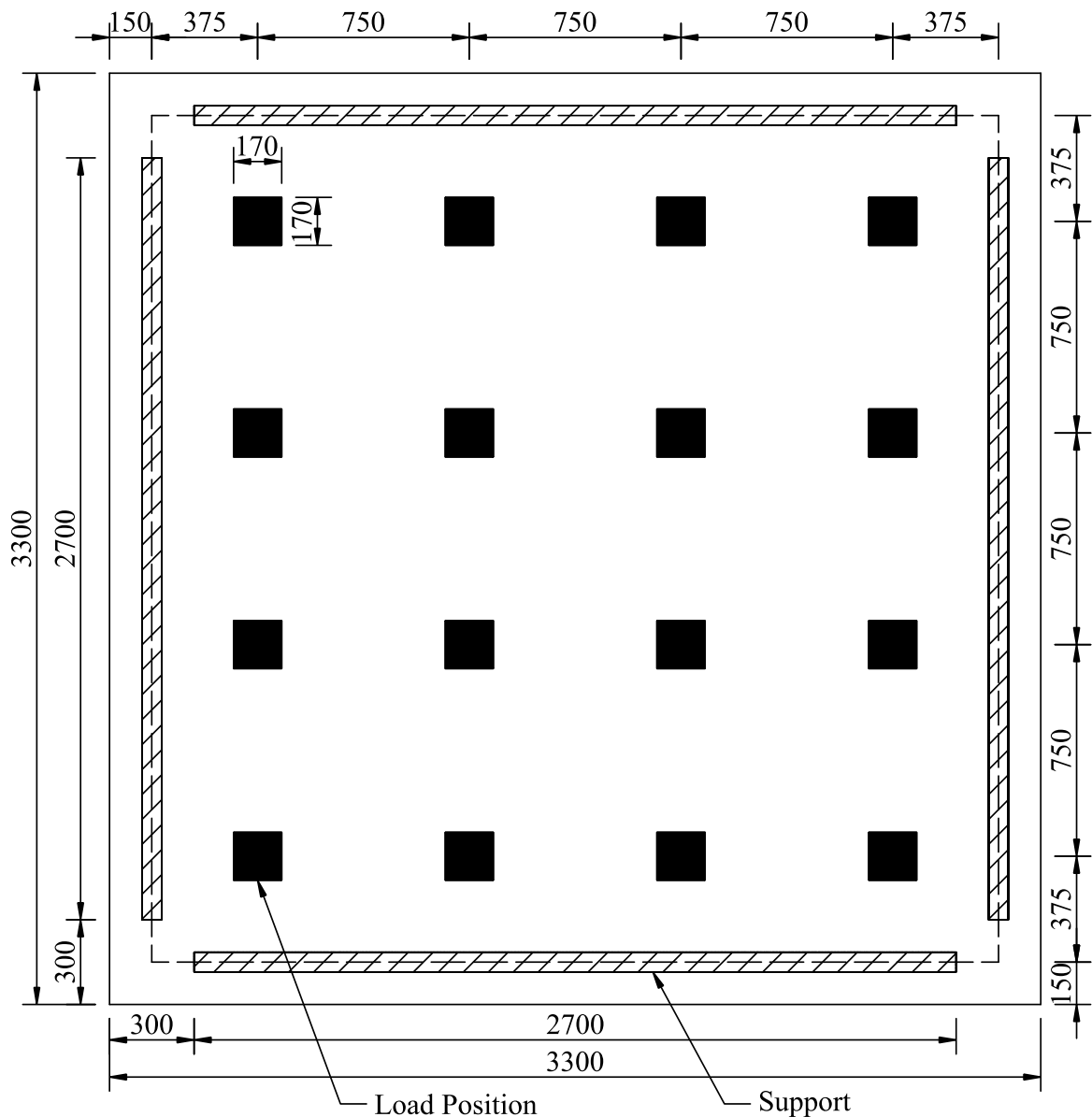


Figure 3.22 – Schematic Test Set-up (Sixteen-point Bending) – Phase I: Load up to 1000 kN





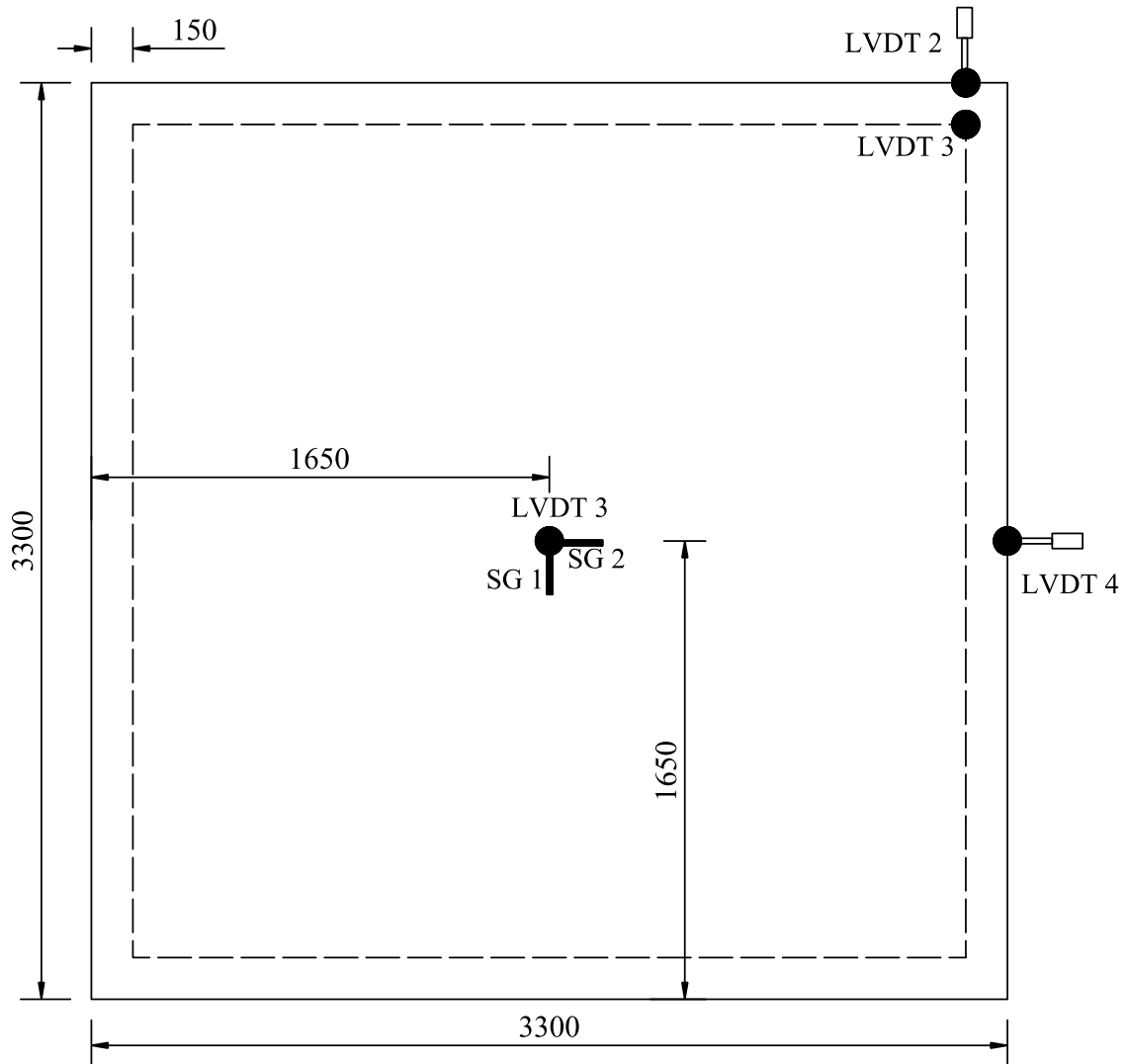
All dimensions are in mm

Figure 3.23 – Position of Sixteen-point (Patch) Load

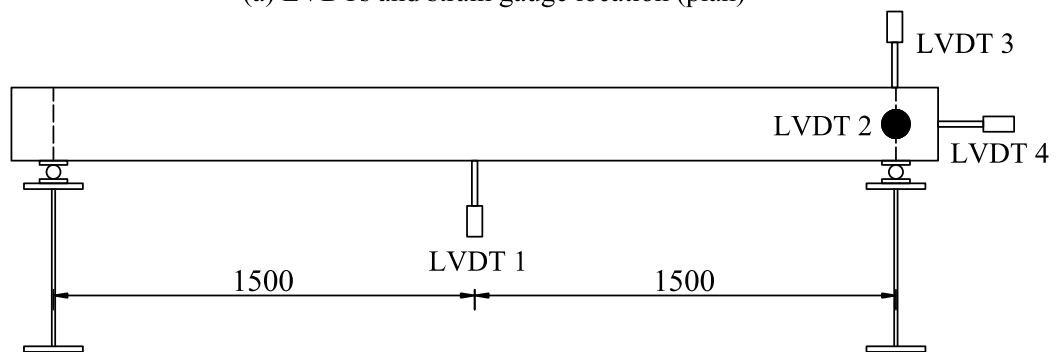
**(ii) Instrumentation**

Applied loads, deflections, and strain in reinforcements were measured through appropriate instruments. Load-cells with a capacity of 1000 kN were used to measure the applied load. One LVDT with a measurement range of  $\pm 100$  mm were used to measure the deflections at mid-span. The corner uplift, translations in lateral and longitudinal directions were measured using three LVDTs with a measurement range of  $\pm 20$  mm. Figure 3.24 shows the schematic arrangement of LVDTs. Strain in the bottom reinforcements located at the centre of slab specimens was measured by strain gauges with 10 mm gauge length. Strain gauges were

provided in the longitudinal and transverse direction of bottom reinforcements, as shown Figure 3.24. A data acquisition system was used to obtain real-time experimental data which has the facility to record the load, deflection, and strain simultaneously.



(a) LVDTs and strain gauge location (plan)



(b) LVDTs location (elevation)

All dimensions are in mm

Figure 3.24 – Instrumentation of Test Specimen (Sixteen-point Bending) – Phase I

### (iii) Testing Procedure

Displacement controlled monotonic tests were performed with a 1000 kN capacity pseudo-dynamic hydraulic actuator. The rate of loading was 0.05 mm/sec. In order to ensure the safety of measuring and loading devices, the tests were terminated when the load reached the actuator capacity. Beyond which the test was continued up to failure by load control using hydraulic jacks and the details of the same is explained (below) in section 3.2.3.3.

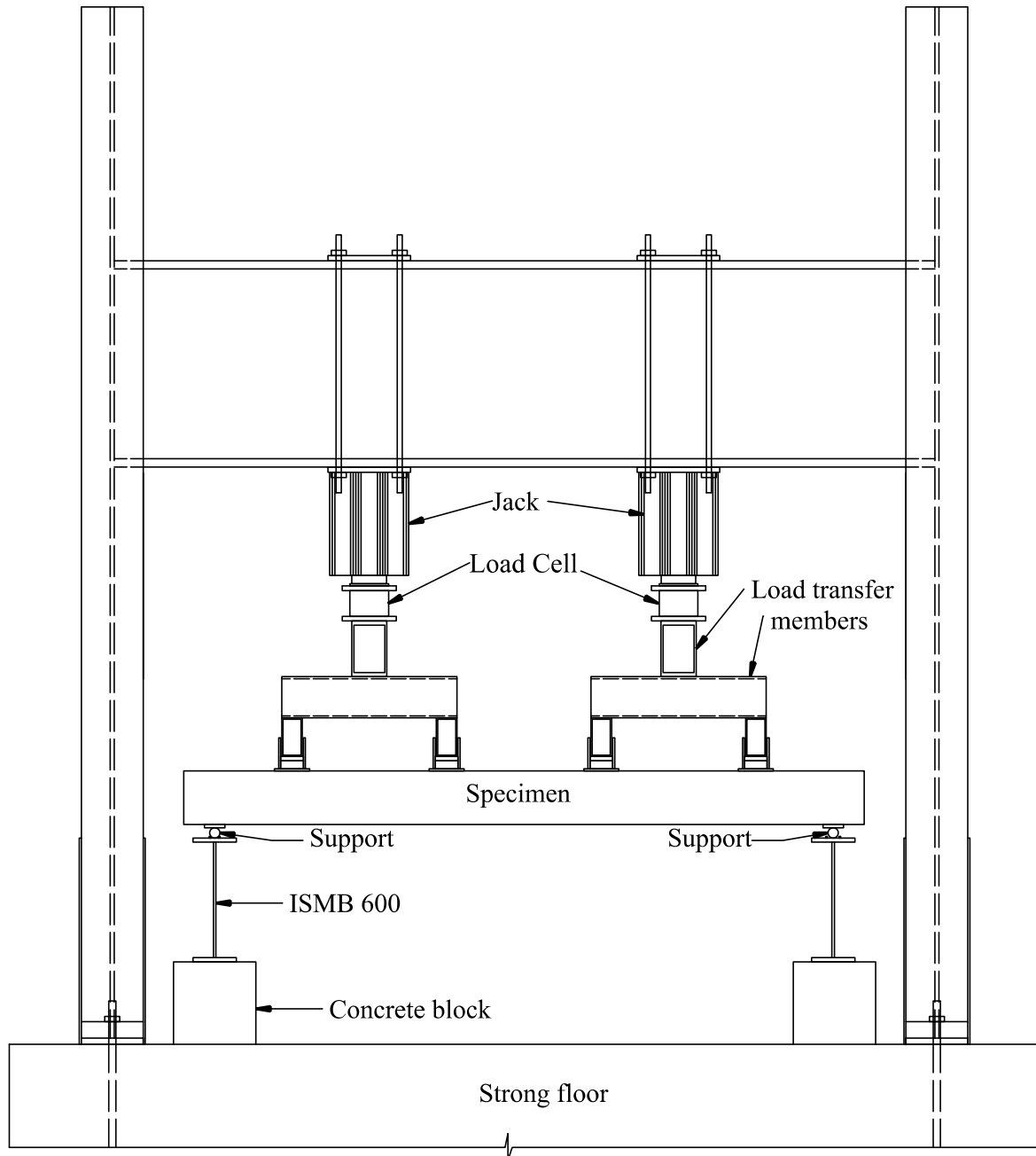


Figure 3.25 – Schematic Test Set-up (Sixteen-point Bending) – Phase I: Load up to Ultimate

### **3.2.3.3 Two-way Flexure: Phase I (Load up to Ultimate Failure)**

The test set-up remains the same as explained earlier (in section 3.2.3.2) except the loading device. Two 1500 kN capacity hydraulic jacks were used to apply the load. Figure 3.25 shows the schematic test set-up. Load-cells with a capacity of 1000 kN were used to measure the applied load. One LVDT with a measurement range of  $\pm 100$  mm were used to measure the deflections at mid-span. Load controlled monotonic test was performed with a pair of hydraulic jacks. The jacks were synchronised and operated using a single master control system to ensure equal load distribution across each jack. The test was terminated immediately after observing a significant drop in applied load; it ensures the safety of measuring and loading devices and avoids any permanent damage to load transfer members.

### **3.2.3.4 Two-way Flexure: Phase II**

In Phase II of the two-way flexural test, cuboid voided slab specimens (TF-CV-1, TF-CV-2, and TF-CV-3) were tested.

#### **(i) Test Set-up**

The test set-up remains the same as explained earlier (in section 3.2.3.2) except the loading device. Two 500 kN capacity pseudo-dynamic hydraulic actuator were used to apply the load. Figure 3.26 shows the schematic test set-up.

#### **(ii) Instrumentation**

Applied loads, deflections, and strain in reinforcements were measured through appropriate instruments. In-built load-cells of actuators were used to measure the applied load. One LVDT with a measurement range of  $\pm 100$  mm were used to measure the deflections at mid-span. Four LVDTs with a measurement range of  $\pm 100$  mm were used to measure the deflections at one-fourth span of the slab. The corner uplift, translations in lateral and longitudinal directions were measured using three LVDTs with a measurement range of  $\pm 20$  mm. Figure 3.27 shows the schematic arrangement of LVDTs. Strain in the bottom reinforcements located at the centre of slab specimens was measured by strain gauges with 10 mm gauge length. Strain gauges were provided in the longitudinal and transverse direction of bottom reinforcements, as shown in Figure 3.27. A data acquisition system was used to obtain real-time experimental data which has the facility to record the load, deflection, and strain simultaneously.

### (iii) Testing Procedure

Displacement controlled monotonic tests were performed with two pseudo-dynamic hydraulic actuators. Equal load distribution across each actuator was ensured by synchronising the actuators and operating with a single master control system. The rate of loading was 0.05 mm/sec. In order to ensure the safety of measuring and loading devices, the tests were terminated when the load reached the actuator capacity.

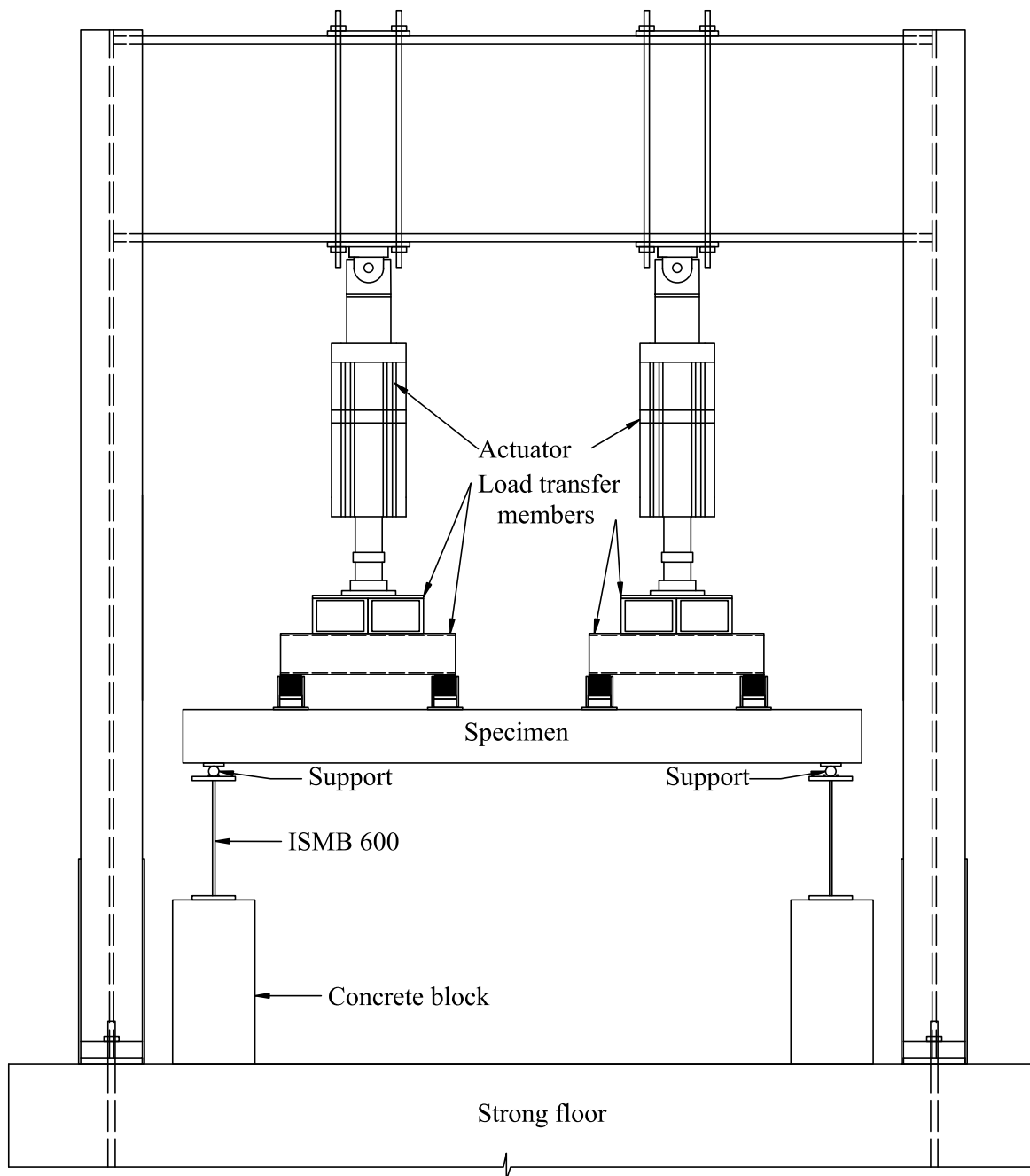
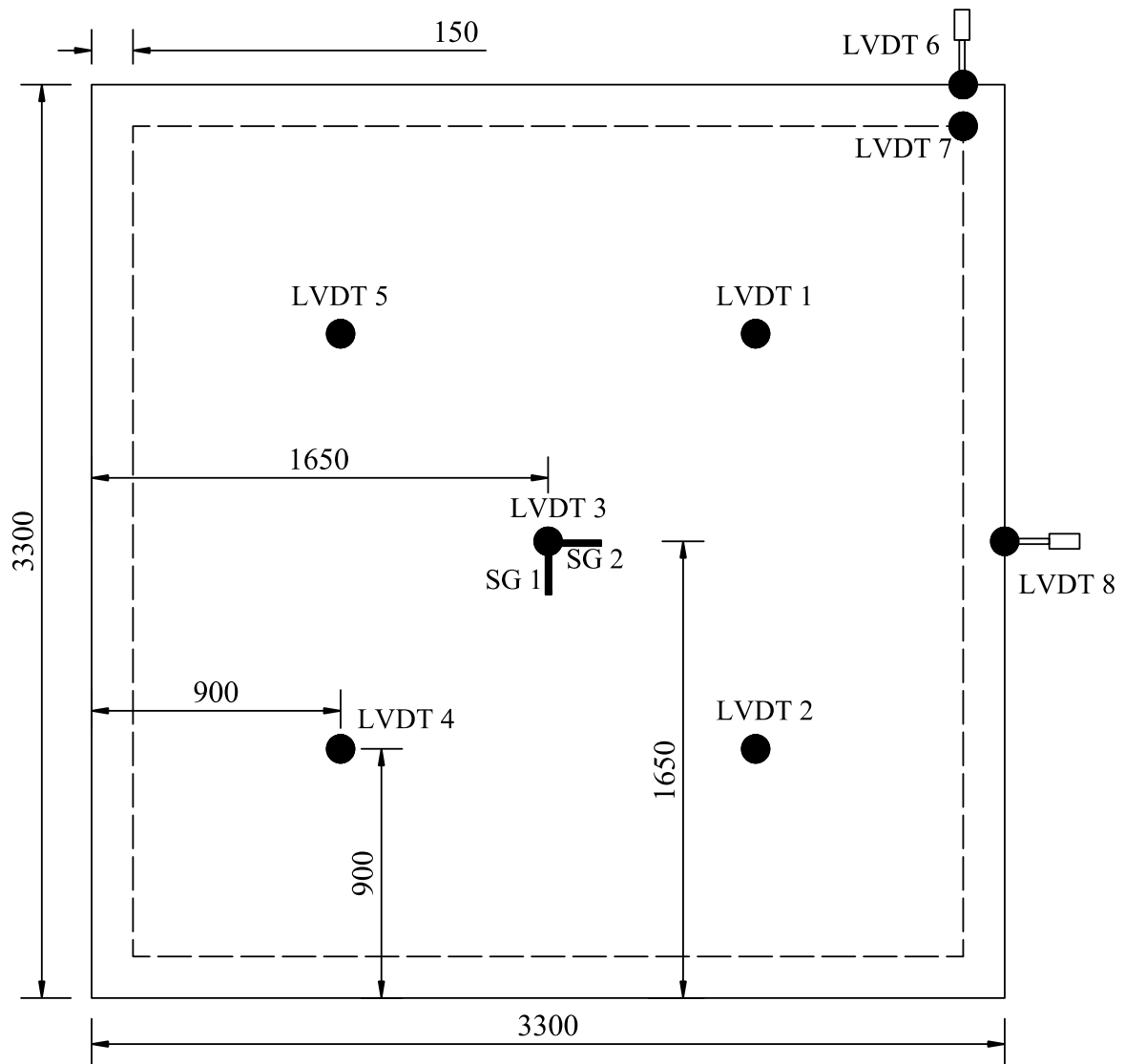
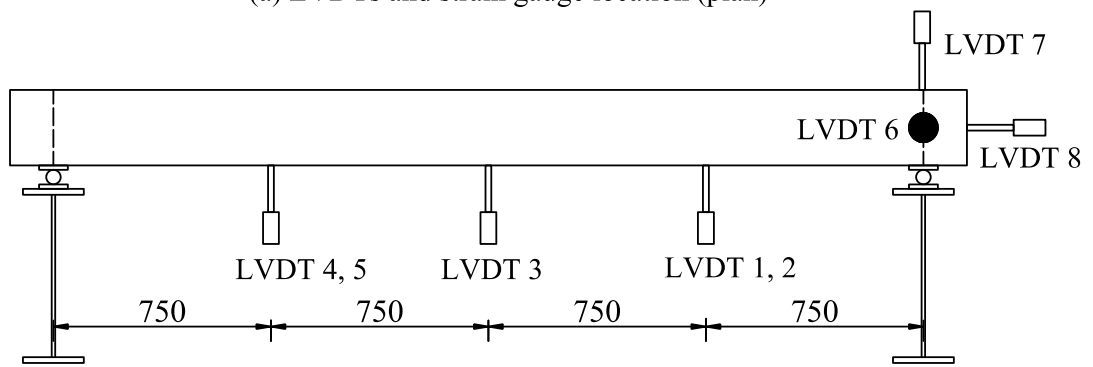


Figure 3.26 – Schematic Test Set-up (Sixteen-point Bending) – Phase II



(a) LVDTs and strain gauge location (plan)



(b) LVDTs location (elevation)

All dimensions are in mm

Figure 3.27 – Instrumentation of Test Specimen (Sixteen-point Bending) – Phase II

### 3.2.4 Fabrication of Loading and Support Frame

The loading and support frames were fabricated as per the requirement of various tests. Figure 3.28 shows the fabricated loading frame components ('A' frames and box girder) and support frame. Epoxy-based anti-corrosive paint was applied on these frames. The safe load carrying capacity of the loading frame is 1000 kN. The support frame is fabricated such that any plan size of specimens ranging from 1 m × 1 m to 5 m × 5 m can be tested. The support frame is reconfigurable to test rectangular specimens as well.



(a) Loading Frame Components – 'A' Frames and Box Girder



(b) Support Frame with Plan Dimension of 5 m × 5 m

Figure 3.28 – Loading and Support Frame

### 3.2.4.1 Erected Test Set-up

Typical erected test set-up for each test is shown in Figure 3.29 – Figure 3.32.



Figure 3.29 – Ono-way Flexural Test Set-up





Figure 3.30 – Two-way Flexural Test Set-up: Phase I (Load up to 1000 kN)



Figure 3.31 – Two-way Flexural Test Set-up: Phase I (Load up to Ultimate)



Figure 3.32 – Two-way Flexural Test Set-up: Phase II

### 3.2.6 Results and Discussion

#### 3.2.6.1 One-way Flexure

##### (i) Load Deflection Behaviour

All biaxial voided slabs showed typical flexural behaviour under one-way bending. Initially, all specimens remained elastic until cracking followed by inelastic actions such as yielding of bottom reinforcement and ultimate failure due to crushing of concrete at the top of the slab. Overall load versus deflection of all specimens showed ductile behaviour (Figure 3.33 – Figure 3.36). The load versus mid-span deflection behaviour for sphere and cuboid voided slab specimens are shown in Figure 3.37 and Figure 3.38, respectively. The critical stages (cracking, yielding and ultimate) are marked in Figure 3.37 and Figure 3.38 for easy understanding.

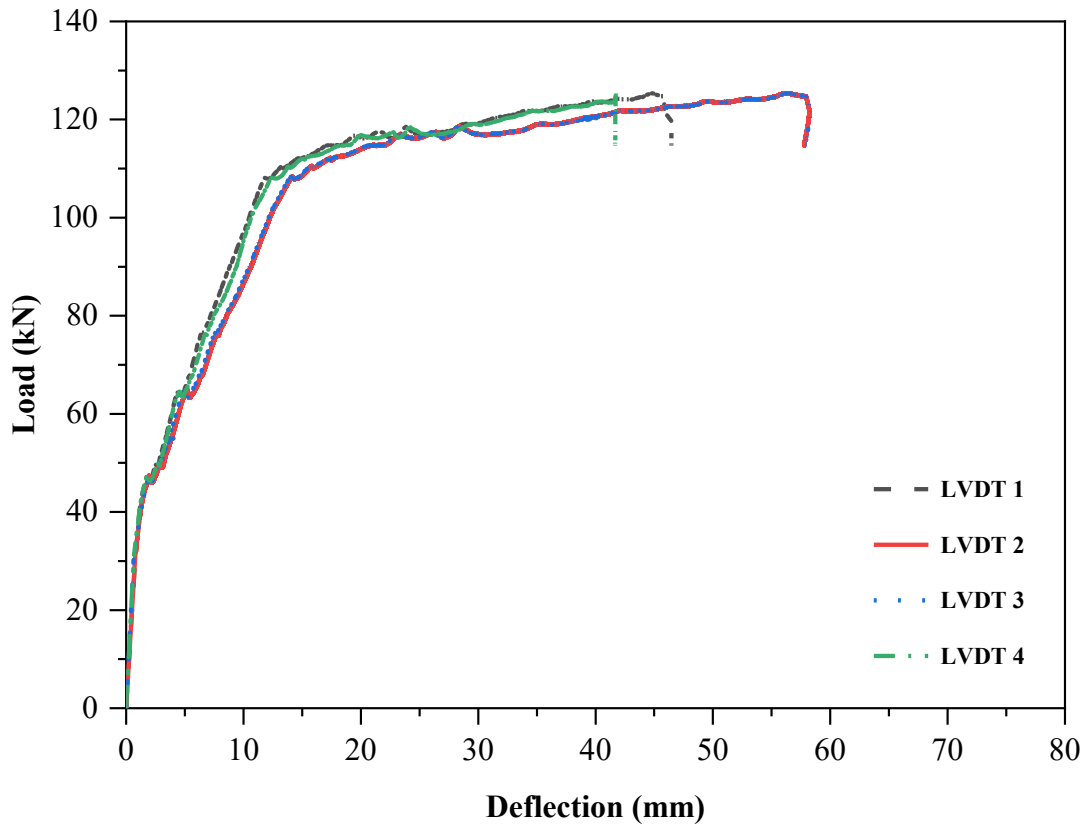


Figure 3.33 – Load versus Deflection Behaviour of Specimen OF-S180V

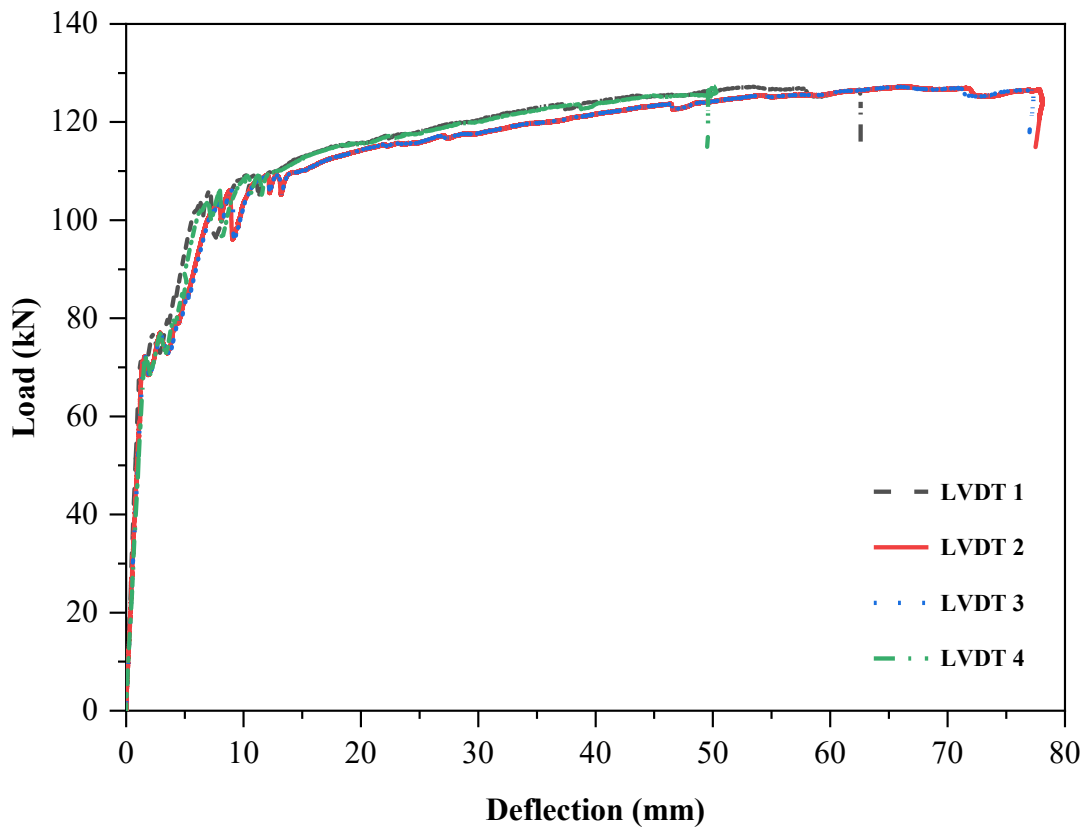


Figure 3.34 – Load versus Deflection Behaviour of Specimen OF-CV-1

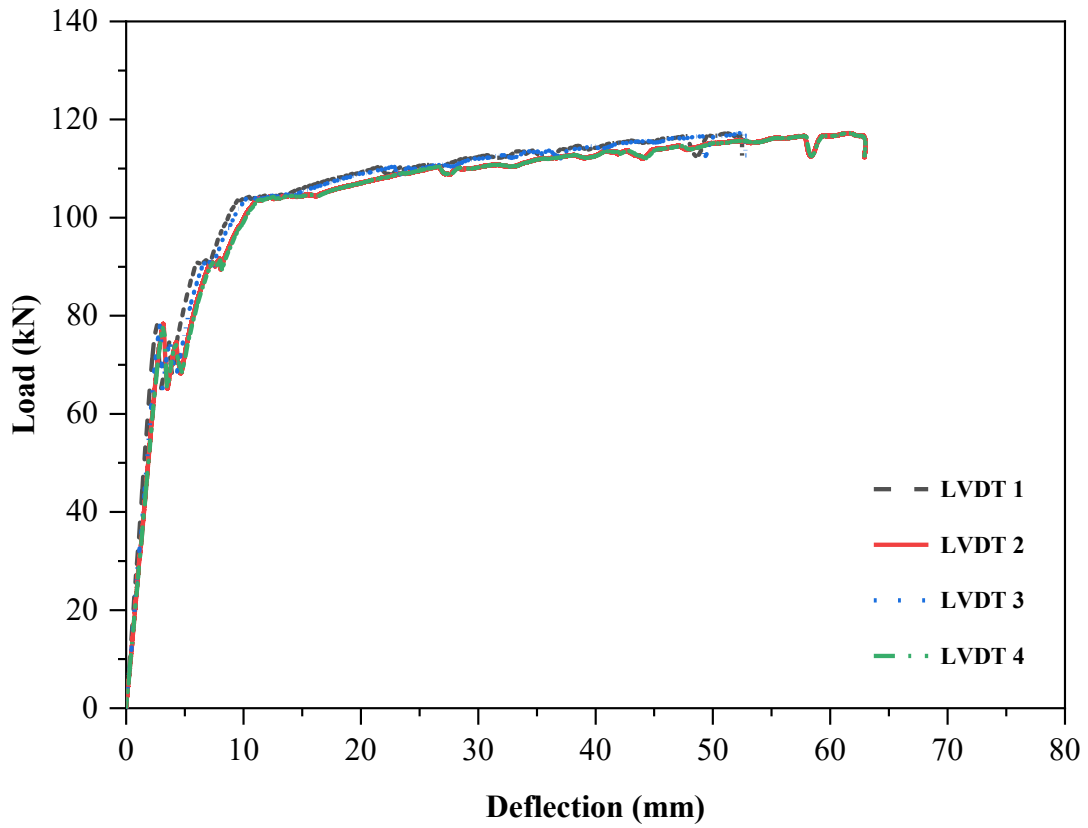


Figure 3.35 – Load versus Deflection Behaviour of Specimen OF-CV-2

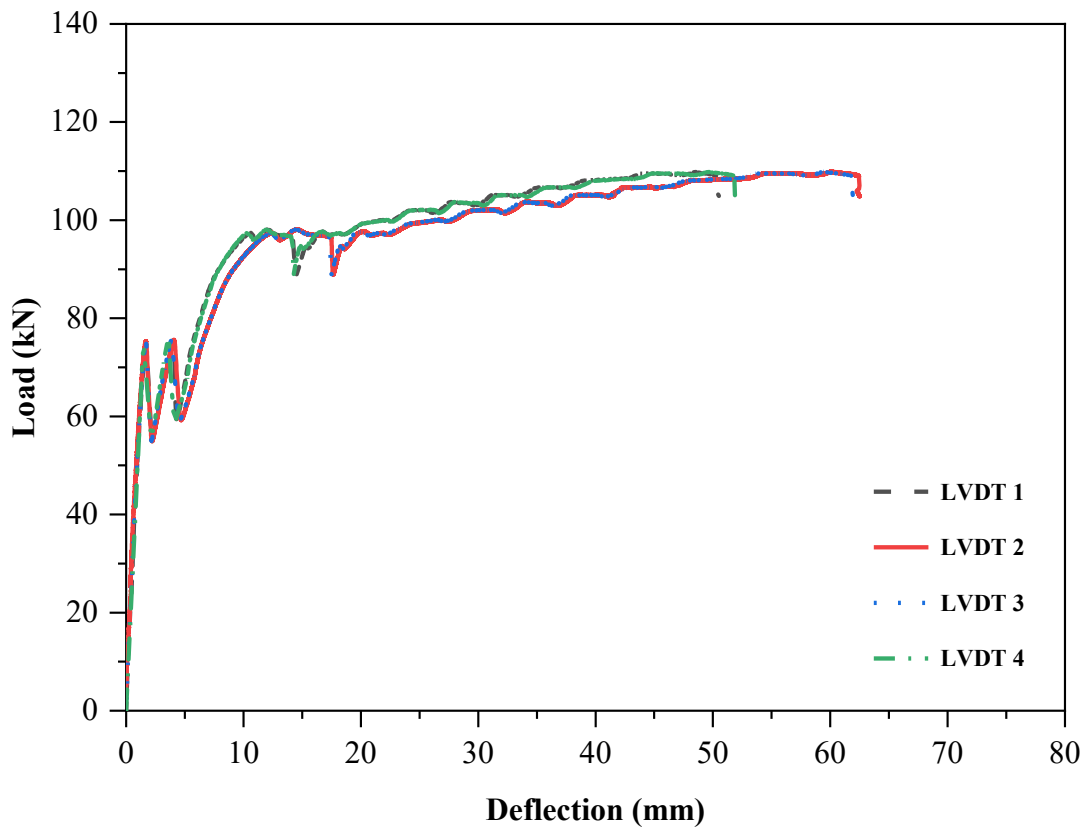


Figure 3.36 – Load versus Deflection Behaviour of Specimen OF-CV-3

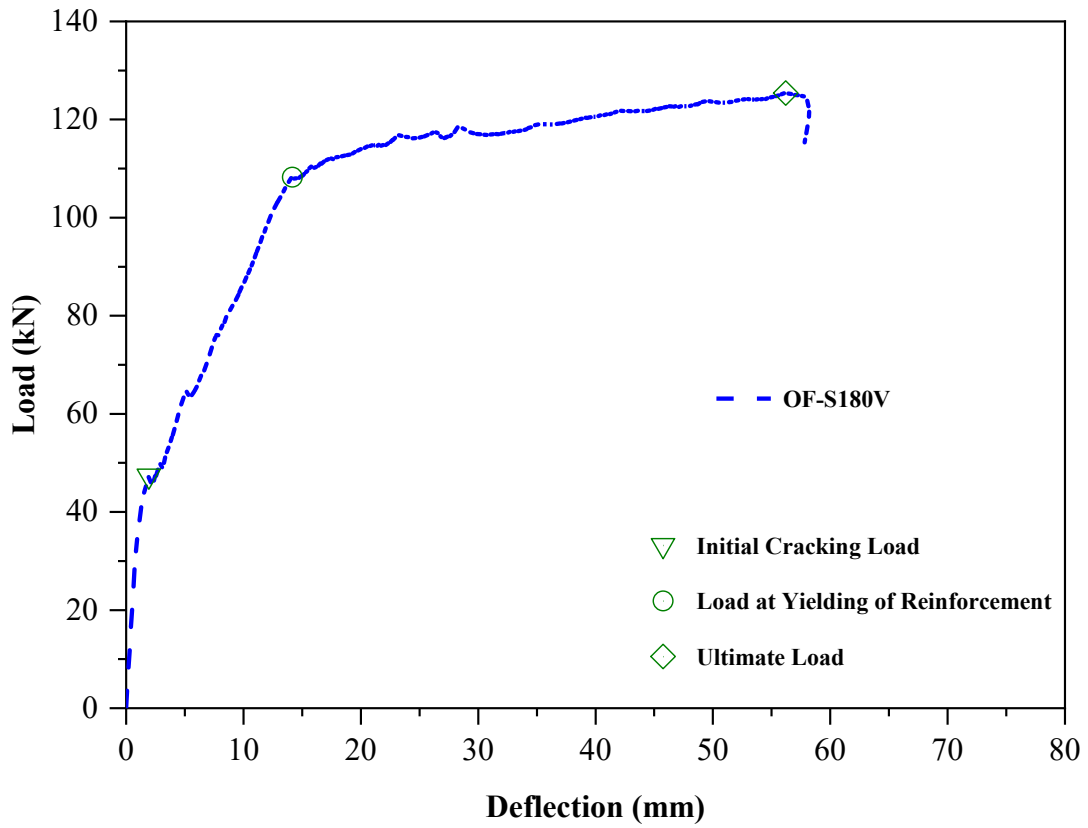


Figure 3.37 – Load versus Mid-span Deflection of Sphere Voided Specimen

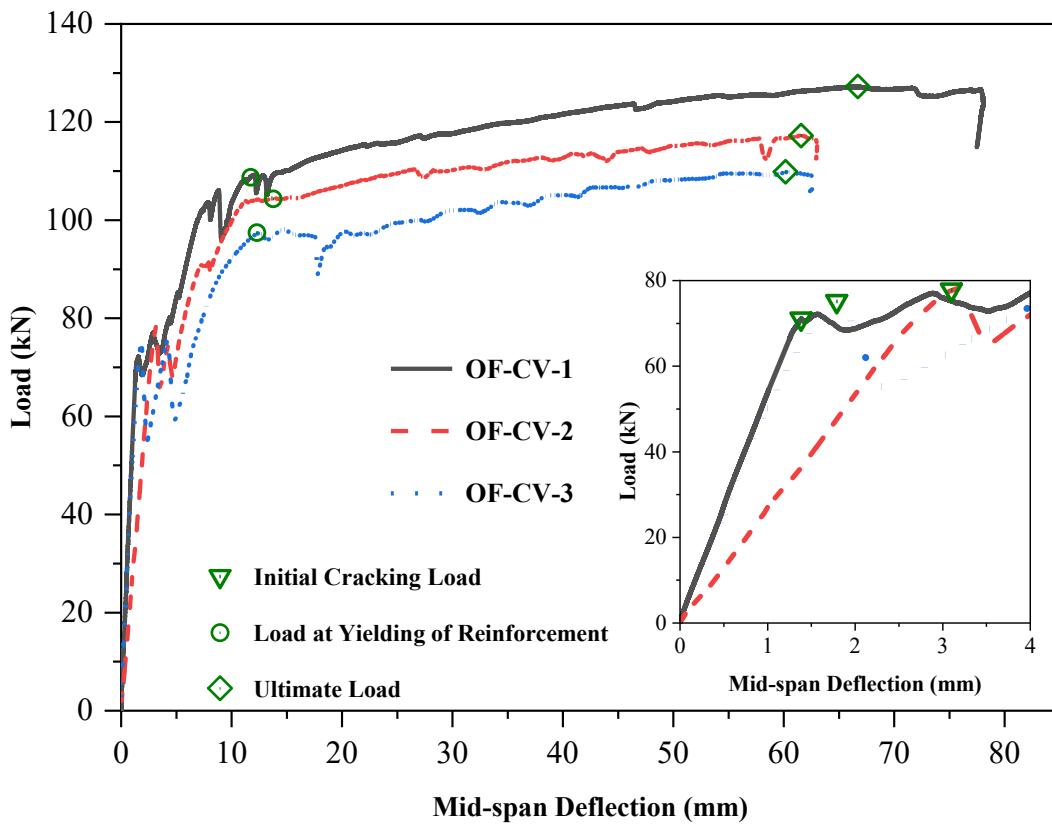


Figure 3.38 – Load versus Mid-span Deflection of Cuboid Voided Specimens

**(ii) Crack Pattern**

Figure 3.39 – Figure 3.42 shows the observed crack pattern on the front elevation and bottom surfaces of slab specimens (actual and digitised). In general, the cracks were formed between loading positions (lines emanating in the transverse direction) along the width of the slab.

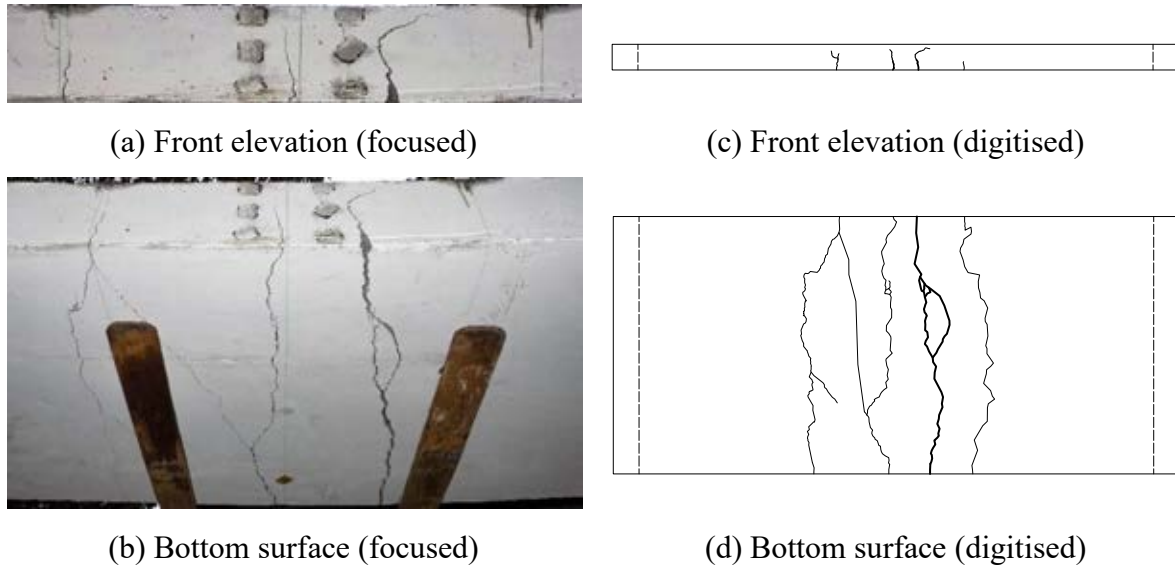


Figure 3.39 – Observed Crack Pattern of Slab Specimen OF-S180V

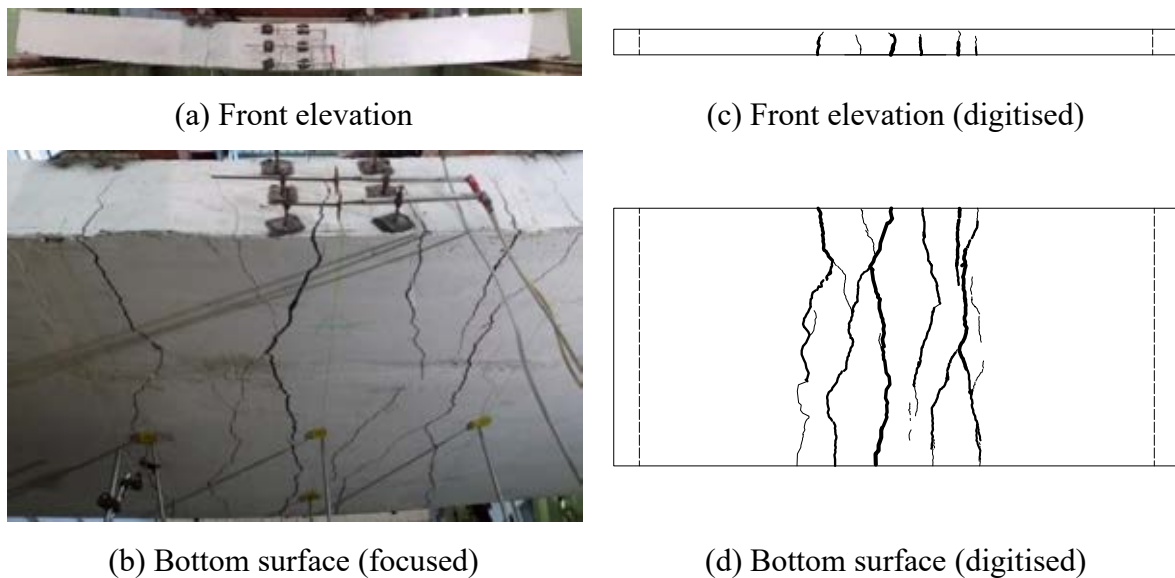
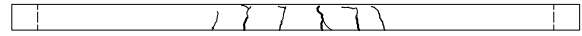


Figure 3.40 – Observed Crack Pattern of Slab Specimen OF-CV-1



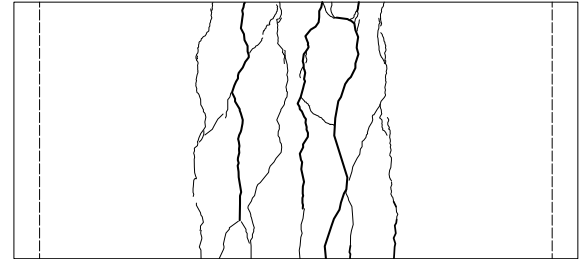
(a) Front elevation (focused)



(c) Front elevation (digitised)



(b) Bottom surface (focused)

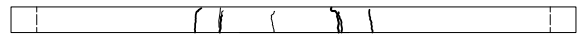


(d) Bottom surface (digitised)

Figure 3.41 – Observed Crack Pattern of Slab Specimen OF-CV-2



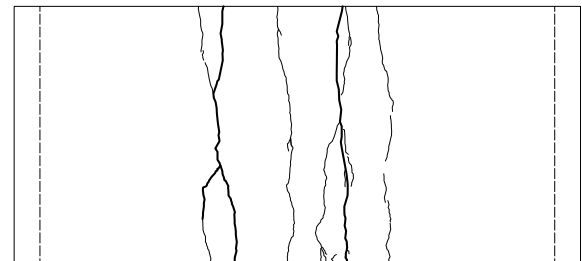
(a) Front elevation (focused)



(c) Front elevation (digitised)



(b) Bottom surface (focused)



(d) Bottom surface (digitised)

Figure 3.42 – Observed Crack Pattern of Slab Specimen OF-CV-3

### (iii) Load Carrying Capacity

Initial cracking, yield & ultimate load and corresponding mid-span deflection are summarised for all tested specimens in Table 3.3. A self-weight correction based on initial stiffness is applied for all figures and values. The load corresponding to initial cracking and yield was defined based on strain in bottom reinforcement (i.e., load corresponding to a sudden change in strain in its elastic state and yield strain, respectively).

Table 3.3 – Experimental Results: One-way Flexure

Specimen	At initial crack		At yielding		At ultimate		At service	
	$P_r$	$\delta_r$	$P_y$	$\delta_y$	$P_u$	$\delta_u$	$P_s$	$\delta_s$
	(kN)	(mm)	(kN)	(mm)	(kN)	(mm)	(kN)	(mm)
<b>OF-S180V</b>	<b>47.3</b>	<b>1.94</b>	<b>108.3</b>	<b>14.16</b>	<b>125.4</b>	<b>56.21</b>	<b>62.7</b>	<b>4.82</b>
OF-CV-1	71.1	1.39	108.7	11.73	127.2	66.72	63.6	1.20
OF-CV-2	77.8	3.10	104.4	13.77	117.2	61.58	58.6	2.19
OF-CV-3	75.1	1.79	97.5	12.31	109.9	60.16	55.0	1.12
<b>OF-CV (Mean)</b>	<b>74.7</b>	<b>2.09</b>	<b>103.5</b>	<b>12.60</b>	<b>118.1</b>	<b>62.82</b>	<b>59.1</b>	<b>1.50</b>

Note:  $P_r$ ,  $P_y$  and  $P_u$  are load corresponding to the first crack, yielding of reinforcement and ultimate failure, respectively;  $\delta_r$ ,  $\delta_y$  and  $\delta_u$  are deflections at mid-span corresponding to  $P_r$ ,  $P_y$  and  $P_u$ , respectively;  $\delta_s$  is deflections at mid-span corresponding to service load  $P_s$  and  $P_s$  is assumed as 50% of ultimate load,  $P_u$ .

#### (iv) Strain of Bottom Reinforcement

Usually, reinforced concrete member behaviour is governed by material (e.g., strain in concrete or reinforcement) and section properties (e.g., moment-curvature); this section focuses on material properties. In this section, strain in bottom reinforcement (at the centre, along both directions) was examined. The load versus reinforcement strain of specimens (OF-S180V and OF-CV-1) showed that the behaviour of reinforcement in both directions was not identical. Along transverse direction, strain in reinforcement is zero; it indicates one-way flexural behaviour during entire period of loading. Thus, reinforcement along transverse direction does not influence load carrying capacity or one-way flexure behaviour of the slab (Figure 3.43); similar behaviour was observed for other specimens.

#### (v) Strain of Concrete Surface along Depth of Slab

The concrete surface strain was measured along with the depth of slab at three different locations (at the centre, bottom and top reinforcement level) using LVDTs (LVDTs 5-7). These measurements were taken at mid-span of slab, where there exist pure bending, i.e., it is the location at which the influence of shear due to applied external load is zero. The load versus concrete surface strain along the depth of slab of specimens (OF-S180V and OF-CV-1) evidenced that bottom, and top reinforcement was in tension. Therefore, the neutral axis of the slab lies in concrete above the top reinforcement (Figure 3.44); similar behaviour was observed



for other specimens. For specimen OF-S180V, the LVDT 7 data is not presented as it was malfunctioned during the experiment.

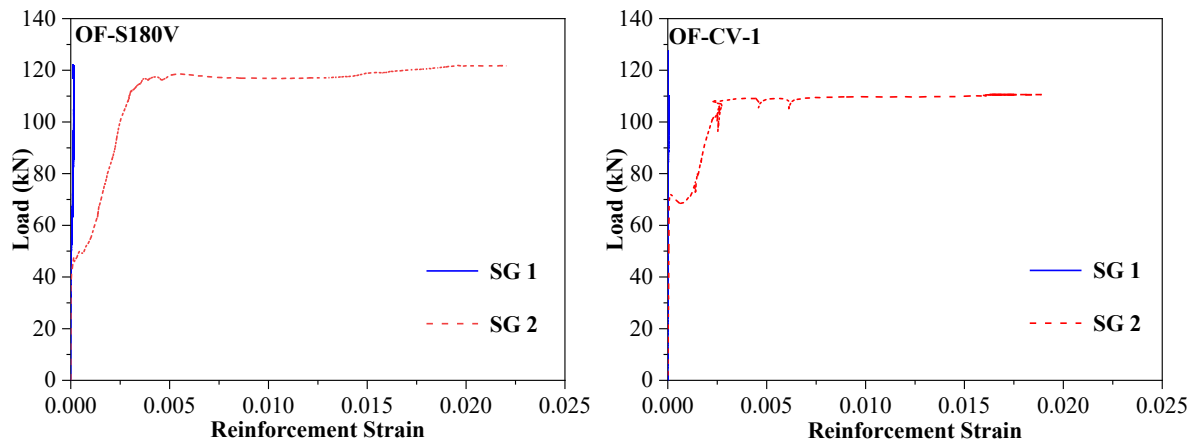


Figure 3.43 – Load versus Reinforcement Strain: One-way Flexure

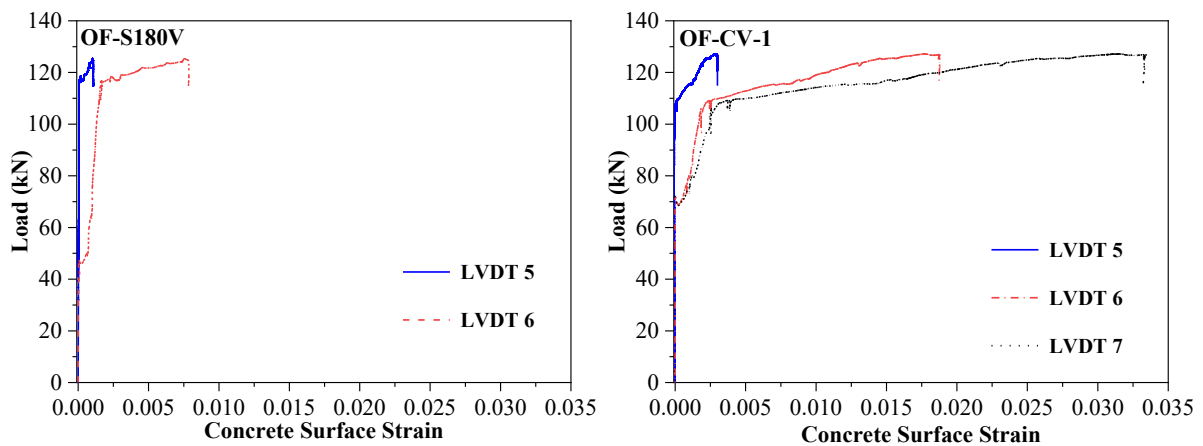


Figure 3.44 – Load versus Concrete Surface Strain along Depth of Slab

### 3.2.6.2 Two-way Flexure

#### (i) Load Deflection Behaviour

All slab specimens exhibited typical flexural behaviour under two-way bending. The specimens remained elastic until cracking, thereafter bottom reinforcements of the slab start yielding initiating the inelastic action. The load versus mid-span deflection for all the tested specimens is shown in Figure 3.45 – Figure 3.47. The specimens with and without voids, having same reinforcement and dimensions (TF-Solid and TF-S90V), show identical load-deflection behaviour after cracking, though the initial stiffness of solid slab specimen (TF-Solid) is 37 % more than that of the voided slab specimen (TF-S90V). The effect of self-weight of load transfer members are considered based on initial stiffness, and the correction is applied

for all figures and values. In addition, the load-displacement behaviour of TF-Solid, TF-S90V and TF-S180V, obtained from displacement controlled test (load up to 1000 kN) and load controlled test (load up to ultimate failure) are combined based on the stiffness. The load-deflection behaviour of the specimen TF-CV-1 is not reported in Figure 3.47 as bolt connection between the loading frame, and the strong floor gave up during the experiment; hence the recorded values are improper. However, the recorded values are shown in Figure 3.48 and Figure 3.49 for the specimen TF-CV-1. The load versus deflection is shown in Figure 3.50 and Figure 3.52 for specimens TF-CV-2 and TF-CV-3, respectively. It is seen that deflections at one-fourth span of the slab are almost the same, which indicates the equal load distribution over the slab area. In the load versus deflection plots, the LVDT7 shows negative deflection, which is attributed to the corner uplift. The load versus lateral deformation is shown in Figure 3.51 and Figure 3.53 for specimens TF-CV-2 and TF-CV-3, respectively. The insignificant initial negative lateral deformation (Figure 3.51 and Figure 3.53) may be attributed to the initial setting of specimens.

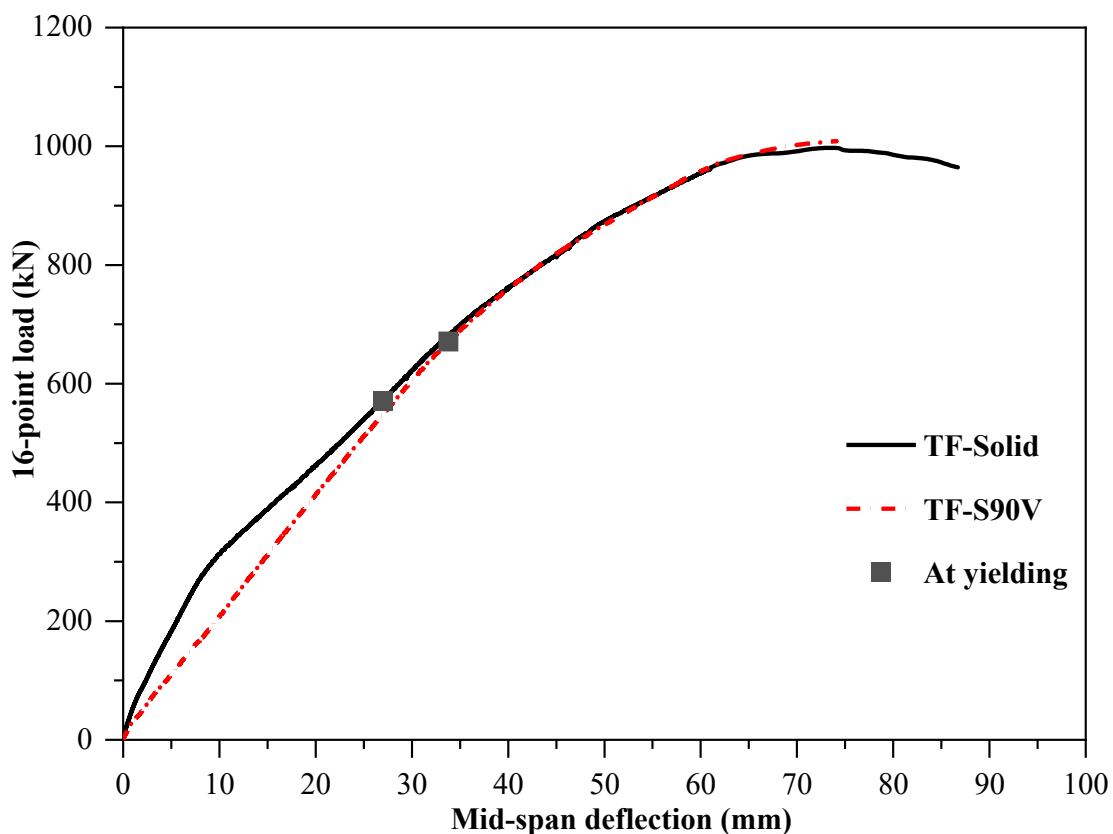


Figure 3.45 – Load versus Mid-span Deflection of Specimens TF-Solid and TF-S90V

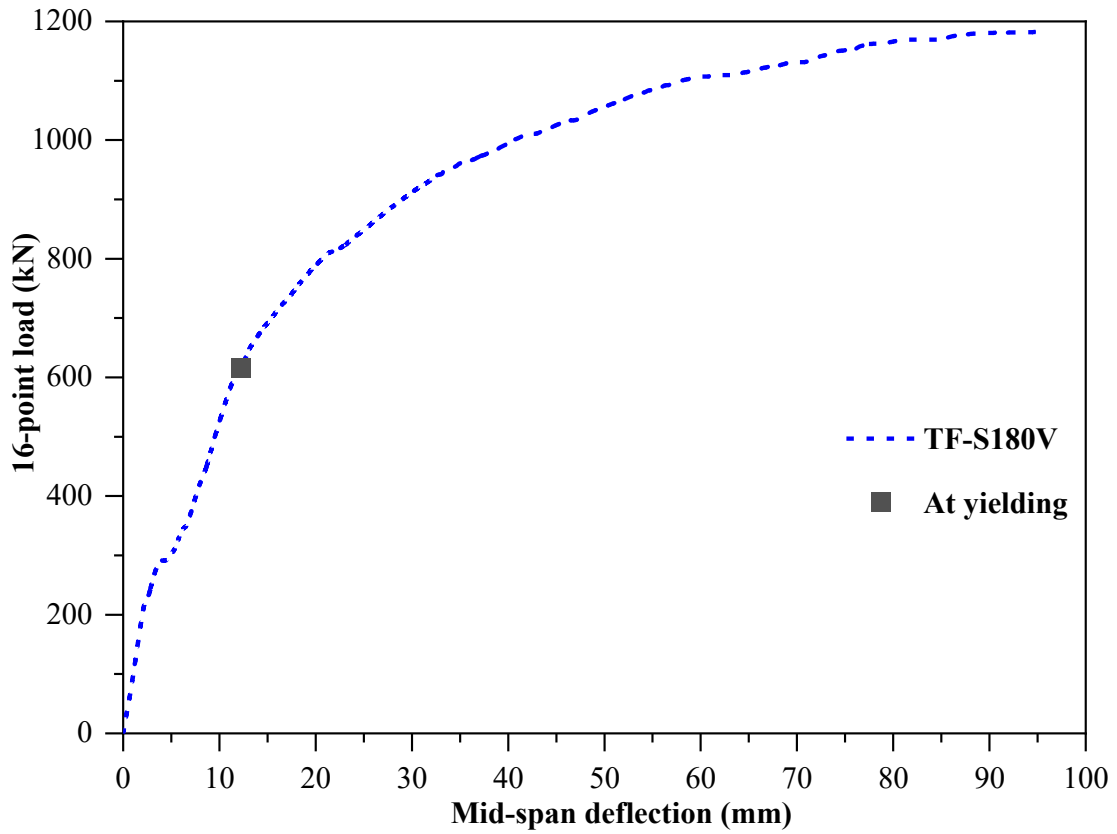


Figure 3.46 – Load versus Mid-span Deflection of Specimen TF-S180V

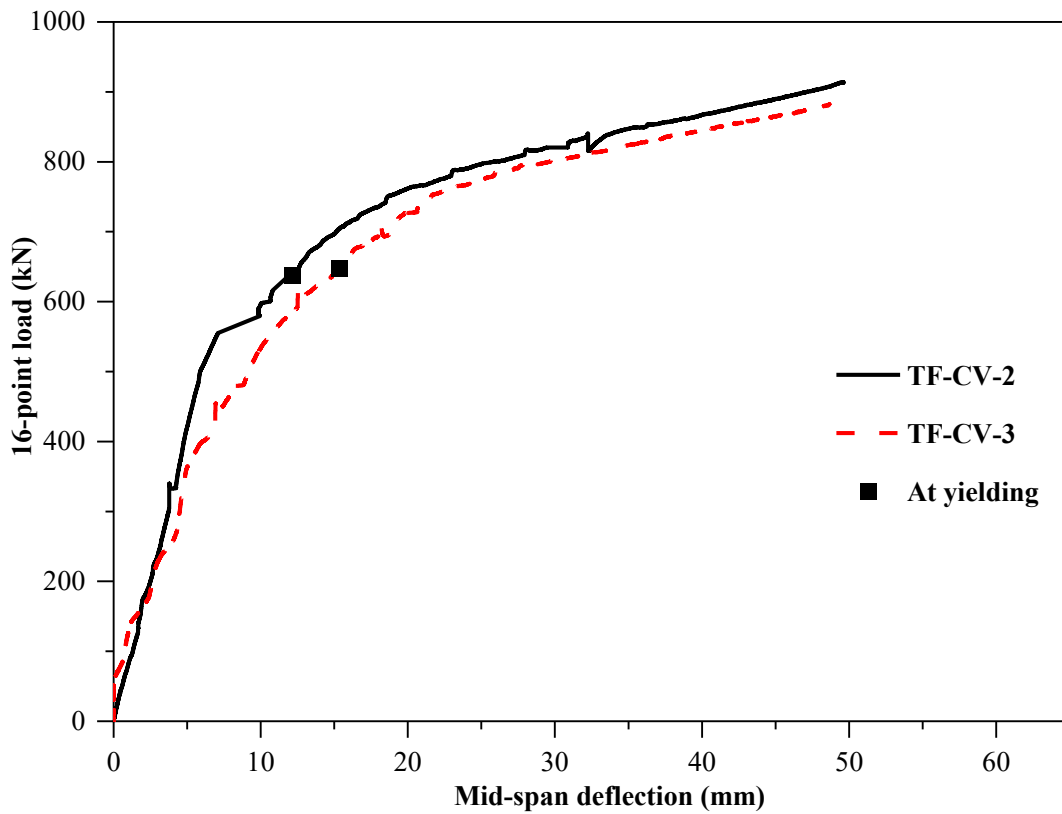


Figure 3.47 – Load versus Mid-span Deflection of Specimens TF-CV-2 and TF-CV-3

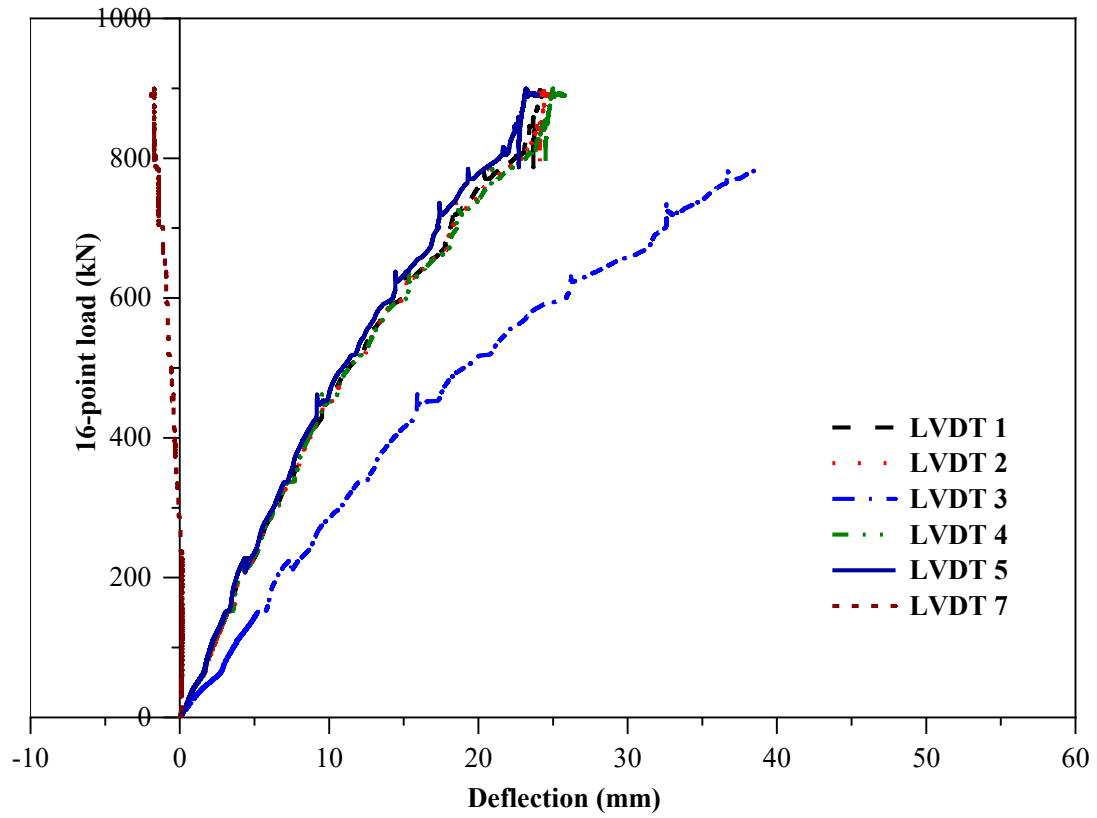


Figure 3.48 – Load versus Deflection of Specimen TF-CV-1

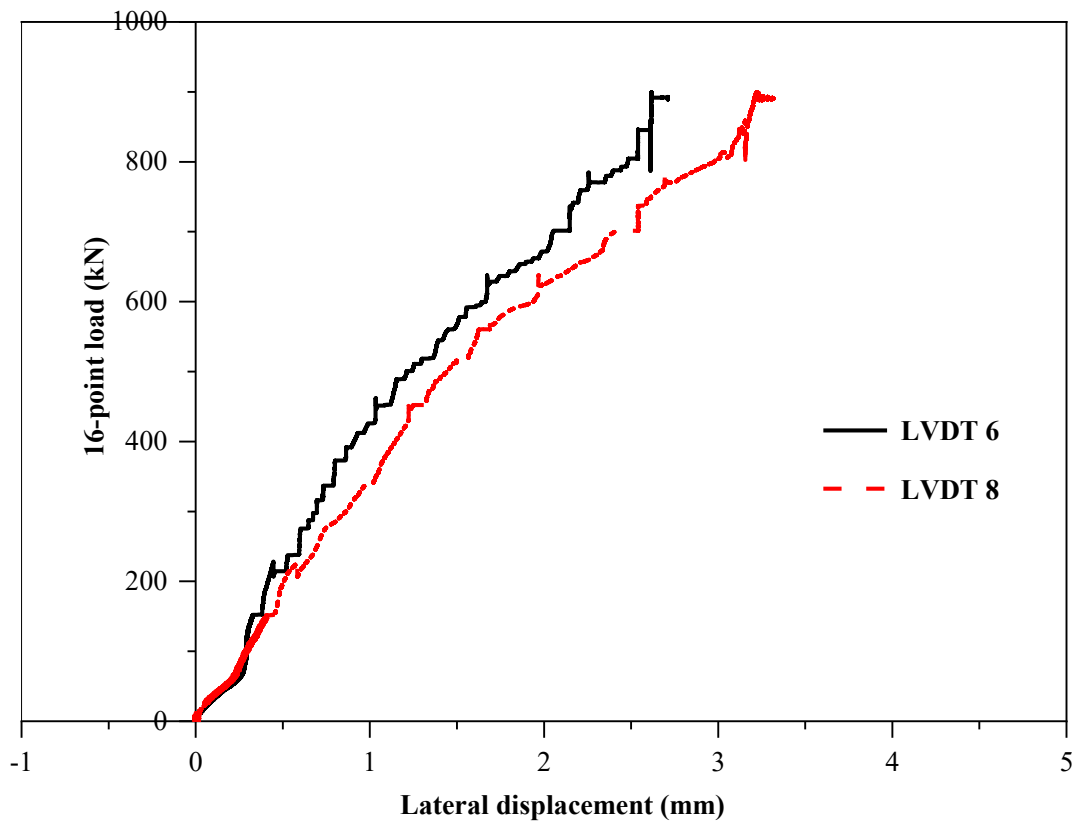


Figure 3.49 – Load versus Lateral Displacement of Specimen TF-CV-1

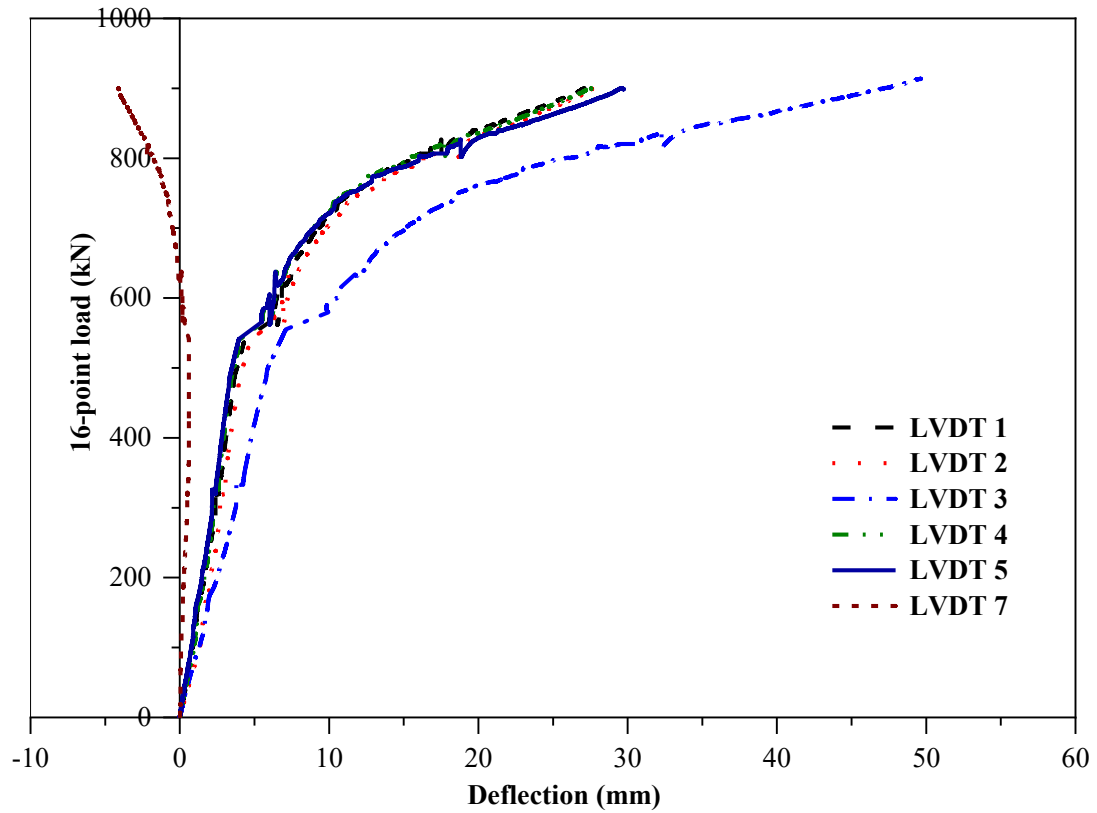


Figure 3.50 – Load versus Deflection of Specimen TF-CV-2

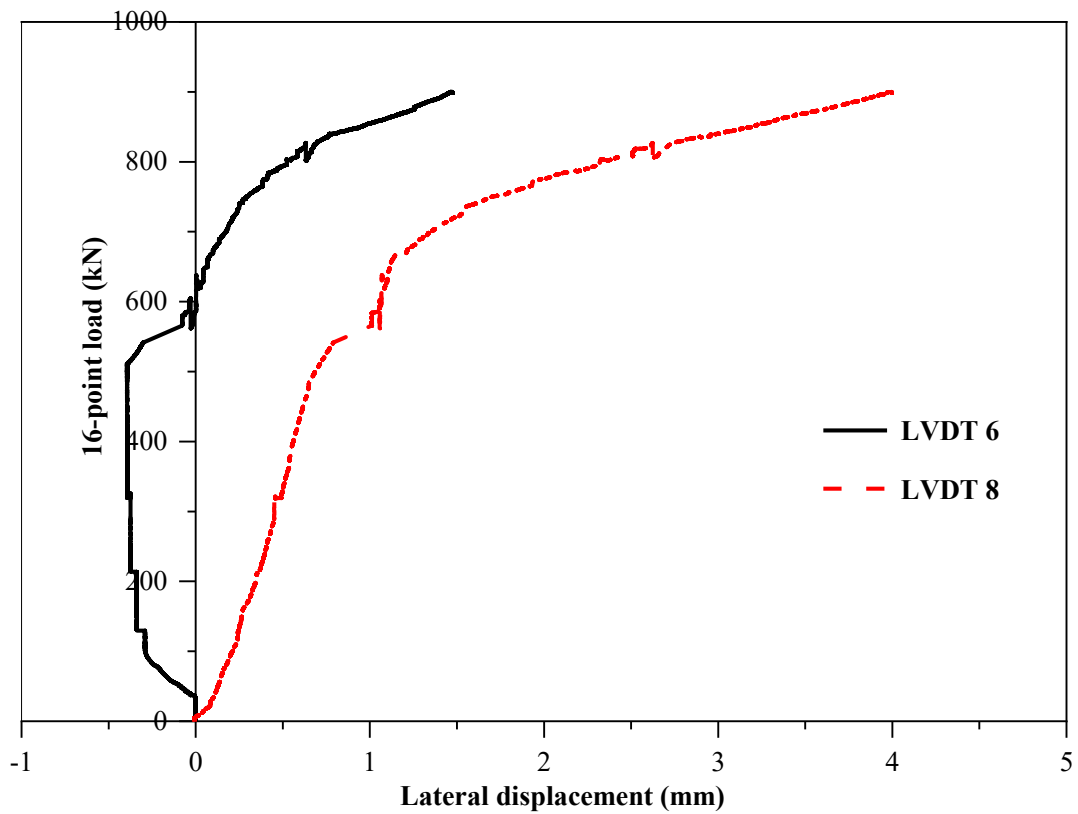


Figure 3.51 – Load versus Lateral Displacement of Specimen TF-CV-2

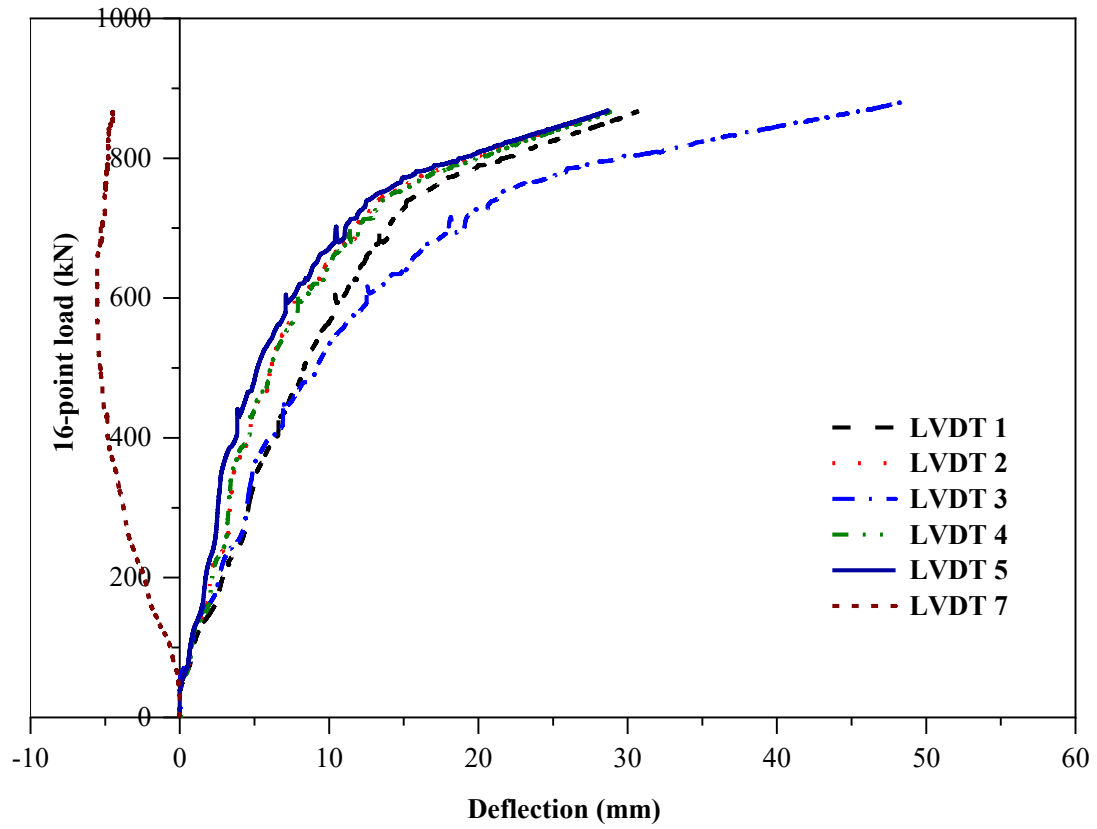


Figure 3.52 – Load versus Deflection of Specimen TF-CV-3

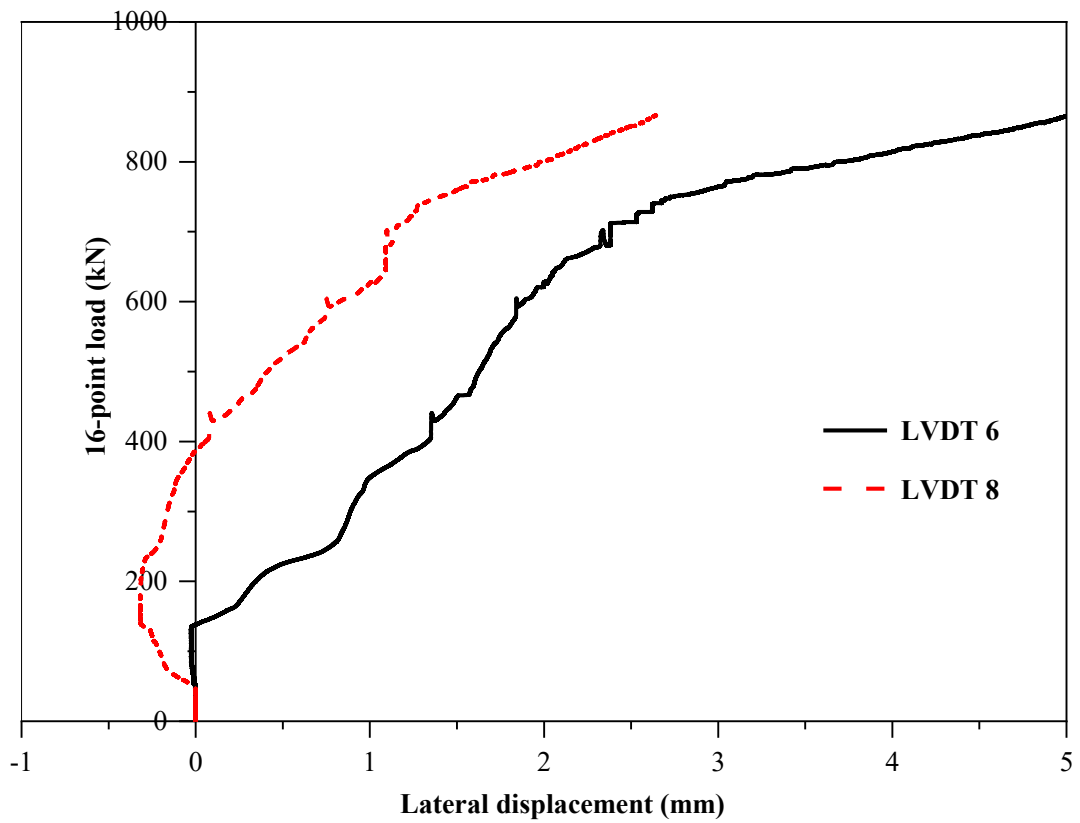


Figure 3.53 – Load versus Lateral Displacement of Specimen TF-CV-3

## (ii) Crack Pattern

The idealised crack pattern observed on the bottom surface of slab specimens is shown in Figure 3.54. Typically the cracks were originated from the centre of the slab and formed X-shape along the diagonals. Corner lever effect was observed in all the test specimens. The photograph of tested specimens with observed cracks are shown in Figure 3.55 – Figure 3.59. The observed different crack distribution mode is attributed to the void shape, size and position.

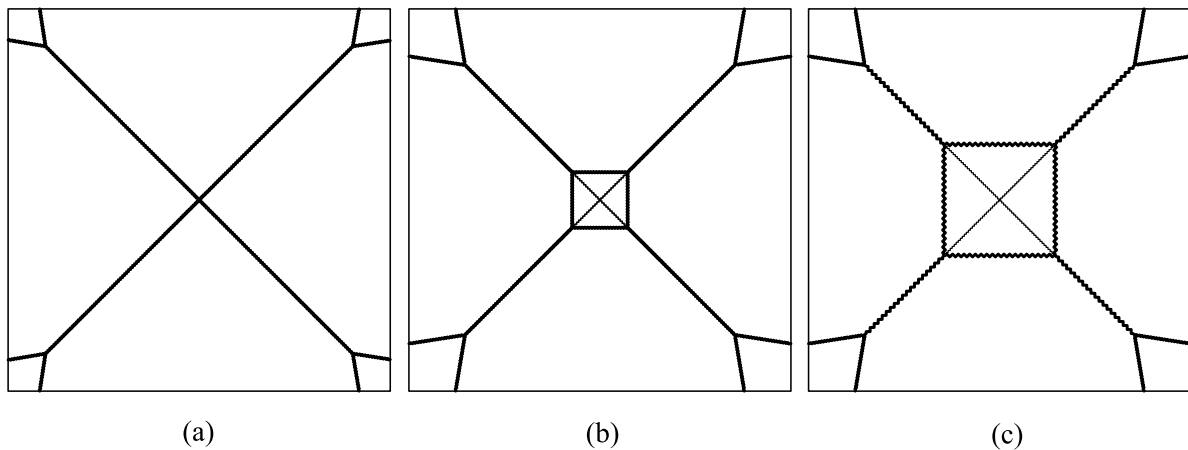


Figure 3.54 – Observed Typical Crack Pattern



Figure 3.55 – Observed Crack Pattern of Slab Specimen TF-Solid



Figure 3.56 – Observed Crack Pattern of Slab Specimen TF-S180V



Figure 3.57 – Observed Crack Pattern of Slab Specimen TF-CV-1





Figure 3.58 – Observed Crack Pattern of Slab Specimen TF-CV-2



Figure 3.59 – Observed Crack Pattern of Slab Specimen TF-CV-3

### (iii) Load Carrying Capacity

The load-carrying capacity of voided slabs was the same as that of a solid slab. Load and mid-span deflection are summarised for all the tested specimens in Table 3.4. The load corresponding to yield was defined based on the strain in bottom reinforcement, i.e. load corresponding to yield strain.

Table 3.4 – Experimental Results: Two-way Flexure

Specimen	At yield		At ultimate				Crack pattern (Fig. 3.54)
	$P_y$ (kN)	$\delta_y$ (mm)	$P_u$ (kN)	$\delta_u$ (mm)	$W_u$ (kN)	$W_{u1}$ (kN)	
TF-Solid	571.45	26.95	997.48	73.64	1120.76	1160.36	a
TF-S90V	670.98	33.78	1008.69	74.08	1133.36	1169.36	a
TF-S180V	616.71	12.29	1184.90*	95.88	1331.35	1386.15	b
TF-CV-1 <sup>#</sup>	–	–	913.29*	–	1026.17	1082.08	c
TF-CV-2	637.23	12.19	913.57*	49.62	1026.48	1082.38	c
TF-CV-3	647.02	15.36	882.55*	48.65	991.63	1047.53	c

Note: \*Specimen did not reach the ultimate stage, maximum observed values are reported; #Displacement values not reported as the measured values are improper due to loading frame connection failure;  $P_y$  and  $P_u$  are load corresponding to yielding of reinforcement and maximum observed load, respectively;  $\delta_y$  and  $\delta_u$  are deflections at mid-span corresponding to  $P_y$  and  $P_u$ , respectively;  $W_u$  and  $W_{u1}$  are equivalent UDL ( $= 0.89P_u$ ) of  $P_u$  without and with considering self-weight of slab, respectively.

### (iv) Strain of Bottom Reinforcement

The load versus reinforcement strain of specimens (Figure 3.60) showed that the behaviour of reinforcement in both directions was not identical. It is mainly because of the difference in effective depth in  $x$ - and  $y$ -directions.

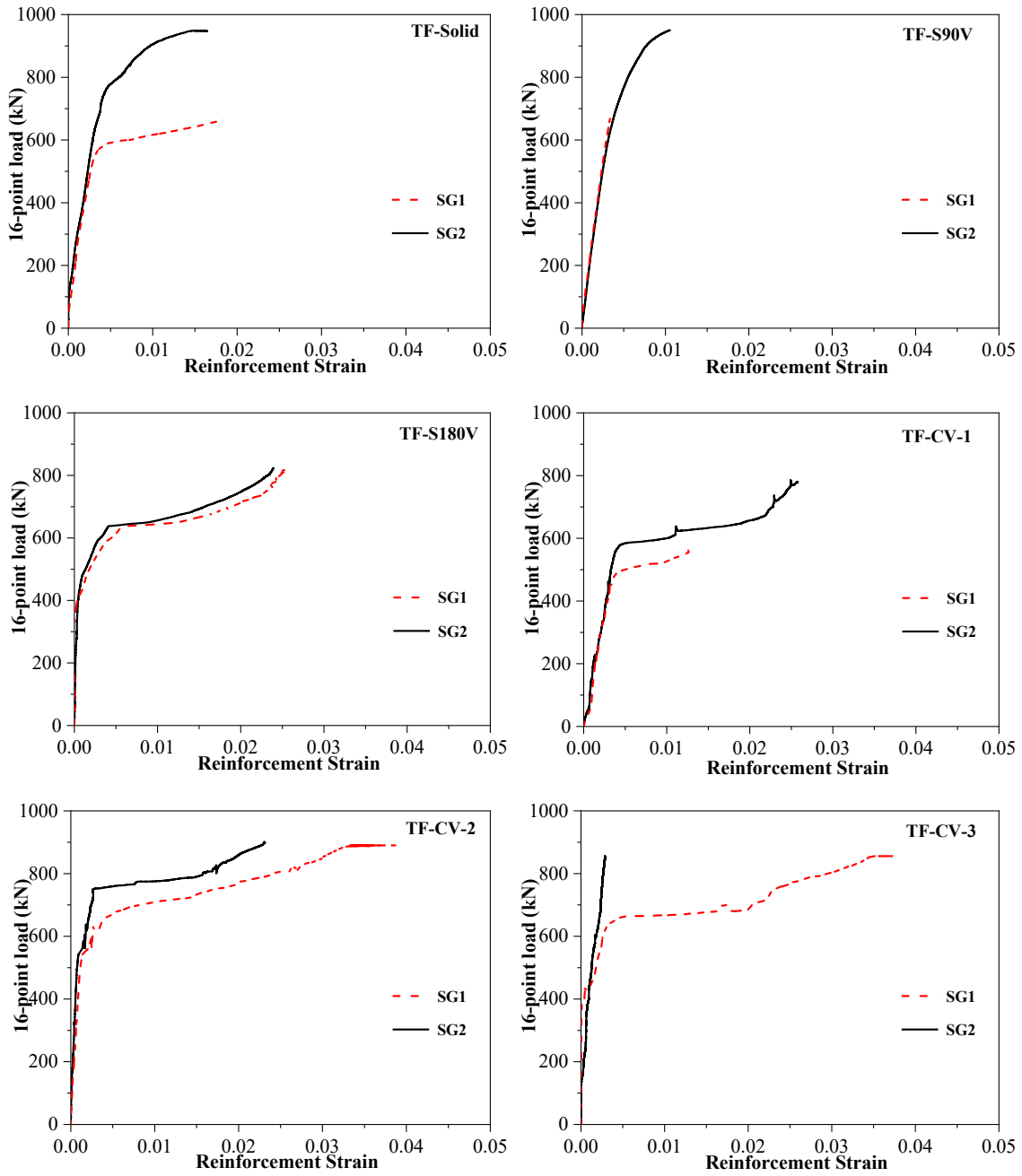


Figure 3.60 – Load versus Reinforcement Strain: Two-way Flexure

### 3.3 Analytical Study

The flexural capacity and the flexural stiffness are calculated based on the existing provisions of IS 456 (2000) & ACI 318 (2019) and yield line analysis. The obtained values are compared with experimental results. It is observed from experimental results that the presence of voids influences the flexural stiffness without significant change in the flexural capacity. The same is verified through theoretical estimations. Further, the applicability of tensile membrane action to biaxial voided slab and the influence of reinforcement orientation on the ultimate capacity is investigated.

#### 3.3.1 One-way Flexure

##### 3.3.1.1 Load Carrying Capacity

The ultimate load-carrying capacity of slab specimens under flexure can be estimated based on the yield line method. Usually, yield line method uses rigid plastic theory to compute failure loads correspond to plastic moment resistance in various parts of the slab (Chung et al., 2018b; Darwin et al., 2002; Hsueh, 1966). It is an inelastic approach and has great potential to predict the failure load of reinforced concrete slabs (Darwin et al., 2002; Hognestad, 1953; Pillai and Menon, 2012). Hence, the ultimate load-carrying capacity of test specimens was estimated using the yield line method.

Initially, crack patterns, and failure modes of the slab were assumed to calculate its ultimate load-carrying capacity. Therefore, in rectangular slabs, yield line was assumed to generate at mid-span under one-way flexural action along transverse direction; it results in dividing the slabs into two equal parts (Figure 3.61). In the case of four-point bending, the yield line may form at load positions or anywhere in between load positions. But, irrespective of the location of yield line the ultimate load-carrying capacity of specimen will be the same.

The *external work done* ( $W_E$ ) by two-line loads is formulated by multiplying the external loads and displacements and given by:

$$W_E = \frac{P_u}{2} \times \left( \frac{2}{3} \delta_u \right) \times 2 = \frac{2}{3} P_u \delta_u \quad \text{Eq. 3.1}$$

where,  $\delta_u$  is the deflection at the centre of the slab under the ultimate load ( $P_u$ ).

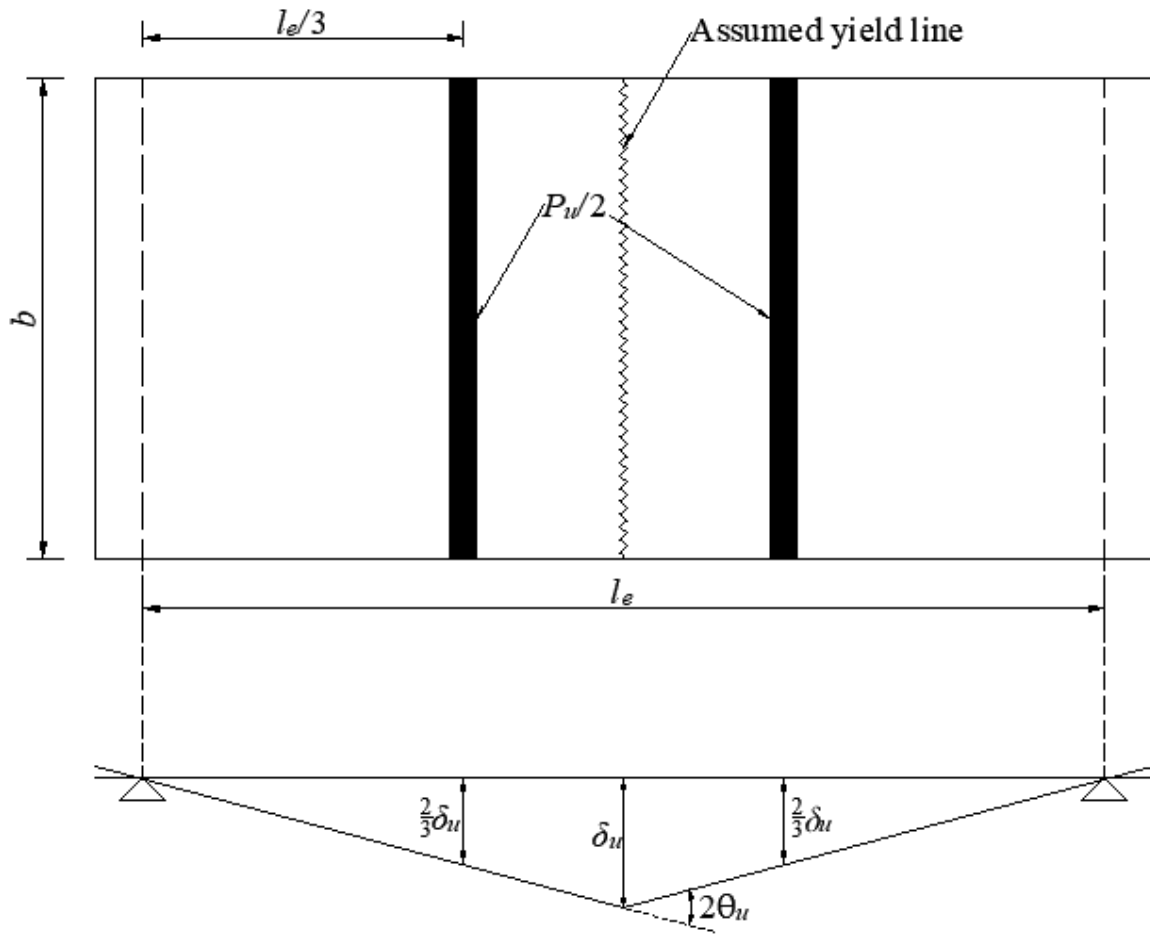


Figure 3.61 – Assumed Yield Line Pattern and Failure Mode: One-way Flexure

The *internal work done* ( $W_I$ ) by in-plane moment ( $m$ ) for width  $b$  along the yield line is expressed in terms of in-plane moment and rotation angle ( $\theta_u$ ). The rotation angle ( $\theta_u$ ) along the yield line is calculated with an assumption that the rotation is small (Figure 3.61) and given by:

$$\theta_u = \frac{2\delta_u}{l_e} \quad \text{Eq. 3.2}$$

where,  $l_e$  is the effective length between simple supports. Then, the internal work done ( $W_I$ ) is calculated as:

$$W_I = m \times \theta_u \times 2 = \frac{4m\delta_u}{l_e} \quad \text{Eq. 3.3}$$

As per the principle of conservation of energy, external work done ( $W_E$ ) and internal work done ( $W_I$ ) should be equal; therefore, the ultimate load-carrying capacity ( $P_u$ ) of the slab specimen is calculated and given by:

$$P_u = \frac{6m}{l_e} \quad \text{Eq. 3.4}$$

Similarly, for the self-weight of the slab, which is uniformly distributed over the span, the relation between self-weight ( $W_{DL}$ ) and in-plane moment ( $m_{DL}$ ) can be derived as:

$$W_{DL} = \frac{8m_{DL}}{l_e} \quad \text{Eq. 3.5}$$

### 3.3.1.2 Moment Capacity of Slab Section

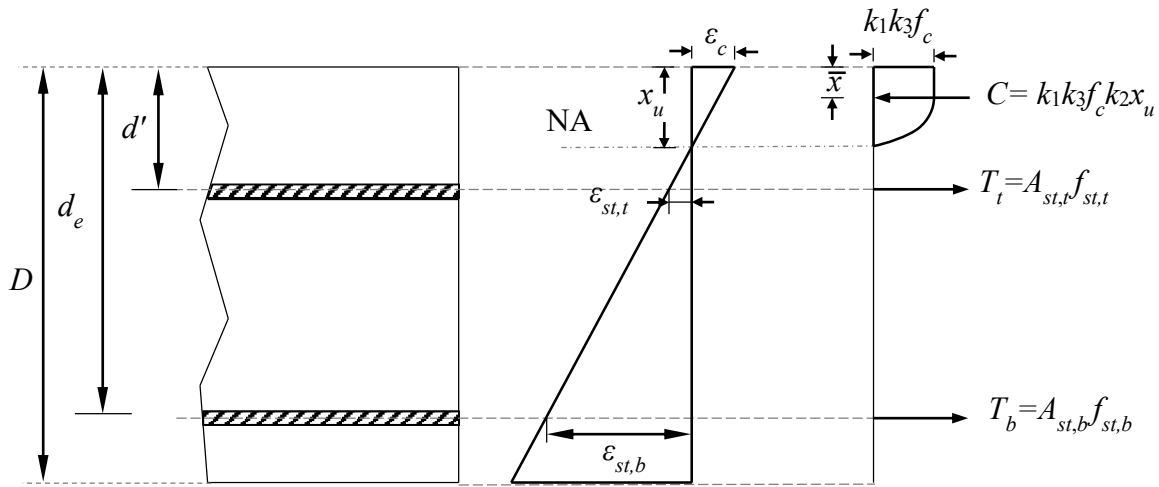


Figure 3.62 – Strain and Stress Distribution in a Slab Section

The moment capacity ( $m$ ) of a slab section per unit length can be calculated by Eq. 3.6 based on the stress distribution shown in Figure 3.62. A layer of reinforcements was provided at the top to place the void formers. It was observed from experiments that the neutral axis lies within the cover concrete to the top reinforcement, i.e. top and bottom reinforcements are in tension. Hence, the contribution from the top and bottom reinforcements are considered for the capacity calculation. Moreover, if the slab's NA lies in the location of the void, then the contribution from compression side reinforcement (top) can be ignored conservatively. In addition, the presence of concrete below the top cover concrete to the void former can be ignored conservatively, as the area of concrete available to resist the compressive force is very small in the biaxial voided slab due the presence of voids.

$$m = T_b (d_e - \bar{x}) + T_t (d' - \bar{x}) \quad \text{Eq. 3.6}$$

where,  $T_b$  and  $T_t$  are the force in the bottom and top reinforcements, respectively,  $d_e$  and  $d'$  are effective depth to bottom and top reinforcements, respectively, and  $\bar{x}$  is the depth of resultant

compressive force in concrete, which depends on neutral axis depth ( $x_u$ ). The neutral axis depth needs to be arrived based on iteration by equating compressive and tensile force.

The theoretical ultimate moment capacity of the slab section is estimated using Eq. 3.6. The change in the magnitude of the moment capacity with respect to the stress-strain relationship of concrete in compression is insignificant as the neutral axis depth ( $x_u$ ), and strain in concrete ( $\varepsilon_c$ ) are small in-comparison with effective depth ( $d_e$ ) and strain in reinforcement ( $\varepsilon_{st,b}$ ), respectively. Here, the moment capacity was calculated based on the stress-strain relationship of concrete in compression given in IS 456 (Eq. 3.7 and Figure 3.63) and ACI 318 (Eq. 3.9 and Figure 3.64).

**(i) IS 456:2000**

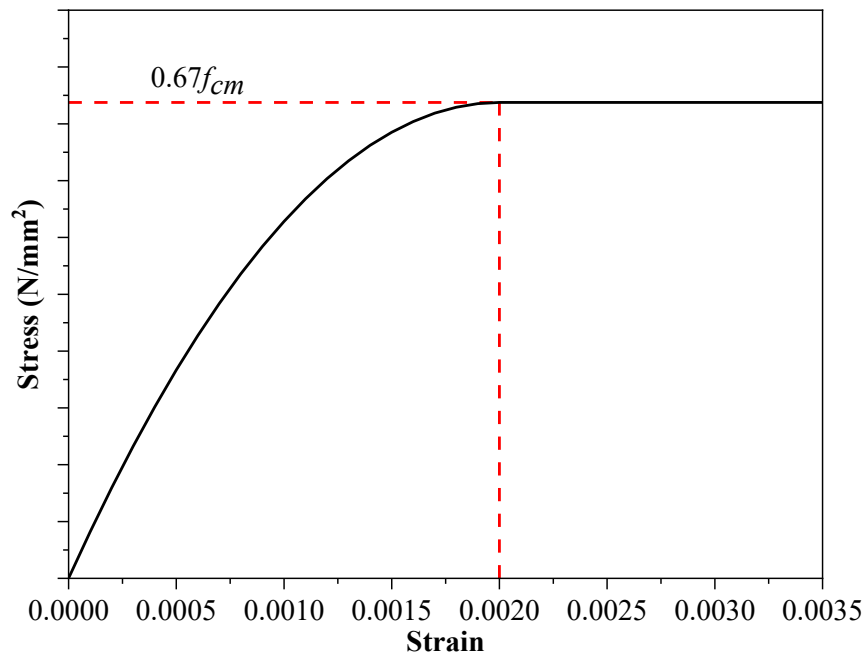


Figure 3.63 – Stress versus Strain Behaviour of Concrete (IS 456)

$$f_c = k_1 k_3 f_{cm} \quad \text{Eq. 3.7}$$

$$f_c = \begin{cases} 0.67 f_{cm} \left[ 2 \left( \frac{\varepsilon}{0.002} \right) - \left( \frac{\varepsilon}{0.002} \right)^2 \right] & \text{for } \varepsilon < 0.002 \\ 0.67 f_{cm} & \text{for } 0.002 \leq \varepsilon \leq 0.0035 \end{cases} \quad \text{Eq. 3.8}$$

where,  $f_c$  is flexural compressive stress in concrete,  $k_1$  is concrete stress factor which depends on the strain  $\varepsilon_c$  (Eq. 3.8),  $k_3$  ( $= 0.67$ ) is a factor to account for size effect and conversion of cube strength to cylinder strength, and  $f_{cm}$  is mean concrete cube strength.

(ii) ACI 318-19

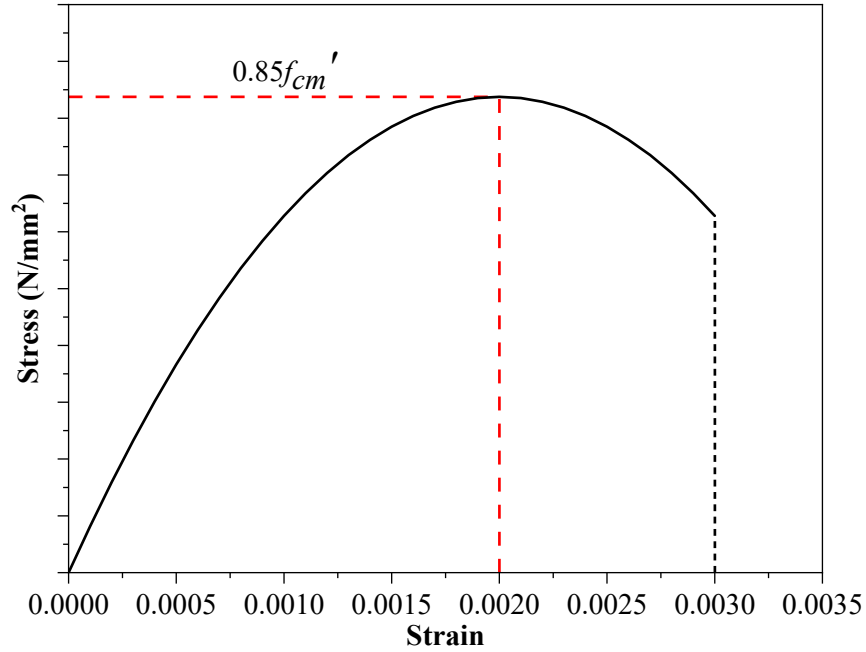


Figure 3.64 – Stress versus Strain Behaviour of Concrete (ACI 318)

$$f_c = k_1 k_3 (0.85 f_{cm}') \quad \text{Eq. 3.9}$$

$$k_1 = 2 \left( \frac{\varepsilon_c}{\varepsilon_0} \right) - \left( \frac{\varepsilon_c}{\varepsilon_0} \right)^2 \quad \text{for } \varepsilon_c \leq 0.003 \quad \text{Eq. 3.10}$$

where,  $f_c$  is flexural compressive stress in concrete,  $k_1$  is concrete stress factor which depends on the strain  $\varepsilon_c$  (Eq. 3.10),  $k_3$  ( $\approx 0.8$ ) is a factor to account for conversion of cube strength to cylinder strength,  $f_{cm}'$  is mean compressive strength of concrete cylinders,  $\varepsilon_c$  is strain in concrete and  $\varepsilon_0$  is strain in concrete at the maximum concrete stress. In ACI 318, the stress-strain relationship of concrete in compression is converted as equivalent rectangular with respect to maximum limiting strain in the concrete of 0.003 for easy calculation purposes.

Based on the stress-strain relationship of concrete, slab specimen dimensions (Figure 3.5 and Figure 3.6) and materials' properties (Table 3.1 and Figure 3.11), load-carrying capacity corresponding to initial crack, yield and ultimate stages are estimated and summarised in Table 3.5.

### 3.3.1.3 Flexural Stiffness

Theoretically estimated flexural stiffness and effective moment of inertia ( $I_{eff}$ ) of solid slabs were compared with flexural stiffness of the biaxial voided slab (from the experimental study);



here the flexural stiffness is defined as the ratio of load and its corresponding deflection. Flexural stiffness is estimated by taking secant stiffness ( $K_s$ ) corresponding to service load ( $P_s$ ) of biaxial voided slab specimen (Eq. 3.11).

$$K_s = \frac{P_s}{\delta_s} \quad \text{Eq. 3.11}$$

Typically, deflection of slab depends on load, modulus of elasticity ( $E$ ) of material and geometrical properties (such as the moment of inertia of section  $I$ , effective length  $l_e$ ). Hence, the deflection at the centre of the slab ( $\delta_c$ ) under two-line loads ( $P/2$  each) (Figure 3.61) is calculated using Eq. 3.12.

$$\delta_c \approx \frac{Pl_e^3}{56EI} \quad \text{Eq. 3.12}$$

The effective moment of inertia of the specimens was estimated as per IS 456 at yield load; here the short-term deflection is calculated using short-term modulus of elasticity of concrete ( $E_c = 5000 f_{ck}^{0.5}$ ) and effective moment of inertia ( $I_{eff}$ ) (Eq. 3.13 and Eq. 3.14).

$$I_{eff} = \frac{I_r}{1.2 - \frac{M_r}{M} \frac{z}{d} \left(1 - \frac{x}{d}\right) \frac{b_w}{b_c}}; I_r \leq I_{eff} \leq I_{gr} \quad \text{Eq. 3.13}$$

$$\text{cracking moment, } M_r = \frac{f_{cr} I_{gr}}{y_t} \quad \text{Eq. 3.14}$$

where,  $I_r$  is the moment of inertia of cracked section,  $f_{cr}$  ( $= 0.7 f_{ck}^{0.5}$ ) is the modulus of rupture of concrete,  $I_{gr}$  is the moment of inertia of gross-section about the centroidal axis (ignoring reinforcement),  $y_t$  is the distance from centroidal axis of gross section to extreme fibre in tension (ignoring reinforcement),  $M$  is the maximum moment under service load,  $z$  is the lever arm distance,  $x$  is the depth of neutral axis,  $d$  is the effective depth,  $b_w$  is the breadth of web and  $b_c$  is the breadth of compression face.

The estimate of deflection based on IS 456 results in large deflection. Therefore, the cracking moment ( $M_r$ ) may be reduced by approximately 30 % (Pillai and Menon, 2012) to estimate deflection based on Eq. 3.12. The effective moment of inertia of the voided slab is calculated based on the critical cross-section that corresponds to the section located at the centre of the void as shown in Figure 3.65. The uncracked moment of inertia ( $I_{g,v}$ ) was calculated using Eq. 3.15 and Eq. 3.16 for sphere shape voided slab and using Eq. 3.15 and Eq. 3.17 for cuboid

shape voided slab, accounting for the loss of concrete due to voids. The location of the centre of gravity from the base ( $C_y$ ) was calculated for sphere and cuboid shape voids using Eq. 3.18 and Eq. 3.19, respectively. Researchers suggested that the cracked moment of inertia of voided slab ( $I_{r,V}$ ) may be taken as 90 % of the cracked moment of inertia of solid slab ( $I_{r,Solid}$ ) (BubbleDeck Technology, 2008; Midkiff, 2013). However, the ratio of  $I_{r,V}$  to  $I_{r,Solid}$  needs to be arrived based on the maximum void ratio at a section ( $\alpha$ ) as given in Eq. 3.20.

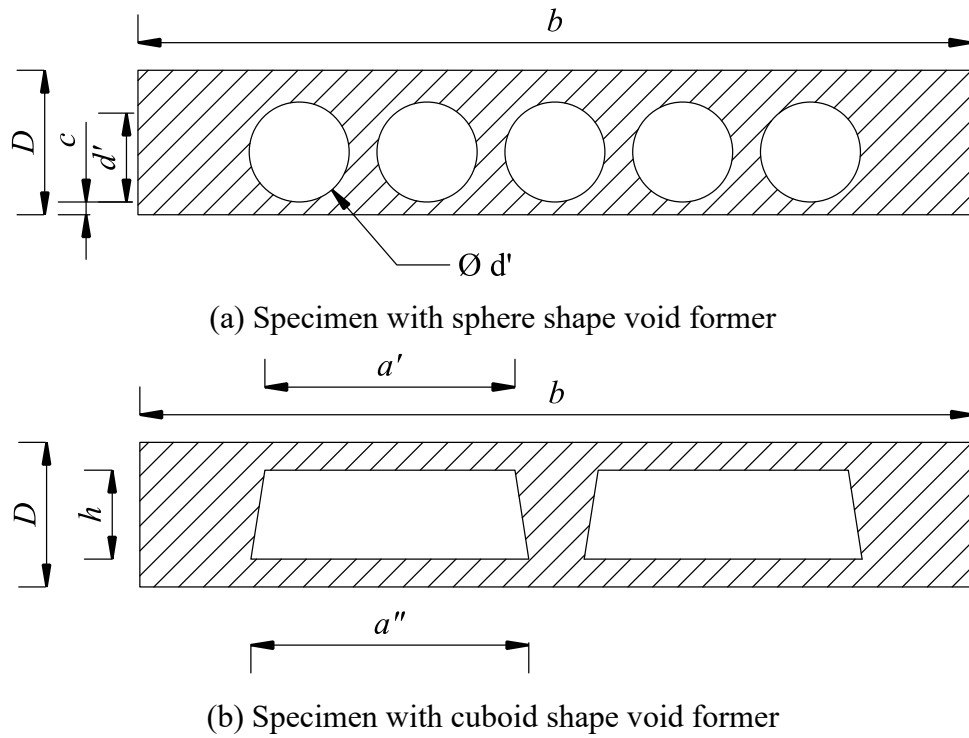


Figure 3.65 – Voided Slab Sections used to Calculate Moment of Inertia

$$I_{g,V} = I_{g,Solid} - n(I_V) \quad \text{Eq. 3.15}$$

$$I_{V,S} = \frac{\pi d'^4}{64} + \frac{\pi d'^2}{4} \left( \frac{D}{2} - C_{y,S} \right)^2 \quad \text{Eq. 3.16}$$

$$I_{V,C} = \frac{h^3}{36} \left( \frac{a'^2 + 4a'a'' + a''^2}{a' + a''} \right) + \frac{h(a' + a'')}{2} \left( \frac{D}{2} - C_{y,C} \right)^2 \quad \text{Eq. 3.17}$$

$$C_{y,S} = c + \frac{d'}{2} \quad \text{Eq. 3.18}$$

$$C_{y,C} = \left( \frac{D-h}{2} \right) + \frac{h}{3} \left( \frac{2a' + a''}{a' + a''} \right) \quad \text{Eq. 3.19}$$

$$I_{r,V} = (1 - \alpha) I_{r,Solid} \quad \text{Eq. 3.20}$$

where,  $I_{g,Solid}$  is the uncracked moment of inertia of solid slab and  $n$  is the number of voids in a section. The theoretical results of mid-span deflection are summarised in Table 3.5.

Table 3.5 – Analytical Results: One-way Flexure

Specimen	At initial crack	At yielding	At ultimate	At service	
	$P_r$ (kN)	$P_y$ (kN)	$P_u$ (kN)	$P_s$ (kN)	$\delta_s$ (mm)
OF-S180V	67.7	88.8	119.9	60.0	4.92
OF-Solid	84.0	88.8	119.9	60.0	0.52
<b>Ratio</b>	<b>0.81</b>	<b>1.00</b>	<b>1.00</b>	<b>1.00</b>	–
OF-CV	71.6	107.4	128.7	64.4	1.54
OF-Solid	84.6	107.4	128.7	64.4	0.57
<b>Ratio</b>	<b>0.85</b>	<b>1.00</b>	<b>1.00</b>	<b>1.00</b>	–

Note:  $P_r$ ,  $P_y$  and  $P_u$  are load corresponding to the first crack, yielding of reinforcement and ultimate failure, respectively;  $\delta_s$  is deflections at mid-span corresponding to service load  $P_s$  and  $P_s$  is assumed as 50% of ultimate load,  $P_u$ .

Table 3.6 – Comparison of Results: One-way Flexure

Specimen	At initial crack	At yielding	At ultimate	At service		
	$P_r$ (kN)	$P_y$ (kN)	$P_u$ (kN)	$P_s$ (kN)	$\delta_s$ (mm)	$K_s$ (kN/mm)
<b>Specimen with sphere shape void (OF-S180V)</b>						
Calculated	67.7	88.8	119.9	60.0	4.92	12.19
Experiment	47.3	108.3	125.4	62.7	4.82	13.01
<b>Ratio</b>	<b>1.43</b>	<b>0.82</b>	<b>0.96</b>	<b>0.96</b>	–	<b>0.94</b>
<b>Specimen with cuboid shape void (OF-CV)</b>						
Calculated	71.6	107.4	128.7	64.4	1.54	41.82
Experiment	74.7	103.5	118.1	59.0	1.50	39.33
<b>Ratio</b>	<b>0.96</b>	<b>1.04</b>	<b>1.09</b>	<b>1.09</b>	–	<b>1.06</b>

Note:  $P_r$ ,  $P_y$  and  $P_u$  are load corresponding to the first crack, yielding of reinforcement and ultimate failure, respectively;  $\delta_s$  is deflections at mid-span corresponding to service load  $P_s$  and  $P_s$  is assumed as 50% of ultimate load,  $P_u$ ;  $K_s$  is secant stiffness corresponding to  $P_s$ .

The comparison of experimental and analytical results are given in Table 3.6. From the comparison of results, it is observed that the one-way flexure behaviour of voided slabs could be well established using provisions of IS 456 with necessary correction for the loss of cross-section due to voids. As the voids lie below the neutral axis, the load-carrying capacity of the voided slab remains same as that of solid slab. However, the initial flexural stiffness affected significantly. The loss of cross-section due to voids should be considered for calculating flexural stiffness of voided slab based the maximum void ratio at a section.

### **3.3.2 Two-way Flexure**

#### **3.3.2.1 Load Carrying Capacity**

The experimental results based on the test data available in the literature (7 specimens) and current study (5 specimens) were compared with the estimations by YLA in conjunction with IS 456 and ACI 318. The specimen details and results of slab specimens are summarised in Table 3.7 and Table 3.8, respectively. The ultimate capacity of the slab may be calculated based on suitable assumptions of failure modes and crack patterns. Therefore, the yield line for the square slabs was assumed to form in X-shape along the diagonals, under two-way flexural action. This results in dividing the slabs into four equal triangular parts. The expression for collapse load for the assumed yield line pattern could be derived by considering the equilibrium of the slab and its various segments. It may be carried out either by the direct application of static equilibrium (equilibrium of slab parts) or by the concept of virtual displacements. In this study, an expression for collapse load was derived based on the equilibrium of slab parts. The schematic slab with yield line and deformation contour is shown in Figure 3.66, Figure 3.67, and Figure 3.68 for 16-point, 12-point and uniformly distributed loading type, respectively. The detailed procedure to obtain the collapse load for the slab specimen with 16-point load alone is explained here.

Table 3.7 – Details of Slab Specimens of Various Researchers

Reference	ID	Slab type	Dimension, mm	Reinforcement area, mm <sup>2</sup> /m				Loading type	Concrete strength <sup>#</sup> , N/mm <sup>2</sup>	Reinforcement strength, N/mm <sup>2</sup>	
				Top		Bottom				Yield (Strain)	Tensile
				<i>x</i>	<i>y</i>	<i>x</i>	<i>y</i>				
Taylor et al. 1966	S1	Solid	1980 × 1980 × 50.80	–	233.78	280.53	16-point	35.05	375.76 (0.0039)	486.76	
	S9		1980 × 1980 × 76.20	–	146.11	155.85		33.23	375.76 (0.0039)	486.76	
Brotchie and Holley 1971	12	Solid	400 × 400 × 38.10	–	309.88		UDL	23.30	379.21 (0.0019)	482.63	
	19		400 × 400 × 76.20	–	657.86			16.14	365.42 (0.0018)	484.70	
Chung et al. 2018b*	Solid	Solid	3300 × 3300 × 250	432.30	767.90		12-point	19.36	473.00 (0.0024)	665.00	
	TF-D-S-P.P	Voided	3300 × 3300 × 250	432.30	767.90			19.36	473.00 (0.0024)	665.00	
	TF-D-M-P.P	Voided	3300 × 3300 × 250	432.30	767.90			19.36	473.00 (0.0024)	665.00	
Current study	TF-Solid	Solid	3300 × 3300 × 150	343.00	343.00		16-point	31.20	560.00 (0.0033)	650.00	
	TF-S90V	Voided	3300 × 3300 × 150	343.00	343.00			31.00	560.00 (0.0033)	650.00	
	TF-S180V	Voided	3300 × 3300 × 250	257.00	257.00			29.40	560.00 (0.0033)	650.00	
	TF-CV-2	Voided	3300 × 3300 × 260	146.00	274.00			22.9	560.00 (0.0033)	650.00	
	TF-CV-3	Voided	3300 × 3300 × 260	146.00	274.00			24.4	560.00 (0.0033)	650.00	

**Note:** # Concrete cylinder strength is taken as 80 % of cube strength if required.

\* The contribution from the presence of top reinforcement is not considered as it is above neutral axis and under compression.

Table 3.8 – Experimental Results

Reference	ID	Maximum observed load, $W_u$ , kN	Mid-span deflection, $\delta_u$ , mm
Taylor et al. 1966	S1	166*	81.28
	S9	151	83.82
Brotchie and Holley 1971	12	81	13.36
	19	326	2.46
Chung et al. 2018b	Solid	2039	56.60
	TF-D-S-P.P	1934	60.69
	TF-D-M-P.P	2018	70.50
Current study	TF-Solid	1160	73.64
	TF-S90V	1169	74.08
	TF-S180V	1386*	95.88
	TF-CV-2	1082*	49.62
	TF-CV-3	1048*	48.65

\*Specimen did not reach the ultimate stage, maximum observed values are reported.

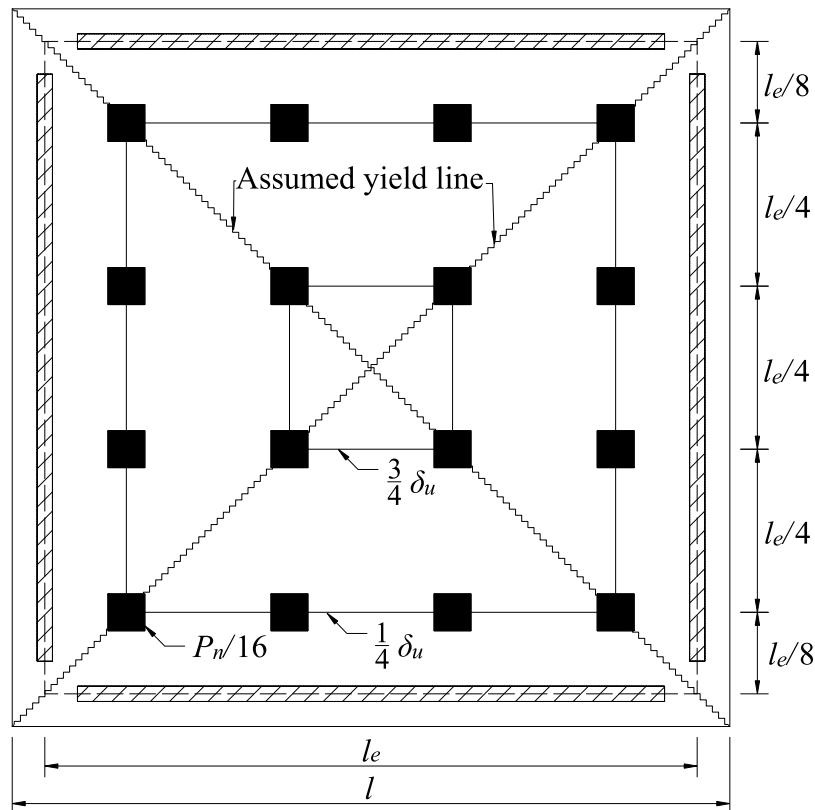


Figure 3.66 – Assumed Yield Line Pattern with Deformation Contour: 16-point Load

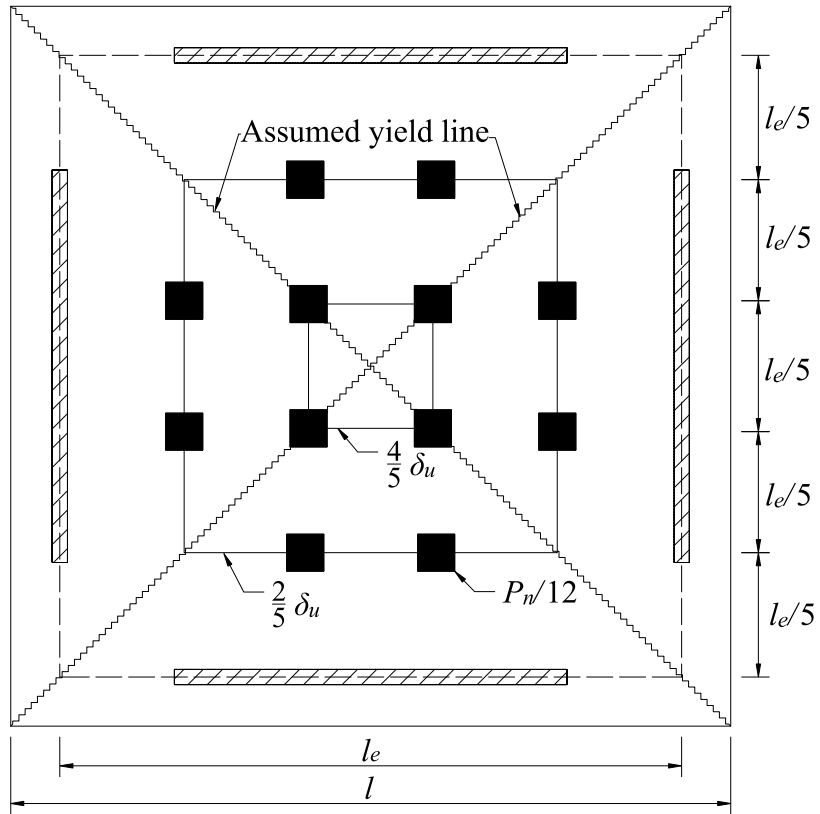


Figure 3.67 – Assumed Yield Line Pattern with Deformation Contour: 12-point Load

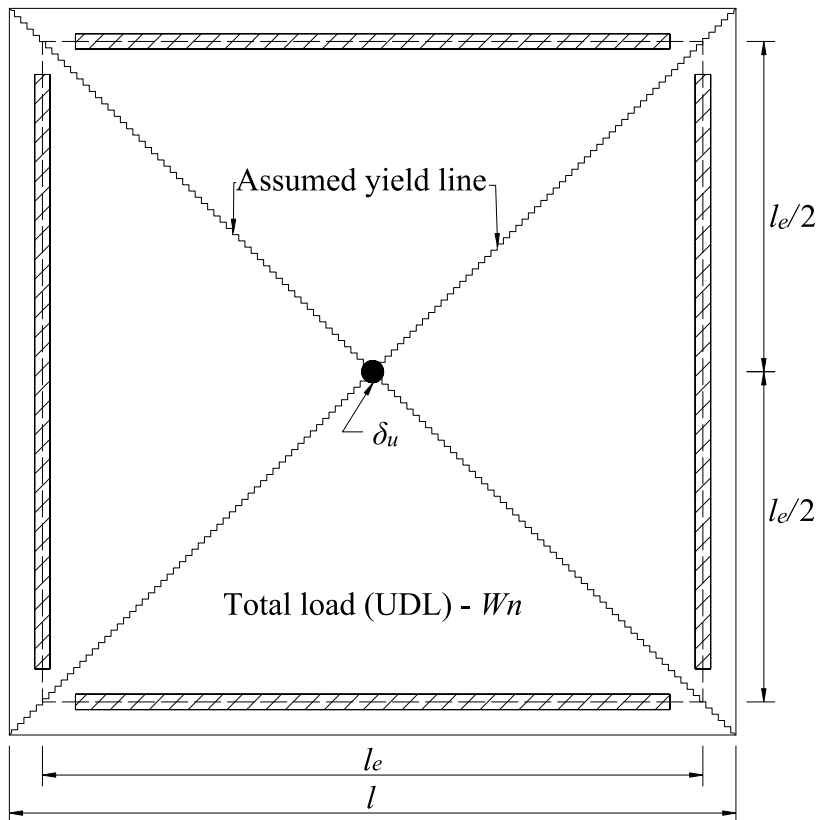


Figure 3.68 – Assumed Yield Line Pattern with Deformation Contour: UDL

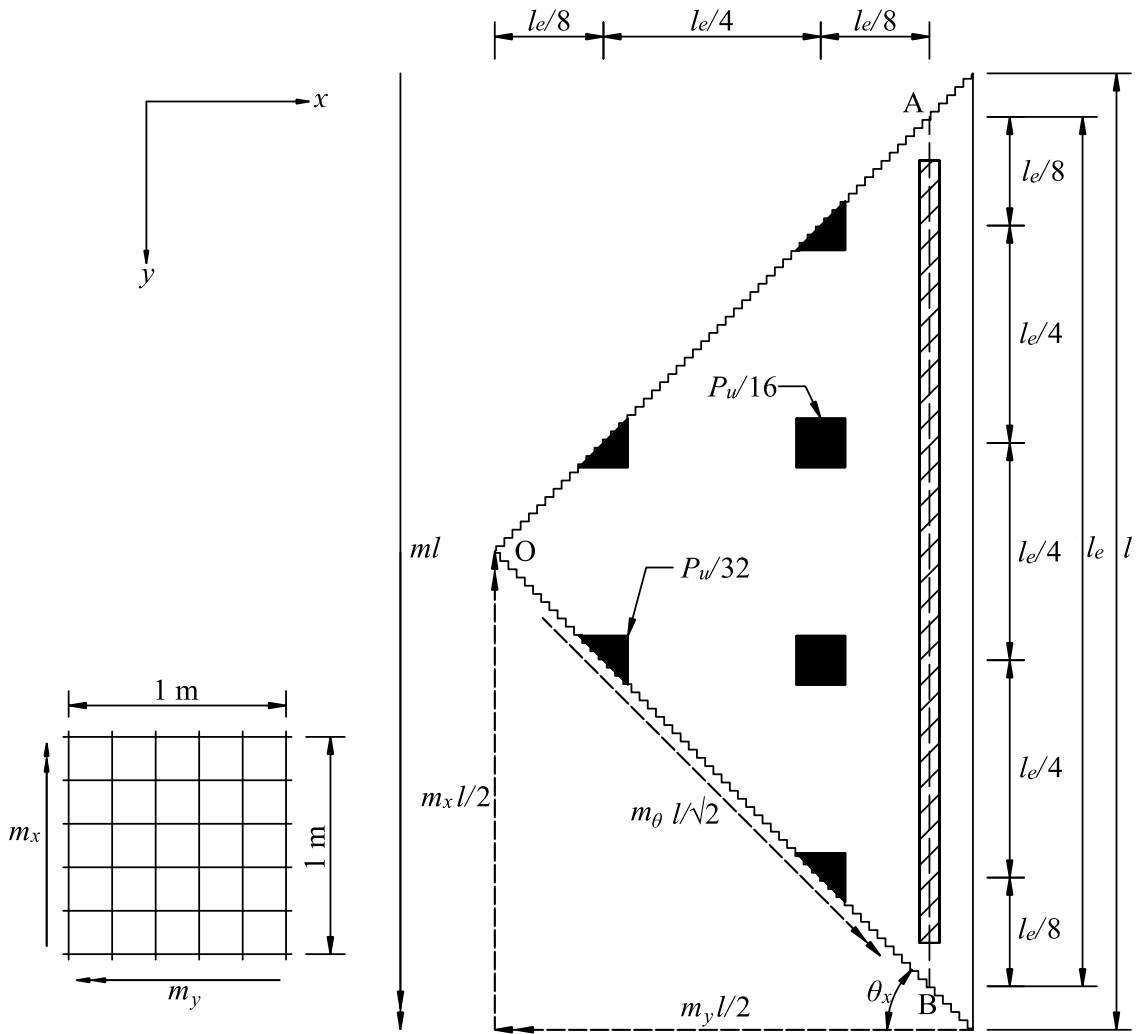


Figure 3.69 – Moment Capacity of a Yield Line and Application of Equilibrium of Slab Parts

The ultimate moment capacity per unit length of the yield line ( $m_\theta$ ) can be calculated by considering moment equilibrium in the direction of  $m_\theta$  (Figure 3.69) and given by Eq. 3.21.

$$m_\theta = m_x \sin^2 \theta_x + m_y \cos^2 \theta_x \quad \text{Eq. 3.21}$$

where,  $m_x$  and  $m_y$  are ultimate moment capacity of slab per unit length in  $x$  and  $y$  directions, respectively, and  $\theta_x$  is the inclination of yield line with respect to  $x$ -direction. As given in Table 3.9, the values of  $m_x$  and  $m_y$  are either equal or with a small difference (Eq. 3.22). The slab specimens are square-shaped, and reinforcements were arranged symmetrically in both longitudinal and transverse directions; hence the value of  $\theta_x$  can be assumed to be  $45^\circ$ . Based on Eq. 3.22 and the above-assumed value of  $\theta_x$ , the equation of flexural strength (Eq. 3.21) can be written as Eq. 3.23.

$$m_x = m_y = m \quad \text{Eq. 3.22}$$



$$m_{\theta} = m \quad \text{Eq. 3.23}$$

From Eq. 3.23, it can be interpreted that if the flexural capacity of slab per unit length is the same in the two orthogonal directions, then the flexural capacity of the slab will remain the same in any direction. The estimated capacity of slab section (Table 3.9) based on ACI 318 and IS 456 provision is observed to same as the yielding of reinforcement governs the failure, and the compressive strain in concrete is less than 0.002.

Yield line pattern with deformation contour for test configuration is shown in Figure 3.66. The moment developed by the externally applied load must be balanced by the component of the yield line moments, as shown in Figure 3.69.

$$\sum M_{AB} = 0 \Rightarrow \left( \frac{P_n}{16} \times \frac{3l_e}{8} \right) + \left( \frac{3P_n}{16} \times \frac{l_e}{8} \right) - m_{\theta}l = 0 \quad \text{Eq. 3.24}$$

From Eq. 3.24, the ultimate load-carrying capacity ( $P_n$ ) of the slab specimen is calculated as:

$$P_n = \frac{64m_{\theta}l}{3l_e} \quad \text{Eq. 3.25}$$

Similarly, for the slab subjected to 12-point load (Figure 3.67), the ultimate load-carrying capacity ( $P_n$ ) is derived as:

$$P_n = \frac{15m_{\theta}l}{l_e} \quad \text{Eq. 3.26}$$

Similarly, for the slab subjected to UDL (Figure 3.68), the ultimate load-carrying capacity ( $W_n$ ) is derived as:

$$W_n = \frac{24m_{\theta}l}{l_e} \quad \text{Eq. 3.27}$$

The expression for collapse load was derived based on the equilibrium of slab parts and given in Eq. 3.25, Eq. 3.26 and Eq. 3.27 for 16-point, 12-point and uniformly distributed loading type, respectively. It is observed that, if the ultimate deflection, moment capacity of slab and length remain the same in all the three loading types, then the ratio of UDL to 12-point load is

0.625. Similarly, the ratio of UDL to 16-point load is 0.89. Equivalent UDL values ( $W_u$  and  $W_n$ ) corresponding to 12-point and 16-point loads are computed based on these ratios as listed in Table 3.8 and Table 3.9. It is to be noted that the actual ultimate deflection may not be the same for different loading type. However, in this thesis, for comparison of the ultimate load carrying capacity of slab specimens with the different loading type is converted to equivalent UDL based on the above-estimated ratios.

Table 3.9 – Capacity of Slab by YLA

Reference	ID	Moment capacity, kN-m/m		Ratio	Load by YLA
		$m_x$	$m_y$	$\mu = m_x / m_y$	$W_n$ , kN
Taylor et al. 1966	S1	3.56	3.75	0.95	94.9
	S9	3.60	3.56	1.01	93.0
Brotchie and Holley 1971	12	3.07	3.07	1.00	77.4
	19	12.78	12.78	1.00	322.0
Chung et al. 2018b	Solid	70.59	70.59	1.00	1961.7
	TF-D-S-P.P	70.59	70.59	1.00	1961.7
	TF-D-M-P.P	70.59	70.59	1.00	1961.7
Current study	TF-Solid	23.96	24.17	0.99	635.3
	TF-S90V	23.94	24.15	0.99	634.8
	TF-S180V	31.51	31.12	1.01	826.7
	TF-CV-2	32.27	33.68	0.96	870.5
	TF-CV-3	32.20	33.61	0.96	868.7

### 3.3.2.2 Tensile Membrane Action in Slabs

The theoretically predicted ultimate load of the slab by yield line method is usually lesser than the experimental value; the same is observed in this study as well. The difference is mainly due to the effects of tensile membrane (TM) action, which developed post-yield stage at large deflection and effects of strain hardening in reinforcements. Depending on the magnitude of these effects, the predictions of yield line theory can underestimate the ultimate capacity of the slab. Various researchers attempted to develop a relationship between deflection and ultimate load, which accounts for load enhancement due to tensile membrane action. In this study, the

load enhancement factor is calculated based on the theory developed by Bailey (2001). The key parameters are summarised below.

The load enhancement factor ( $e$ ) is expressed as the sum of enhancement factor due to membrane forces ( $e_m$ ) and enhancement factor due to bending action ( $e_b$ ) as follows:

$$e_m = \frac{2b}{3(3+g_0)} \left( \frac{w}{d_{e,n}} \right) \quad \text{Eq. 3.28}$$

$$e_b = 1 - \frac{b^2(1-g_0)}{3(3+g_0)} \quad \text{Eq. 3.29}$$

$$e = e_m + e_b \geq 1.0 \quad \text{Eq. 3.30}$$

where,  $b$  is parameter defining the magnitude of membrane force given by Eq. 3.31,  $g_0$  is a parameter to fix the depth of compressive stress block when no membrane force is present,  $w$  is the deflection of yield line and  $d_{e,n}$  is the effective depth of the slab.

$$b = 1.5 \left( \frac{f_u}{f_y} \right) \quad \text{Eq. 3.31}$$

where,  $f_u$  and  $f_y$  are ultimate and yield stress of reinforcement, respectively.

The calculated load enhancement factor for all twelve tested specimens are summarised in Table 3.10. The enhancement factor is based on the deflection observed at maximum load in the experiment (Table 3.7).

### 3.3.2.3 Effect of Reinforcement Orientation

Based on the test results of various researchers explained in Section 2.3.4, the enhancement factor ( $f_o$ ) to account for the effect of reinforcement orientation is taken as 1.15. The effect of reinforcement orientation may not be significant if the slab is not undergoing large displacement or plastic rotation which will take place along with tensile membrane action alone. Hence, if the enhancement factor ( $e$ ) is equal to unity, then the factor ( $f_o$ ) is also equal to unity. This implies that the effects of tensile membrane action and reinforcement orientation are mutually influencing. However, the mutual influence observation needs to be validated with more experiments with different reinforcement orientation. After including the effects of tensile membrane action and reinforcement orientation on the estimated capacity by YLA closely matches with experimentally observed capacity with a mean ( $W_u/W_{n2}$ ) of 1.086 (Table 3.10).

Table 3.10 – Experimental and estimated capacity comparison

Reference	ID	Experiment results $W_u$ , kN	Capacity by YLA $W_n$ , kN	Factor $e$	Capacity with TM $W_{n1}$ , kN	Rein. Oren. Factor $f_o$	Net capacity $W_{n2}$ , kN	Ratio $W_u/W_{n2}$
Taylor et al. 1966	S1	166	94.9	1.607	153	1.15	175	0.95
	S9	151	93.0	1.391	129	1.15	149	1.01
Brotchie and Holley 1971	12	81	77.4	1.000	77	1.00	77	1.05
	19	326	322.0	1.000	322	1.00	322	1.01
Chung et al. 2018b	Solid	2039	1961.7	1.000	1962	1.00	1962	1.04
	TF-D-S-P.P	1934	1961.7	1.000	1962	1.00	1962	0.99
	TF-D-M-P.P	2018	1961.7	1.000	1962	1.00	1962	1.03
Current study	TF-Solid	1160	635.3	1.184	752	1.15	865	1.34
	TF-S90V	1169	634.8	1.185	752	1.15	865	1.35
	TF-S180V	1386	826.7	1.169	966	1.15	1111	1.25
	TF-CV-2	1082	870.5	1.064	926	1.15	1065	1.02
	TF-CV-3	1048	868.7	1.060	921	1.15	1059	0.99
Average								1.086
Standard Deviation								0.136
Coefficient of Variation								0.125

### **3.4 Summary**

In this chapter, the results of full-scale specimens tested under one-way and two-way flexure are discussed. It is evidenced that the voids do not have a significant effect on the ultimate load-carrying capacity. However, as the concrete area reduces due to the presence of voids, the initial flexural stiffness of biaxial voided slab is observed to be lesser than that of a solid slab. The stiffness and load-carrying capacity is estimated based on the yield line analysis and found that the conventional design and analysis procedure available for solid slab can be used for biaxial voided slab as well by incorporating a necessary correction for the presence of voids. In case of two-way flexure, the beneficial effect of tensile membrane action at large deflection is observed to be applicable for biaxial voided slab like solid slab, which is evidenced based on the twelve specimens data (five – current study and seven – reported in the literature). In addition, the comparison of experimental and analytical results shows that the ultimate capacity can be predicted by yield line analysis including the effects of tensile membrane action and reinforcement orientation.

This page is intentionally left blank.

## CHAPTER 4

### BEHAVIOUR OF VOIDED SLABS IN PUNCHING SHEAR

#### 4.1 Overview

This chapter explains the experiments that are carried out to study the structural behaviour of biaxial voided slab subject to concentrated load (punching shear). Under the heading of the experimental study (Section 4.2), the details of void formers, test specimens, test set-up, instrumentation, loading procedure and observed test results are summarised. Similarly in Section 4.3, the applicability of the existing procedure to obtain the punching shear capacity of solid slab given in ACI 318 (2014), EN 1992-1-1 (2004) and IS 456 (2000) to the biaxial voided slab is explained with the test results of the current study and reported in the literature.

#### 4.2 Experimental Study

In this section, the details of the void formers, specimen details, materials' properties, test set-up, instrumentation, test procedure and experimental observations & results are explained.

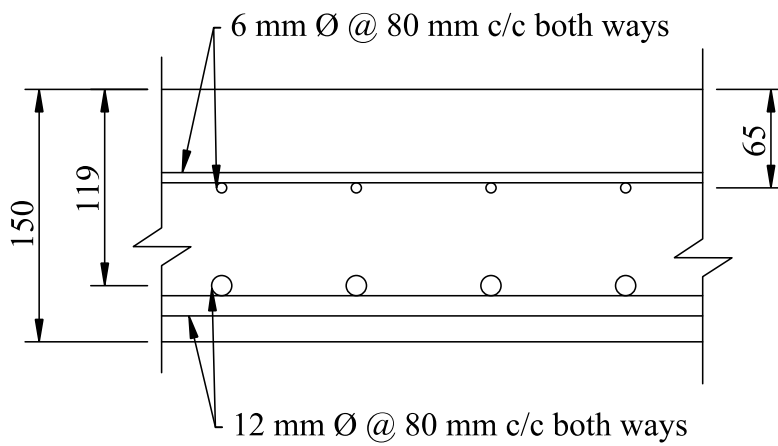
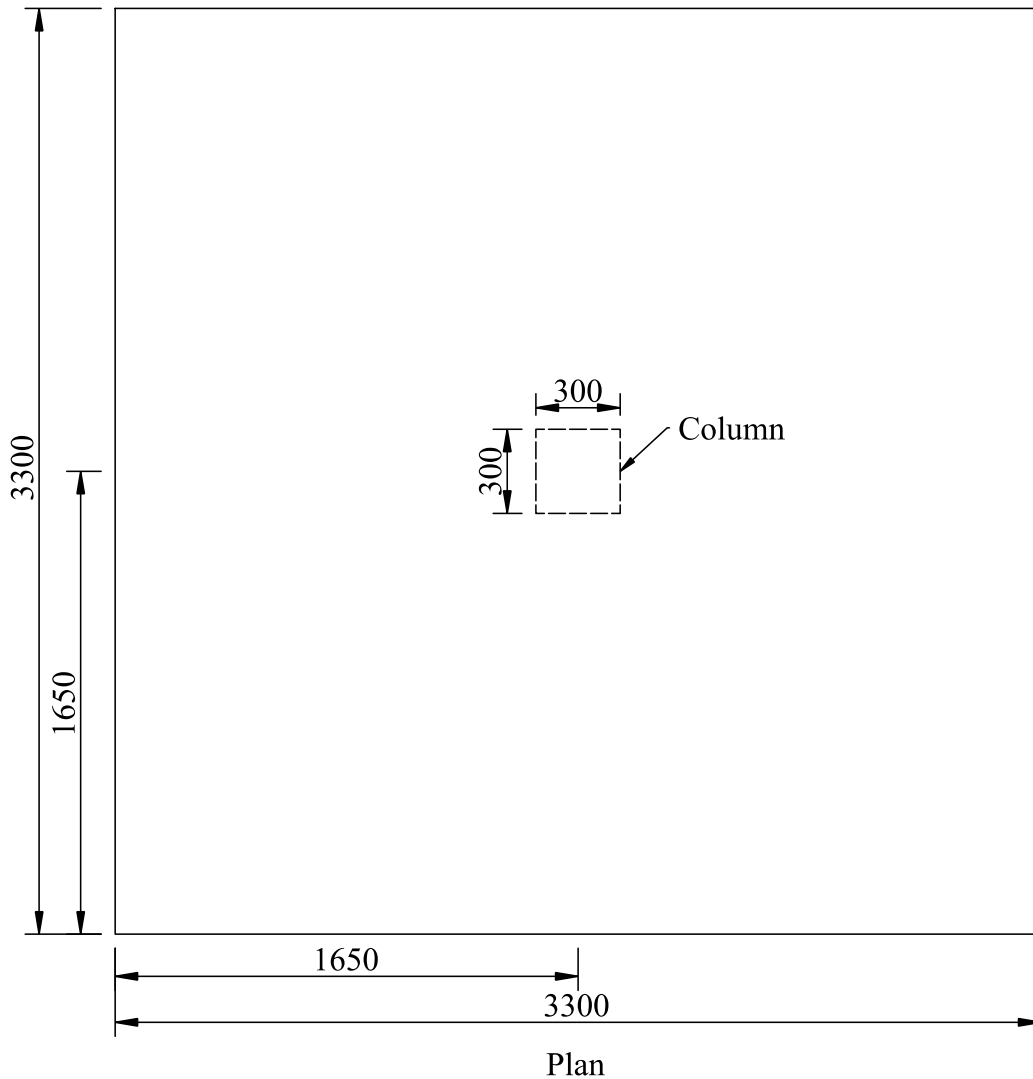
##### 4.2.1 Details of Void Formers

Void formers of sphere and cuboid, manufactured from recycled polypropylene were used to cast the voided slab specimens. The specifications of the void formers are explained in Section 3.2.1.

##### 4.2.2 Details of Test Specimens

In total eight specimens were tested under punching shear (single point load) – one RC solid slab, four sphere and three cuboid voided slabs. The overall plan dimensions of punching shear test specimens were 3300 mm × 3300 mm. The detailed specifications about test specimens such as dimensions, cross-section and reinforcement details are summarised in Table 4.1. The reinforcement was arranged as top and bottom mesh in longitudinal and transverse directions, such that the voids can be placed between the reinforcement gauges. The detailed arrangement of reinforcement and void formers are shown in Figure 4.1 – Figure 4.6. The column was reinforced with four numbers of 16 mm diameter bars in the longitudinal direction and 8 mm diameter stirrup at 50 mm c/c. The column was cast monolithically with the slab to simulate

actual site condition. For all type of voided slab, reference solid slab specimens were not cast and tested as the maximum lifting capacity of crane facility available is 5 ton.

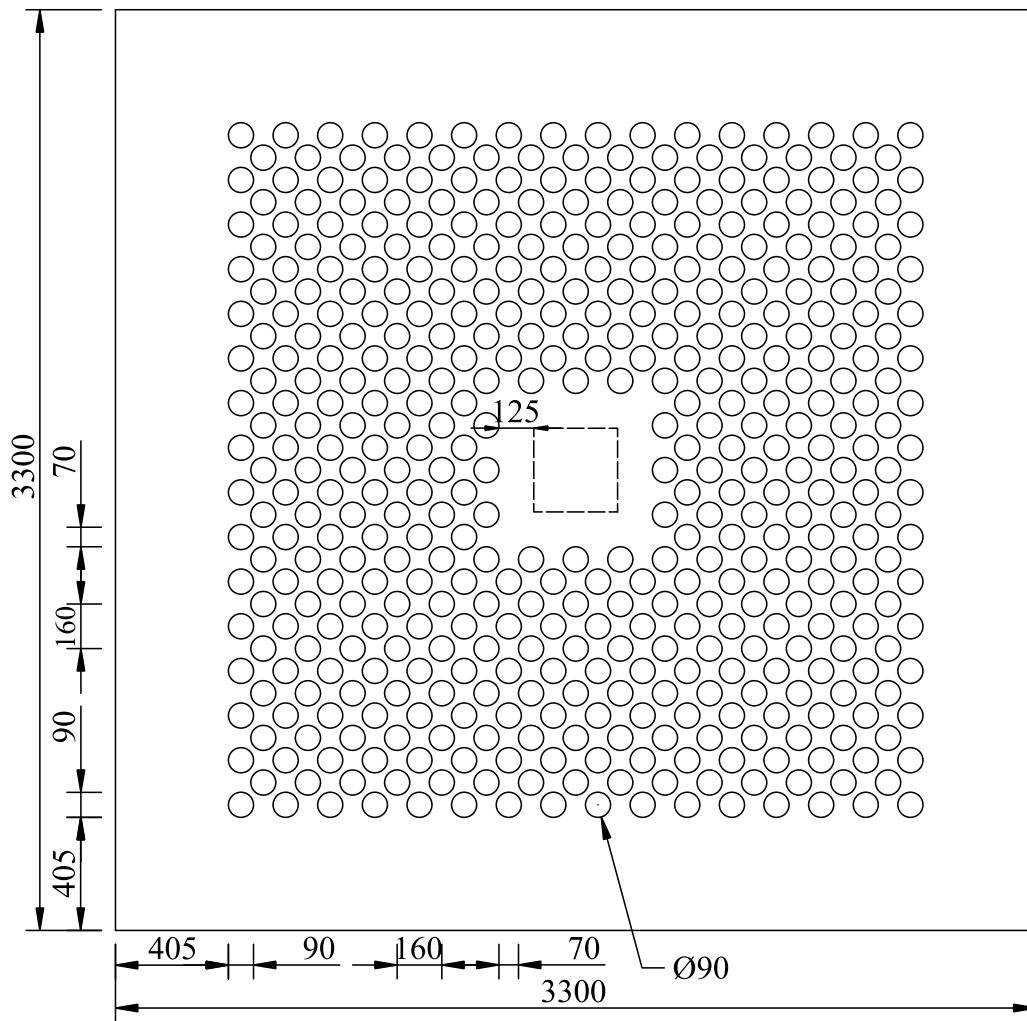


Typical Section

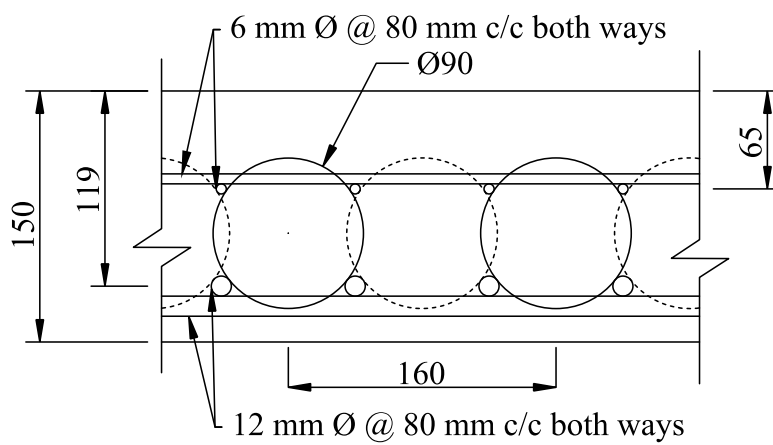
All dimensions are in mm

Figure 4.1 – Details of Test Specimen S





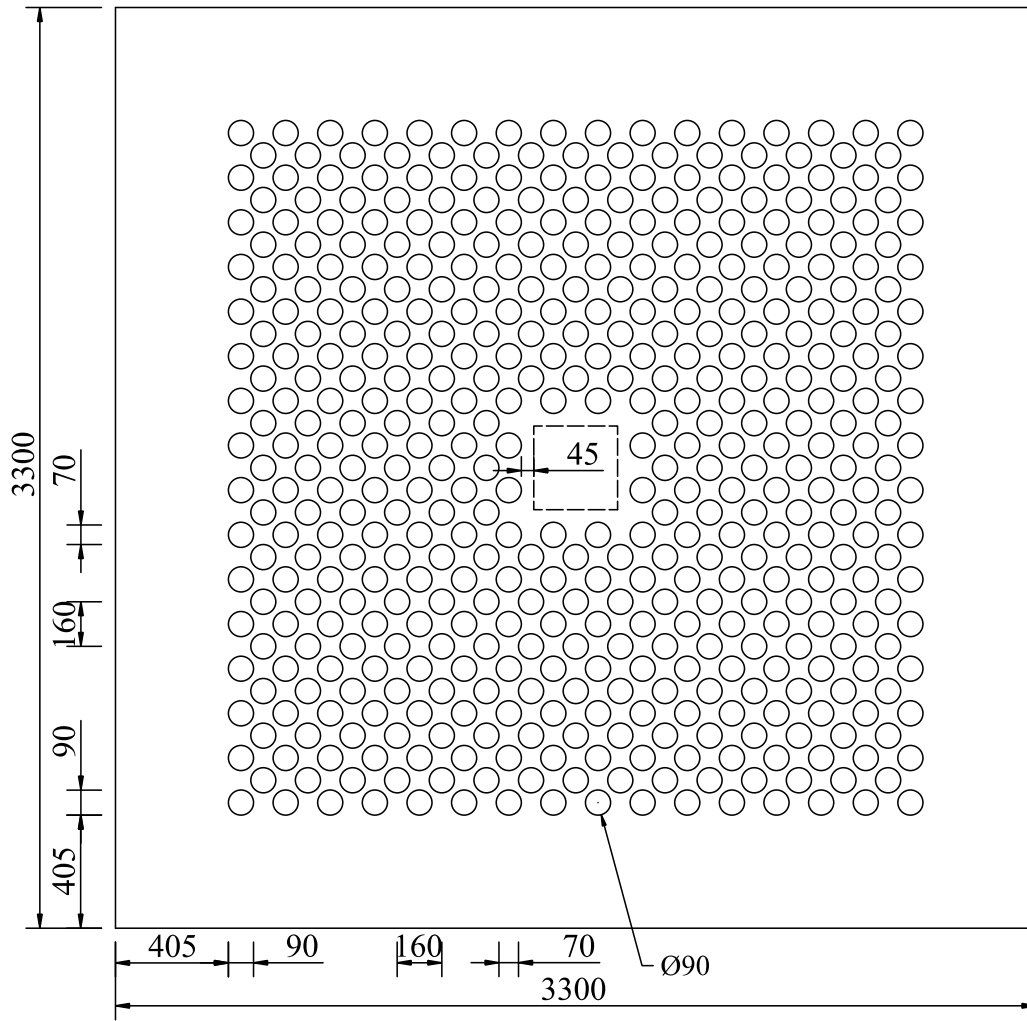
Plan



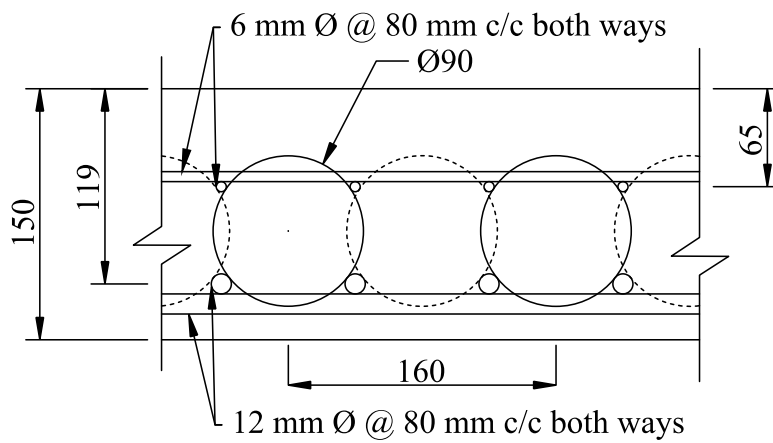
Typical Section

All dimensions are in mm

Figure 4.2 – Details of Test Specimen V1



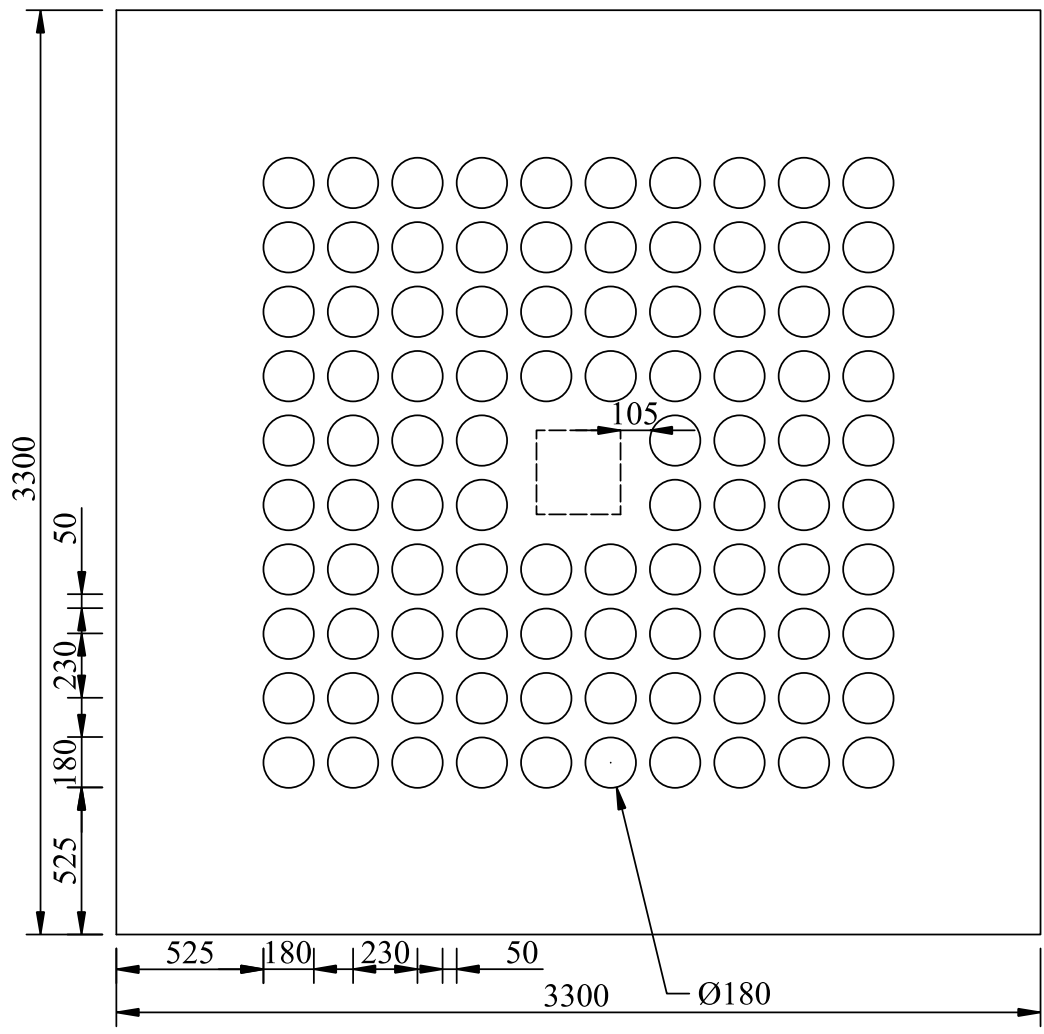
Plan



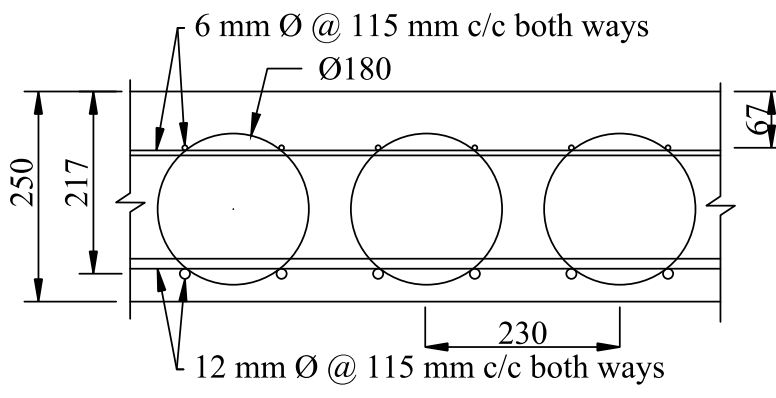
Typical Section

All dimensions are in mm

Figure 4.3 – Details of Test Specimen V2



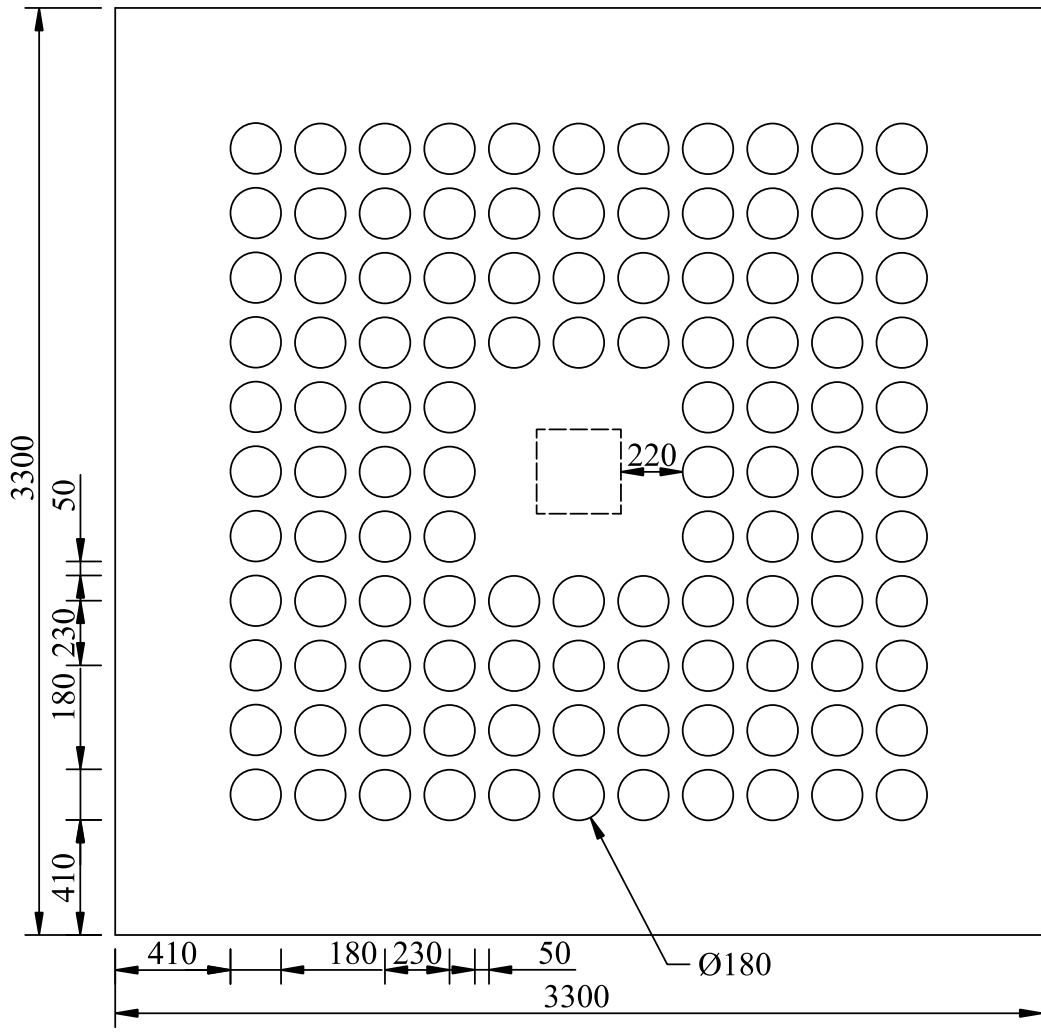
Plan



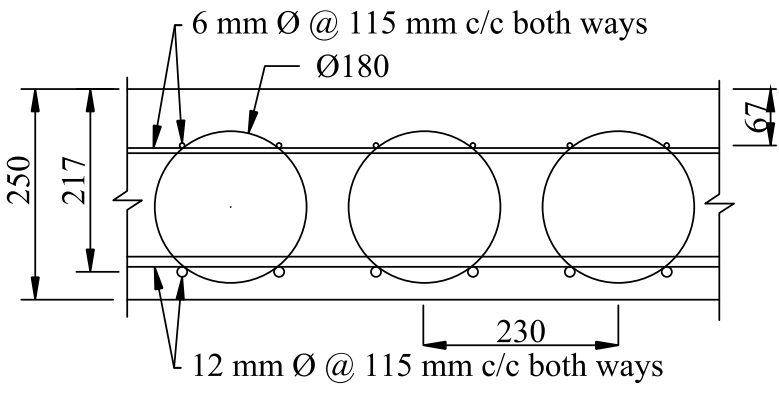
Typical Section

All dimensions are in mm

Figure 4.4 – Details of Test Specimen V3



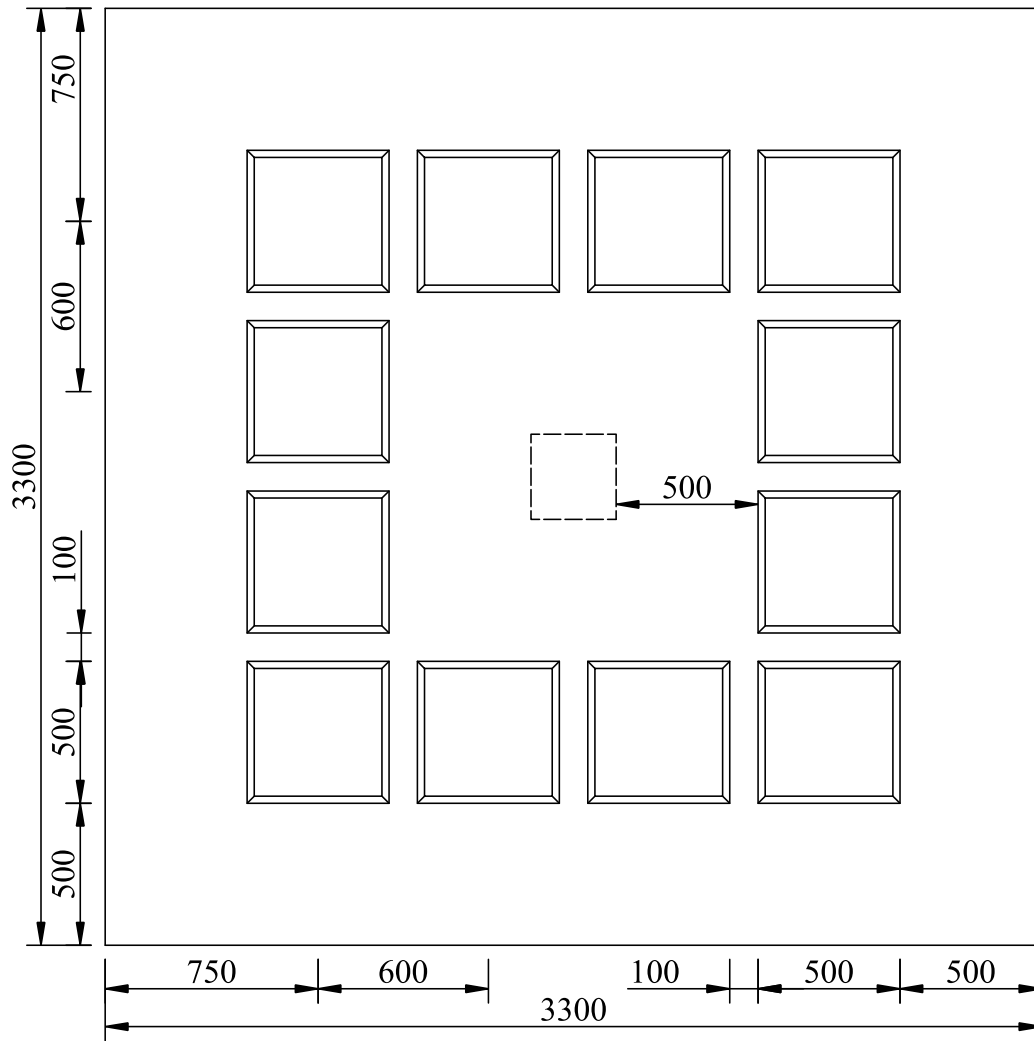
Plan



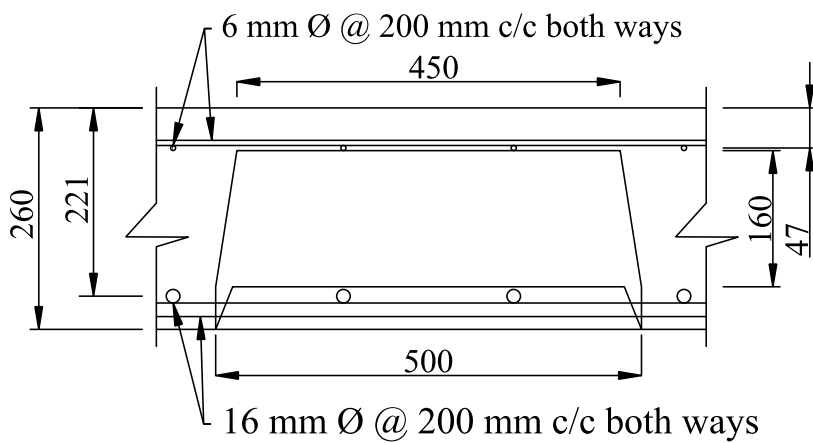
Typical Section

All dimensions are in mm

Figure 4.5 – Details of Test Specimen V4



Plan



Typical Section

All dimensions are in mm

Figure 4.6 – Details of Test Specimen V5 – V7

Table 4.1 – Details of Punching Shear Test Specimens

ID	Void location	Void details	Dimension (mm)	$A_{st}$ (mm <sup>2</sup> /m)		$f_{cm}$ (N/mm <sup>2</sup> )
				Top	Bottom	
S	–	–				28.1
V1	1.05 <i>d</i>	Ø 90 mm Sphere	3300 × 3300 × 150	353	1413	28.1
V2	0.38 <i>d</i>					28.1
V3	0.51 <i>d</i>	Ø 180 mm Sphere	3300 × 3300 × 250	246	983	26.7
V4	1.07 <i>d</i>					26.7
V5						25.0
V6	2.26 <i>d</i>	Cuboid	3300 × 3300 × 260	141	1005	25.0
V7						25.0

Note: The given void location is from the face of the column.

#### 4.2.2.1 Material Properties

The specimens were cast using concrete, with mix proportion of 1 : 2.25 : 4.5 (cement : fine aggregate : coarse aggregate) with a water-cement ratio of 0.55. Cube specimens were cast with a size of 150 mm and cured under similar exposure condition as that of slab specimens. The compression test on cubes was carried out simultaneously with the flexure test on the companion slab specimen. The observed mean compressive strength for each test specimen is summarised in Table 4.1. Likewise, the nominal yield strength of the selected reinforcement of size 6 mm, 12 mm and 16 mm diameter was 500 N/mm<sup>2</sup>, conforming to IS 1786 (2008). Tensile tests of reinforcement were conducted as per IS 1608 (Part 1) 2018, and the properties are summarised in Table 4.2. The idealised stress-strain behaviour of the reinforcements is shown in Figure 4.7.

Table 4.2 – Mechanical Properties of Reinforcement

Reinforcement diameter (mm)	Strength (N/mm <sup>2</sup> )			Strain (%)	
	Nominal	Yield	Ultimate	Yield	Ultimate
6	500	545	643	0.33	6.11
12	500	582	664	0.35	9.28
16	500	528	625	0.37	10.47

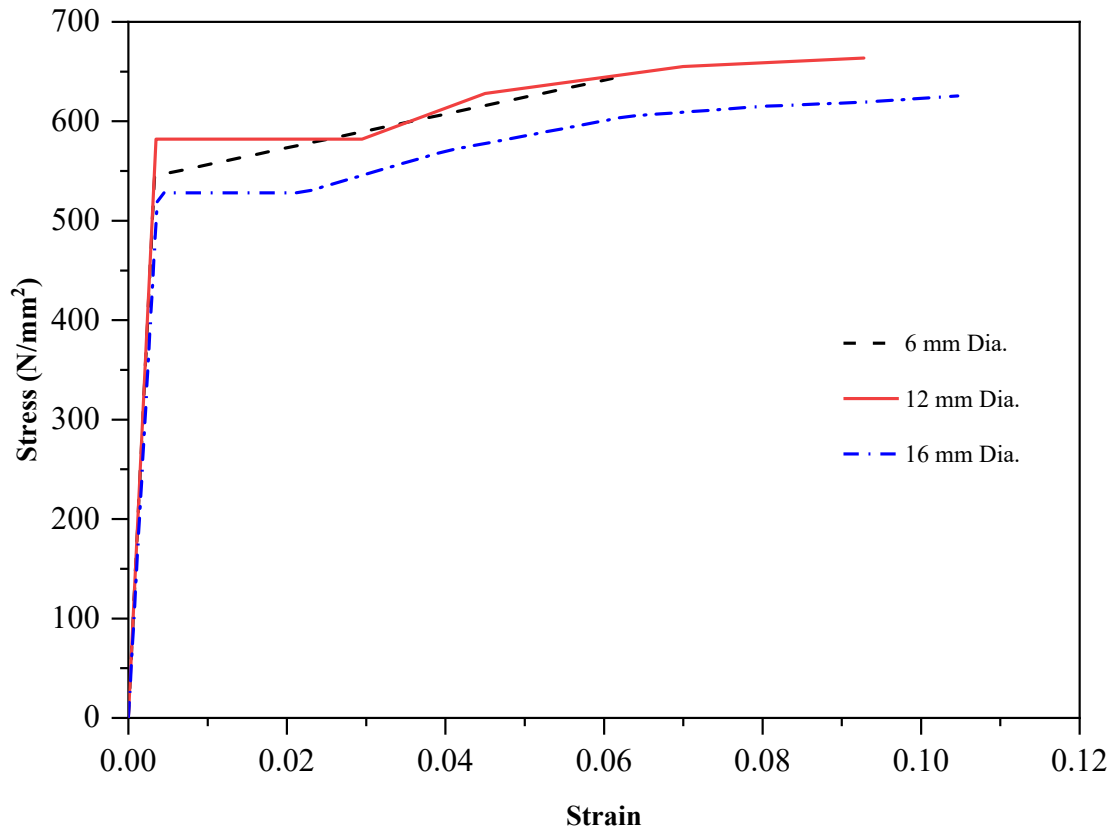


Figure 4.7 – Idealised Stress versus Strain Behaviour of Reinforcements

#### 4.2.2.2 Casting of Specimens

Reinforcement gauge was prepared as per the details given in Table 4.1 and Figure 4.1 – Figure 4.6. Various stages of specimens casting are shown in Figure 4.8 – Figure 4.11.



Figure 4.8 – Punching Shear Test Specimen V1



Figure 4.9 – Punching Shear Test Specimen V3





Figure 4.10 – Punching Shear Test Specimen V5



Figure 4.11 – Typical Punching Shear Test Specimen after Cast

### **4.2.3 Test Set-up and Instrumentation**

#### **4.2.3.1 Punching Shear: Phase I**

In Phase I of punching shear test, sphere voided slab specimens (V1 – V4) along with reference solid slab specimen (S) were tested.

**(i) Test Set-up**

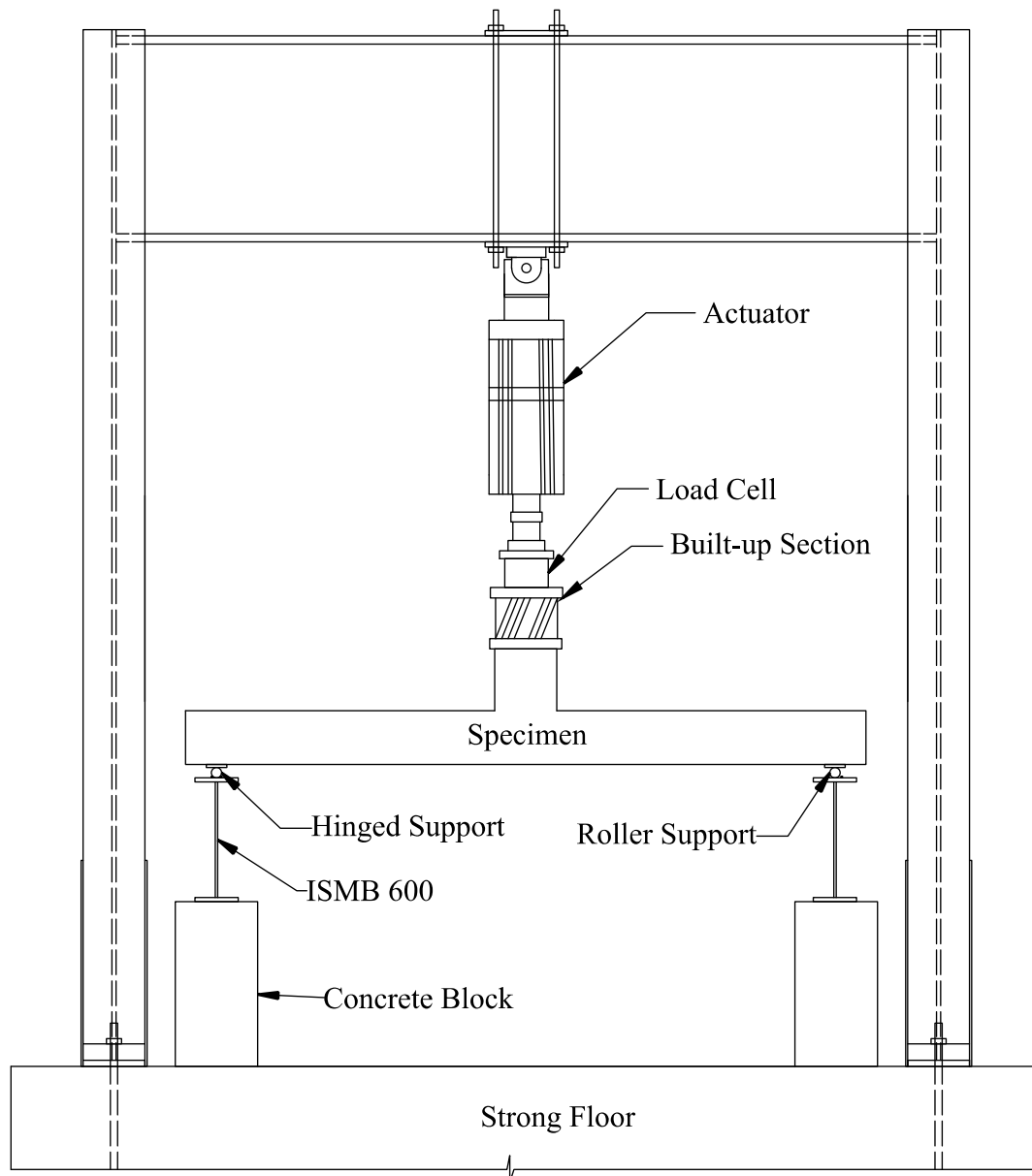


Figure 4.12 – Schematic Test Set-up (Punching Shear) – Phase I

A single-point load test was conducted to study the punching shear behaviour of the slab. Figure 4.12 shows the schematic test set-up. The photograph of the erected test set-up is shown in Figure 4.13. The point load was applied through the column of size 300 mm × 300 mm located at mid-span, as shown in Figure 4.14. The load was applied using a pseudo-dynamic hydraulic actuator of 1000 kN capacity. The load was transferred through hot rolled steel section to the column of slab specimens. The slab specimens were supported at its all four sides using line-type reaction hinge of length 2800 mm, and the location of support was 150 mm from specimen edges. The discontinuity of supports at corner minimises the experimental

errors such as the stress concentration and generation of fixed end moment, from the support condition (Chung et al. 2018).

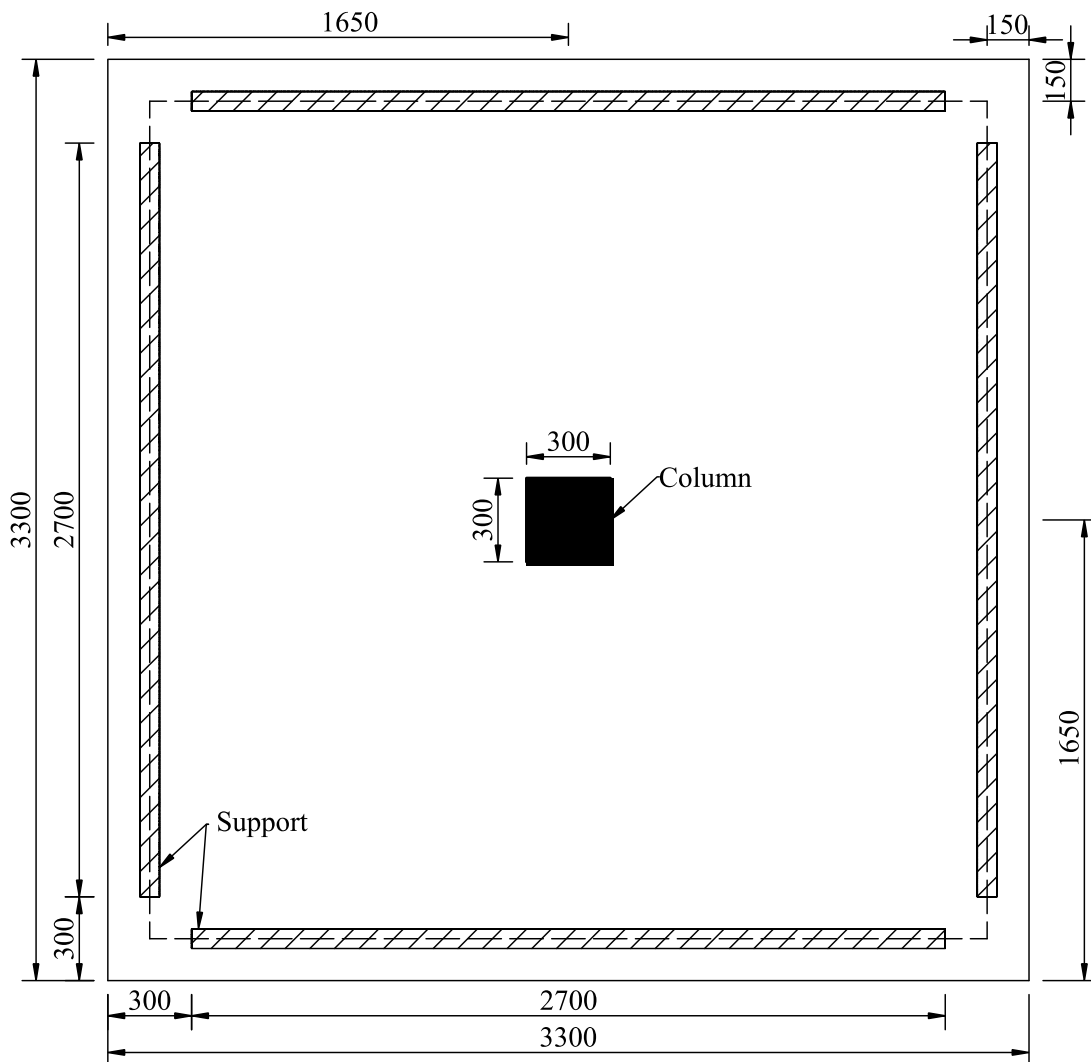


Figure 4.13 – Punching Shear Test Set-up: Phase I

### **(ii) Instrumentation**

Applied load, deflections, and strain in reinforcements were measured through appropriate instruments. Load-cells with a capacity of 1000 kN were used to measure the applied load. One LVDT with a measurement range of  $\pm 100$  mm were used to measure the deflections at mid-span. Four LVDTs with a measurement range of  $\pm 100$  mm were used to measure the deflections at one-fourth span of the slab. The corner uplift, translations in lateral and longitudinal directions were measured using three LVDTs with a measurement range of  $\pm 20$  mm. Figure 4.15 shows the schematic arrangement of LVDTs. Strain in the bottom reinforcements located at the centre of slab specimens was measured by strain gauges with 10 mm gauge length. Strain gauges were provided in the longitudinal and transverse direction of bottom reinforcements, as shown in Figure 4.15. A data acquisition system was used to obtain

real-time experimental data which has the facility to record the load, deflection, and strain simultaneously.

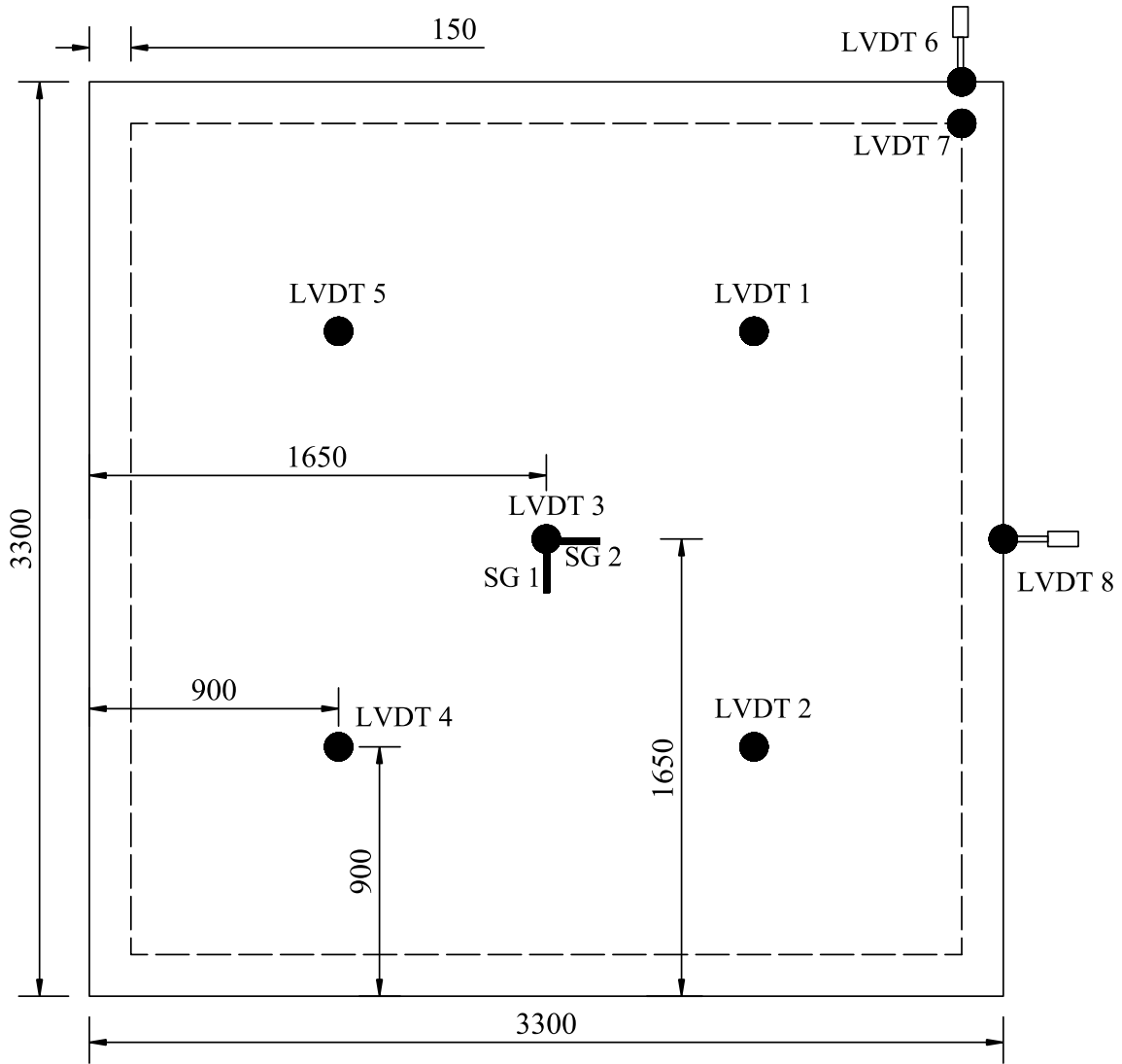


All dimensions are in mm

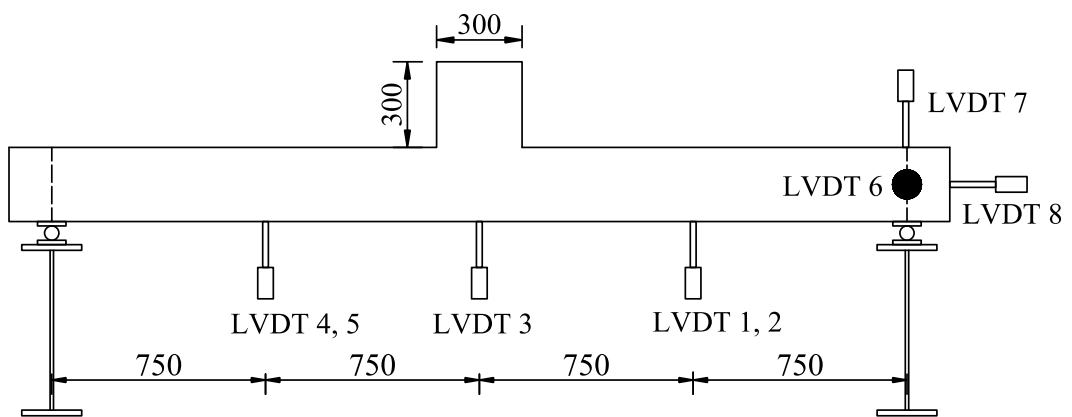
Figure 4.14 – Position of Point Load (Column)

### (iii) Testing Procedure

Displacement controlled monotonic tests were performed with a pseudo-dynamic hydraulic actuator of the capacity of 1000 kN. The rate of loading was 0.05 mm/sec. The test was terminated at ultimate failure (due to punching shear) as it ensures the safety of measuring and loading devices.



(a) LVDTs and strain gauge location (plan)



(b) LVDTs location (elevation)

All dimensions are in mm

Figure 4.15 – Instrumentation of Test Specimen (Punching Shear Test) – Phase I

#### 4.2.3.2 Punching Shear: Phase II

In Phase II of punching shear test, cuboid voided slab specimens (V5 – V7) were tested.

##### (i) Test Set-up

The test set-up remains the same as explained earlier in Phase I of punching shear test except the loading device. Two 500 kN capacity pseudo-dynamic hydraulic actuators were used to apply the load. Figure 4.16 shows the schematic test set-up. The photograph of the erected test set-up is shown in Figure 4.17

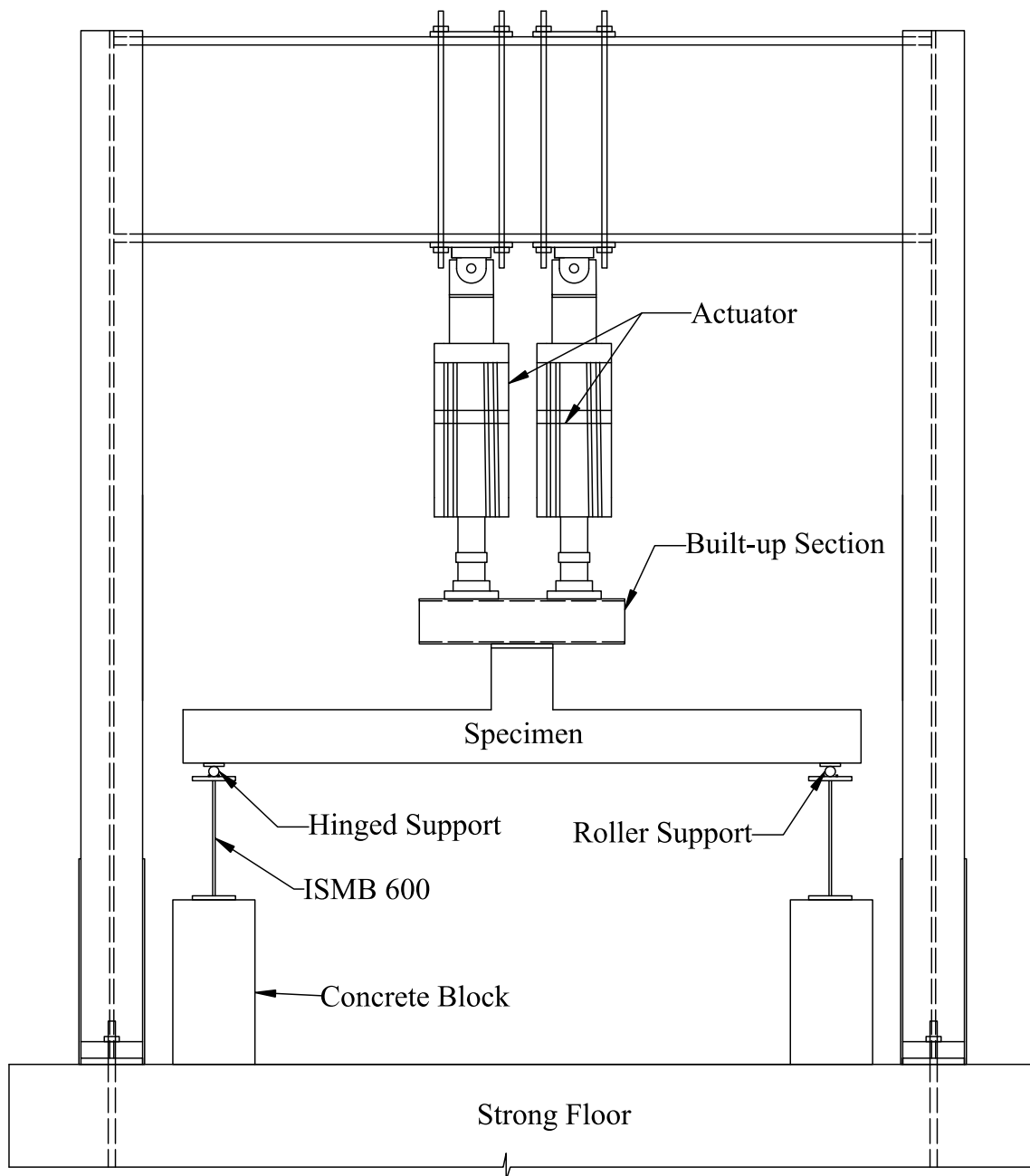


Figure 4.16 – Schematic Test Set-up (Punching Shear) – Phase II



Figure 4.17 – Punching Shear Test Set-up: Phase II

### **(ii) Instrumentation**

The instrumentation remains the same as explained earlier in Phase I of punching shear test except the load measurement method. In-built load-cells of actuators were used to measure the applied load.

### **(iii) Testing Procedure**

Displacement controlled monotonic tests were performed with two pseudo-dynamic hydraulic actuators. Equal load distribution across each actuator was ensured by synchronising the actuators and operating with a single master control system. The rate of loading was 0.05 mm/sec. The test was terminated at ultimate failure (due to punching shear) as it ensures the safety of measuring and loading devices.

## 4.2.4 Results and Discussion

### 4.2.4.1 Load Deflection Behaviour

All slab specimens showed typical punching shear failure. The load versus mid-span displacement for all the tested specimens is shown in Figure 4.18 – Figure 4.20. By comparing the plots for voided slab specimen V1 and reference solid slab S, it can be observed that both the specimens show nearly identical load-displacement behaviour. Such an observation can also be made from the experimental test data (PS and PD-N-4) of Chung et al. (2018). This is reasonable because, after cracking, a little portion of the void is expected to be present above the neutral axis in low reinforced members like slabs. A clear illustration of this behaviour has been observed in two-way flexure tests as well. However, specimen V2 showed a flexible response in comparison to the solid slab S. The reduced stiffness is attributed to higher stress concentrations due to the presence of voids (at  $0.38d$ ) near to the column. The load versus displacement for all the tested specimens is shown in Figure 4.21 – Figure 4.28.



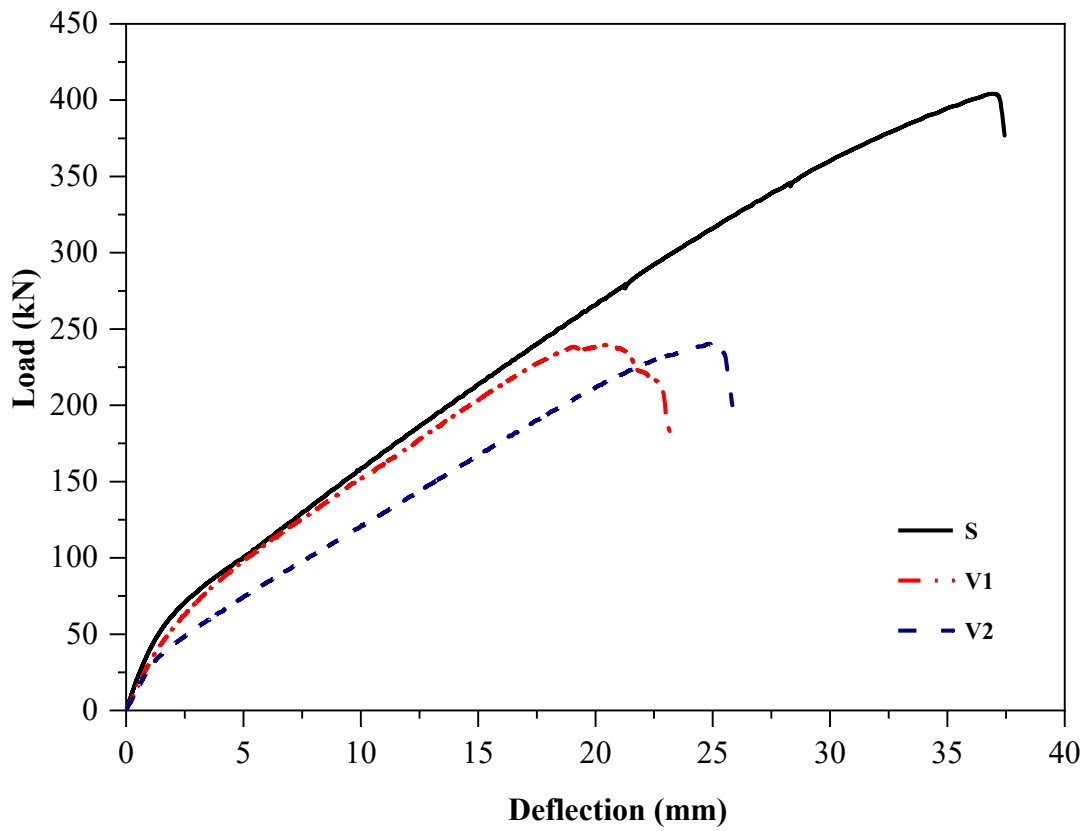
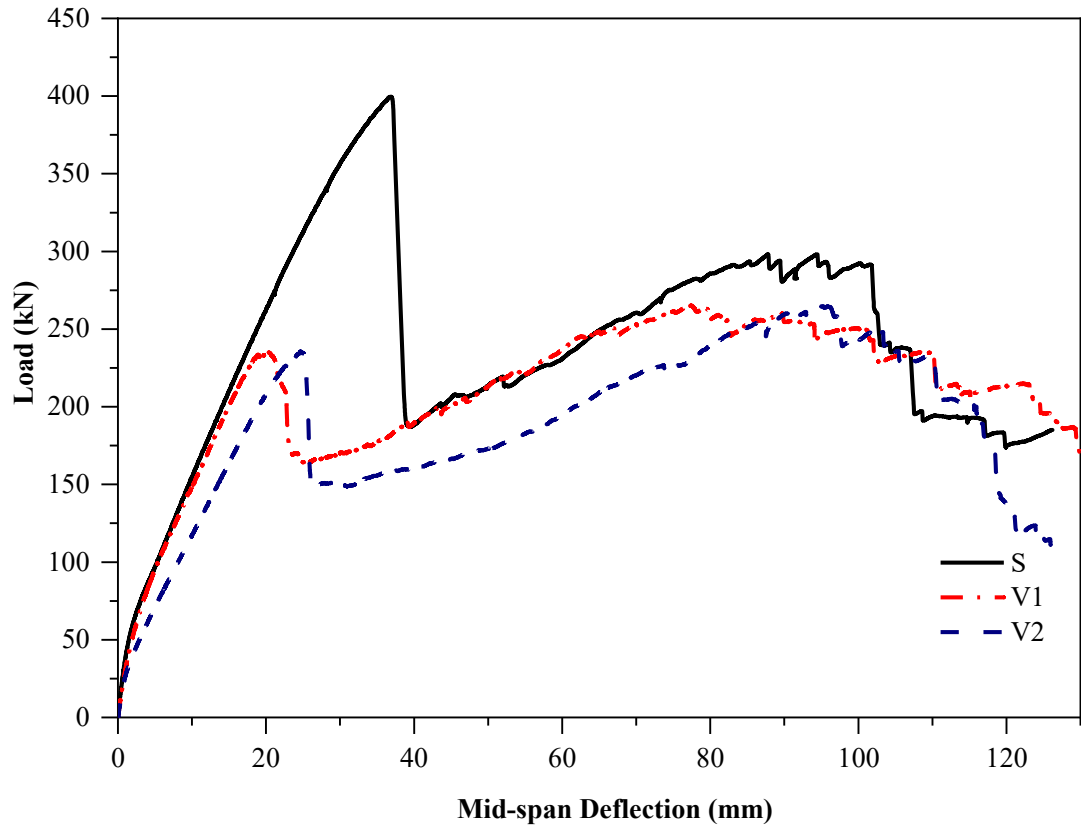


Figure 4.18 – Load versus Mid-span Deflection of Specimens S, V1 and V2

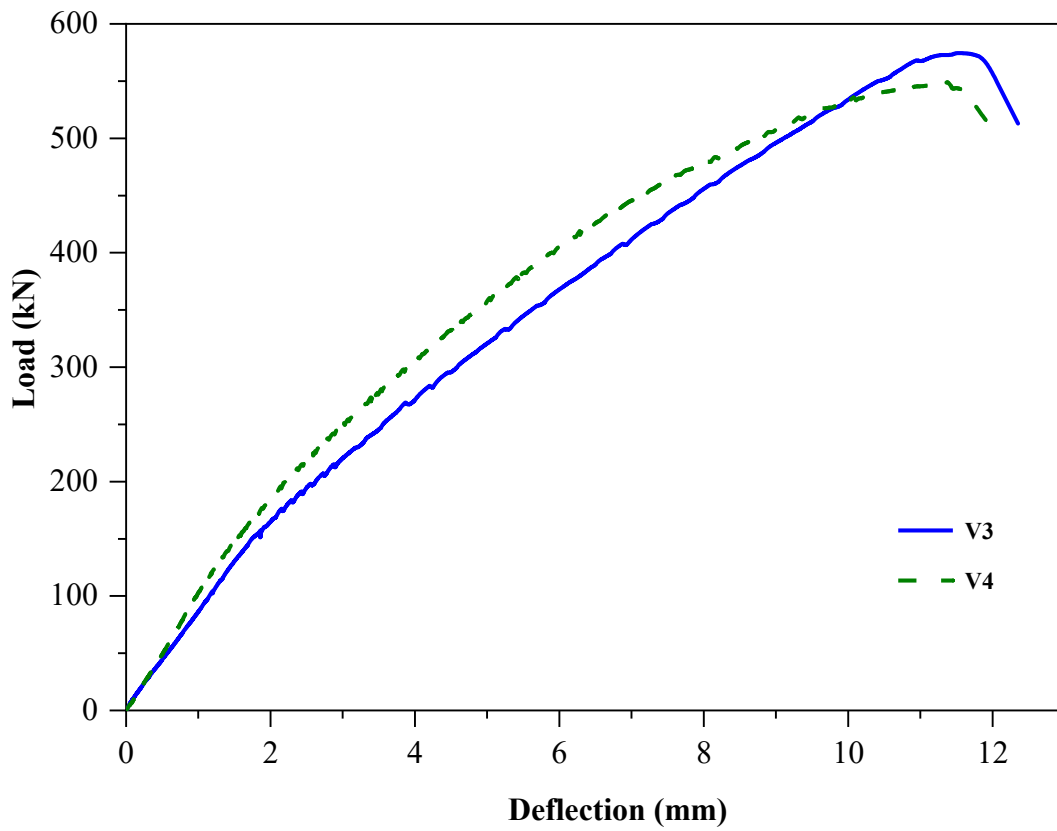
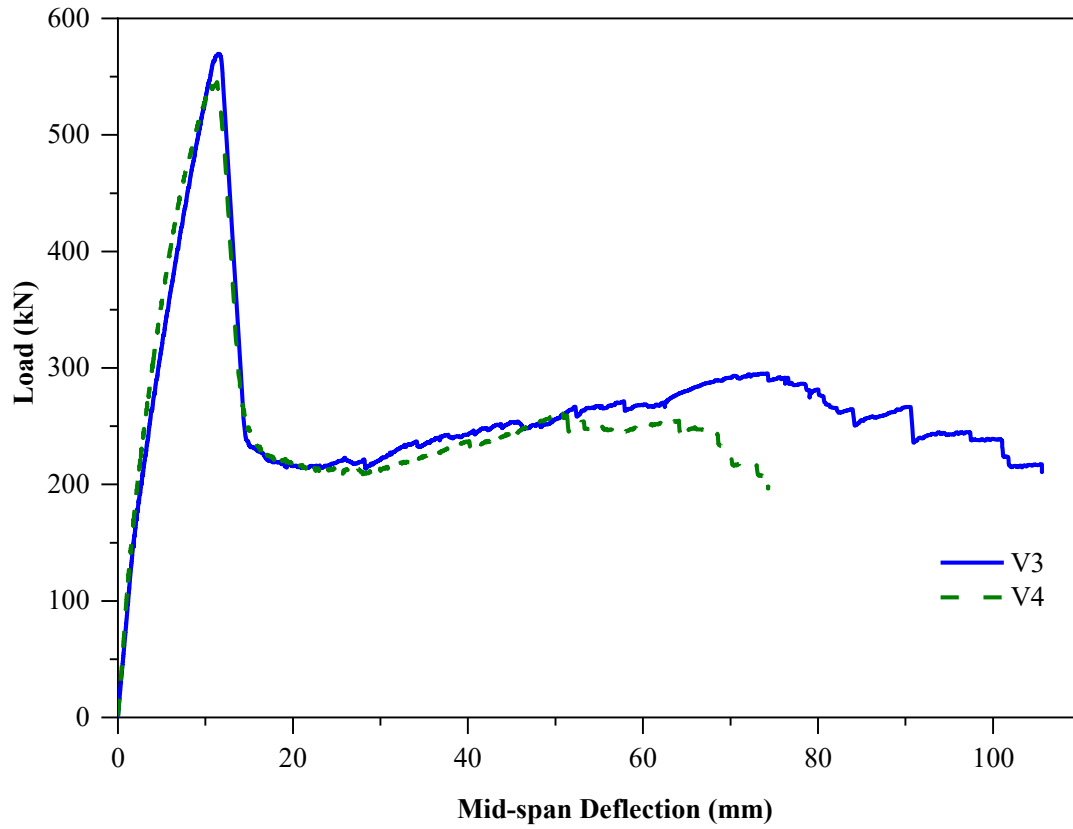


Figure 4.19 – Load versus Mid-span Deflection of Specimens V3 and V4

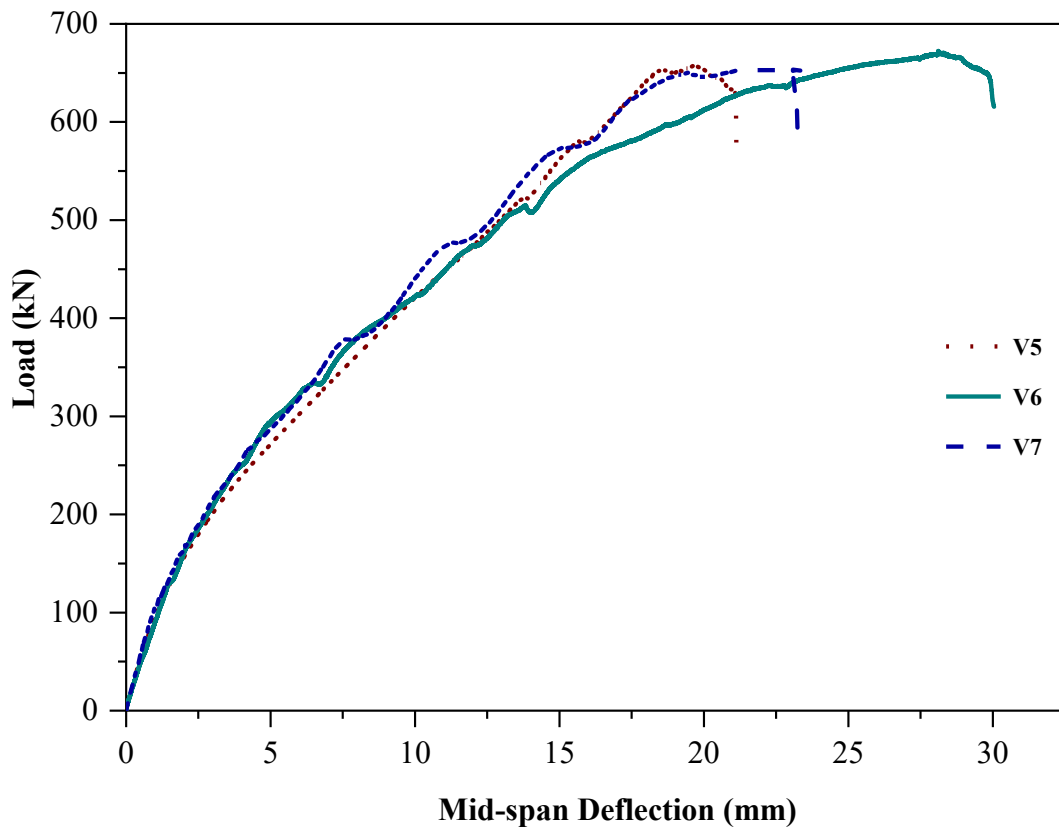
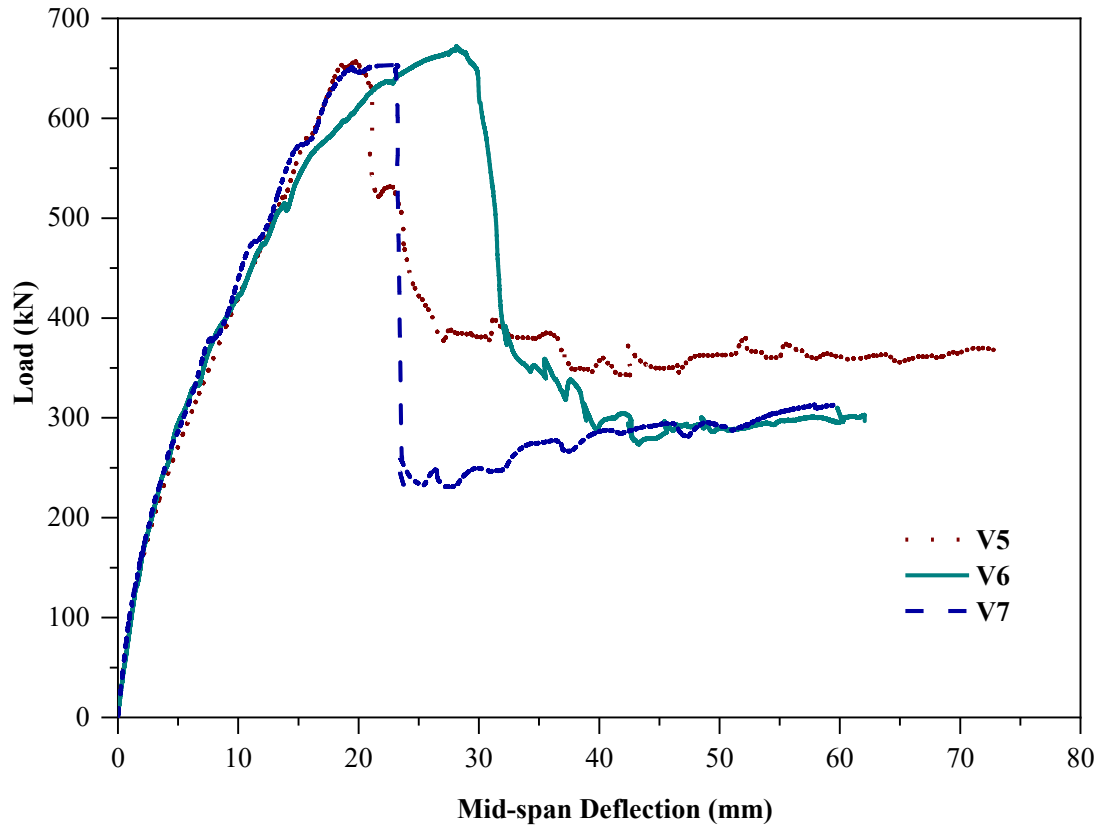


Figure 4.20 – Load versus Mid-span Deflection of Specimens V5, V6 and V7

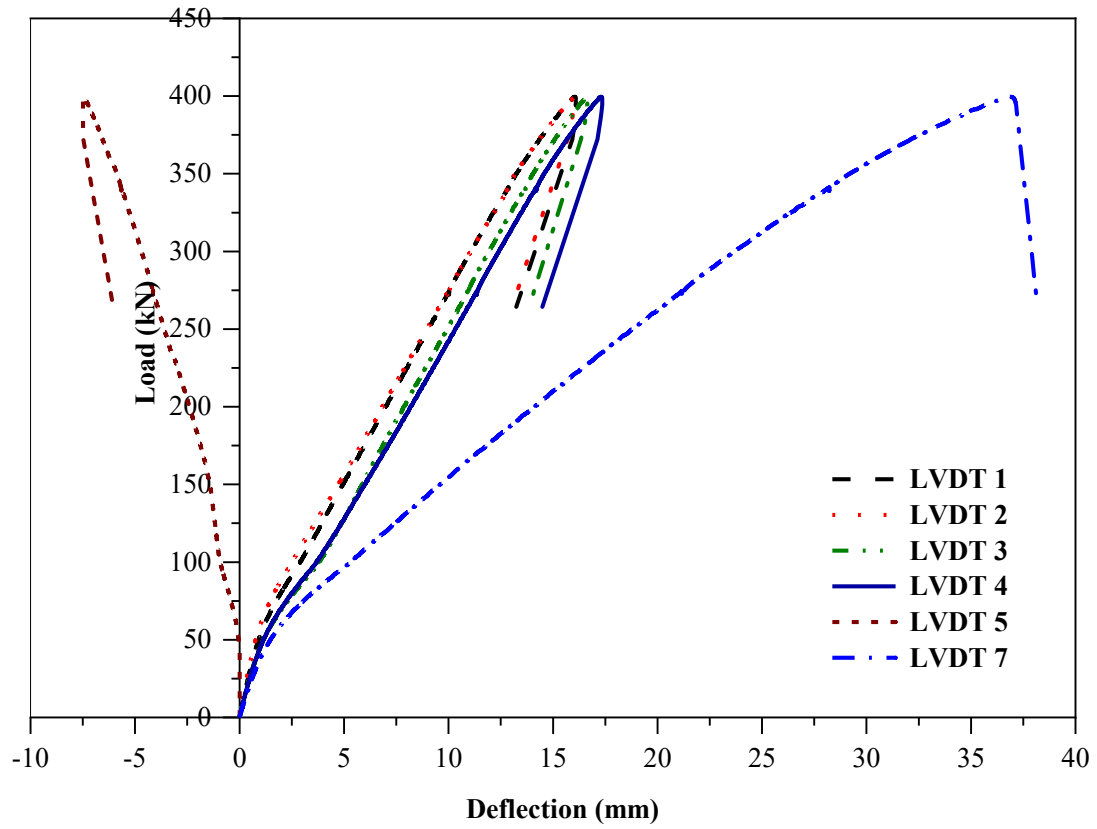


Figure 4.21 – Load versus Deflection of Specimens S

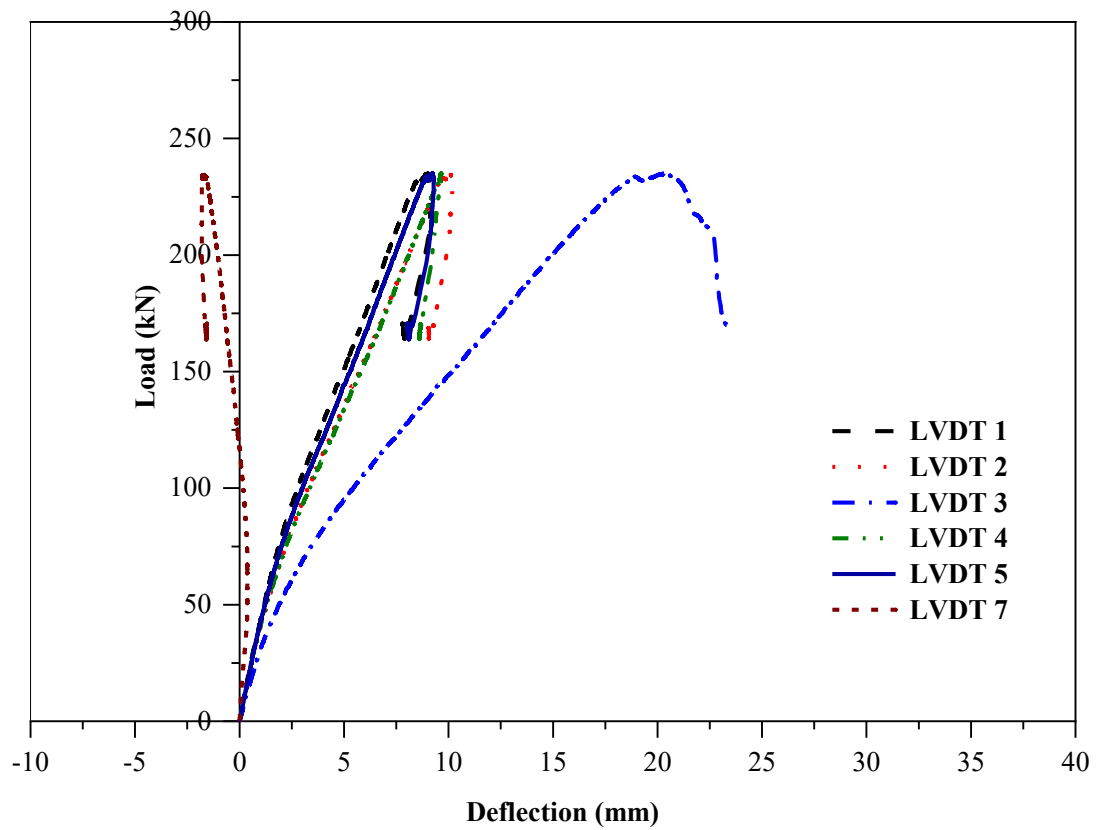


Figure 4.22 – Load versus Deflection of Specimens V1

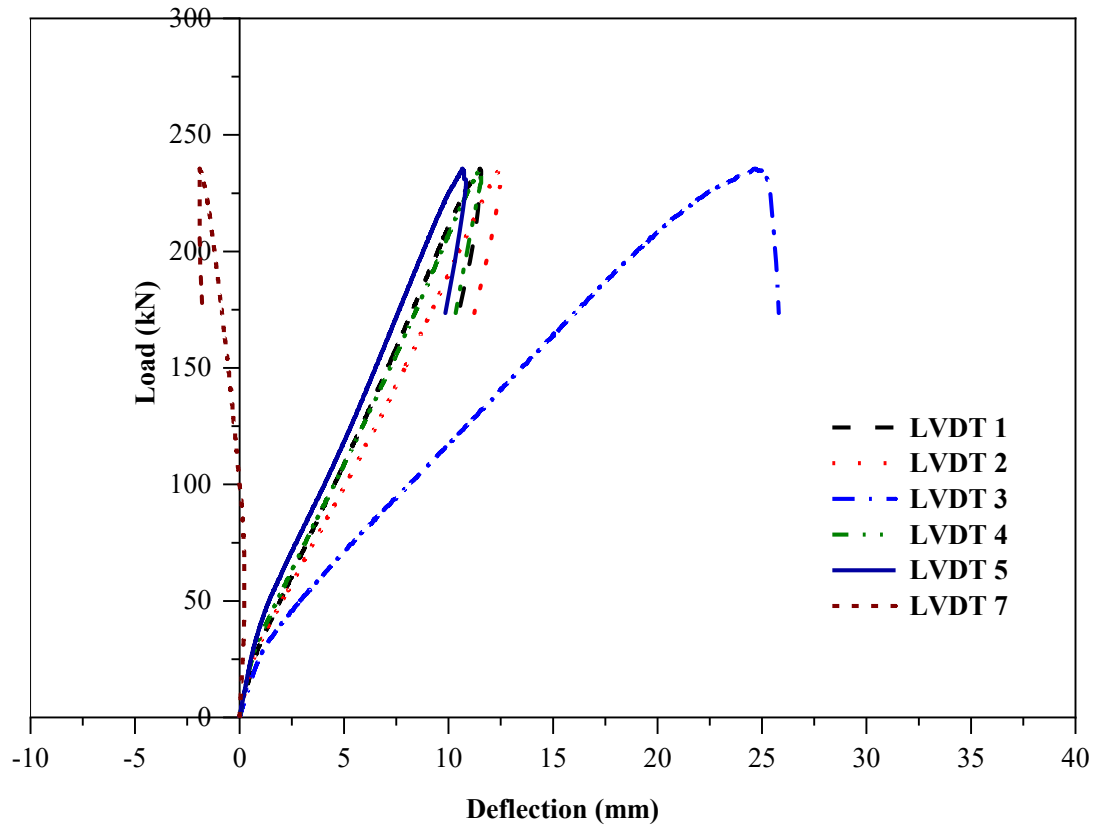


Figure 4.23 – Load versus Deflection of Specimens V2

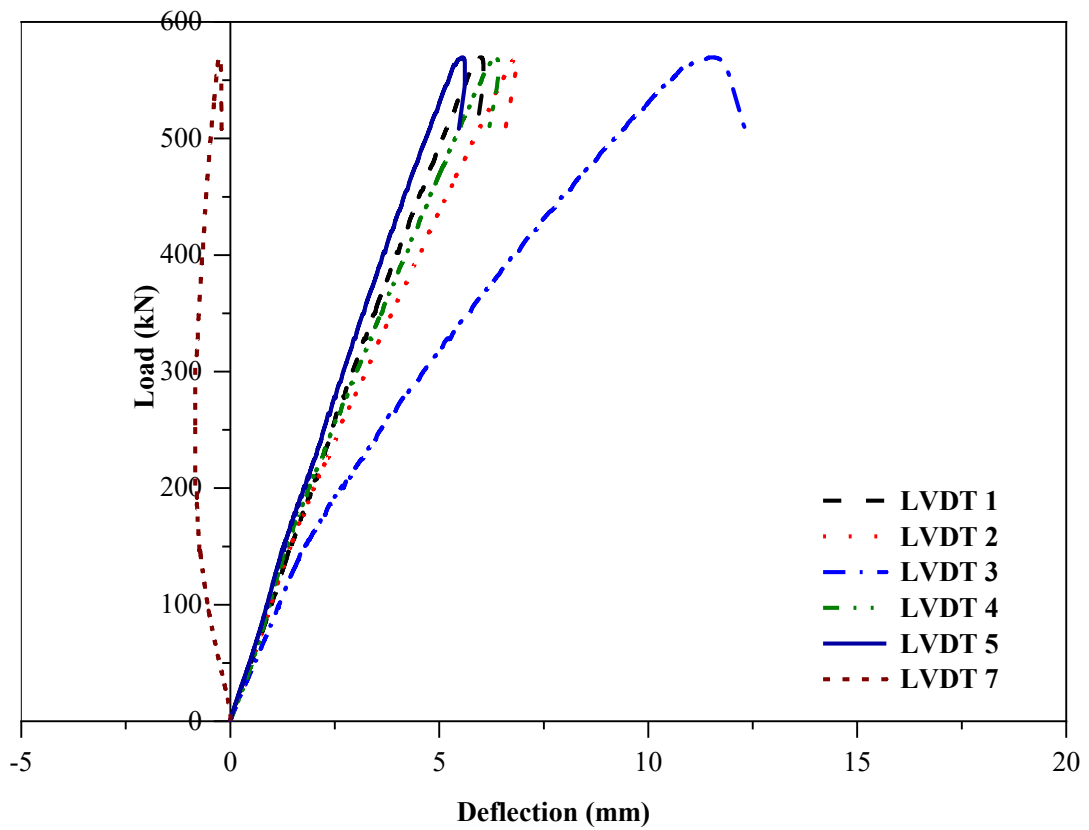


Figure 4.24 – Load versus Deflection of Specimens V3

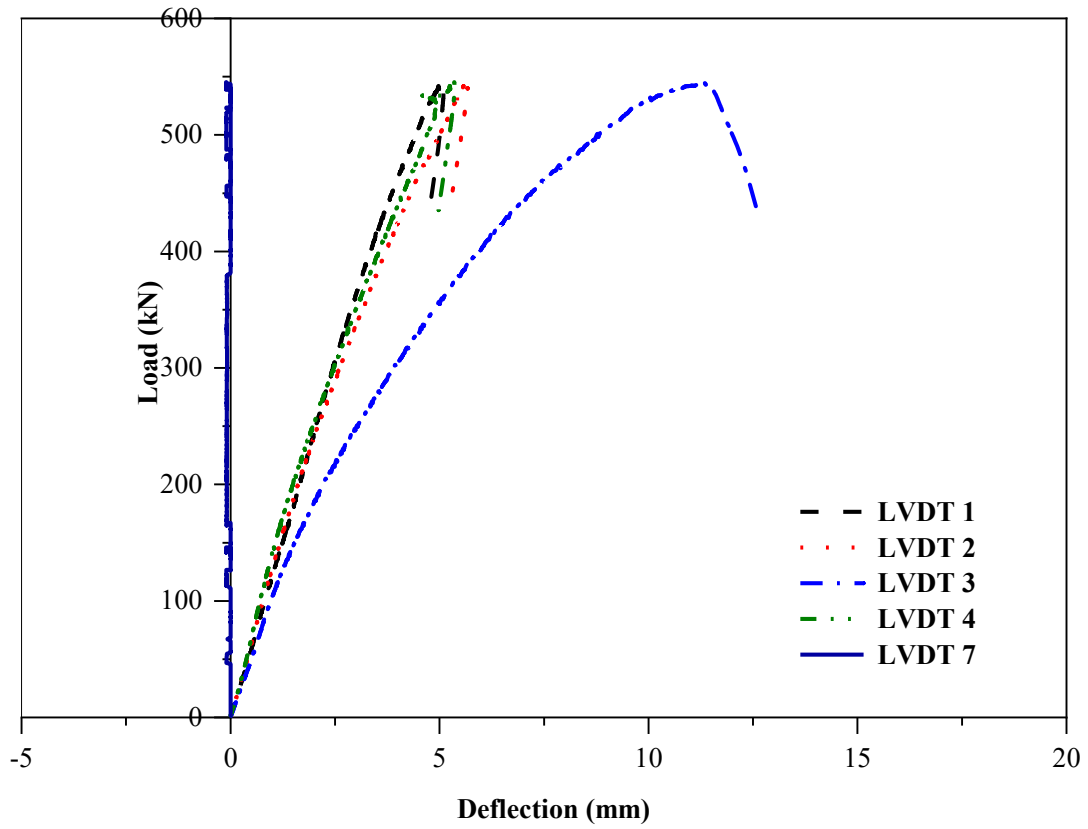


Figure 4.25 – Load versus Deflection of Specimens V4

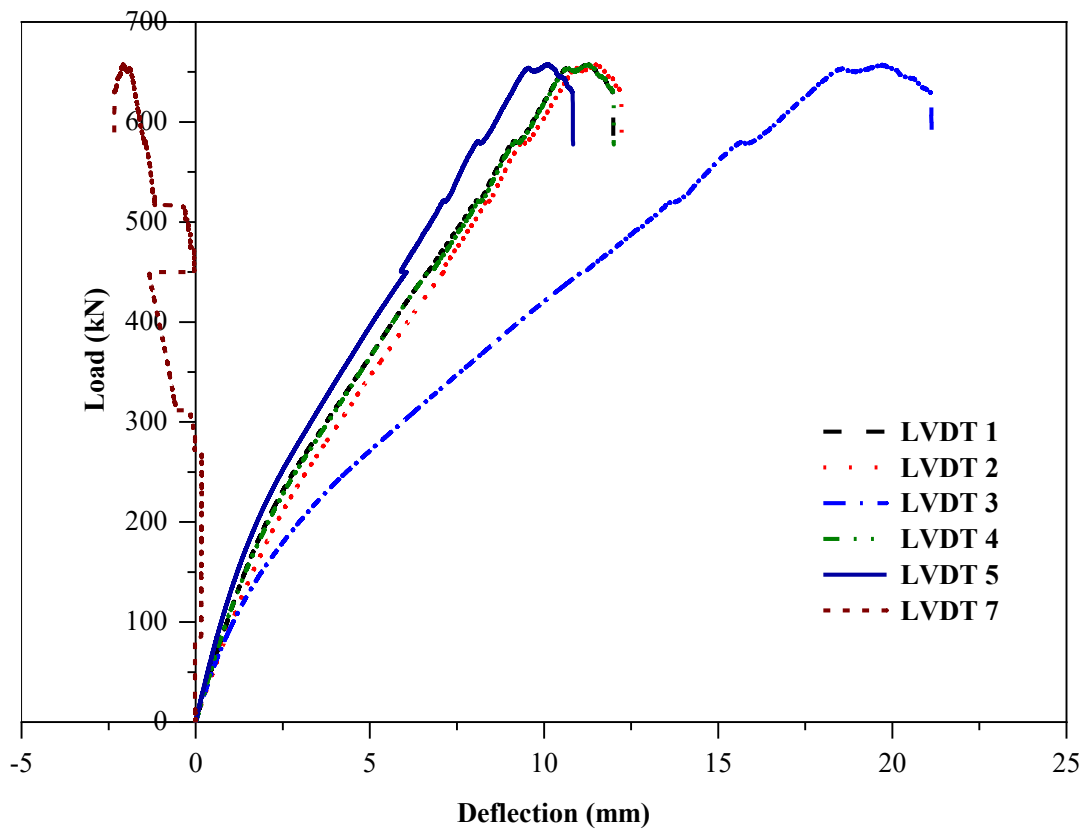


Figure 4.26 – Load versus Deflection of Specimens V5

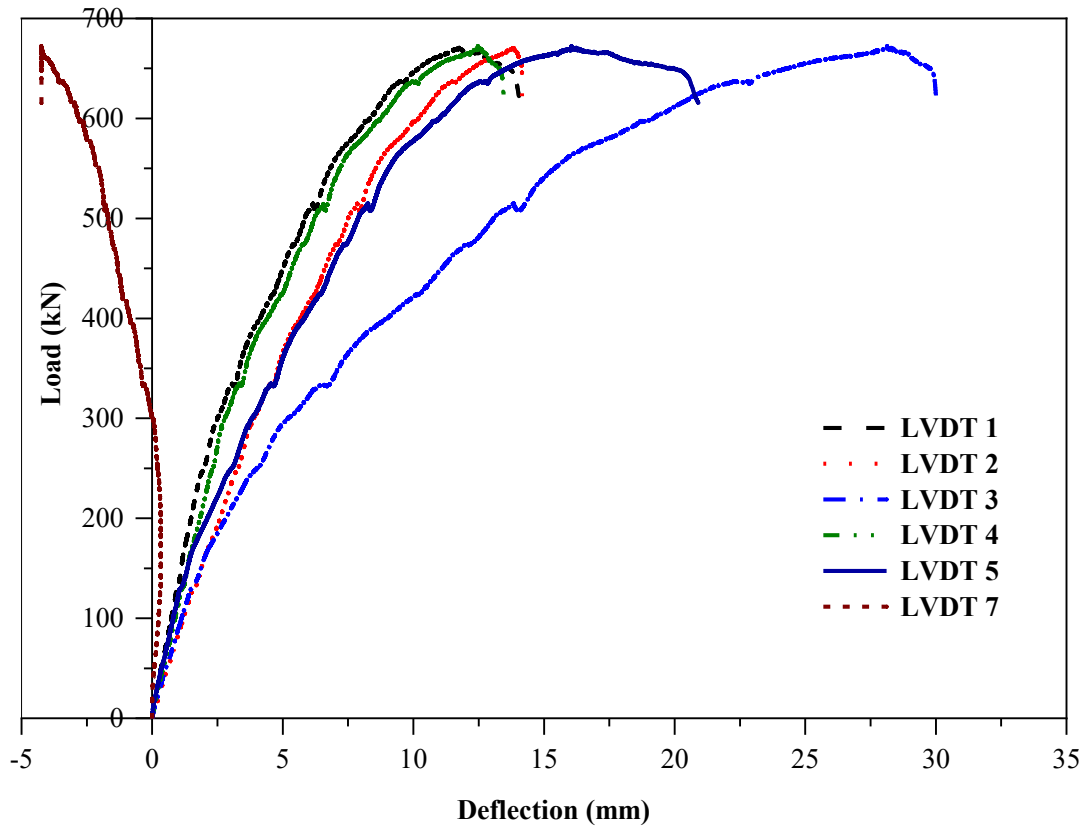


Figure 4.27 – Load versus Deflection of Specimens V6

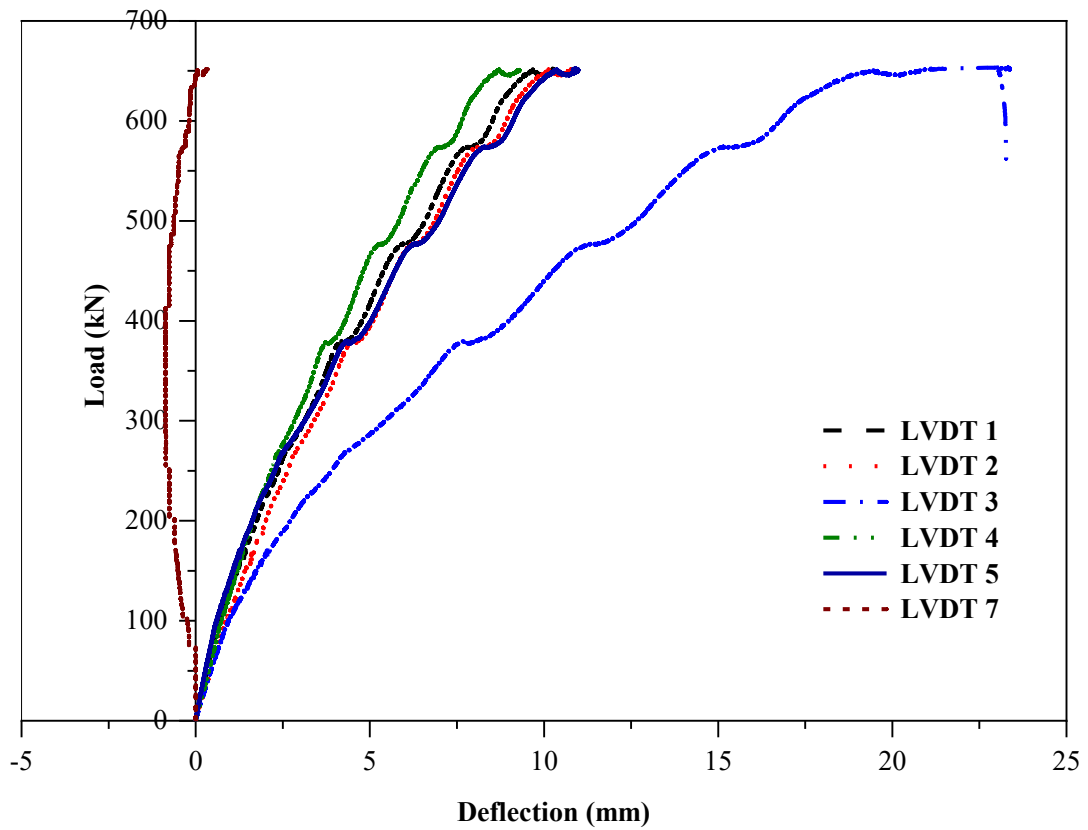


Figure 4.28 – Load versus Deflection of Specimens V7

#### 4.2.4.2 Crack Pattern

The photograph of tested specimens with observed cracks are shown in Figure 4.29 – Figure 4.36.



Figure 4.29 – Observed Crack Pattern of Slab Specimen S



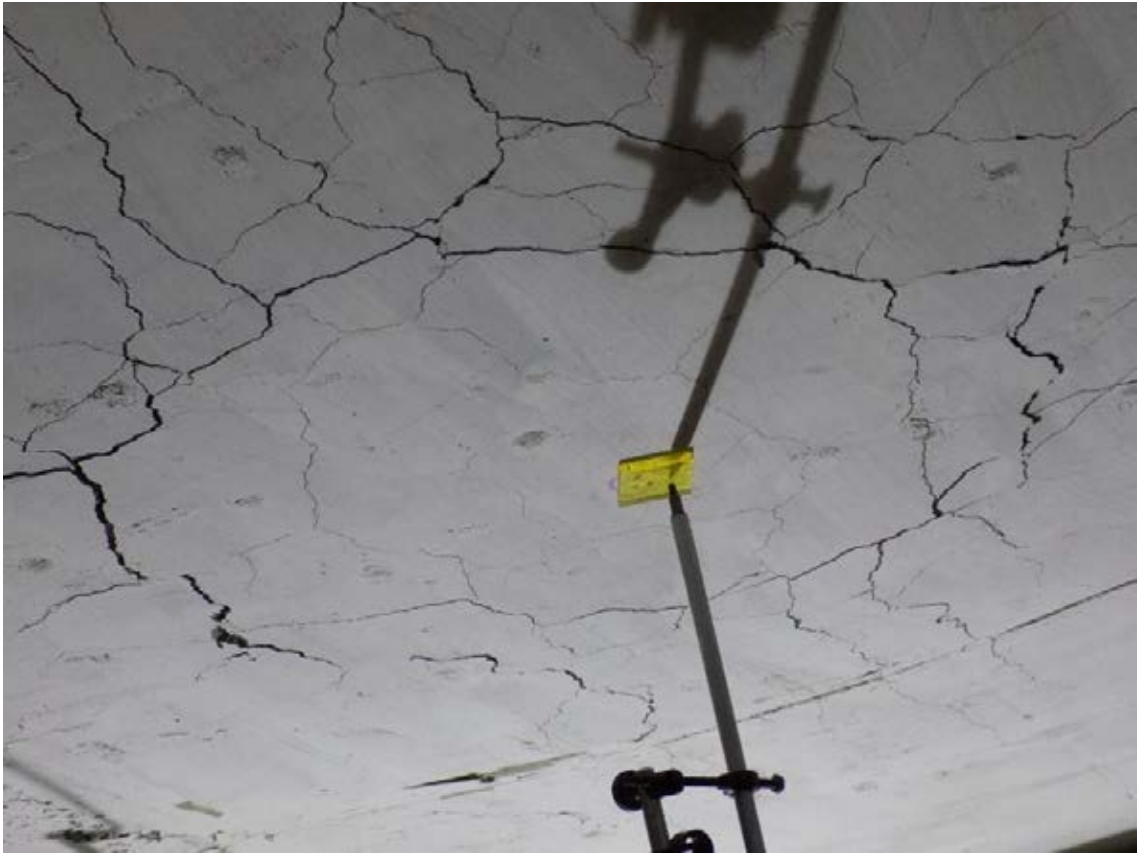


Figure 4.30 – Observed Crack Pattern of Slab Specimen V1



Figure 4.31 – Observed Crack Pattern of Slab Specimen V2



Figure 4.32 – Observed Crack Pattern of Slab Specimen V3



Figure 4.33 – Observed Crack Pattern of Slab Specimen V4



Figure 4.34 – Observed Crack Pattern of Slab Specimen V5



Figure 4.35 – Observed Crack Pattern of Slab Specimen V6



Figure 4.36 – Observed Crack Pattern of Slab Specimen V7

#### 4.2.4.3 Load Carrying Capacity

Ultimate load and corresponding mid-span displacement are summarised for all eight tested specimens in Table 4.3. From the test results of specimens S, V1 and V2, it is observed that the load-carrying capacity of voided slabs was 60 % of solid slab capacity. The load-carrying capacity of voided slab specimens (V1 & V2 and V3 & V4) were observed to be almost same irrespective of void location, i.e., the void located anywhere within  $d$  distance from the face of the column. This is reasonable, as the presence of voids close to column changes the critical section of failure. The ultimate load of identical voided slab specimens (V5 – V7) was almost the same; however, the displacement corresponding to the ultimate load was observed to vary significantly. It may be due to uncertainty in material properties.

Table 4.3 – Punching Shear Capacity of Test Specimens

<b>ID</b>	<b>Ultimate load, <math>V_u</math> (kN)</b>	<b>Displacement at ultimate load, <math>\delta_u</math> (mm)</b>	<b>Ratio, <math>V_{u, void} / V_{u, solid}</math></b>
S	404.21	36.89	–
V1	239.77	20.51	0.593
V2	240.38	24.83	0.595
V3	574.43	11.52	–
V4	548.91	11.37	–
V5	657.18	19.70	–
V6	672.34	28.12	–
V7	653.61	23.13	–

#### 4.2.4.4 Strain of Bottom Reinforcement

The load versus reinforcement strain of specimens (Figure 4.37) showed that the behaviour of reinforcement in both directions was not identical. It is mainly because of the difference in effective depth in x- and y-directions.

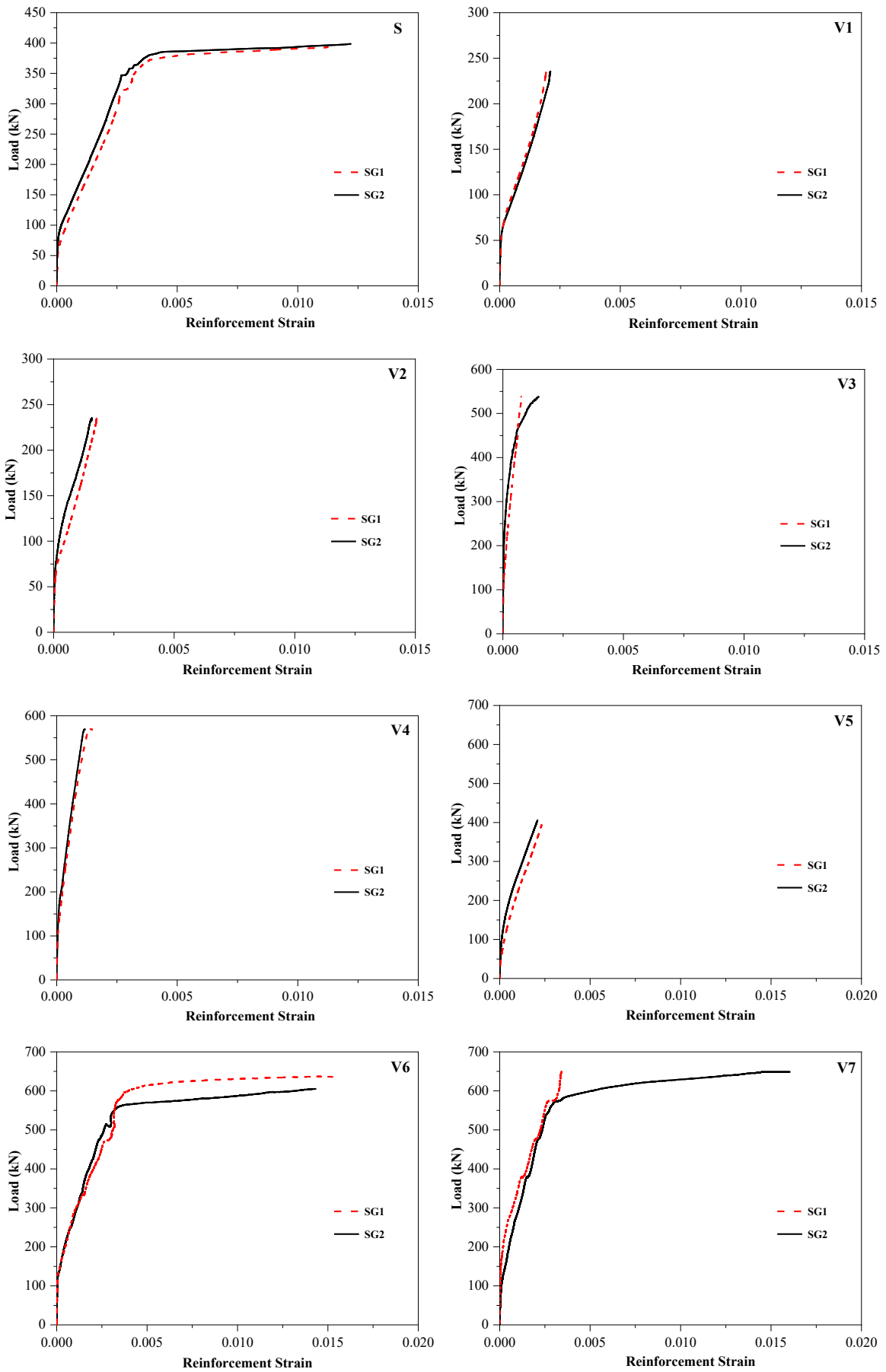


Figure 4.37 – Load versus Reinforcement Strain

### 4.3 Analytical Study

#### 4.3.1 Punching Shear Capacity Prediction of Solid Slabs by Various Standards

The punching shear capacity of the solid slab can be predicted by various standards, such as ACI 318 (2014), EN 1992-1-1 (2004) and IS 456 (2000). It varies for each standard based on three key parameters such as (i) critical section for punching shear which governs the control perimeter, (ii) permissible shear strength of concrete, and (iii) effect of flexural reinforcement. The equations to predict the punching shear capacity of the solid slab with these parameters are summarised below.

##### 4.3.1.1 ACI 318

As per ACI 318, the critical section for punching shear is located at a distance of  $0.5d$  from the face of the column, as shown in Figure 4.38(a). The punching shear capacity of the solid slab ( $V_c$ ) is least of Eq. 4.1, Eq. 4.2 and Eq. 4.3.

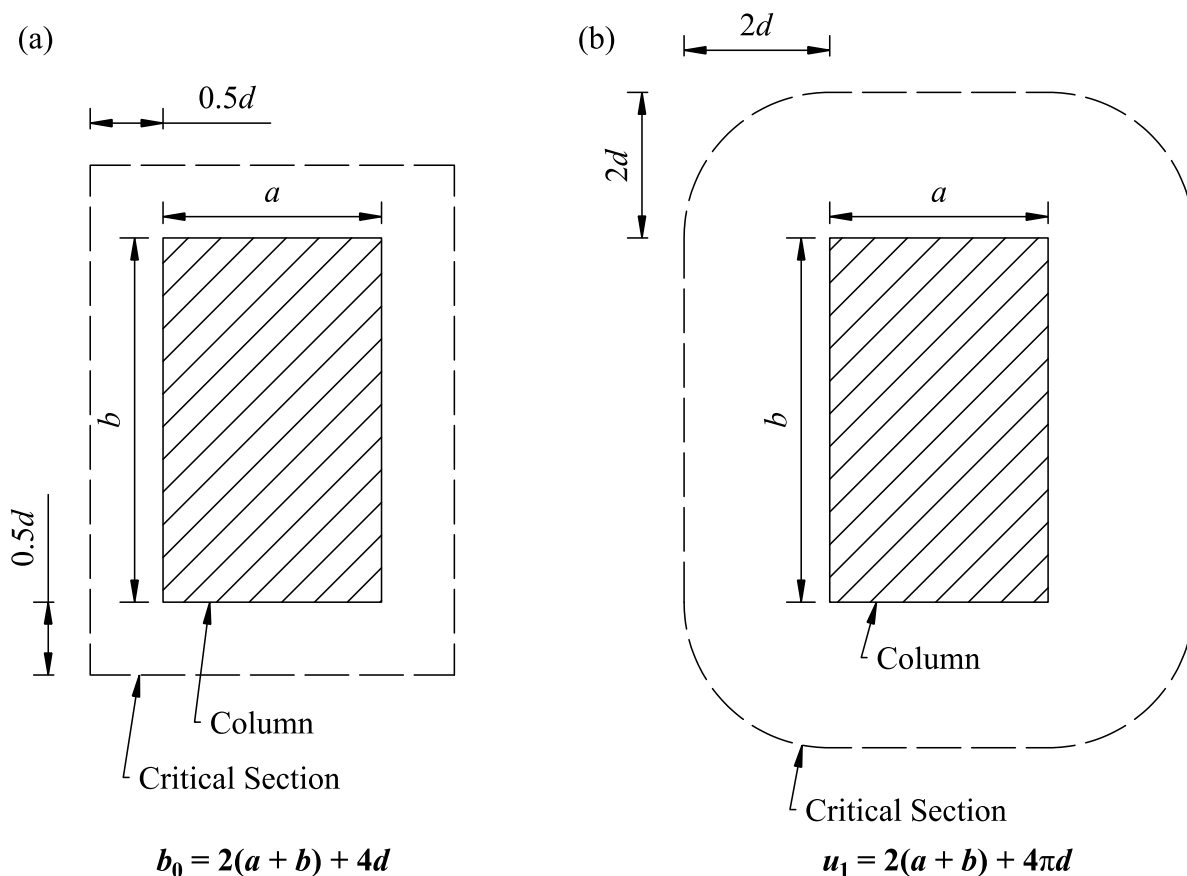


Figure 4.38 – Critical section for punching shear as per (a) ACI 318 and IS 456, (b) EN 1992-



$$V_c = 0.33\lambda\sqrt{f'_c}A \quad \text{Eq. 4.1}$$

$$V_c = 0.17\left(1 + \frac{2}{\beta}\right)\lambda\sqrt{f'_c}A \quad \text{Eq. 4.2}$$

$$V_c = 0.083\left(2 + \frac{\alpha_s d}{b_0}\right)\lambda\sqrt{f'_c}A \quad \text{Eq. 4.3}$$

where,  $\lambda$  is modification factor to reflect the reduced mechanical properties of light-weight concrete relative to normal-weight concrete of the same compressive strength, and equal to 1.0 for normal-weight concrete,  $f'_c$  is specified compressive cylinder strength of concrete,  $b_0$  is perimeter of critical section for two-way shear in slabs,  $d$  is distance from extreme compression fibre to centroid of longitudinal tension reinforcement, i.e., effective depth,  $\beta$  is ratio of long side to short side of the column,  $\alpha_s$  is constant and equal to 40 for interior column, and  $A$  is concrete area ( $= b_0 d$ ).

The design punching shear capacity of the solid slab ( $V_n$ ) is given by Eq. 4.4, where  $\Phi$  is stress reduction factor and equal to 0.75.

$$V_n = \Phi V_c \quad \text{Eq. 4.4}$$

#### 4.3.1.2 EN 1992-1-1

As per EN 1992-1-1, the critical section for punching shear is located at a distance of  $2d$  from the face of the column, as shown in Figure 4.38(b). The punching shear capacity of the solid slab ( $V_{Rd,c}$ ) is given in Eq. 4.5.

$$V_{Rd,c} = C_{Rd,c} k (100 \rho_l f'_c)^{1/3} A \geq V_{min} \quad \text{Eq. 4.5}$$

where,  $C_{Rd,c}$  is equal to 0.18,  $f'_c$  is characteristic compressive cylinder strength of concrete,  $u_1$  is the perimeter of critical section for two-way shear in slabs,  $d$  is effective depth of slab,  $k$  is size effect factor and calculated as per Eq. 4.6,  $\rho_l$  is reinforcement ratio for longitudinal reinforcement and calculated as per Eq. 4.7,  $\rho_{ly}$  and  $\rho_{lz}$  are reinforcement ratios for longitudinal reinforcement in  $y$ - and  $z$ -direction, respectively,  $V_{min}$  is defined as minimum punching shear capacity of the solid slab and calculated as per Eq. 4.8 and  $A$  is concrete area ( $= u_1 d$ ).

$$k = 1 + \sqrt{\frac{200}{d}} \leq 2.0 \quad \text{Eq. 4.6}$$

$$\rho_l = \sqrt{\rho_{ly} \rho_{lz}} \leq 0.02 \quad \text{Eq. 4.7}$$

$$V_{min} = 0.035k^{3/2}\sqrt{f_c}A \quad \text{Eq. 4.8}$$

The design punching shear capacity of the solid slab ( $V_n$ ) is given by Eq. 4.9, where  $\gamma_c$  is partial factor for concrete and equal to 1.5.

$$V_n = V_{Rd,c} / \gamma_c \quad \text{Eq. 4.9}$$

#### 4.3.1.3 IS 456

As per IS 456, the critical section for punching shear is located at a distance of  $0.5d$  from the face of the column, as shown in Figure 4.38(a). The punching shear capacity of the solid slab ( $V_c$ ) is given in Eq. 4.10.

$$V_c = 0.25\sqrt{1.5f_{ck}}k_sA \quad \text{Eq. 4.10}$$

where,  $f_{ck}$  is characteristic compressive cube strength of concrete,  $b_0$  is the perimeter of critical section for two-way shear in slabs,  $d$  is effective depth of slab,  $k_s$  calculated as per Eq. 4.11,  $\beta_c$  is defined as ratio of short side to long side of the column and  $A$  is concrete area ( $= b_0d$ ).

$$k_s = 0.5 + \beta_c \leq 1.0 \quad \text{Eq. 4.11}$$

The design punching shear capacity of the solid slab ( $V_n$ ) is given by Eq. 4.12, where  $\gamma_c$  is partial safety factor for material strength and equal to 1.5 for concrete.

$$V_n = V_c / \sqrt{\gamma_c} \quad \text{Eq. 4.12}$$

#### 4.3.2 Experimental Test Data and Prediction of Punching Shear Capacity

The experimental results based on present study (7 voided slab) and the test data available in the literature (33 specimens) were compared with the estimations by provisions in the building standards (specified for solid slabs). The details and experimental results of voided slab specimens (in total 40 test specimens) are summarised in Table 4.4. These test specimens cover a wide range of void former shapes (sphere, cylinder, donut, hexahedron and cuboid), void locations from the column face ( $0.07d - 3.40d$ ), concrete cylinder strengths ( $20 - 68.5 \text{ N/mm}^2$ ) and longitudinal reinforcement ratios ( $0.303 - 1.803 \%$ ).

Table 4.4 – Details and Experimental Results of Voided Slab Specimens of Various Researchers

Reference	Void details	ID	Void location from column face	Effective depth, $d$ (mm)	Square column size, $a$ (mm)	Concrete strength <sup>#</sup> , N/mm <sup>2</sup>		Rein. Ratio, $\rho_l$ (%)	Failure load, $V_u$ (kN)
						Cube	Cylinder		
						( $f_{ck}$ )	( $f_c'$ )		
Held and Pfeffer (2002)	Sphere	D1-24	0.31 $d$	190.0	300	44.40	35.52	1.803	520
		D2-24	0.31 $d$	190.0	300	50.80	40.64	1.803	580
		D3-24	0.31 $d$	190.0	300	46.70	37.36	1.803	525
		D4-45	0.18 $d$	380.0	300	29.60	23.68	1.060	935
		D5-45	0.18 $d$	380.0	300	37.90	30.32	1.060	990
		D6-45	0.18 $d$	380.0	300	40.50	32.40	1.060	1180
Han and Lee (2014)	Cylinder	V1	0.66 $d$	373.5	267	41.25	33.00	0.791	1297
		V2	0.34 $d$	373.5	267	41.25	33.00	0.791	1071
		V3	0.34 $d$	373.5	267	41.25	33.00	0.791	1111
		V4	0.34 $d$	373.5	267	41.25	33.00	0.791	944
Oukaili and Husain (2017)	Sphere	BD1	2.00 $d$	77.0	100	37.70	30.50	0.734	140
		BD3	2.00 $d$	105.0	100	34.00	28.00	1.068	205
		BD5	1.00 $d$	77.0	100	36.40	29.50	0.734	120
		BD7	1.00 $d$	105.0	100	39.60	31.70	1.068	190
		BD9	2.00 $d$	77.0	100	74.00	65.00	0.734	180
		BD11	2.00 $d$	105.0	100	74.70	66.50	1.068	325

Reference	Void details	ID	Void location from column face	Effective depth, $d$ (mm)	Square column size, $a$ (mm)	Concrete strength#, N/mm <sup>2</sup>		Rein. Ratio, $\rho_l$ (%)	Failure load, $V_u$ (kN)
						Cube	Cylinder		
						( $f_{ck}$ )	( $f_c'$ )		
		BD13	1.00 $d$	77.0	100	75.70	67.00	0.734	170
		BD15	1.00 $d$	105.0	100	76.40	68.00	1.068	290
Valivonis et al. (2017a)*	Hexahedron with rounded edges	BPR1-1	0.34 $d$	234.6	350	31.64	26.51	0.487	600.2
		BPR1-2	0.34 $d$	234.8	350	31.64	26.51	0.486	600.1
		BPR2-1	0.34 $d$	232.9	350	34.78	28.95	0.493	776.3
		BPR2-2	0.34 $d$	235.0	350	34.78	28.95	0.485	704.5
		BPR3-1	3.33 $d$	152.9	350	32.02	27.96	0.403	385.4
		BPR3-2	3.40 $d$	150.0	350	32.02	27.96	0.416	428.1
Valivonis et al. (2017b)	Hexahedron with rounded edges	BP1-1	2.18 $d$	233.9	350	36.15	31.01	0.306	772.7
		BP1-2	2.19 $d$	232.5	350	36.15	31.01	0.308	800.5
		BP2-1	0.35 $d$	225.7	350	34.54	32.07	0.317	443.1
		BP2-2	0.34 $d$	236.3	350	34.54	32.07	0.303	450.9
		BP3-1	0.35 $d$	231.1	350	34.82	30.38	0.310	630.4
		BP3-2	0.34 $d$	234.0	350	34.82	30.38	0.306	658.4
Chung et al. (2018a)	Donut	PD-N-0	1.31 $d$	217.0	300	26.75	21.40	0.800	556.4
		PD-N-4	0.07 $d$	217.0	300	27.75	22.20	0.800	515.7
		PD-N-8	0.07 $d$	217.0	300	33.50	26.80	0.800	480.2

Reference	Void details	ID	Void location from column face	Effective depth, $d$ (mm)	Square column size, $a$ (mm)	Concrete strength#, N/mm <sup>2</sup>		Rein. Ratio, $\rho_l$ (%)	Failure load, $V_u$ (kN)
						Cube	Cylinder		
						( $f_{ck}$ )	( $f_c'$ )		
Current Study	Sphere	V1	$1.05d$	119.0	300	28.10	22.48	1.130	239.8
		V2	$0.38d$	119.0	300	28.10	22.48	1.130	240.4
		V3	$0.51d$	205.0	300	26.70	21.36	0.800	574.4
		V4	$1.07d$	205.0	300	26.70	21.36	0.800	548.9
	Cuboid	V5	$2.26d$	221.0	300	25.00	20.00	0.430	657.2
		V6	$2.26d$	221.0	300	25.00	20.00	0.430	672.3
		V7	$2.26d$	221.0	300	25.00	20.00	0.430	653.6

**Note:** # Concrete cylinder strength is taken as 80 % of cube strength and vice versa, if required.

\* The contribution from the presence of shear reinforcement is not considered as it is not significant in comparison with observed failure load.

#### 4.3.2.1 Prediction of Capacity by Various Standards

The punching shear capacity of all 40 specimens (Table 4.4) is calculated based on the provisions of building standards, applicable for solid slabs, are summarised in Section 4.3.1. The calculated capacity using various standards are summarised in Table 4.5; here, the strength reduction factor / partial safety for the material is removed to compare with experimental test data. Based on the above comparison, the following observations are made. The punching shear capacity of voided slabs is greatly overestimated (mean  $\approx 1.3$ , and COV  $\approx 0.3$ ) by the provisions of the building standards considered in this study; slabs with voids within  $0.5d$  distance from the column face is particularly unsafe ( $V_c / V_u \approx 2.3$ ). Since the estimation of punching shear capacity of the biaxial voided slab by existing provisions for solid slabs in standards does not lead to satisfactory results, an effective area method is proposed to predict the punching shear capacity of the biaxial voided slab.

#### 4.3.2.2 Prediction of Capacity by Effective Concrete Area

The presence of voids is considered by modifying the critical section depending on the void location. In addition, the gross concrete area available ( $A$ ) to resist the punching shear load is reduced to an effective concrete area ( $A_e$ ) by acknowledging the presence of voids. The effective concrete area ( $A_e$ ) is estimated based on the Eq. 4.13 and Eq. 4.14.

For, ACI 318 and IS 456,

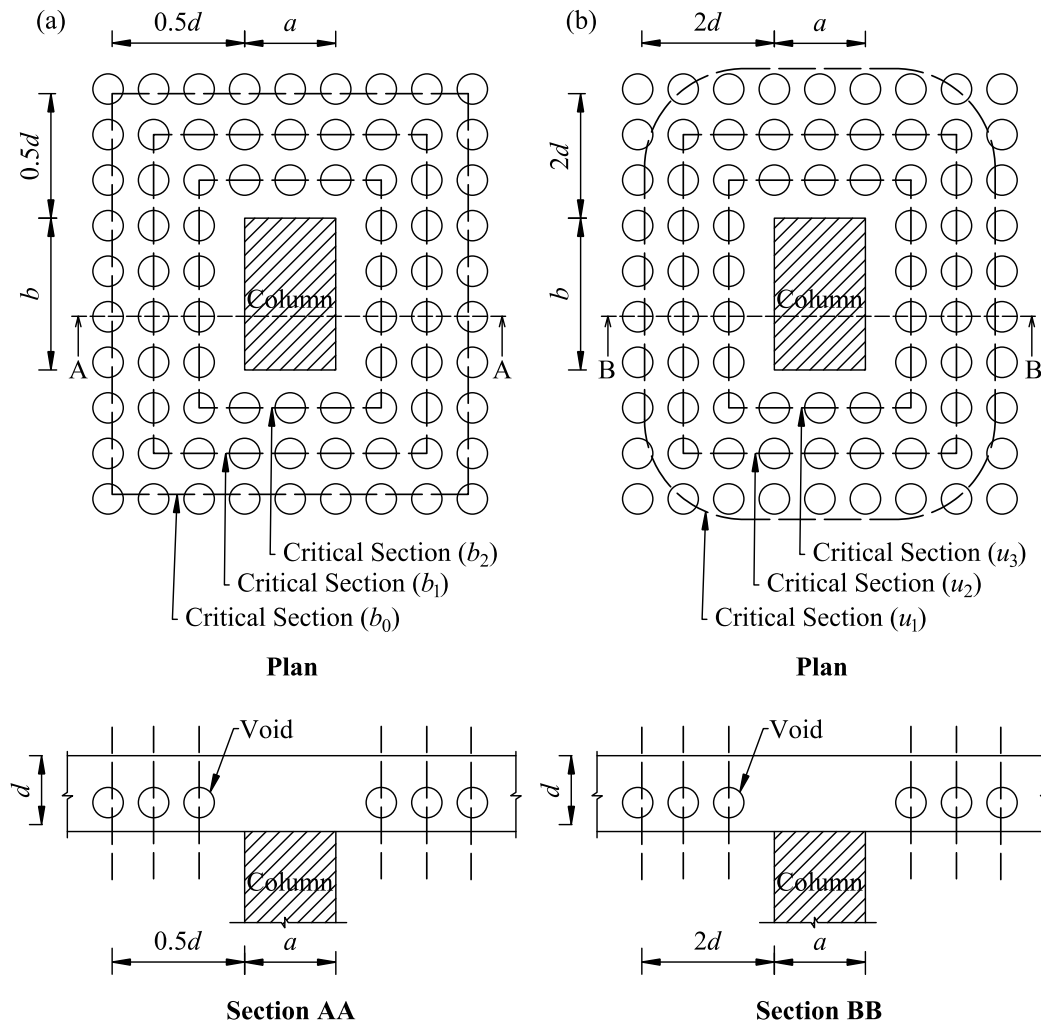
$$A_e = b_i d - A_{i-void} \quad \text{Eq. 4.13}$$

where,  $b_i$  is control perimeter (depending on the void location), and  $A_{i-void}$  is the area of void at  $i^{\text{th}}$  critical section ( $i = 0, 1, \dots, n$ ). The smallest value of  $A_e$  should be considered. Typical details are shown in Figure 4.39a.

For, EN 1992-1-1

$$A_e = u_i d - A_{i-void} \quad \text{Eq. 4.14}$$

where,  $u_i$  is control perimeter depends on void location and/or as per design code, and  $A_{i-void}$  is the area of void at  $i^{\text{th}}$  critical section ( $i = 1, 2, \dots, n$ ). The smallest value of  $A_e$  should be considered. Typical details are shown in Figure 4.39b.



Drawings are Not To Scale

Figure 4.39 – Typical critical sections based on void locations for (a) ACI 318 and IS 456, (b) EN 1992-1-1

The punching shear capacity of the voided slab is predicted by considering the effective concrete area, and the results are summarised in Table 6; here the strength reduction factor / partial safety for material is removed to compare with experimental test data. Based on the comparison of calculated and experimental capacity for each building standard, the following observations are made.

- After modifying the critical perimeter and the effective concrete area, the provisions of (ACI 318, EN 1992-1-1, IS 456) predict the experimental data reasonably well (mean  $\approx 1.0$ , and COV  $\approx 0.21$ ).
- After including the strength reduction factor / partial safety for material for the predicted capacity, the observed conservatism (mean) is 22 %, 35 % and 13 % for ACI 318, EN 1992-1-1, and IS 456, respectively.

Table 4.5 – Punching shear capacity of voided slabs calculated by various standards without considering the voids

Reference (year)	ID	Failure load, $V_u$ (kN)	ACI 318		EN 1992-1-1		IS 456	
			$V_c$ (kN)	$V_c / V_u$	$V_{Rdc}$ (kN)	$V_{Rdc} / V_u$	$V_c$ (kN)	$V_c / V_u$
Held and Pfeffer (2002)	D1-24	520	732.4	1.41	981.8	1.89	759.8	1.46
	D2-24	580	783.4	1.35	1026.9	1.77	812.7	1.40
	D3-24	525	751.2	1.43	998.5	1.90	779.2	1.48
	D4-45	935	1659.8	1.78	2070.2	2.21	1721.8	1.84
	D5-45	990	1878.2	1.90	2248.0	2.27	1948.3	1.97
	D6-45	1180	1941.5	1.65	2298.3	1.95	2014.0	1.71
Han and Lee (2014)	V1	1297	1814.0	1.40	1987.8	1.53	1881.8	1.45
	V2	1071	1814.0	1.69	1987.8	1.86	1881.8	1.76
	V3	1111	1814.0	1.63	1987.8	1.79	1881.8	1.69
	V4	944	1814.0	1.92	1987.8	2.11	1881.8	1.99
Oukaili and Husain (2017)	BD1	140	99.4	0.71	106.9	0.76	102.5	0.73
	BD3	205	150.4	0.73	201.7	0.98	153.7	0.75
	BD5	120	97.7	0.81	105.7	0.88	100.7	0.84
	BD7	190	160.0	0.84	210.3	1.11	165.9	0.87
	BD9	180	145.0	0.81	137.5	0.76	143.6	0.80
	BD11	325	231.7	0.71	269.2	0.83	227.9	0.70
	BD13	170	147.3	0.87	138.9	0.82	145.2	0.85
	BD15	290	234.3	0.81	271.2	0.94	230.4	0.79



Reference (year)	ID	Failure load, $V_u$ (kN)	ACI 318		EN 1992-1-1		IS 456	
			$V_c$ (kN)	$V_c / V_u$	$V_{Rdc}$ (kN)	$V_{Rdc} / V_u$	$V_c$ (kN)	$V_c / V_u$
Valivonis et al. (2017a)	BPR1-1	600.2	932.1	1.55	827.0	1.38	944.8	1.57
	BPR1-2	600.1	932.9	1.55	827.3	1.38	945.7	1.58
	BPR2-1	776.3	964.2	1.24	849.2	1.09	980.6	1.26
	BPR2-2	704.5	976.4	1.39	852.9	1.21	993.0	1.41
	BPR3-1	385.4	536.5	1.39	409.7	1.06	532.7	1.38
	BPR3-2	428.1	523.5	1.22	401.9	0.94	519.8	1.21
Valivonis et al. (2017b)	BP1-1	772.7	1003.9	1.30	742.6	0.96	1005.7	1.30
	BP1-2	800.5	995.5	1.24	740.6	0.93	997.3	1.25
	BP2-1	443.1	971.3	2.19	723.3	1.63	935.3	2.11
	BP2-2	450.9	1035.3	2.30	761.2	1.69	996.9	2.21
	BP3-1	630.4	976.8	1.55	729.5	1.16	970.2	1.54
	BP3-2	658.4	994.0	1.51	737.8	1.12	987.3	1.50
Chung et al. (2018a)	PD-N-0	556.4	685.1	1.23	774.8	1.39	710.7	1.28
	PD-N-4	515.7	697.8	1.35	784.4	1.52	723.8	1.40
	PD-N-8	480.2	766.6	1.60	835.2	1.74	795.3	1.66
Current Study	V1	239.8	312.1	1.30	339.4	1.41	323.7	1.35
	V2	240.4	312.1	1.30	339.4	1.42	323.7	1.35
	V3	574.4	631.6	1.10	714.2	1.24	655.2	1.14
	V4	548.9	631.6	1.15	714.2	1.30	655.2	1.19

Reference (year)	ID	Failure load, $V_u$ (kN)	ACI 318		EN 1992-1-1		IS 456	
			$V_c$ (kN)	$V_c / V_u$	$V_{Rdc}$ (kN)	$V_{Rdc} / V_u$	$V_c$ (kN)	$V_c / V_u$
	V5	657.2	679.7	1.03	632.1	0.96	705.1	1.07
	V6	672.3	679.7	1.01	632.1	0.94	705.1	1.05
	V7	653.6	679.7	1.04	632.1	0.97	705.1	1.08
Minimum				0.71		0.76		0.70
Maximum				2.30		2.27		2.21
Mean				1.325		1.345		1.349
SD				0.391		0.431		0.391
COV				0.295		0.320		0.289

Table 4.6 – Punching shear capacity of voided slabs calculated by various standards with effective concrete area

Reference (year)	ID	Failure load, $V_u$ (kN)	ACI 318		EN 1992-1-1		IS 456	
			$V_c$ (kN)	$V_c / V_u$	$V_{Rdc}$ (kN)	$V_{Rdc} / V_u$	$V_c$ (kN)	$V_c / V_u$
Held and Pfeffer (2002)	D1-24	520	465.7	0.90	432.7	0.83	483.1	0.93
	D2-24	580	498.2	0.86	452.5	0.78	516.8	0.89
	D3-24	525	477.7	0.91	440.0	0.84	495.5	0.94
	D4-45	935	753.5	0.81	1071.4	1.15	781.7	0.84
	D5-45	990	852.6	0.86	1163.4	1.18	884.5	0.89
	D6-45	1180	881.4	0.75	1189.4	1.01	914.3	0.77
Han and Lee (2014)	V1	1297	1814.0	1.40	618.5	0.48	1881.8	1.45
	V2	1071	1268.9	1.18	801.5	0.75	1316.3	1.23
	V3	1111	921.0	0.83	710.0	0.64	955.4	0.86
	V4	944	921.0	0.98	710.0	0.75	955.4	1.01
Oukaili and Husain (2017)	BD1	140	99.4	0.71	106.9	0.76	102.5	0.73
	BD3	205	150.4	0.73	201.7	0.98	153.7	0.75
	BD5	120	97.7	0.81	105.7	0.88	100.7	0.84
	BD7	190	160.0	0.84	210.3	1.11	165.9	0.87
	BD9	180	145.0	0.81	137.5	0.76	143.6	0.80
	BD11	325	231.7	0.71	269.2	0.83	227.9	0.70
	BD13	170	147.3	0.87	138.9	0.82	145.2	0.85
	BD15	290	234.3	0.81	271.2	0.94	230.4	0.79

Reference (year)	ID	Failure load, $V_u$ (kN)	ACI 318		EN 1992-1-1		IS 456	
			$V_c$ (kN)	$V_c / V_u$	$V_{Rdc}$ (kN)	$V_{Rdc} / V_u$	$V_c$ (kN)	$V_c / V_u$
Valivonis et al. (2017a)	BPR1-1	600.2	503.9	0.84	622.7	1.04	510.8	0.85
	BPR1-2	600.1	504.8	0.84	623.2	1.04	511.7	0.85
	BPR2-1	776.3	964.2	1.24	636.8	0.82	980.6	1.26
	BPR2-2	704.5	976.4	1.39	642.8	0.91	993.0	1.41
	BPR3-1	385.4	536.5	1.39	409.7	1.06	532.7	1.38
	BPR3-2	428.1	523.5	1.22	401.9	0.94	519.8	1.21
Valivonis et al. (2017b)	BP1-1	772.7	1003.9	1.30	742.6	0.96	1005.7	1.30
	BP1-2	800.5	995.5	1.24	740.6	0.93	997.3	1.25
	BP2-1	443.1	500.4	1.13	242.1	0.55	481.8	1.09
	BP2-2	450.9	564.4	1.25	278.5	0.62	543.5	1.21
	BP3-1	630.4	976.8	1.55	544.6	0.86	970.2	1.54
	BP3-2	658.4	994.0	1.51	554.7	0.84	987.3	1.50
Chung et al. (2018a)	PD-N-0	556.4	685.1	1.23	499.9	0.90	710.7	1.28
	PD-N-4	515.7	639.0	1.24	506.0	0.98	662.9	1.29
	PD-N-8	480.2	443.8	0.92	538.8	1.12	460.3	0.96
Current Study	V1	239.8	312.1	1.30	233.3	0.97	323.7	1.35
	V2	240.4	269.0	1.12	233.3	0.97	279.1	1.16
	V3	574.4	631.6	1.10	432.5	0.75	655.2	1.14
	V4	548.9	631.6	1.15	635.1	1.16	655.2	1.19

Reference (year)	ID	Failure load, $V_u$ (kN)	ACI 318		EN 1992-1-1		IS 456	
			$V_c$ (kN)	$V_c / V_u$	$V_{Rdc}$ (kN)	$V_{Rdc} / V_u$	$V_c$ (kN)	$V_c / V_u$
	V5	657.2	679.7	1.03	632.1	0.96	705.1	1.07
	V6	672.3	679.7	1.01	632.1	0.94	705.1	1.05
	V7	653.6	679.7	1.04	632.1	0.97	705.1	1.08
Minimum				0.71		0.48		0.70
Maximum				1.55		1.18		1.54
<b>Mean</b>				<b>1.045</b>		<b>0.895</b>		<b>1.064</b>
SD				0.237		0.161		0.237
COV				0.227		0.180		0.223
Minimum				0.53		0.50		0.57
Maximum				1.16		1.01		1.26
<b>Mean</b>			Design punching shear capacity, $V_n$	<b>0.783</b>		<b>0.654</b>		<b>0.869</b>
SD			(with partial safety factor)	0.178		0.116		0.193
COV				0.228		0.178		0.222

The results from 40 test specimens were grouped based on the location of voids from the face of the column, such as  $< 0.5d$ ,  $0.5d - 1.0d$ ,  $1.0d - 2.0d$ , and  $> 2.0d$  (Figure 4.40). It helps to understand the variation in the capacity depending on the location of voids. In Figure 4.40, the capacity points located above  $45^\circ$  line are overpredicted by the standards. Such variation between the experimental and estimated capacity is primarily due to change in control perimeter, as it is affected by the presence of voids. Further, it is observed that the capacity of slabs with voids located at  $2d$  distance away from column face is the same as that of solid slab. However, the conservatism in the capacity needs to be investigated with more experiments.

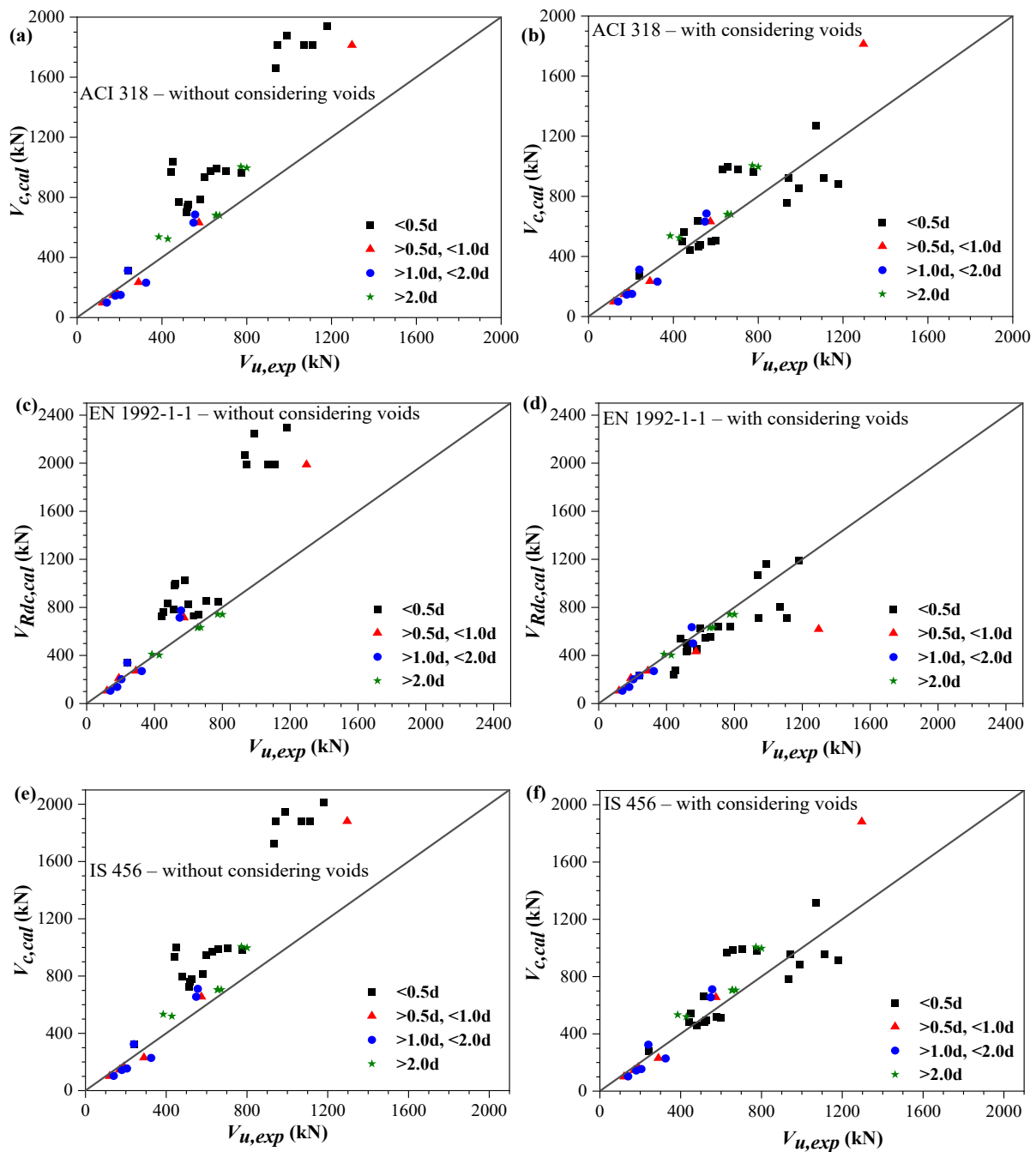


Figure 4.40 – Comparison of punching shear capacity of voided slab specimens

### 4.3.3 Prediction of Punching Shear Capacity by Critical Shear Crack Theory

“The punching shear strength decreases with increasing rotation of the slab, i.e., the shear strength is reduced by the presence of a critical shear crack that propagates through the slab into the inclined compression strut carrying the shear force to the column” (Muttoni and Schwartz, 1991). In continuation with that critical shear crack theory (CSCT) was adopted to develop a failure criterion for punching shear (Muttoni, 2003, 2008). This criterion describes the relationship between the punching shear strength of a solid slab and its rotation at failure (Eq. 4.15).

$$\frac{V_R}{b_0 d \sqrt{f_c'}} = \frac{3/4}{1 + 15 \frac{\psi d}{d_{g0} + d_g}} \quad \text{Eq. 4.15}$$

where,  $V_R$  is punching shear strength,  $f_c'$  is characteristic compressive cylinder strength of concrete,  $b_0$  is perimeter of critical section for two-way shear in slabs (Figure 4.38a),  $d$  is effective depth of slab,  $\psi$  is rotation,  $d_{g0}$  is reference aggregate size (= 16 mm), and  $d_g$  is maximum aggregate size.

The applicability of the Eq. 4.15 for the biaxial voided slab is verified in this section. The CSCT approach requires the ultimate load (punching shear) and corresponding deflection. In this study, the experimental results based on present study (7 voided slab) and test data available in the literature (22 specimens) were compared with the estimations. The details and experimental results of voided slab specimens (in total 29 test specimens) are summarised in Table 4.7. The normalised load and rotation behaviour of the current study is shown in Figure 4.41.

Figure 4.42 shows the data points of the normalised load and rotation of 29 test specimens (Table 4.7). The punching shear capacity of slab specimens with voids located beyond  $2d$  distance from column face is almost the same as that of the solid slab (Figure 4.42). However, if the void is located within  $d$  distance from the column face, then the punching shear capacity is reduced about 30%. Similarly, for slab specimens with voids located very close to column face ( $<d$ ), the punching shear capacity is reduced about 60%. Based on this understanding, the CSCT is applied to all 40 test specimens (Table 4.4) and found that the predictions were observed to be very scattered with a mean and standard deviation of 0.752 and 0.412, respectively (Figure 4.43). This is reasonable as the modified CSCT estimates the capacity with respect to the location of voids and ignores the number of voids. The CSCT approach needs to be modified by including location and amount of voids, which needs more experimental results.

Table 4.7 – Details and Experimental Results of Voided Slab Specimens of Various Researchers

Reference	ID	Void location from column face	Effective depth, $d$ (mm)	Square column size, $a$ (mm)	Concrete strength <sup>#</sup> , $f_c'$ (N/mm <sup>2</sup> )	Max. aggregate size, $d_g$ (mm)	Radius, $r_q$ (mm)	Failure load, $V_u$ (kN)	Deflection, $\delta$ (mm)
Held and Pfeffer (2002)	D2-24	$0.31d$	190.0	300	40.64	16	1125	557.6	4.96
	V1	$0.66d$	373.5	267	33.00	16	900	1297	6.27
Han and Lee (2014)	V2	$0.34d$	373.5	267	33.00	16	900	1071	5.20
	V3	$0.34d$	373.5	267	33.00	16	900	1111	5.38
	V4	$0.34d$	373.5	267	33.00	16	900	944	3.68
	BD1	$2.00d$	77.0	100	30.50	16	700	140	24.50
	BD3	$2.00d$	105.0	100	28.00	16	700	205	20.45
	BD5	$1.00d$	77.0	100	29.50	16	700	120	22.10
Oukaili and Husain (2017)	BD7	$1.00d$	105.0	100	31.70	16	700	190	20.90
	BD9	$2.00d$	77.0	100	65.00	16	700	180	22.10
	BD11	$2.00d$	105.0	100	66.50	16	700	325	18.88
	BD13	$1.00d$	77.0	100	67.00	16	700	170	20.22
	BD15	$1.00d$	105.0	100	68.00	16	700	290	19.75
Valivonis et al. (2017a)	BPR1-1	$0.34d$	234.6	350	26.51	12	1505	600.2	12.27
	BPR1-2	$0.34d$	234.8	350	26.51	12	1505	600.1	11.61
	BPR2-1	$0.34d$	232.9	350	28.95	12	1505	776.3	15.13



Reference	ID	Void location from column face	Effective depth, $d$ (mm)	Square column size, $a$ (mm)	Concrete strength <sup>#</sup> , $f_c'$ (N/mm <sup>2</sup> )	Max. aggregate size, $d_g$ (mm)	Radius, $r_q$ (mm)	Failure load, $V_u$ (kN)	Deflection, $\delta$ (mm)
	BPR2-2	$0.34d$	235.0	350	28.95	12	1505	704.5	10.40
	BPR3-1	$3.33d$	152.9	350	27.96	12	1505	385.4	23.28
	BPR3-2	$3.40d$	150.0	350	27.96	12	1505	428.1	29.13
Chung et al. (2018a)	PD-N-0	$1.31d$	217.0	300	21.40	16	1275	758.1	9.98
	PD-N-4	$0.07d$	217.0	300	22.20	16	1275	677.1	9.53
	PD-N-8	$0.07d$	217.0	300	26.80	16	1275	641.5	9.20
Current Study	V1	$1.05d$	119.0	300	22.48	12	1500	239.8	20.51
	V2	$0.38d$	119.0	300	22.48	12	1500	240.4	24.83
	V3	$0.51d$	205.0	300	21.36	12	1500	574.4	11.52
	V4	$1.07d$	205.0	300	21.36	12	1500	548.9	11.37
	V5	$2.26d$	221.0	300	20.00	12	1500	657.2	19.70
	V6	$2.26d$	221.0	300	20.00	12	1500	672.3	28.12
	V7	$2.26d$	221.0	300	20.00	12	1500	653.6	23.13

**Note:** # Concrete cylinder strength is taken as 80 % of cube strength and vice versa, if required.

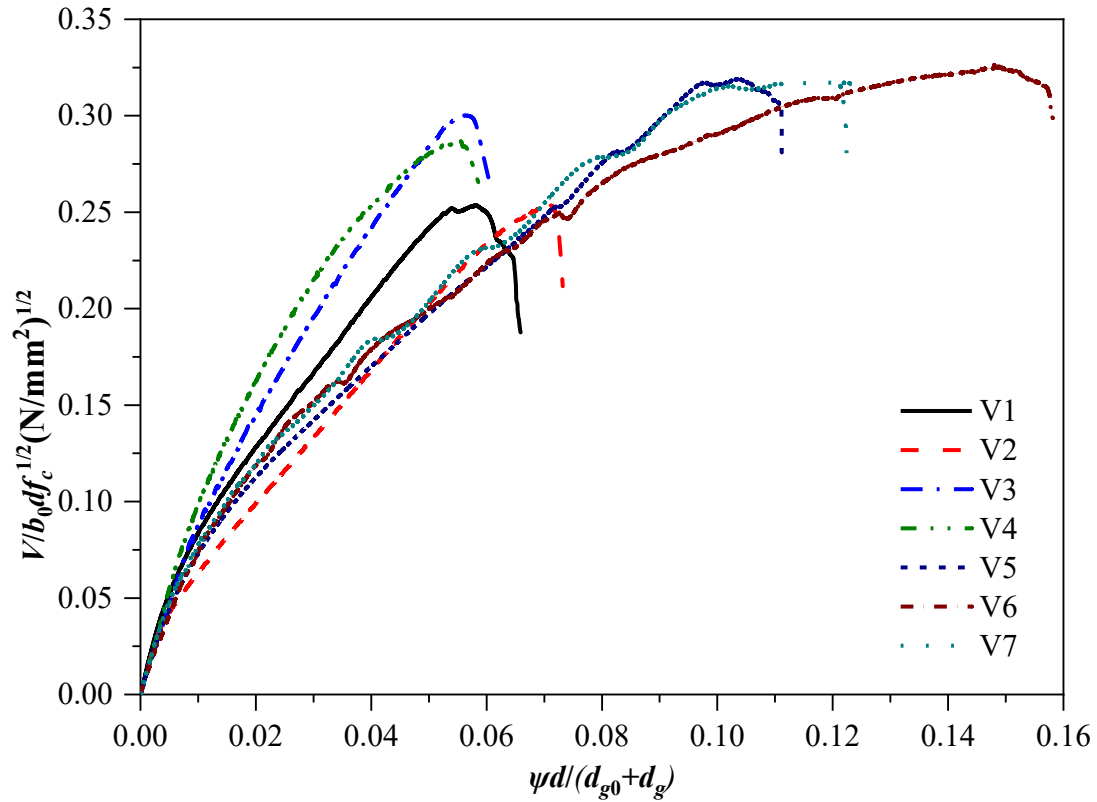


Figure 4.41 – Normalised Load versus Rotation (Current Study)

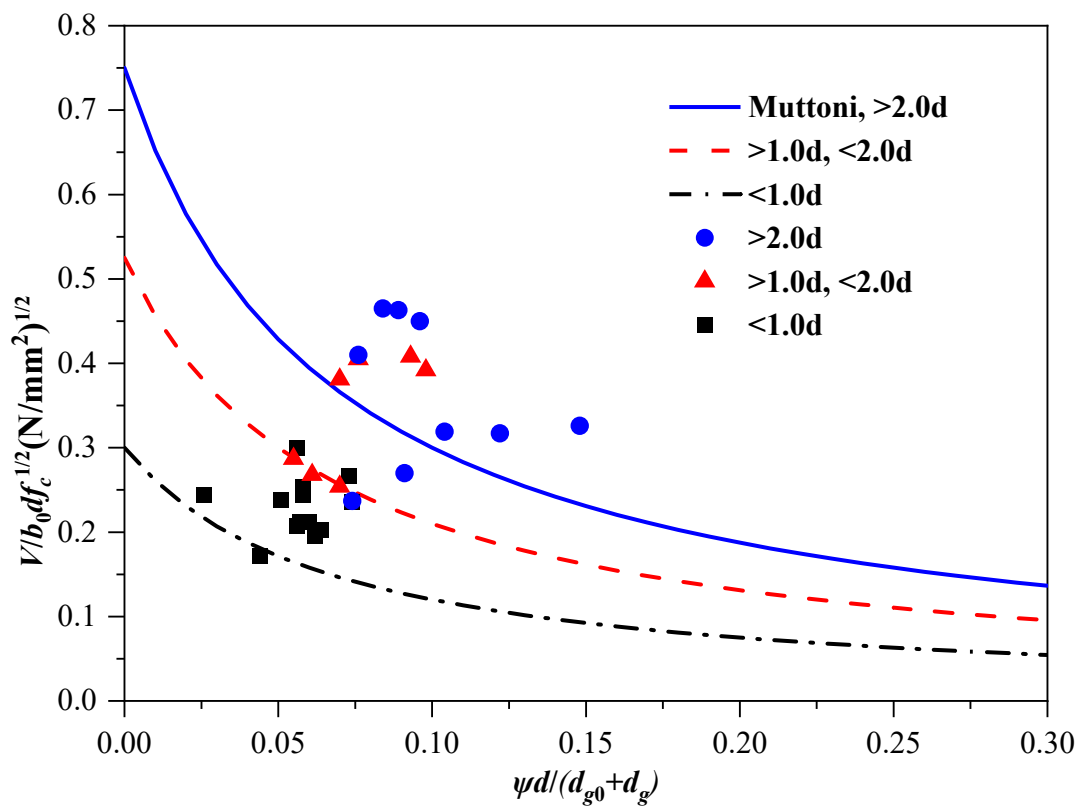


Figure 4.42 – Failure Criterion: Punching Shear Strength as Function of Width of Critical Shear Crack

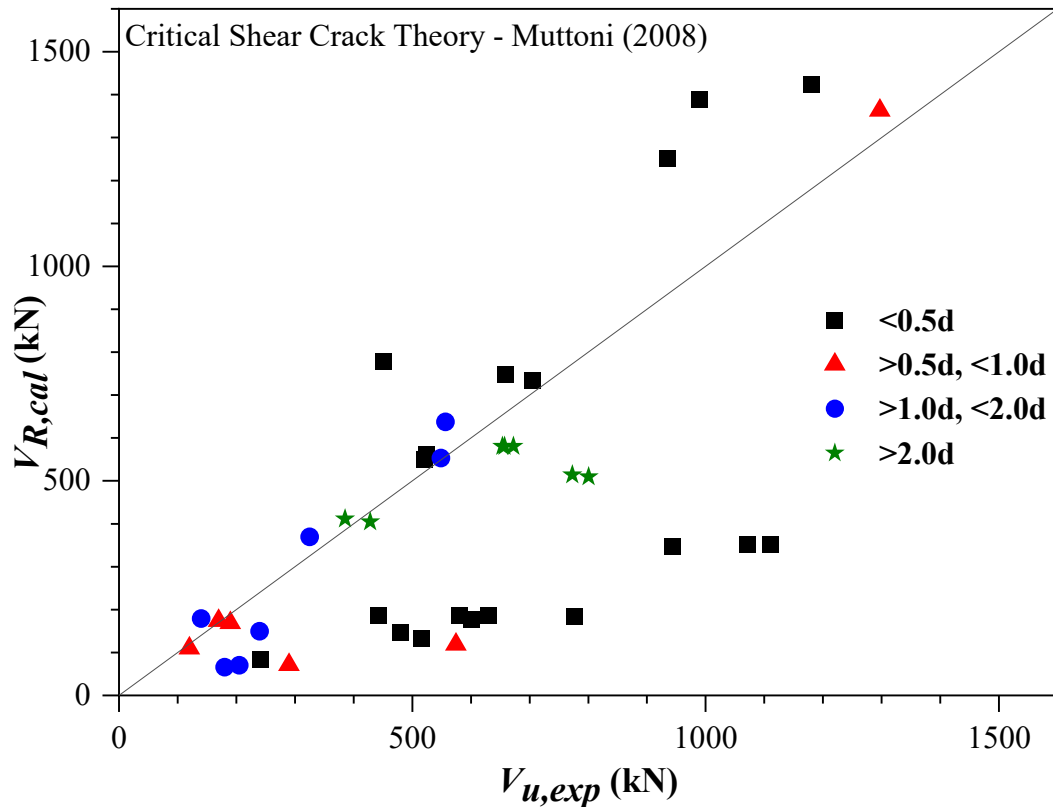


Figure 4.43 – Comparison of punching shear capacity of voided slab specimens obtained from experiments and Critical Shear Crack Theory

#### 4.4 Summary

In this chapter, the results of full-scale specimens tested under punching shear are discussed. It is evidenced that the location of voids has a significant effect on the punching shear capacity. Therefore, an effective way of predicting the punching shear capacity is investigated as the presence of voids alters the critical failure section. The applicability of conventional methods for solid slabs in the design standards, such as ACI 318 (2014), EN 1992-1-1 (2004) and IS 456 (2000) to predict the punching shear capacity of the voided slab is examined. Finally, experimental results of the present study and test data collected from the literature (33 specimens) were compared with predictions by the relevant code provisions. The estimation of punching shear capacity of the biaxial voided slab by existing provisions for solid slabs in standards does not lead to satisfactory results. Hence, the presence of voids is considered by modifying the critical section depending on the void location. Further, only the effective concrete area is considered to predict the punching shear capacity. After the modifications, the predictions by all three building standards lead to satisfactory results. In addition, the applicability of critical shear crack theory to predict the punching shear capacity is investigated.

This page is intentionally left blank.

## CHAPTER 5

### FINITE ELEMENT ANALYSIS

#### 5.1 Overview

This chapter discusses the background of modelling and analysis of biaxial voided slab subject to various loadings conditions, such as one-way and two-way flexure and one-way shear and punching (two-way) shear. The numerical studies are carried out in the finite element software DIANA (DIANA FEA BV., 2017a – d). The adopted properties of materials, such as concrete and reinforcement, are based on the available material models available in the literature and experimental observations of the current study. The detailed procedure to model the slab, meshing the slab with appropriate materials' model, load steps, and non-linear analysis are summarised. The parametric study is carried out in DIANA version 9.4.4, and the numerical study with current experimental specimens is carried out in DIANA version 10.0. The obtained results from numerical studies are compared with the available experimental test results.

#### 5.2 Materials' Properties

In general, the non-linear response is caused by the cracking of the concrete, yielding of reinforcement and non-linear behaviour of concrete (Mohammadi, 2008). The constitutive material models are playing a vital role to obtain realistic results. In this section, the properties of concrete and reinforcement are explained.

##### 5.2.1 Mechanical Properties of Concrete

###### 5.2.1.1 Compression

The stress-strain behaviour of concrete in compression was considered as Hognestad parabola (DIANA FEA BV., 2017d; Ferreira, 2013; Hognestad, Hanson, and Mchenry, 1955) as shown in Figure 5.1(a) and given in Eq. 5.1.

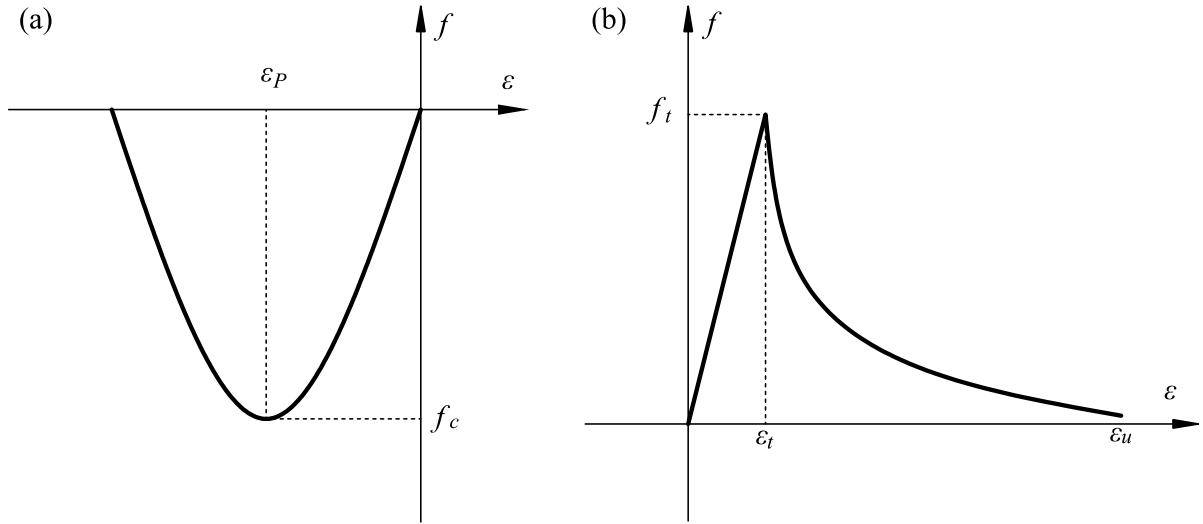


Figure 5.1 – Concrete Behaviour Considered in Finite Element Analysis (a) Compression and (b) Tension

$$f = -f_c \left[ \frac{2\varepsilon}{\varepsilon_p} - \left( \frac{\varepsilon}{\varepsilon_p} \right)^2 \right] \quad \text{Eq. 5.1}$$

$$\varepsilon_p = -\frac{2f_c}{E} \quad \text{Eq. 5.2}$$

where,  $\varepsilon_p$  is strain corresponding to maximum cylinder compressive stress ( $f_c$ ), estimated by Eq. 5.2,  $E$  is Young's modulus of concrete ( $= 5000 f_{cm}^{0.5}$ ), and  $f_{cm}$  is mean cube compressive strength.

### 5.2.1.2 Tension

The linear stress-strain curve (DIANA FEA BV., 2017d) for concrete in tension, as shown in Figure 5.1(b) was considered.

### 5.2.1.3 Tension Softening

The stress-strain relation of concrete in tension after the peak (softening branch) can be defined by tensile strength of concrete, area under the stress-strain curve, and shape of the descending branch (Roesler, Paulino, Park, and Gaedicke, 2007). In this study, the shape of the descending branch was considered as parabolic variation (Cornellissen, Hordijk, and Reinhardt, 1986; Hordijk, 1991; Hordijk & Reinhardt, 1990) as shown in Figure 5.1(b). The relationship between stress-strain (tension softening) is given in Eq. 5.3.

$$\frac{f_n(\varepsilon)}{f_t} = \begin{cases} \left(1 + \left(c_1 \frac{\varepsilon}{\varepsilon_u}\right)^3\right) \exp\left(-c_2 \frac{\varepsilon}{\varepsilon_u}\right) - \frac{\varepsilon}{\varepsilon_u} (1 + c_1^3) \exp(-c_2) & \text{for } \varepsilon_t < \varepsilon < \varepsilon_u \\ 0 & \text{for } \varepsilon_u < \varepsilon < \infty \end{cases} \quad \text{Eq. 5.3}$$

with the parameters  $c_1 = 3$  and  $c_2 = 6.93$ .

#### 5.2.1.4 Tension Cut-off

The tension cut-off of concrete in two-dimensional principal stress spaces (Figure 5.2) is defined by tensile ( $f_t$ ) and compressive ( $f_c$ ) strength. (DIANA FEA BV., 2017d).

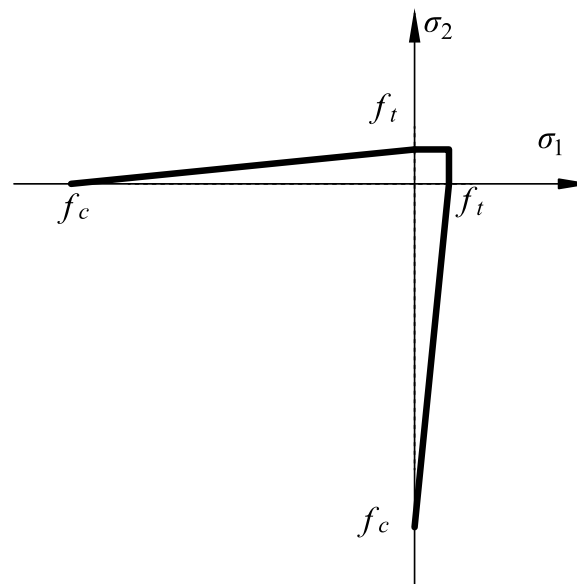


Figure 5.2 – Tension Cut-off: Linear

#### 5.2.1.5 Shear Retention Factor

In the smeared crack models, the transverse stiffness of the concrete reduces due to cracking and it is accounted through shear retention factor ( $\beta$ ) (De Borst, 1987). Thus, the shear stiffness is given by Eq. 5.4.

$$D_{secant}^{II} = \frac{\beta}{1 - \beta} G \quad \text{Eq. 5.4}$$

The parameter  $\beta$  may range from 0 to 1. Based on the recommendations given in the literature (Held and Pfeffer, 2002), the value of shear retention factor ( $\beta$ ) was taken as 0.18.

### 5.2.1.6 Material Model

#### (i) Mohr-Coulomb Plasticity Model

The compressive regime of concrete is defined by the Mohr-Coulomb plasticity model with the help of Eq. 5.5.

$$c = \frac{f_c (1 - \sin \varphi)}{2 \cos \varphi} \quad \text{Eq. 5.5}$$

where,  $c$  is cohesion,  $\varphi$  is friction angle, and  $f_c$  is compressive strength.

#### (ii) Total Strain based Crack Model

In this model, rotating crack orientation was used, as it does not require explicit shear retention function. The total strain based crack model evaluates the principal stresses and strains based on the given material input, i.e., uniaxial stress-strain relationship.

### 5.2.1.7 Element

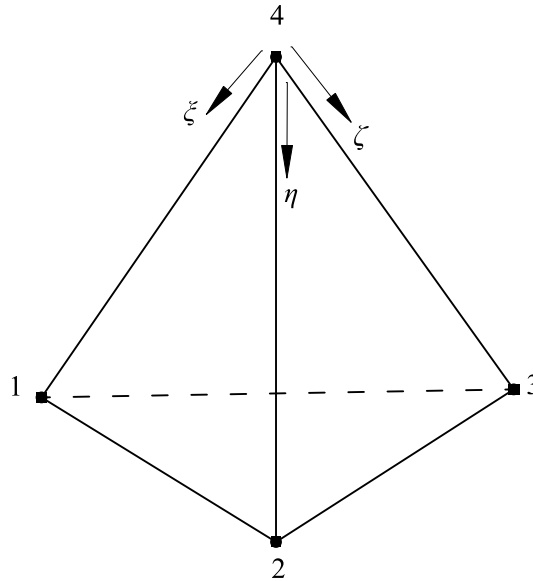


Figure 5.3 – TE12L Element

Four-noded isoparametric solid pyramid elements (TE12L) for concrete is adopted in this study. The TE12L element (Figure 5.3) is a four-node, three-side isoparametric solid pyramid element. The polynomials for the translations  $u_{xyz}$  is given in Eq. 5.6. These polynomials yield a constant strain and stress distribution over the element volume.

$$u_i(\xi, \eta, \zeta) = a_0 + a_1 \xi + a_2 \eta + a_3 \zeta \quad \text{Eq. 5.6}$$



## 5.2.2 Mechanical Properties of Reinforcement

### 5.2.2.1 Uniaxial Stress-Strain

The bilinear stress-strain behaviour of reinforcement (Figure 5.4) was adopted with Von Mises plasticity. For the specimens tested in this study, the observed multi-linear stress-strain behaviour was adopted to compare with the experimental observations.

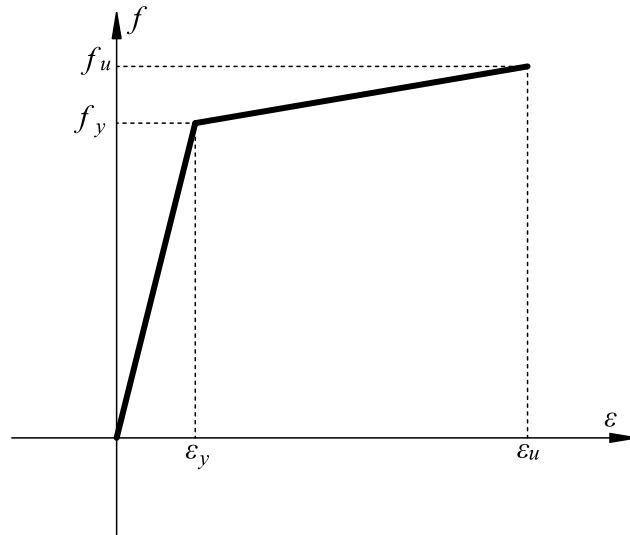


Figure 5.4 – Stress-Strain Behaviour of Reinforcement

### 5.2.2.2 Element

Reinforcements were modelled as embedded line elements in structural elements, i.e. parent element – concrete (Figure 5.5). Based on the assumption of a perfect bond between surrounding material and reinforcement, the strains are computed from the displacement field of the surrounding material (parent elements).

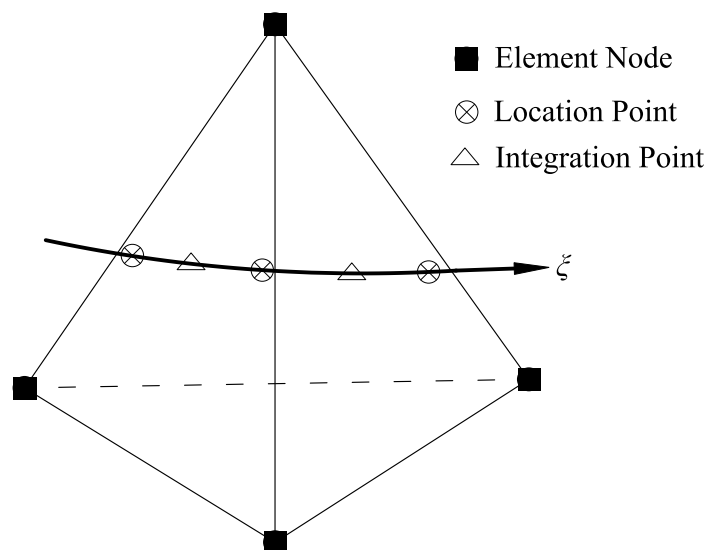


Figure 5.5 – Reinforcement: Embedded Line Element in Solid (TE12L) Element

### 5.3 Finite Element Model – Effect of Void Shape

The geometry of the biaxial hollow slab is complicated due to the presence of voids. Hence, non-linear finite element analysis is required to understand its structural behaviour. The finite element model of the slab is created in displacement analyser (DIANA) software by adopting a three-dimensional model to simulate the actual behaviour of the slab with voids.

#### 5.3.1 Shape of Void Formers

From the literature, it was observed that the void former can be in any shape. In this study, four commonly adopted shapes have been selected for simulation, such as sphere, ellipsoid, cuboid and donut-type with an internal hole (Figure 5.6).

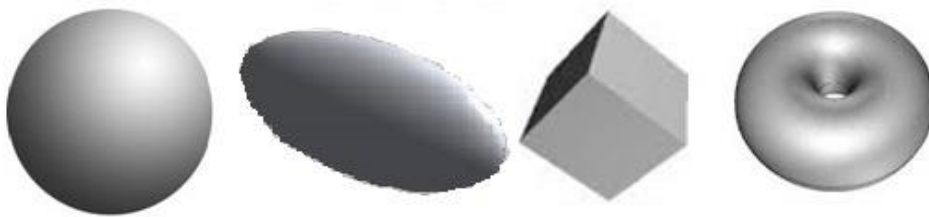


Figure 5.6 – Different Void Former Shapes considered in Numerical Study

#### 5.3.2 Simulation of Voided Slab

The biaxial voided slab was modelled in finite element software DIANA and non-linear analysis carried out with material behaviour explained in Section 5.2. One-quarter of the slab was modelled by taking advantage of symmetry, if applicable to reduce the computation time. In the model of the voided slab, the voids were created by simply removing the concrete in the desired shape of the void; this gives conservative results, i.e. results will be independent of void former materials' properties.

##### 5.3.2.1 Punching Shear

Held and Pfeffer (2002) were conducted punching shear experiment of the biaxial voided slab with sphere-shaped voids. The specimen details are shown in Figure 5.7. Figure 5.8 shows the photograph of the test set-up. In the test, the slab was held down at eight locations radially, and the load is applied through the central column in upward directions. The adopted column size in the experiment was 300 mm × 300 mm. The FE model and model with mesh & boundary conditions are shown in Figure 5.9 and Figure 5.10, respectively. The size of the mesh is chosen as 25 mm based on mesh convergence study. The voids are created by removing the concrete at a required place with a specified shape, as shown in Figure 5.11. Similarly, the finite element

analysis was carried out for the same slab with different void shapes. The slab specimen models with various void shapes are shown in Figure 5.12 and Figure 5.13. The adopted material properties are summarised in Table 5.1. The details of void shapes are summarised in Table 5.2. In the simulation,  $\approx 30\%$  of concrete were removed by providing voids.

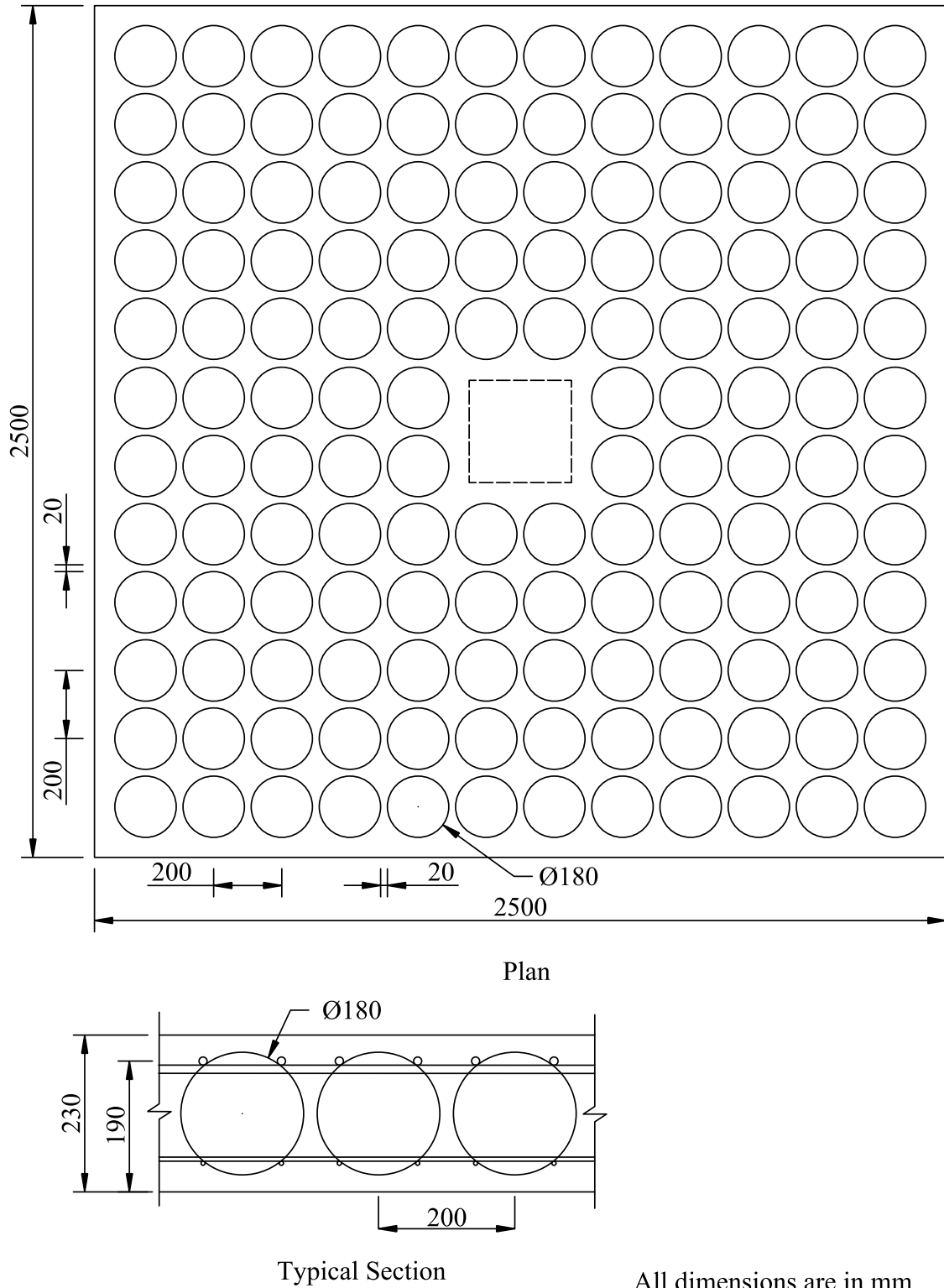


Figure 5.7 – Typical Specimen Details: Punching Shear

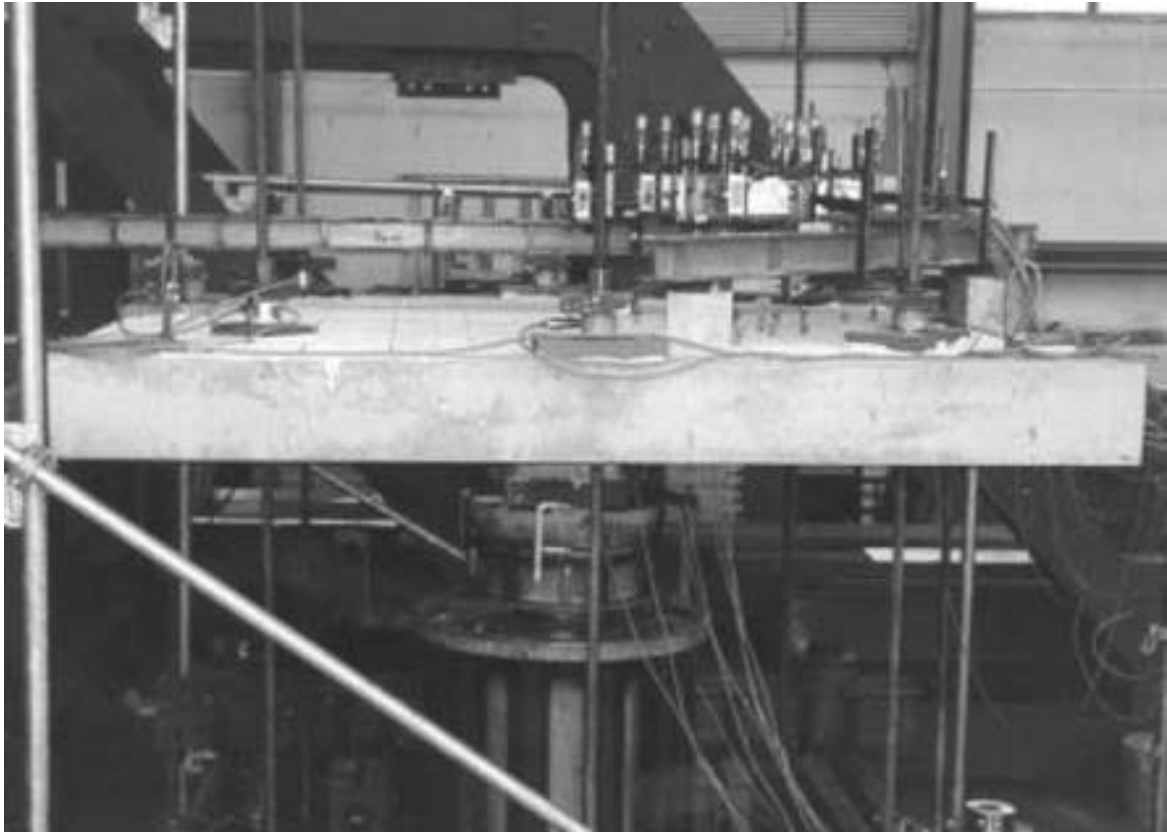


Figure 5.8 – Punching Shear Test Set-up (Held and Pfeffer, 2002)

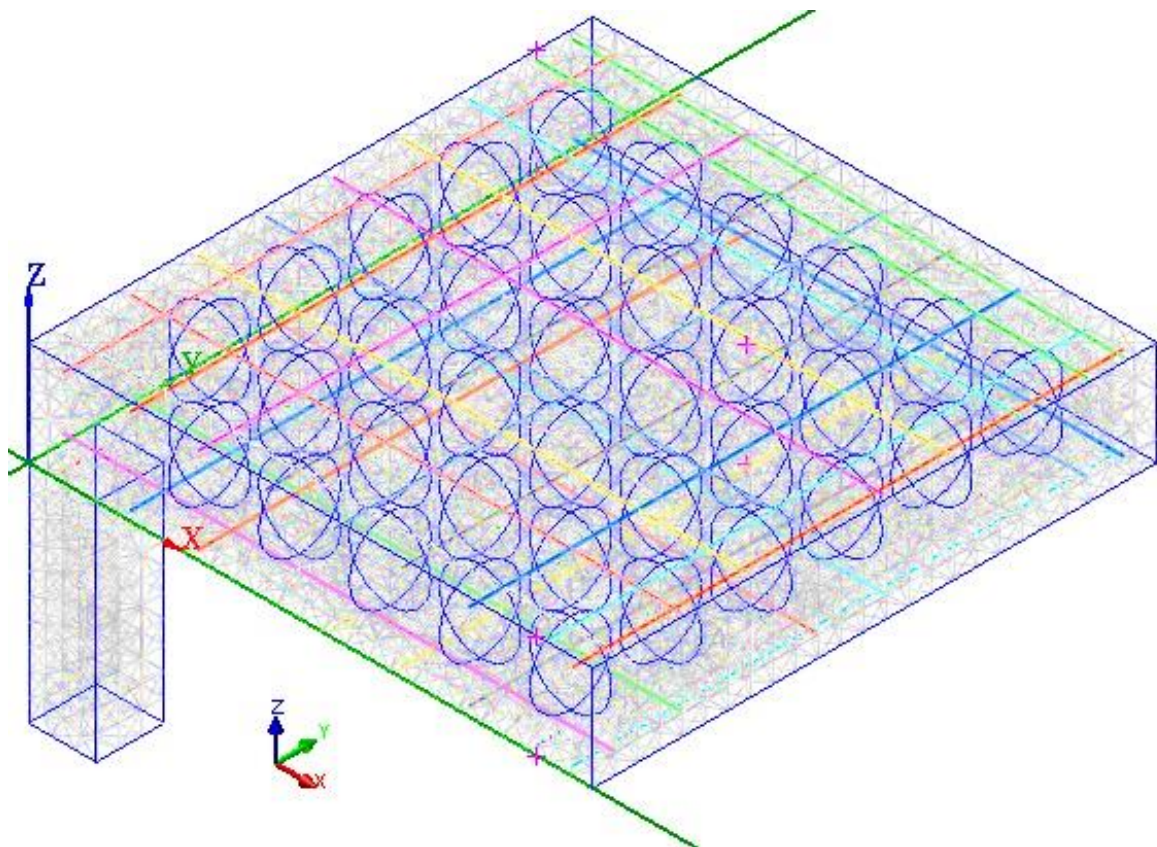


Figure 5.9 – Finite Element Model of Biaxial Sphere Voided Slab

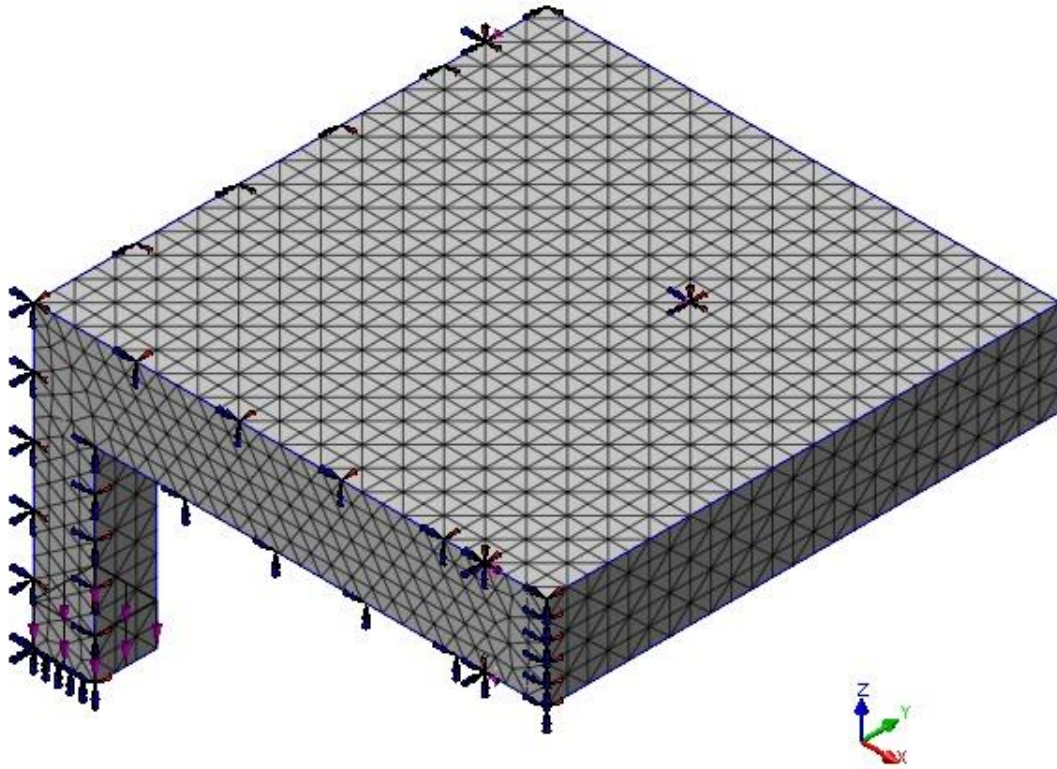


Figure 5.10 – Slab Model with Mesh and Boundary Conditions

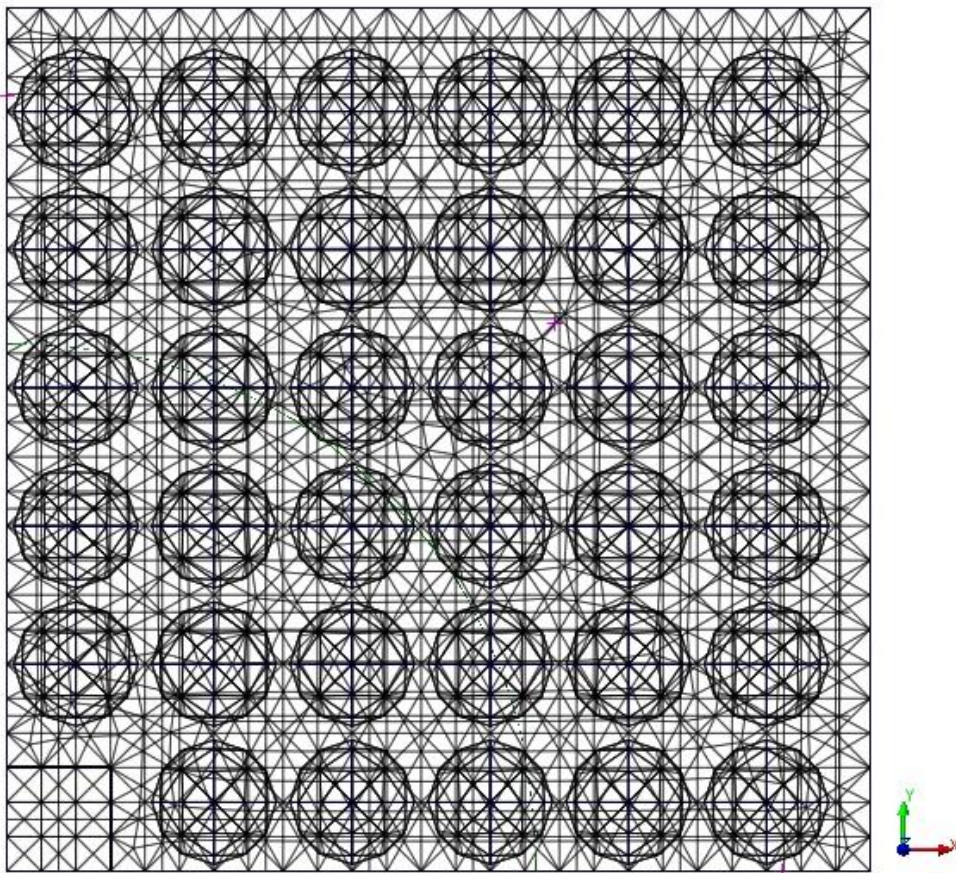


Figure 5.11 – Slab Model with Mesh showing the Sphere Voids

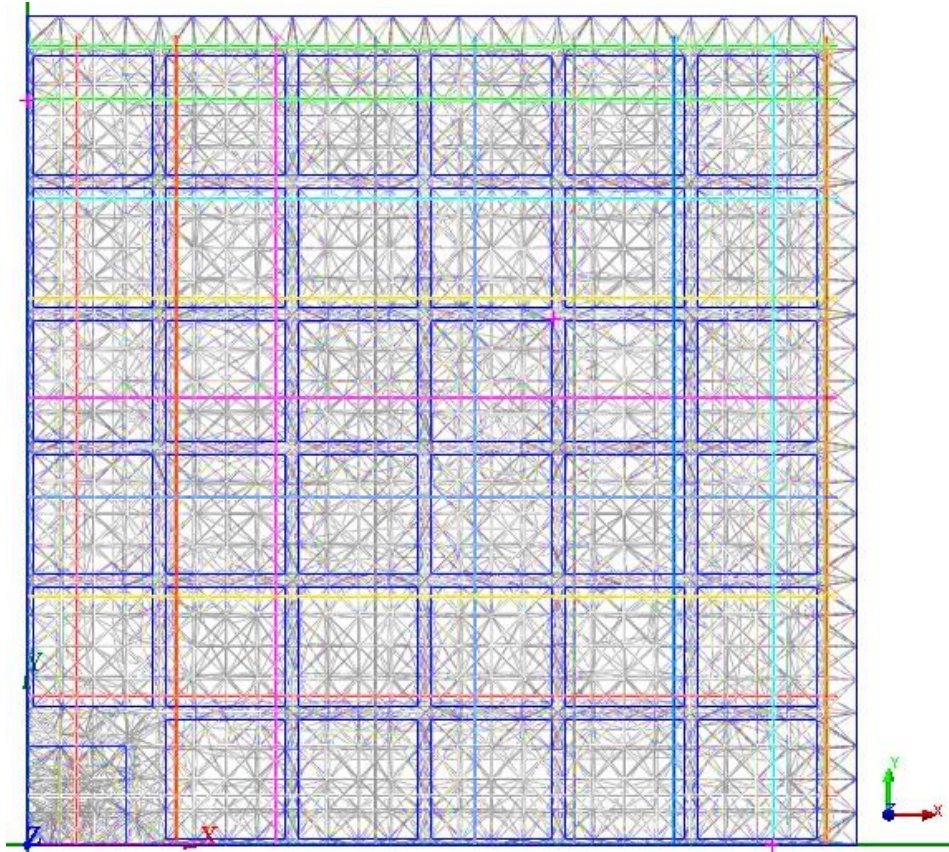


Figure 5.12 – Slab Model with Mesh showing the Cuboid Voids

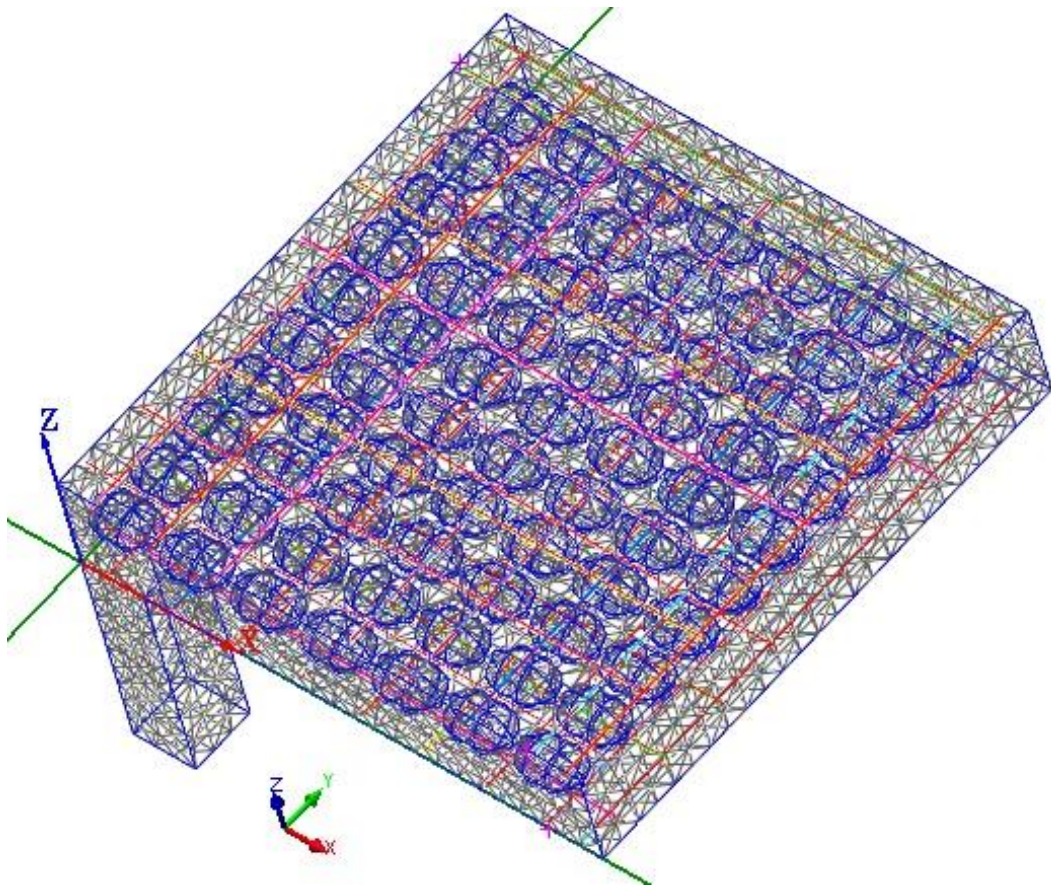


Figure 5.13 – Slab Model with Mesh showing the Ellipsoid Voids

Table 5.1 – Materials’ Properties

Parameter	Value
Compressive strength (mean) of concrete ( $f_{cm}$ )	50.8 N/mm <sup>2</sup>
Tensile strength of concrete ( $f_t$ )	2.5 N/mm <sup>2</sup>
Cohesion ( $c$ )	14.66 N/mm <sup>2</sup>
Fracture energy ( $G_f$ )	0.09 N.mm/mm <sup>2</sup>
Friction angle ( $\phi$ )	30°
Shear retention factor ( $\beta$ )	0.18
Mass Density ( $\rho$ )	2400 kg/m <sup>3</sup>
Poisson’s Ratio ( $\nu$ )	0.2
Yield strength of reinforcement ( $f_y$ )	415 N/mm <sup>2</sup>

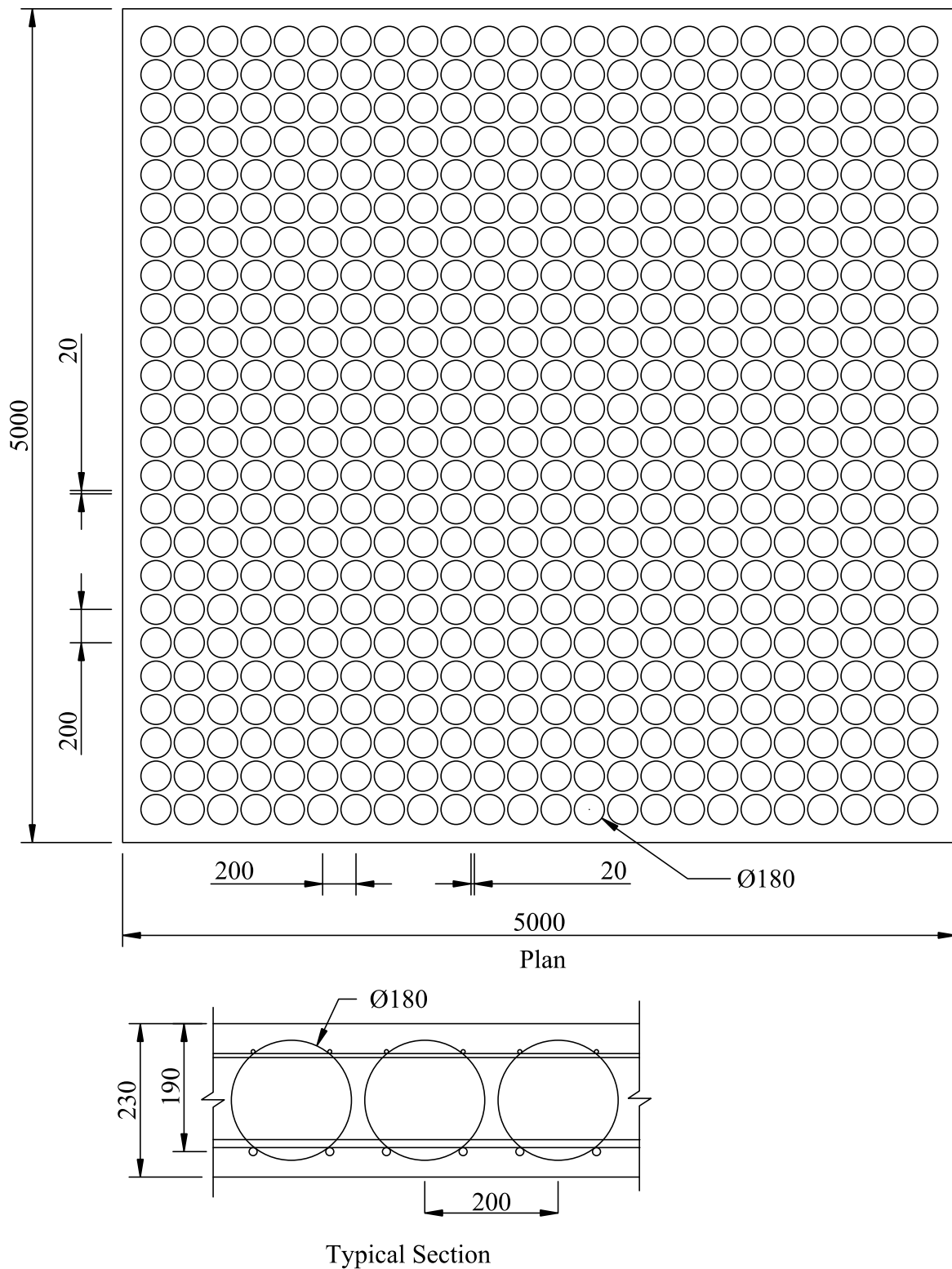
Table 5.2 – Biaxial Voided Slab Specimen Details

Parameter	Description
Slab dimension (punching shear)	2500 × 2500 × 230 mm
Slab dimension (two-way flexure)	5000 × 5000 × 230 mm
Reinforcement at tension side	3425 mm <sup>2</sup> /m
Reinforcement at compression side	1131 mm <sup>2</sup> /m
Sphere void	180 mm Dia.
Cuboid void	180 × 180 × 180 mm
Ellipsoid void	Radius: longer side ( $a$ ) – 90 mm Radius: shorter side ( $b$ ) – 45 mm
Donut void	270 × 270 × 140 mm and 50 mm dia. internal hole

### 5.3.2.2 Two-way Flexure

The numerical study of punching shear was extended to two-way flexure, which helps to understand the influence of void shapes on the behaviour of the biaxial voided slab. The specimen details are shown in Figure 5.14. The FE model with mesh and boundary conditions is shown in Figure 5.15. The slab model with mesh showing the sphere void is shown in Figure 5.16. The adopted material properties are summarised in Table 5.1. The details of void shapes are summarised in Table 5.2. In the simulation,  $\approx 30\%$  of concrete were removed by providing voids. The slab was supported at its all four sides by simple support, i.e. hinge support at two

adjacent edges and roller support at other two adjacent edges. The load is applied as a uniformly distributed load on the top surface of the slab.



All dimensions are in mm

Figure 5.14 – Typical Specimen Details: Two-way Flexure



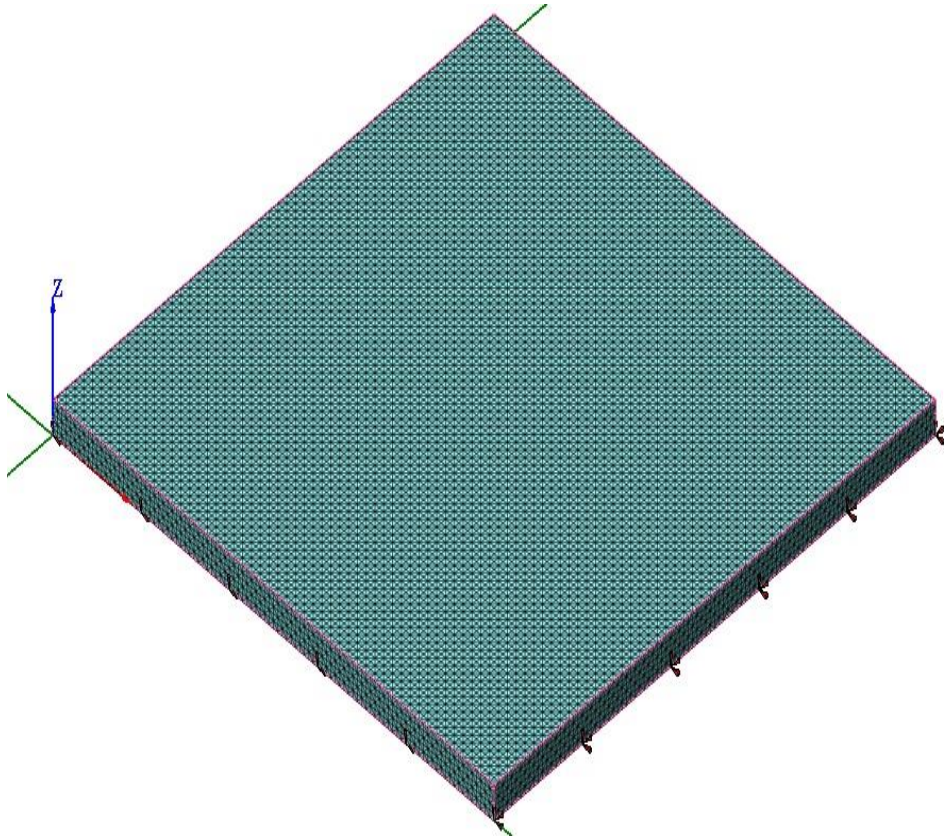


Figure 5.15 – Slab Model with Mesh and Boundary Conditions (Two-way Flexure)

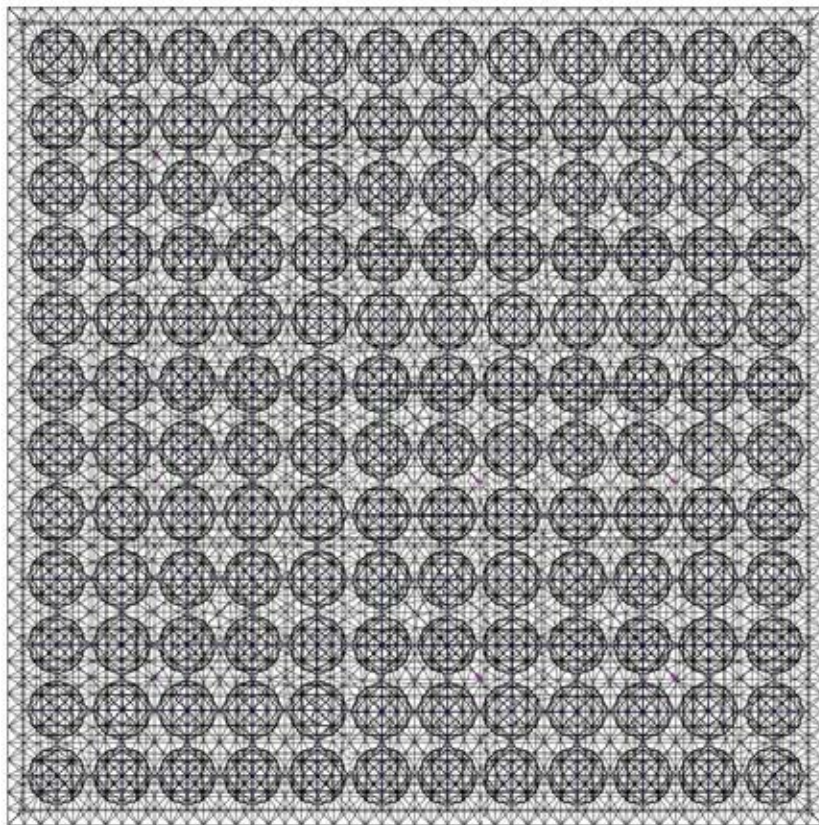


Figure 5.16 – Slab Model with Mesh showing the Sphere Voids (Two-way Flexure)

### 5.3.3 Results and Discussion

#### 5.3.3.1 Punching Shear

The obtained load versus displacement behaviour of the biaxial sphere voided slab is compared with the reported experimental results (Figure 5.17). It was observed that the numerical simulation results closely match with the experimental observations. The load versus mid-span displacement for all the biaxial voided slab with various void shapes are shown in Figure 5.17. It evidences that the shape of the void former affects the behaviour of biaxial voided slab significantly. Also, the sphere voided slab shows higher punching shear capacity and stiffness in comparison with other shape voided slabs. The observed deformed shape and deflection contour are shown in Figure 5.18 and Figure 5.19, respectively.

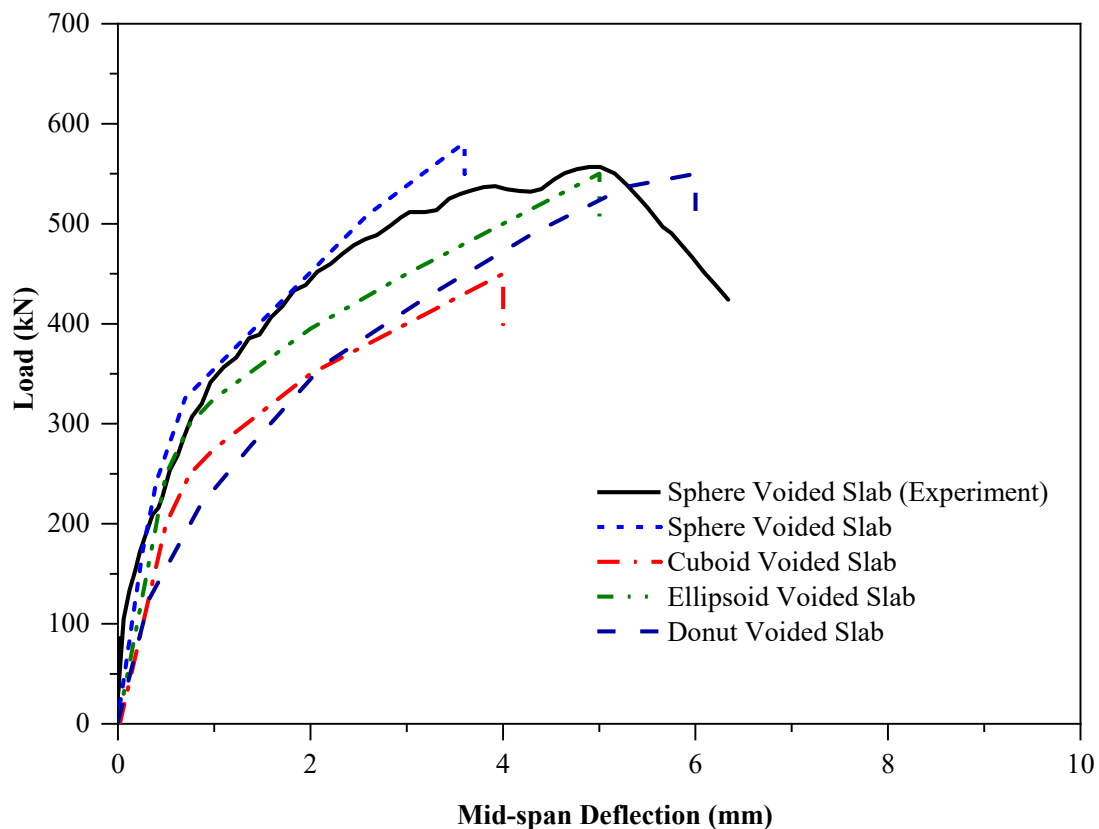


Figure 5.17 – Load versus Mid-span Deflection (Numerical Simulation – Punching Shear)

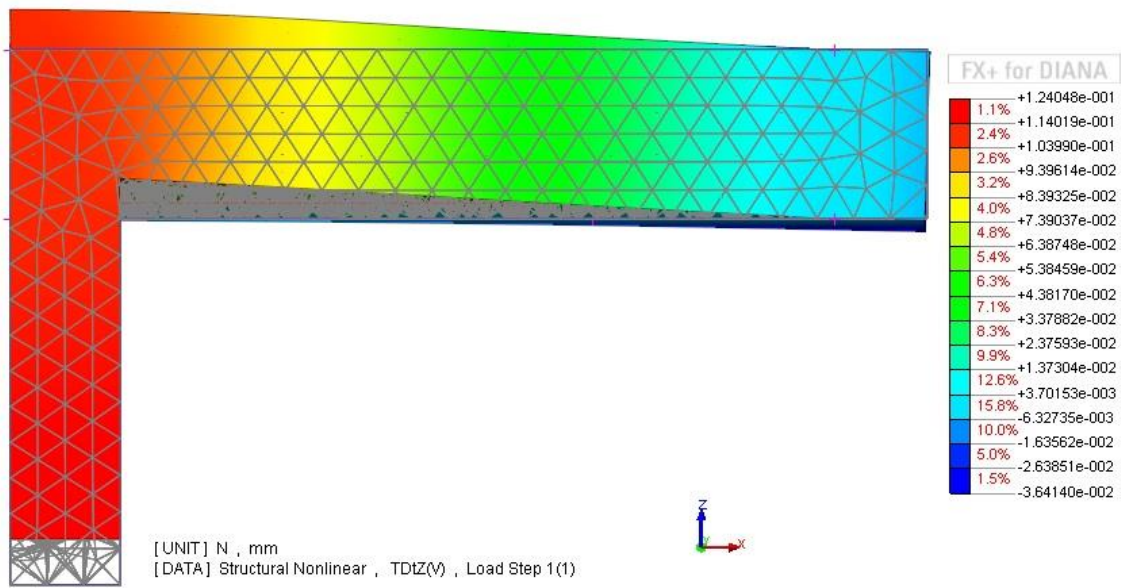


Figure 5.18 – Deformed Configuration (Punching Shear – Sphere Voided Slab)

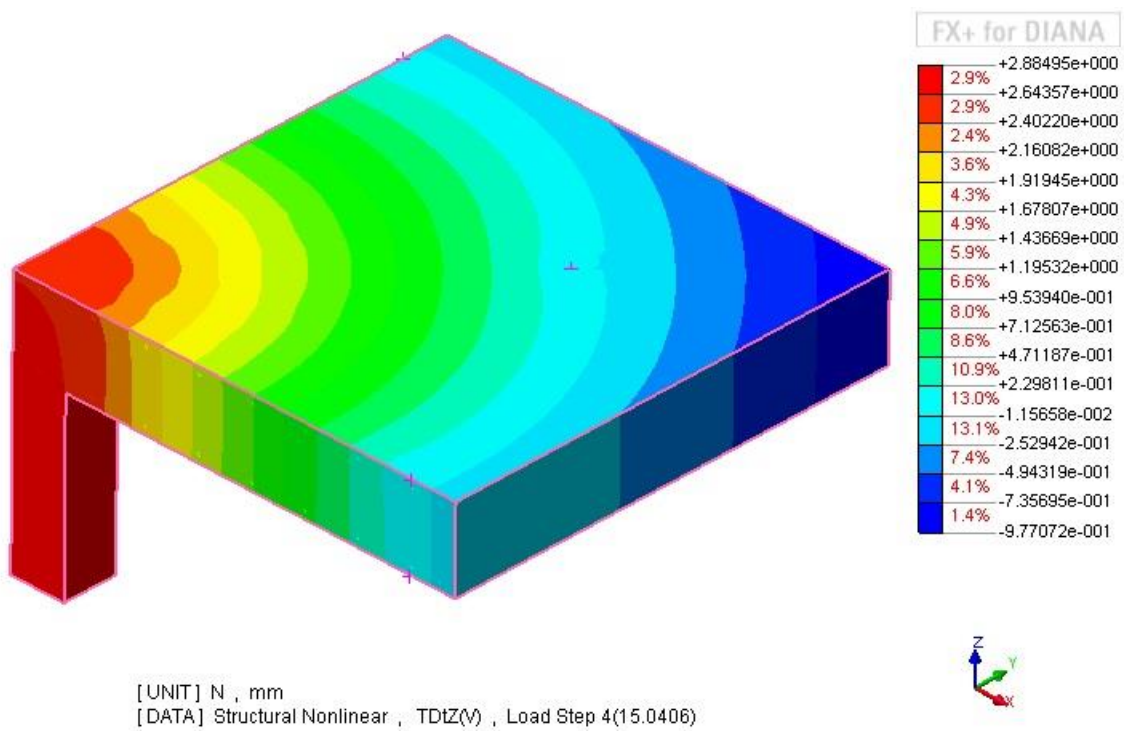


Figure 5.19 – Deflection Contour (Punching Shear – Sphere Voided Slab)

### 5.3.3.2 Two-way Flexure

The observed load versus mid-span displacement for all the biaxial voided slab with various void shapes are shown in Figure 5.20. The sphere voided slab shows higher flexural capacity and stiffness in comparison with other shape voided slabs. The observed typical deflection contour is shown in Figure 5.21.

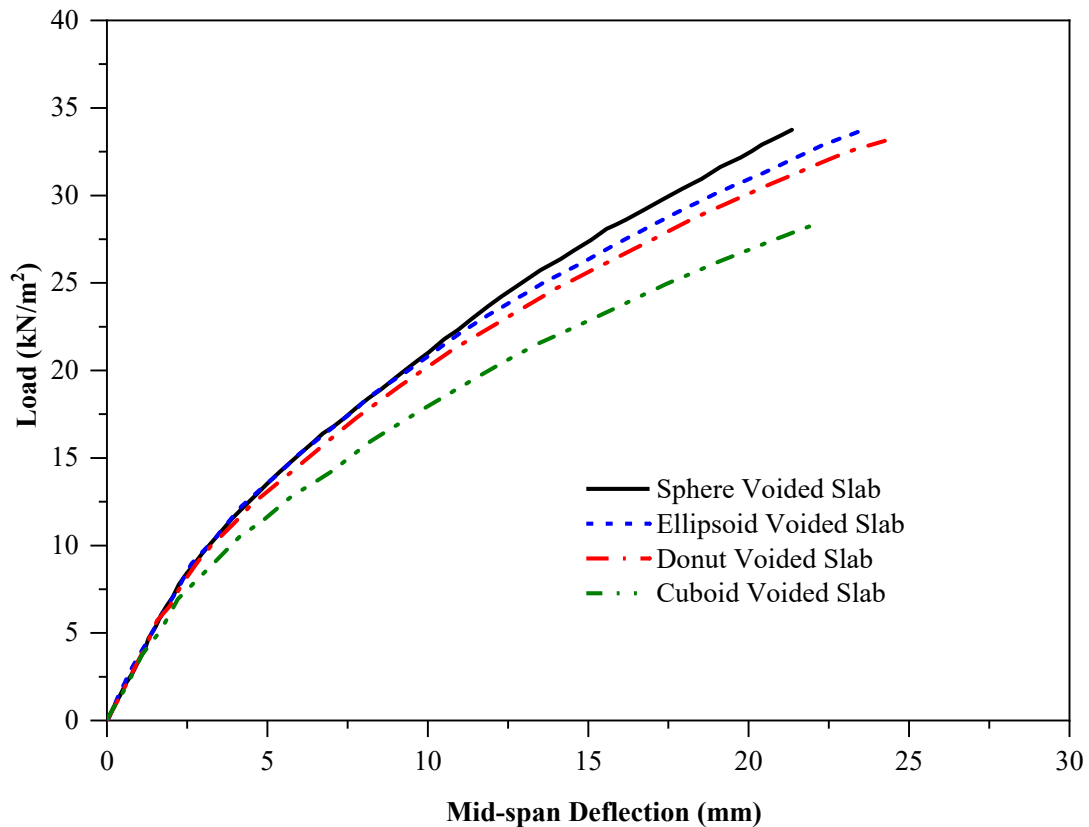


Figure 5.20 – Load versus Mid-span Deflection (Numerical Simulation – Two-way Flexure)

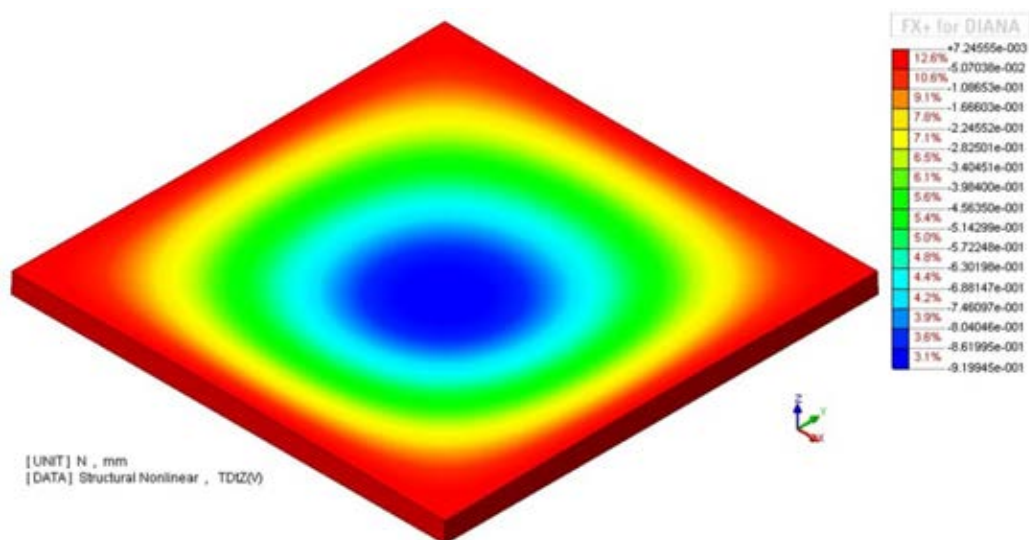


Figure 5.21 – Typical Deflection Contour (Two-way Flexure – Sphere Voided Slab)

## 5.4 Finite Element Model – Based on Current Experimental Study

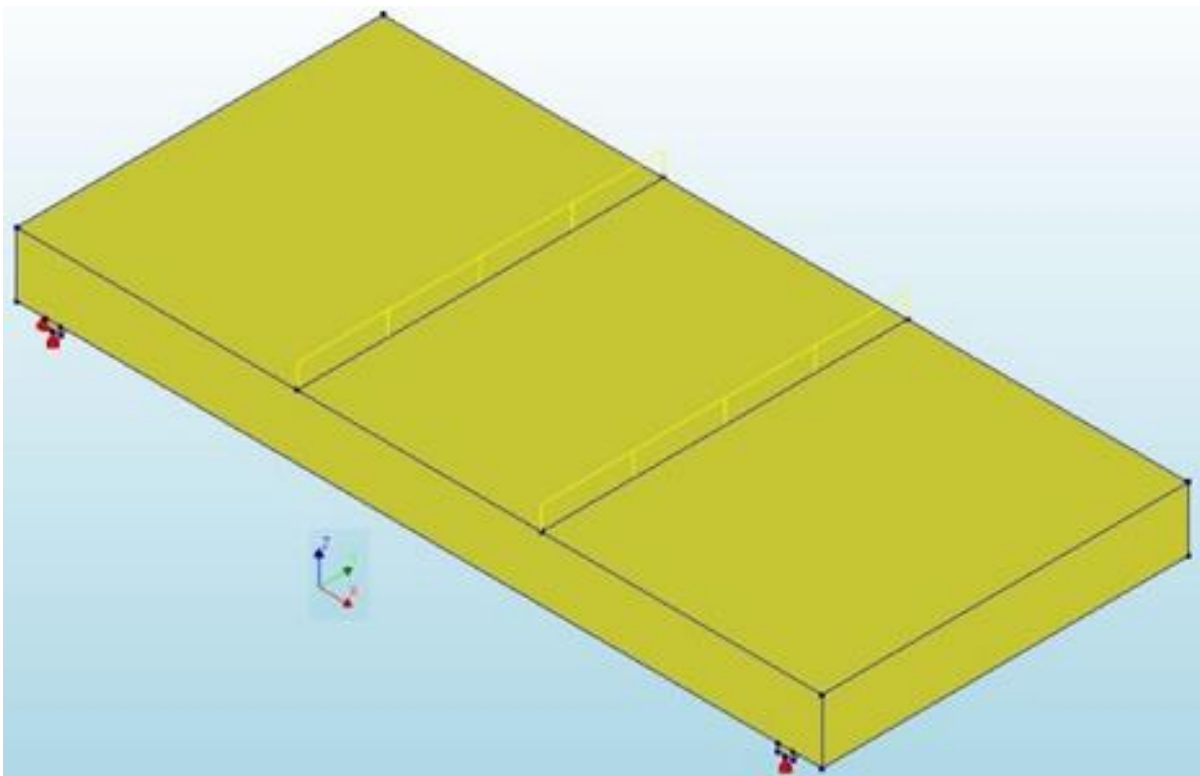
The finite element simulation was carried out for the biaxial cuboid voided slab specimens tested in the current study. This helps to understand the structural behaviour of cuboid voided slab subjected to one- and two-way flexure, shear (one-way) and punching shear.

### 5.4.1 One-way Flexure

Numerical simulation of the slab specimens subjected to one-way flexure was carried out in the finite element software DIANA. A three-dimensional model developed and non-linear analysis was carried out to simulate the actual slab specimens with voids. The specifications of slab like plan dimension, cross-section, reinforcement details and position of void former were considered as per actual test given in Section 3.2.2. The properties of concrete are summarised in Table 5.3. Multi-linear stress-strain curve (Figure 3.11) was used to simulate the reinforcement behaviour, which was obtained by conducting a tensile test on the reinforcements. The adopted materials' model is explained in Section 5.2. In the test, the slab was supported at both ends, with one end hinge and another end roller. Finite element model with the same boundary conditions and mesh are in shown in Figure 5.22 and Figure 5.23, respectively. Displacement controlled non-linear analysis (DIANA FEA BV., 2017a) was carried out with the increment of displacement in a phased manner to capture critical behaviour at initial cracking, yielding and ultimate stages. Deformed shape with deflection contour of the voided slab is shown in Figure 5.24. Cauchy stress ( $\sigma_{xx}$ ) contour of the voided slab prior to the initial crack is shown in Figure 5.25. One-quarter of the slab is shown for better visibility. Sectional views of stress contour at the centre of void along XX and YY planes are shown in Figure 5.25. The stress discontinuity and concentration at void locations can be observed from Figure 5.25. The solid slab with properties of the voided slab was modelled and analysed. The load versus mid-span deflection behaviour of the voided and solid slab is compared with experiment results (Figure 5.26). The slope of the load-deflection graph based on FEA for the voided slab is lower than that from the experiments after the first crack as the stiffness of void former was not considered in modelling. The load at yielding stage is higher for FEA results in comparison with experimental values, due to the assigned idealised stress-strain relationship of reinforcement. Figure 5.27 shows that the strain results obtained from FEA are in good agreement with that from experimental results. Figure 5.28 shows the observed crack pattern on the front elevation of the voided slab specimen (OF-CV-1) in experimental and numerical study. The crack pattern in experimental and numerical studies is observed to be the same.

Table 5.3 – Properties of Concrete

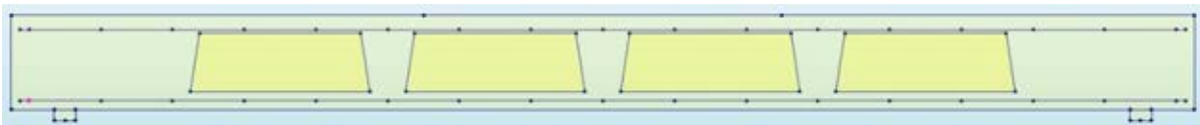
Parameter	Value
Compressive strength (mean) of concrete ( $f_{cm}$ )	24.8 N/mm <sup>2</sup>
Tensile strength of concrete ( $f_t$ )	1.0 N/mm <sup>2</sup>
Fracture energy ( $G_f$ )	0.075 N.mm/mm <sup>2</sup>
Mass Density ( $\rho$ )	2400 kg/m <sup>3</sup>
Poisson's Ratio ( $\nu$ )	0.2
Young's Modulus ( $E_c$ )	24900 N/mm <sup>2</sup>



Three-dimensional View



Elevation



Sectional View

Figure 5.22 – Model of Slab Specimen (OF-CV)

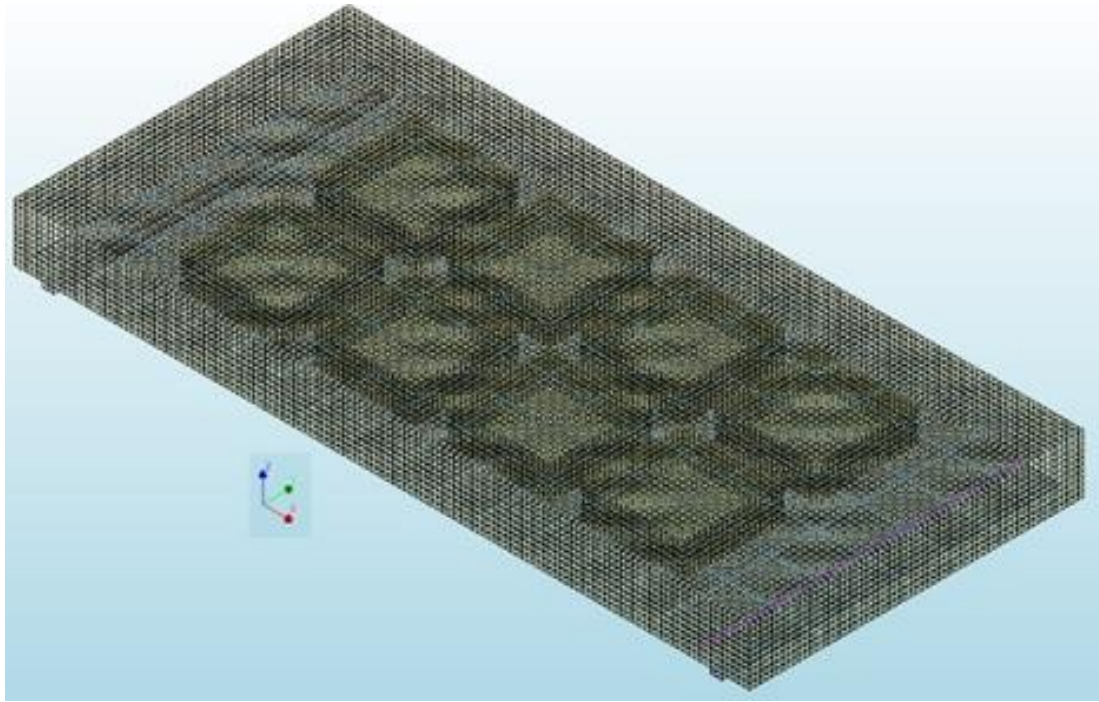


Figure 5.23 – Finite Element Model with Mesh

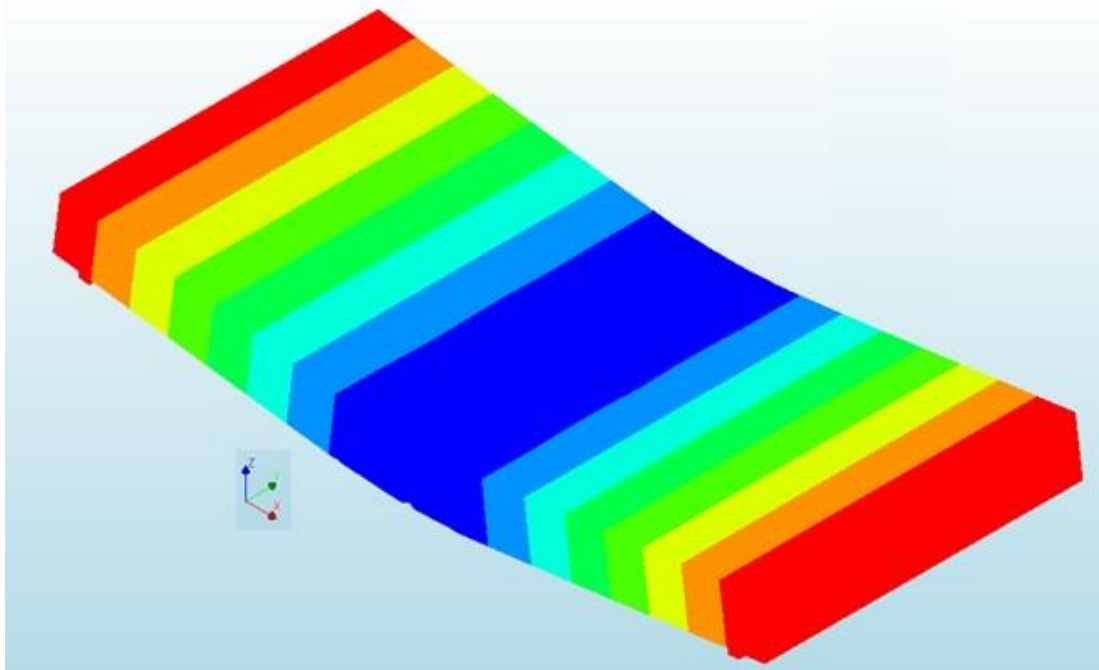


Figure 5.24 – Deformed Shape with Deflection Contour of Voided Slab

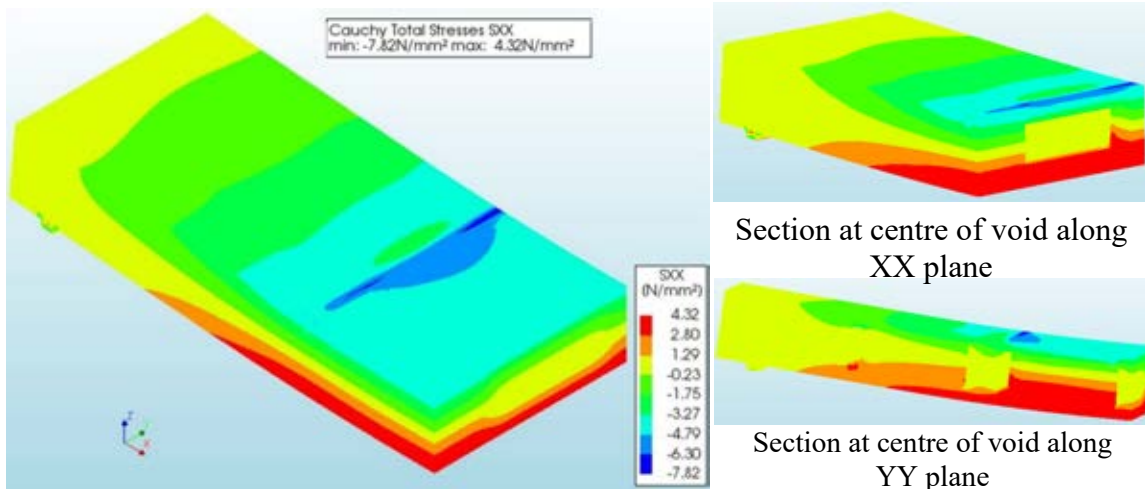


Figure 5.25 – Stress Contour of Voided Slab prior to Initial Crack (One-quarter of Slab)

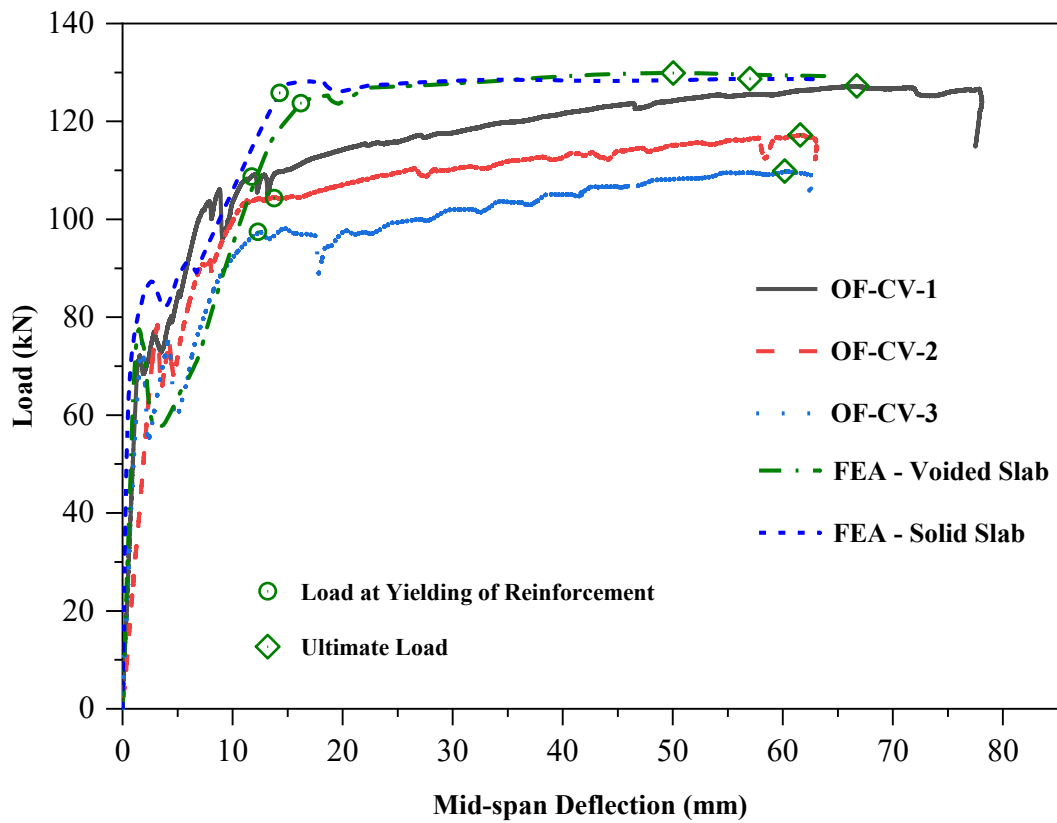


Figure 5.26 – Load versus Mid-span Deflection Behaviour (One-way Flexure)



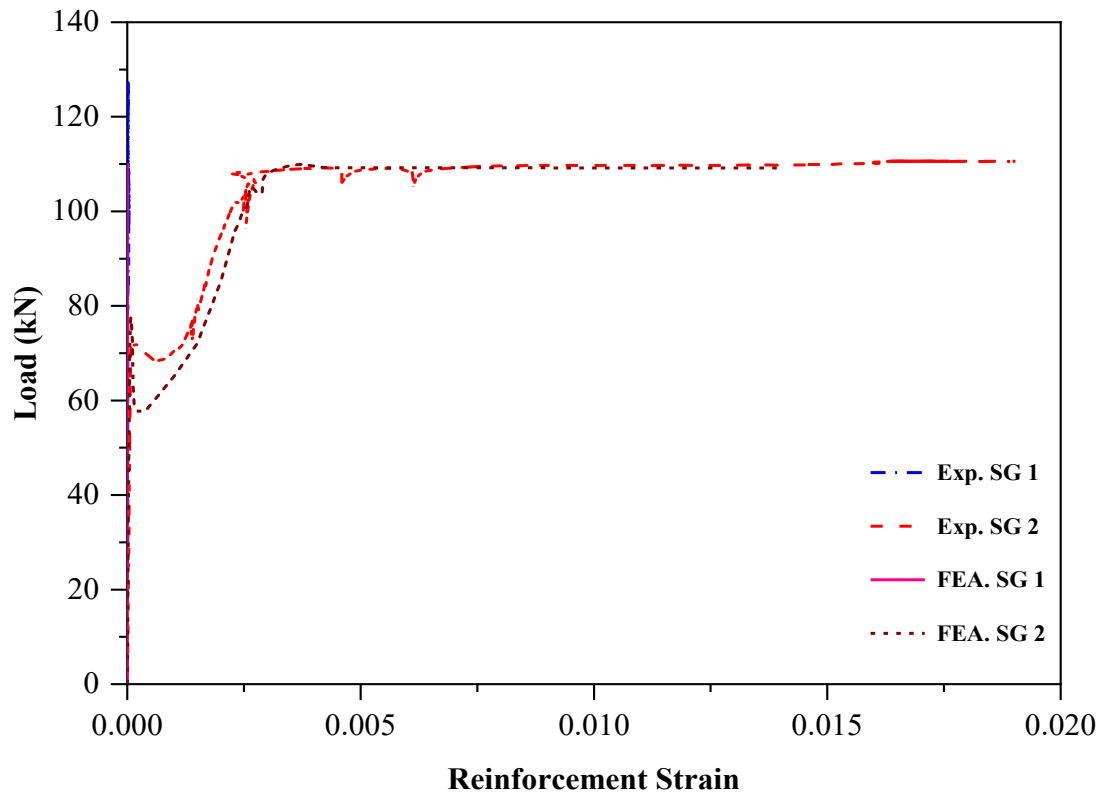
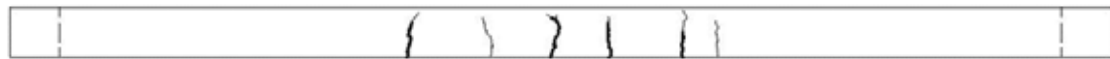


Figure 5.27 – Load versus Reinforcement Strain of Specimen OF-CV-1



(a) Experiment



(b) Simulation

Figure 5.28 – Observed Crack Pattern of Slab Specimen OF-CV-1 (Front Elevation)

Table 5.4 – Numerical Results: One-way Flexure

Specimen	At initial crack	At yielding	At ultimate	At service	
	$P_r$ (kN)	$P_y$ (kN)	$P_u$ (kN)	$P_s$ (kN)	$\delta_s$ (mm)
OF-CV	77.5	123.7	129.9	64.9	0.97
OF-Solid	87.3	125.9	128.7	64.4	0.57
<b>Ratio</b>	<b>0.89</b>	<b>0.98</b>	<b>1.01</b>	<b>1.01</b>	–

Note:  $P_r$ ,  $P_y$  and  $P_u$  are load corresponding to the first crack, yielding of reinforcement and ultimate failure, respectively;  $\delta_s$  is deflections at mid-span corresponding to service load  $P_s$  and  $P_s$  is assumed as 50% of ultimate load,  $P_u$ .

Table 5.5 – Comparison of Results: One-way Flexure

Specimen	At initial crack	At yielding	At ultimate	At service		
	$P_r$ (kN)	$P_y$ (kN)	$P_u$ (kN)	$P_s$ (kN)	$\delta_s$ (mm)	$K_s$ (kN/mm)
Numerical	77.5	123.7	129.9	64.9	0.97	66.91
Experiment	74.7	103.5	118.1	59.0	1.50	39.33
<b>Ratio</b>	<b>1.04</b>	<b>1.19</b>	<b>1.10</b>	<b>1.10</b>	–	<b>1.70</b>

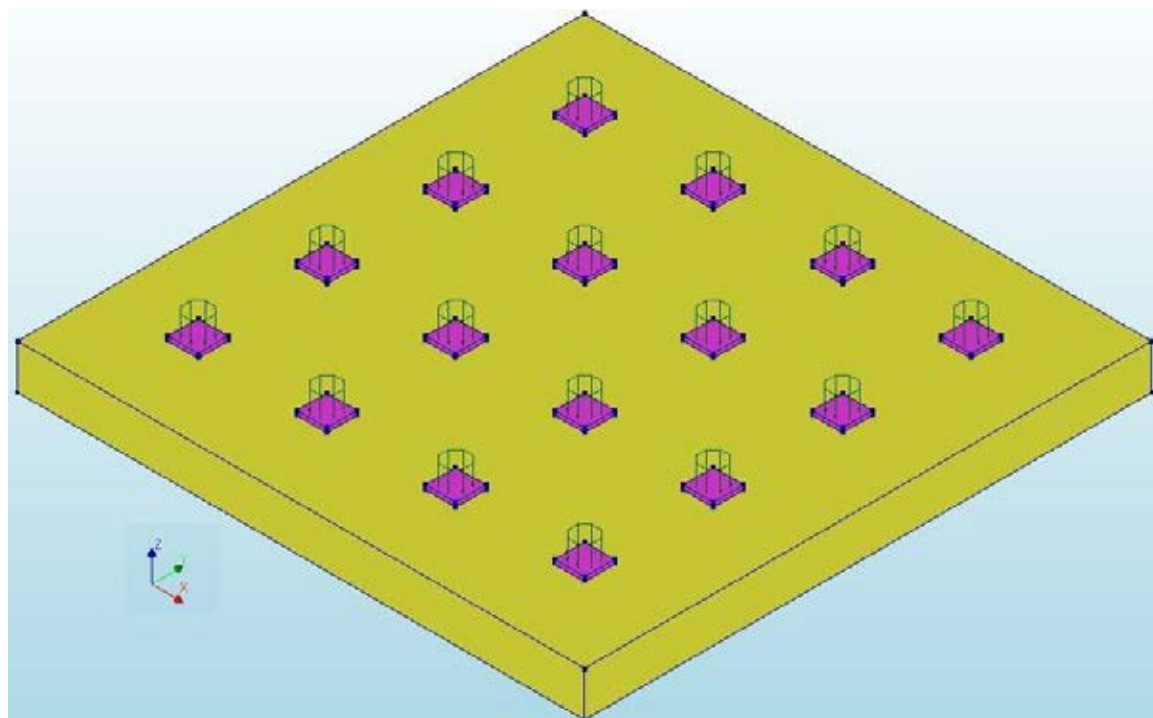
Note:  $P_r$ ,  $P_y$  and  $P_u$  are load corresponding to the first crack, yielding of reinforcement and ultimate failure, respectively;  $\delta_s$  is deflections at mid-span corresponding to service load  $P_s$  and  $P_s$  is assumed as 50% of ultimate load,  $P_u$ ;  $K_s$  is secant stiffness corresponding to  $P_s$ .

The obtained numerical results are summarised in Table 5.4. The comparison of experimental and numerical results are given in Table 5.5. From the comparison of results, it is observed that the one-way flexure behaviour of voided slabs could be well predicted by numerical analysis.

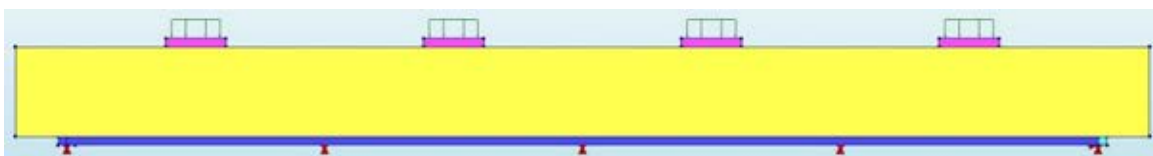
#### 5.4.2 Two-way Flexure

The biaxial voided slab specimen (TF-CV) was modelled and analysed in finite element software DIANA. A three-dimensional model developed and non-linear analysis was carried out to simulate the actual slab specimens with voids. The specifications of slab like plan dimension, cross-section, reinforcement details and position of void former were considered as per actual test given in Section 3.2.2. The properties of concrete are summarised in Table 5.3. Multi-linear stress-strain curve (Figure 3.11) was used to simulate the reinforcement behaviour, which was obtained by conducting a tensile test on the reinforcements. The adopted materials'

model is explained in Section 5.2. The load is applied as distributed point load (16 points). In the test, the slab was supported at its all four sides by simple support, i.e. hinge support at two adjacent edges and roller support at other two adjacent edges, the same boundary conditions were created. In addition, no tension boundary conditions were imposed to allow the corners of the slab to uplift as in the experiment the corners free to lift. Finite element model with boundary conditions and mesh are in shown in Figure 5.29 and Figure 5.30, respectively. Deflection contour of the biaxial cuboid voided slab is shown in Figure 5.31, which was obtained from the structural non-linear analysis. The load versus mid-span deflection behaviour of the voided and solid slab is compared with experiment results (Figure 5.32) and found that the FEA results are having a good agreement with experimental observations.



Three-dimensional View



Elevation



Sectional View

Figure 5.29 – Model of Slab Specimen (TF-CV)

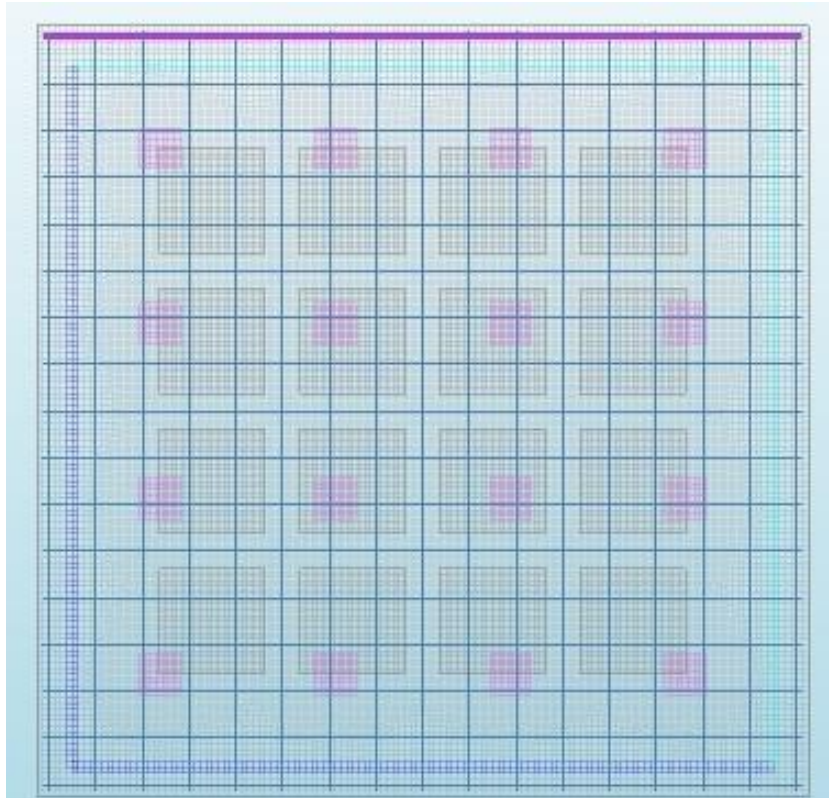


Figure 5.30 – Finite Element Model with Mesh (Two-way Flexure)

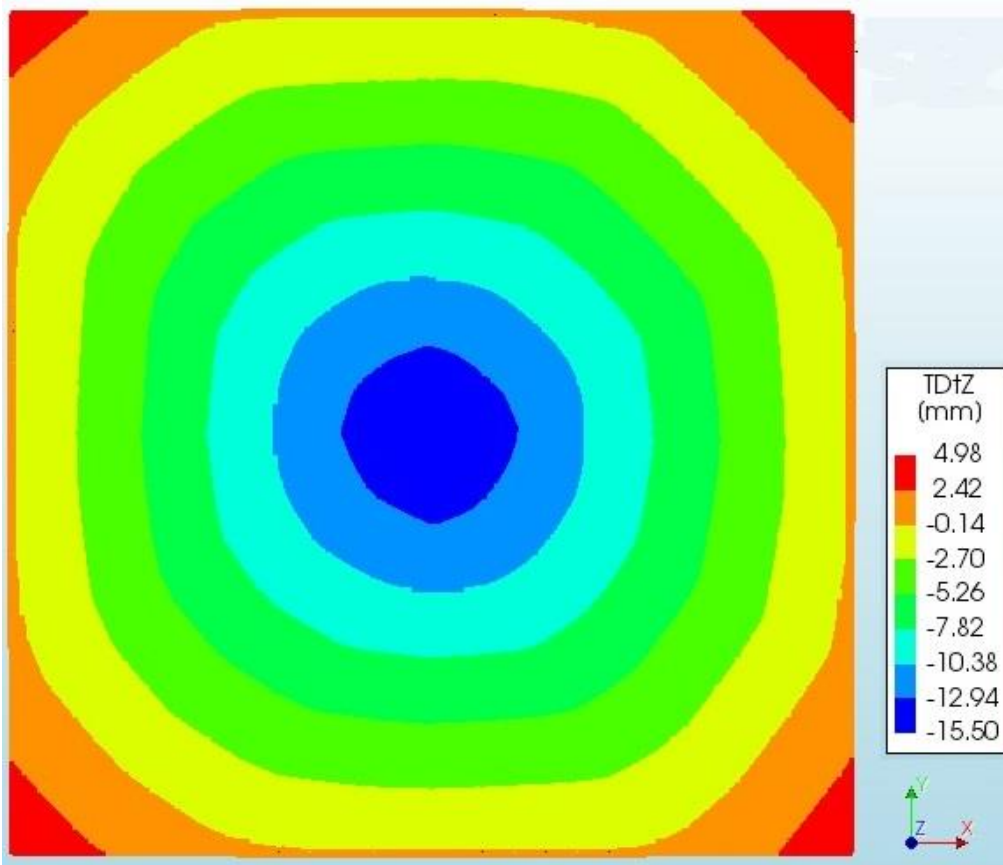


Figure 5.31 – Deflection Contour at 800 kN (Two-way Flexure)

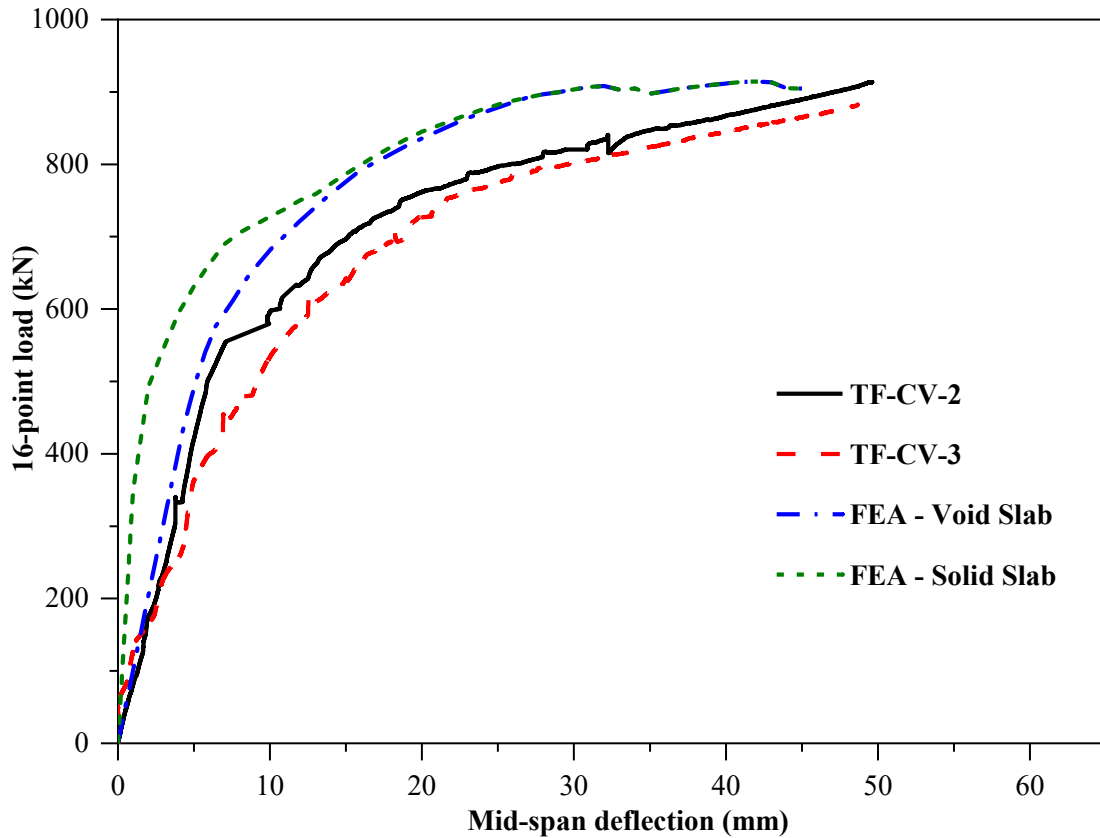


Figure 5.32 – Load versus Mid-span Deflection Behaviour (Two-way Flexure)

Table 5.6 – Comparison of Ultimate Load: Two-way Flexure

Specimen	Voided Slab		Solid Slab	Ratio	
	Experiment, $P_{u, Void-exp}$	Numerical, $P_{u, Void-Num}$	Numerical, $P_{u, Solid-Num}$	$P_{u, Void-Num}$ / $P_{u, Void-exp}$	$P_{u, Void-Num}$ / $P_{u, Solid-Num}$
Ultimate load (kN)	903.1	914.0	914.0	0.99	1.00

The obtained numerical results (ultimate capacity) are summarised in Table 5.6. The comparison of experimental and numerical results shows that the ultimate capacity is comparable; however, the stiffness (between the initial crack and yielding stage) showed a marginal difference.

### 5.4.3 Shear (One-way)

As experiments were not carried out, to study the shear behaviour of the biaxial cuboid voided slab, the numerical simulation was carried out based on the test specimen adopted for one-way flexure (Section 5.4.1). The load is applied as a line load at 240 mm (face of void) from the support. The slab was supported on both ends (one end hinge and another end roller). Finite element model with boundary conditions and mesh are in shown in Figure 5.33 and Figure 5.34, respectively. Displacement controlled analysis was carried out with 0.1 mm increment to capture the shear mode of failure. Deflection contour of the one-way voided slab is shown in Figure 5.35, which was obtained from the structural non-linear analysis. Configuration of nodes before and after shear failure is shown in Figure 5.36, which indicates the shear failure of the voided slab.

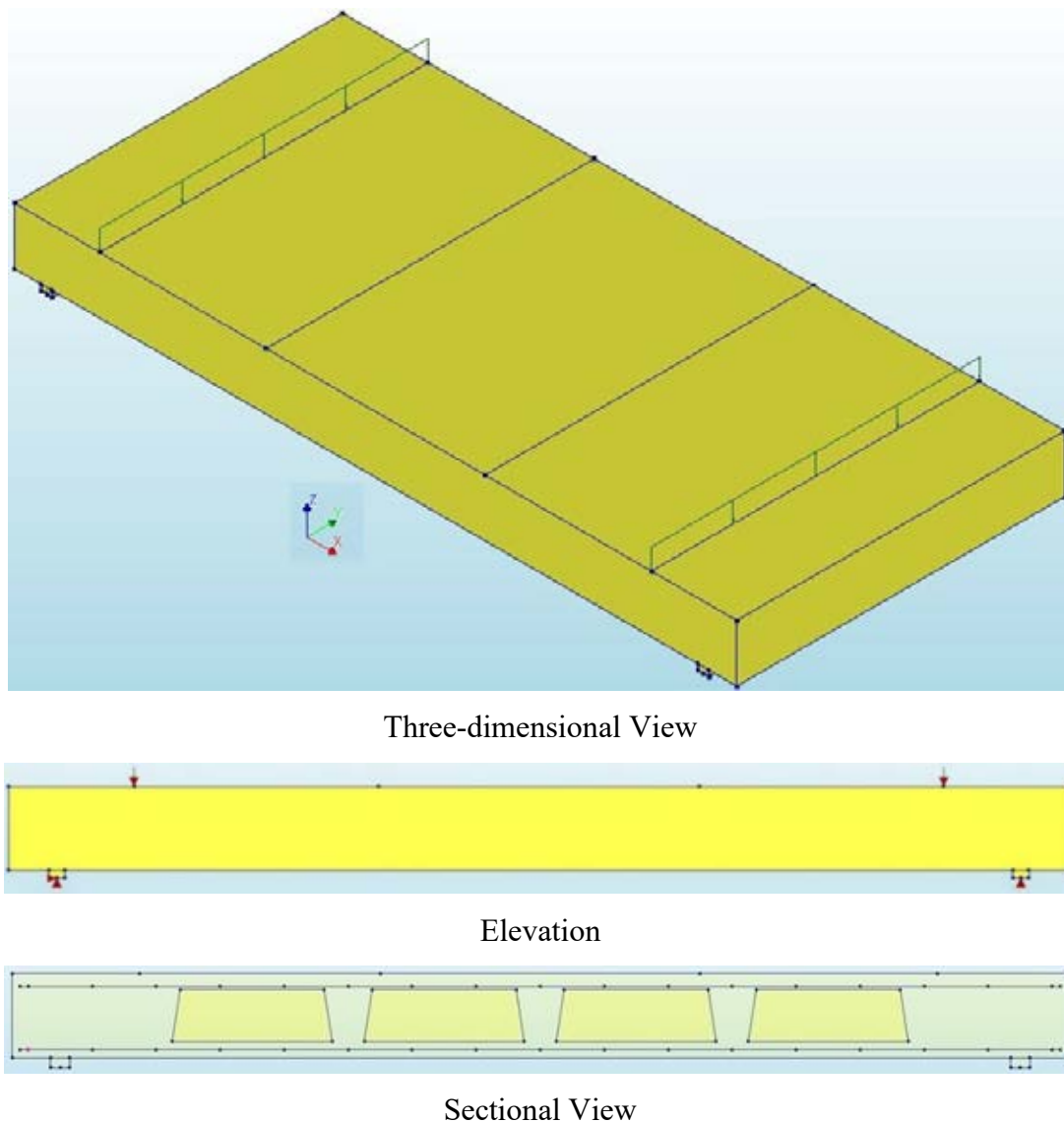


Figure 5.33 – Model of Slab Specimen (OF-CV)

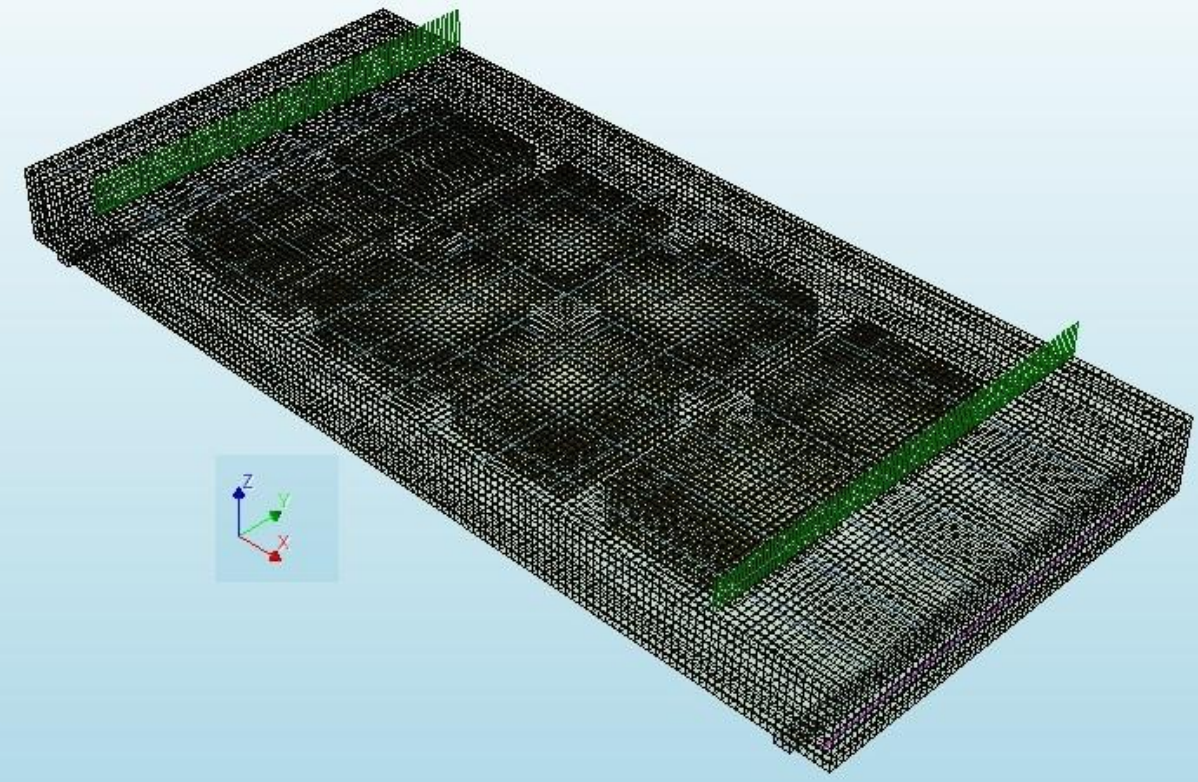
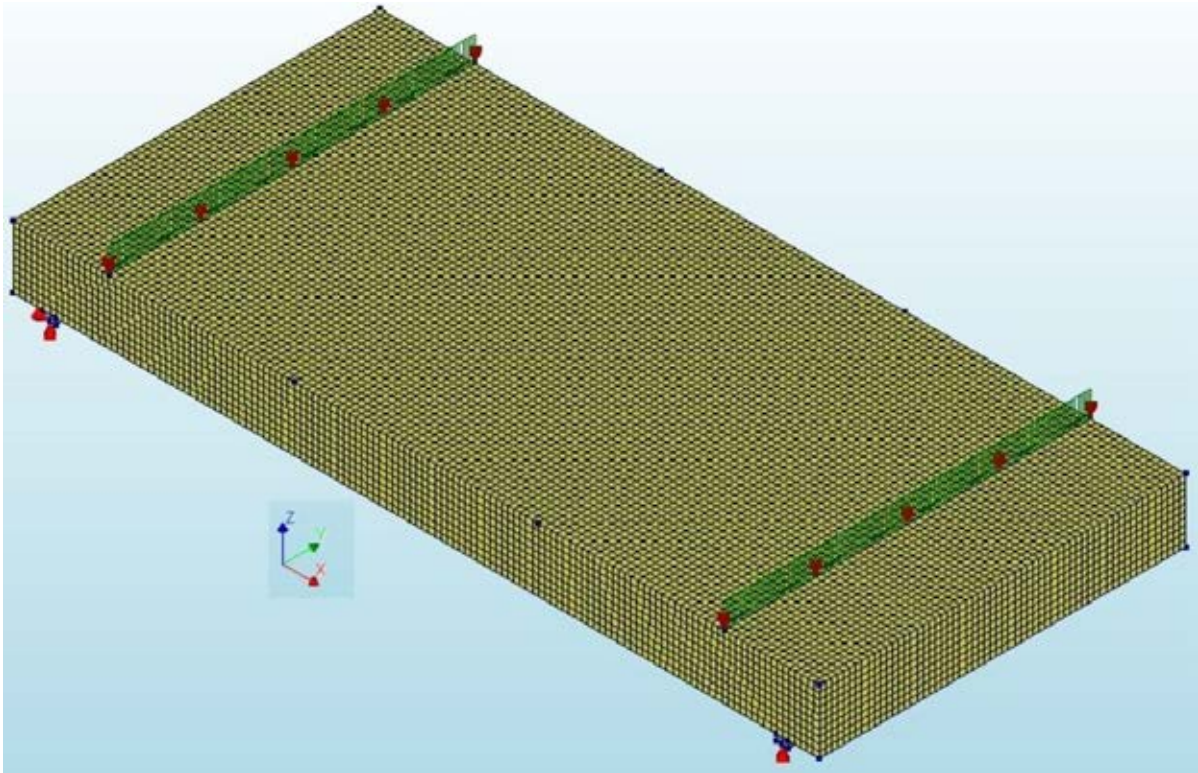


Figure 5.34 – Finite Element Model with Mesh (One-way Shear)

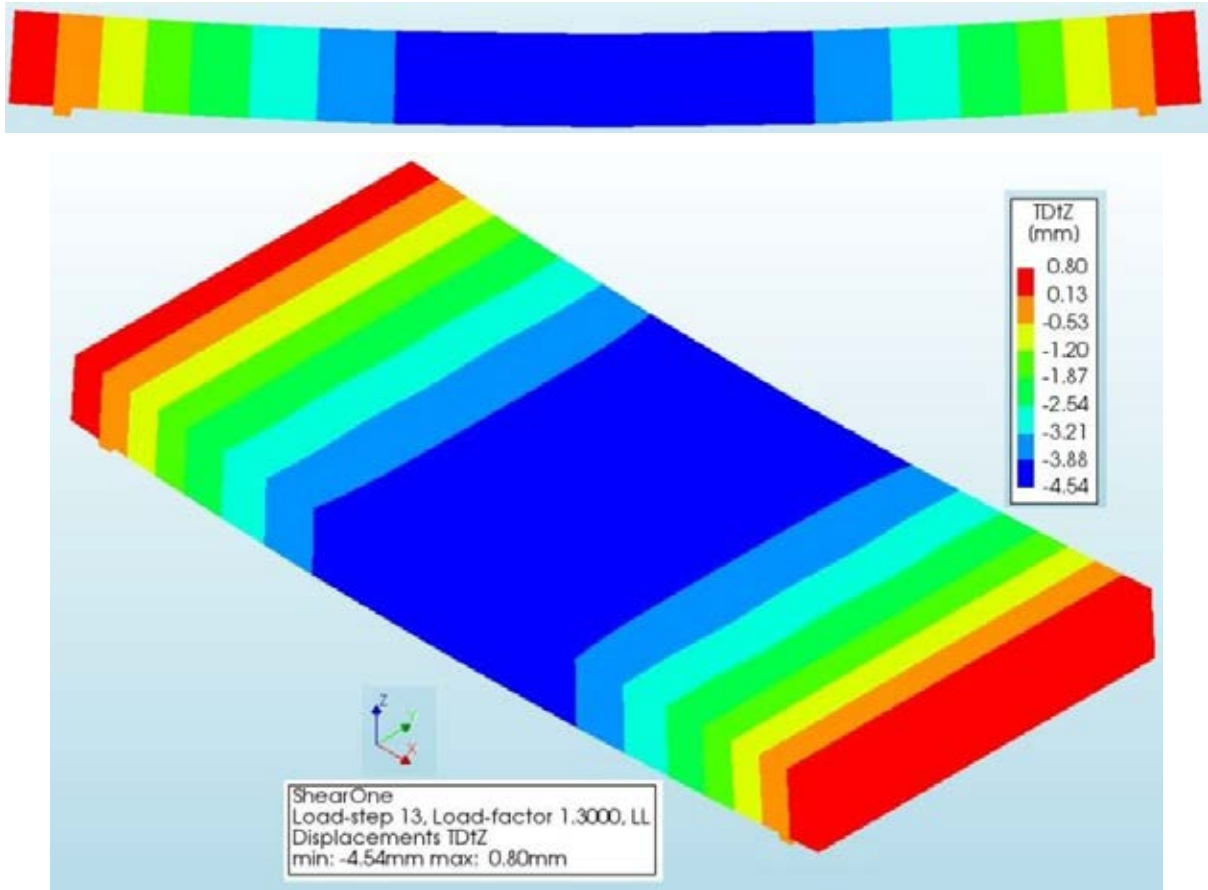


Figure 5.35 – Deflection Contour at 140 kN (One-way Shear)

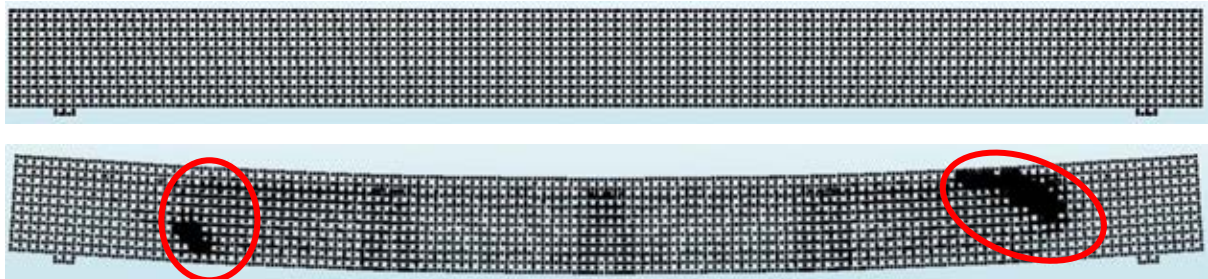


Figure 5.36 – Configuration of Nodes before and after Shear Failure

The load versus displacement of the void and solid slab are compared, as shown in Figure 5.37. The first drop in the load of FEM analysis result is an indication of shear failure. The increase in load beyond the first drop is due to flexural action, i.e., the load is constant with increase in deformation. The recovery of deflection at mid-span of solid slab, after the peak, is due to dowel action of reinforcement which takes place at the time of shear failure. In the case of voided slab, the shear failure is triggered by the void location.



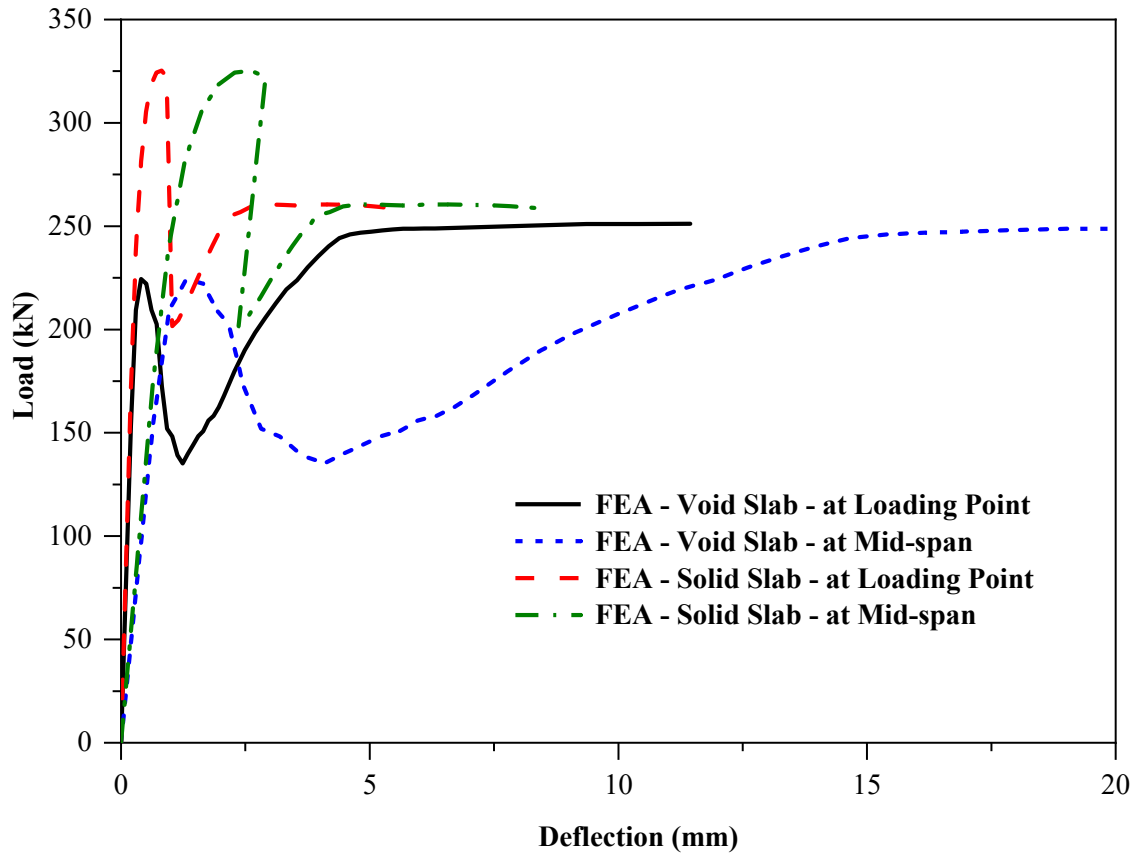


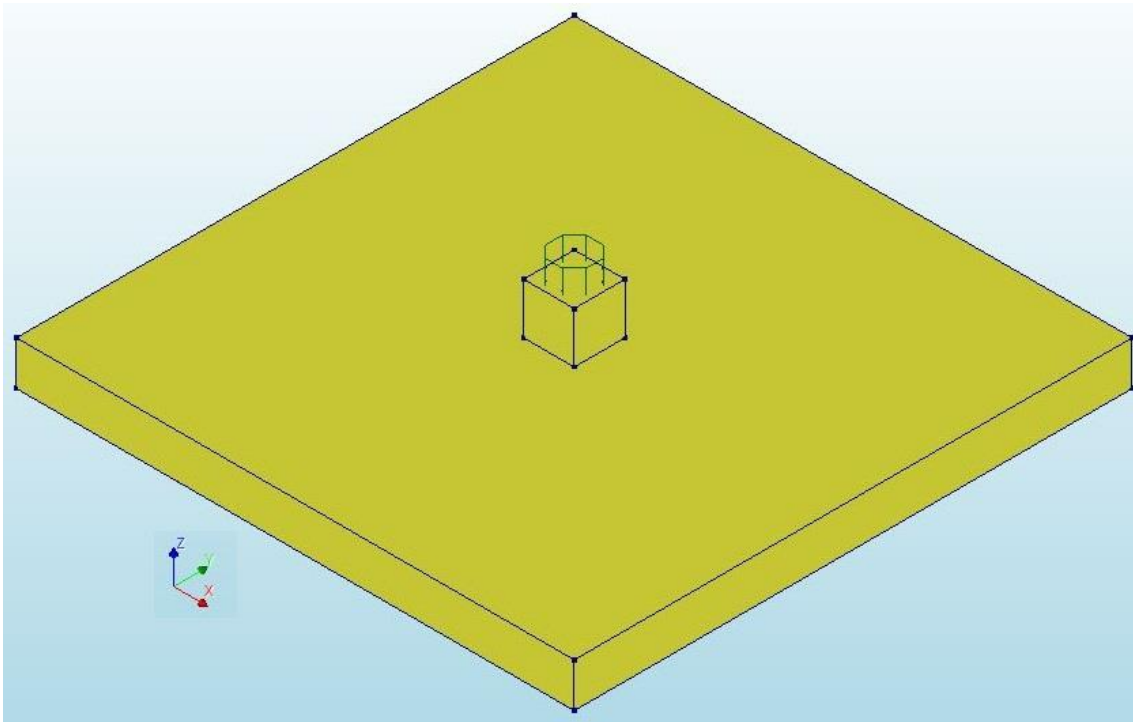
Figure 5.37 – Load versus Deflection Behaviour (One-way Shear)

Table 5.7 – Numerical Results: One-way Shear

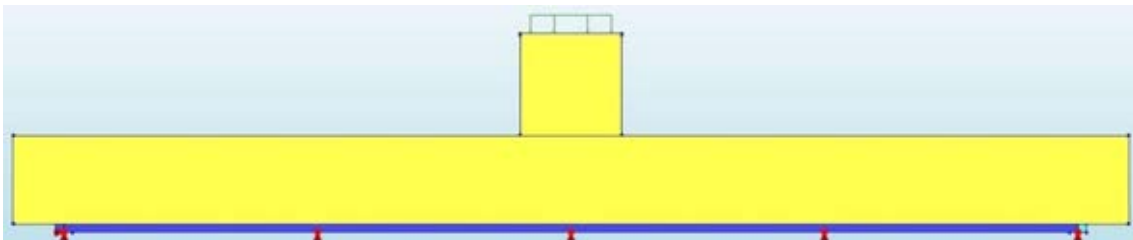
Specimen	Load (kN)	Deflection (mm) at	
		Loading point	Mid-span
Voided slab	224.4	0.40	1.31
Solid slab	325.3	0.81	2.61
<b>Ratio</b>	<b>0.67</b>	–	–

#### 5.4.4 Punching Shear (Two-way)

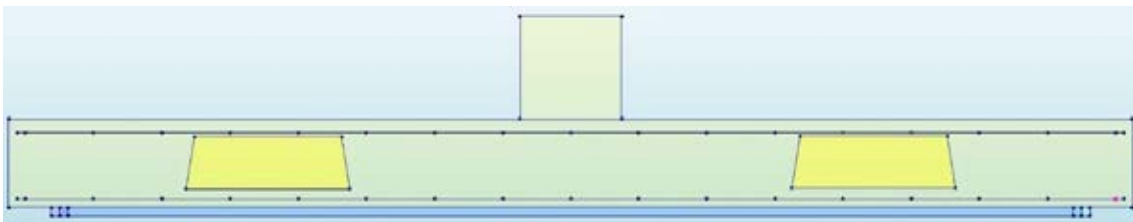
The biaxial voided slab specimen (V5-V7) was modelled and analysed in finite element software DIANA. A three-dimensional model developed and non-linear analysis was carried out to simulate the actual slab specimens with voids. The specifications of slab like plan dimension, cross-section, reinforcement details and position of void former were considered as per actual test given in Section 4.2.2. The properties of concrete are summarised in Table 5.3. Multi-linear stress-strain curve (Figure 4.7) was used to simulate the reinforcement behaviour, which was obtained by conducting a tensile test on the reinforcements. The adopted materials' model is explained in Section 5.2.



Three-dimensional View



Elevation



Sectional View at Column

Figure 5.38 – Model of Slab Specimen (Punching Shear)

The load is applied as uniform pressure at the top cross-section of the column. In the test, the slab was supported at its all four sides by simple support, i.e. hinge support at two adjacent edges and roller support at other two adjacent edges, the same boundary conditions were created. In addition, no tension boundary conditions were imposed to allow the corners of the

slab to uplift as in the experiment the corners free to lift. Finite element model with boundary conditions and mesh are in shown in Figure 5.38 and Figure 5.39, respectively.

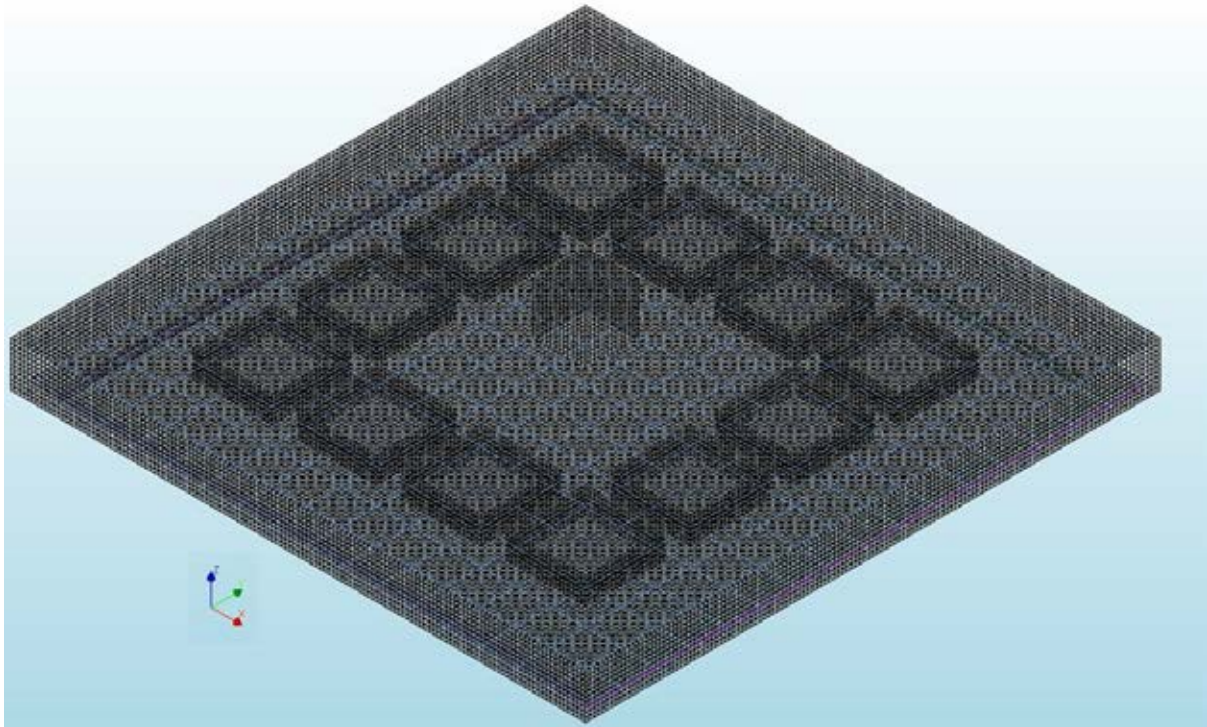


Figure 5.39 – Finite Element Model with Mesh (Punching Shear)

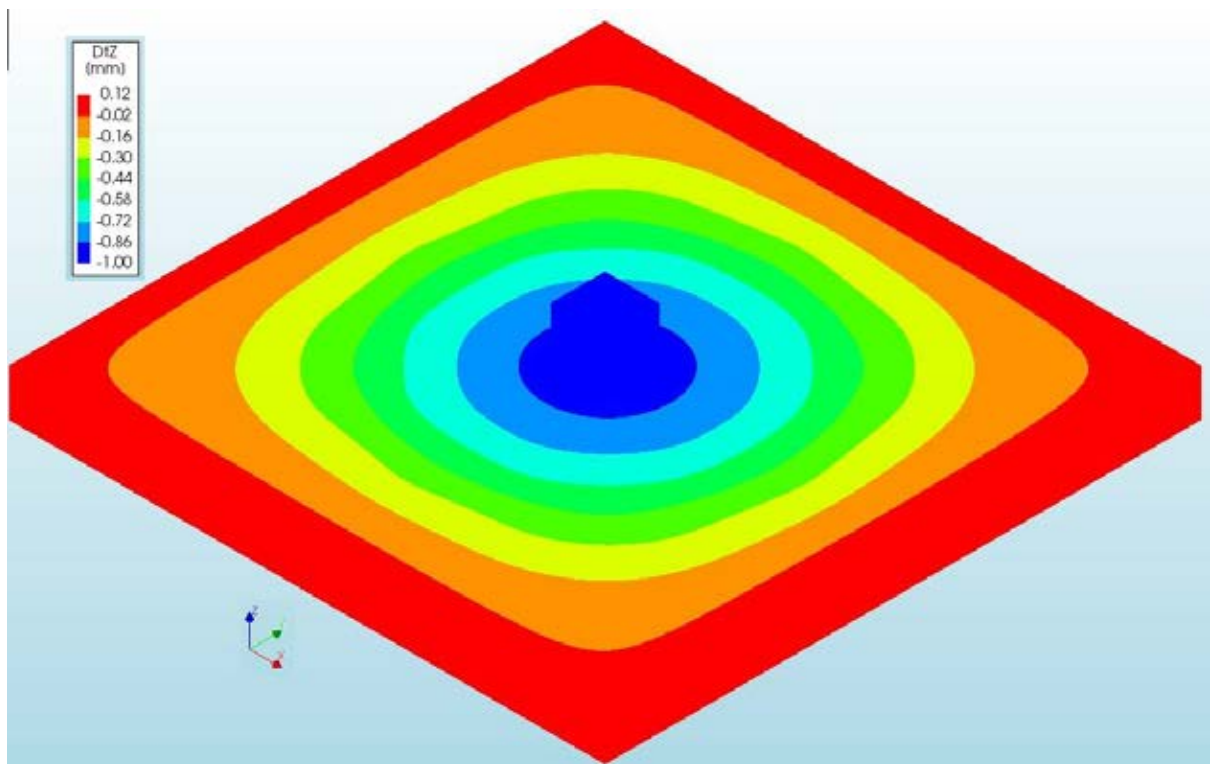


Figure 5.40 – Typical Deflection Contour (Punching Shear)

Typical deflection contour of the biaxial cuboid voided slab is shown in Figure 5.40, which was obtained from the structural non-linear analysis. The load versus mid-span deflection behaviour of the voided and solid slab is compared with experiment results (Figure 5.41) and found that the FEA results are having a good agreement with experimental observations.

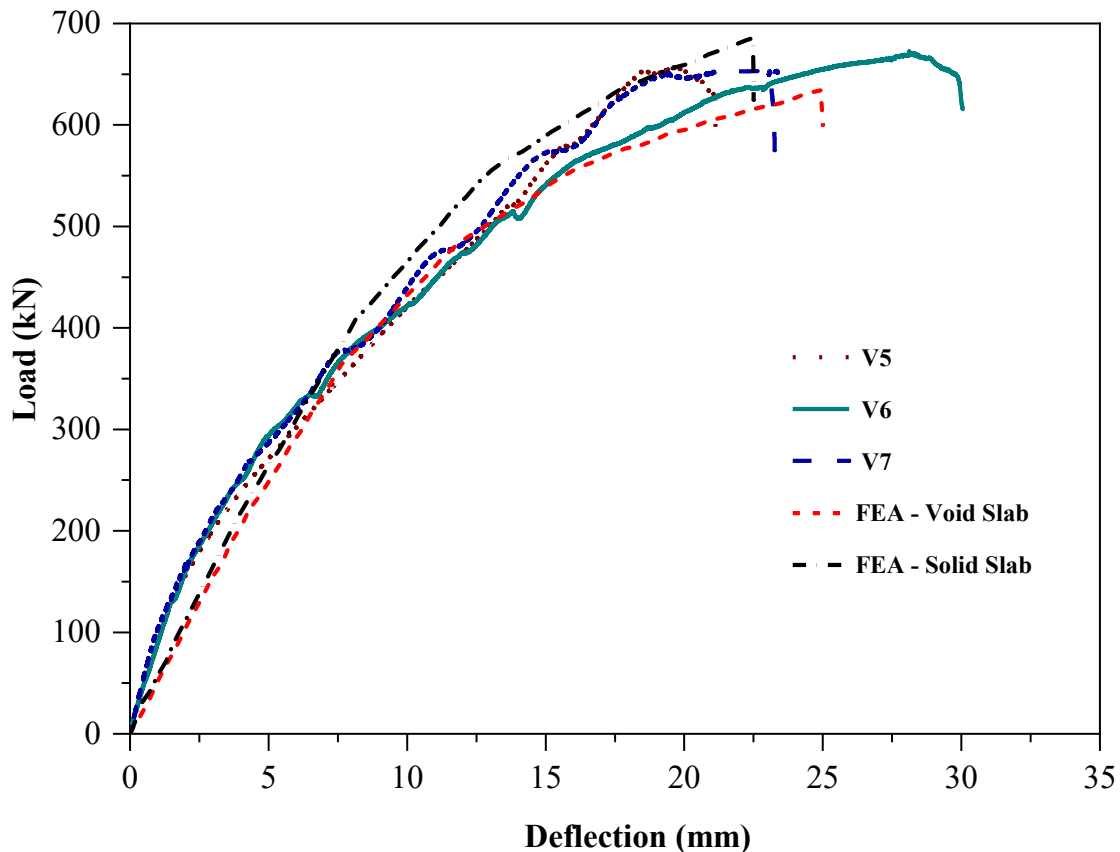


Figure 5.41 – Load versus Mid-span Deflection Behaviour (Punching Flexure)

### 5.5 Summary

In this chapter, the results of the numerical study are discussed. The parametric study with respect to various void shapes evidenced that the shape of the void former affects the behaviour of biaxial voided slab significantly. The sphere voided slab shows higher flexural capacity and stiffness in comparison with other shape voided slabs. Also, the sphere voided slab shows higher punching shear capacity and stiffness in comparison with other shape voided slabs. In addition, the numerical study results of the biaxial cuboid voided slab compared with the experimental results and found that the numerical results are having a good agreement with experimental observations.

## CHAPTER 6

### SUMMARY AND CONCLUSIONS

#### 6.1 Summary

The design procedure for the biaxial voided slab needs to be formulated for wide application of the same in the construction industry. In this thesis, such guidelines are developed for the biaxial voided slabs subjected to flexure and concentrated load (punching shear). In addition, the influence of tensile membrane action and reinforcement orientation on the ultimate flexural capacity found to be significant in RC solid slab. The question of whether such beneficial effect of enhancement in flexural capacity of RC voided slab, is yet to be explored. This would help to determine the ultimate capacity of such slabs with reasonable accuracy. Further, the estimation of the punching shear capacity is significantly influenced by the voids (shape and location). In this study, in addition to the experimental investigation, the data available in the literature are also included to understand the structural behaviour of biaxial voided slabs. Based on this, analytical formulations are developed. Further, parametric study (numerical investigation) to determine the effect of void shape on the structural behaviour of biaxial voided slabs is carried out.

Following the introduction and a detailed literature survey on the voided slab system, the main body of this thesis divided into three main categories based on the structural behaviour and method of investigations (Chapter 3 to Chapter 5).

Chapter 3 deals with the flexural (one-way and two-way) behaviour of biaxial voided slab systems. In total, ten full-scale specimens were tested under flexure. Four of the ten specimens were tested under one-way flexure, and six were tested under two-way flexure. The flexural stiffness was estimated based on the effective section modulus by considering the voids and compared with experimental observations. The capacity corresponding to initial crack, yielding of reinforcement and the ultimate stage was estimated based on the yield line analysis in conjunction with IS 456 (2000) and ACI 318 (2019). The obtained capacity are compared with test results. In the case of two-way flexure, the experimental results based on the test data available in the literature (7 specimens) and current study (5 specimens) were compared with

the estimations by yield line analysis. In addition, the influence of tensile membrane action and reinforcement orientation on the ultimate flexural capacity is investigated.

In Chapter 4, the influence of voids on the punching shear capacity of biaxial voided slab systems is explained. The location (from column face) and shape of voids on the capacity were investigated based on experimental results of the present study (7 specimens) and the test data available in the literature (33 specimens). These test specimens cover a wide range of void former shapes (sphere, cylinder, donut, hexahedron and cuboid), void locations from the column face ( $0.07d - 3.40d$ ), concrete cylinder strengths ( $20 - 68.5 \text{ N/mm}^2$ ) and longitudinal reinforcement ratios ( $0.303 - 1.803 \%$ ). The punching shear capacity is estimated based on the guidelines given in ACI 318 (2014), EN 1992-1-1 (2004) and IS 456 (2000) and compared with experimental observations. Since the estimation of punching shear capacity of the biaxial voided slab by existing provisions for solid slabs in standards does not lead to satisfactory results, an effective area method is proposed to predict the punching shear capacity of the biaxial voided slab.

Chapter 5 explains the numerical investigations which are carried out to understand the influence of void shapes on the structural behaviour of biaxial voided slabs subject to two-way flexure and punching shear. In this study, four commonly adopted shapes have been selected for simulation, such as sphere, ellipsoid, cuboid and donut-type with an internal hole. The details of the materials' model, elements adopted, analysis procedure, and observed results are explained. In addition, the numerical study with current experimental specimens is carried out, and the obtained results are compared with the experimental test results. The study is extended to one-way shear simulation, in addition to the one-way and two-way flexure and punching shear.

## **6.2 Observations and Conclusions**

Based on the detailed study on the structural behaviour of biaxial voided slab subject to flexure and concentrated load (punching shear), the following key observations and conclusions may be drawn.

### 6.2.1 One-way Flexure

- The voided slabs showed typical one-way flexure behaviour similar to a solid slab. The cracks were observed in the region of pure bending. Also, the pattern of crack matched the yield line pattern. The slab specimens ultimately failed by crushing of concrete at the top of slab surface after predominant yielding of bottom reinforcement.
- The ratio of experimental to the theoretical ultimate load-carrying capacity of voided slabs was in the range of 84 - 97 %. The calculated theoretical load-carrying capacity of the solid and voided slab using yield line theory along with IS 456 provisions are the same. Thus, the load-carrying capacity of the voided slab under one-way flexure can be estimated using yield line theory like conventional solid slabs.
- The effective moment of inertia of voided slabs were 31 - 43 % lesser than that of solid slab. The effective moment of inertia showed a similar trend in terms of secant stiffness. Hence, the loss of cross-section due to voids should be considered for calculating flexural stiffness of voided slab.
- The experimental study showed more than 75 % of the ultimate load is within serviceable deflection limit specified in IS 456.
- The one-way flexure behaviour of voided slabs could be well established using provisions of IS 456 with necessary correction for the loss of cross-section due to voids.

### 6.2.2 Two-way Flexure

- The sixteen-point loading condition closely matches with the uniformly distributed loading condition in comparison with single-point, five-point and twelve-point loading condition. Thus sixteen-point load can be adopted to simulate the uniformly distributed load on the slab.
- The voided slabs showed typical two-way flexure behaviour similar to the solid slab. The major cracks were observed in the X shaped pattern, which was originated at the centre of the slab and progressed towards corners.
- The observed maximum load-carrying capacity of voided and solid slabs was equal. The theoretical load-carrying capacity of the solid and voided slab using yield line method along with ACI 318 and IS 456 provisions are the same. Thus, the load-carrying capacity of the voided slab under two-way flexure can be estimated using yield line theory.

- The shape of the void former does not affect the flexural capacity of the biaxial RC voided slab as the neutral axis lies in the cover concrete to the top reinforcement, with a minor difference in the flexural stiffness.
- Though the initial flexural stiffness of solid slab was 37% more than that of the biaxial RC voided slab the secant stiffness corresponding to yield load of voided and solid slab specimens were observed to be almost the same.
- The capacity of the biaxial voided slab can be estimated by conventional flexural theory, and it was observed that the load enhancement effects due to reinforcement orientation and tensile membrane action are applicable for biaxial voided slab as well like a solid slab.

### 6.2.3 Punching Shear

- The load-displacement behaviour of the voided slab (voids located beyond  $0.5d$  distance from the face of column) shows an insignificant difference in comparison with reference solid slab.
- The estimation of punching shear capacity of the biaxial voided slab by existing provisions for solid slabs in standards (ACI 318, EN 1992-1-1 and IS 456) does not lead to satisfactory results. The punching shear capacity of voided slabs is greatly overestimated (mean  $\approx 1.3$ , and COV  $\approx 0.3$ ) by the provisions of the building standards considered in this study; slabs with voids within  $0.5d$  distance from the column face is particularly unsafe ( $V_c / V_u \approx 2.3$ ).
- The predictions of punching shear capacity of voided slabs by the considered building standards (ACI 318, EN 1992-1-1 and IS 456), after suitably modifying the control perimeter and using effective concrete area, are reasonably good in comparison with experimental test data.
- The observed mean conservatism is 22 %, 35 % and 13 % for ACI 318, EN 1992-1-1 and IS 456, respectively; this is obtained after including strength reduction factor / partial safety for material given in building standards for the prediction of punching shear capacity.
- The capacity of slabs with voids located beyond  $2d$  distance from the face of the column is the same as that of solid slab. However, the conservatism in the capacity needs to be investigated with more experiments.



- The capacity estimation by critical shear crack theory (CSCT) available for solid slab was observed to be very scattered with a mean and standard deviation of 0.752 and 0.412, respectively. The CSCT approach needs to be modified by including the influence of location and amount of voids, which needs more experimental results.

#### **6.2.4 Numerical (Parametric) Study**

- The shape of the void former affects the structural behaviour (load-displacement) of biaxial voided slab significantly.
- The sphere voided slab shows higher punching shear capacity and stiffness in comparison with other shape voided slabs, having the same volume of voids.
- The sphere voided slab shows the higher two-way flexural capacity and flexural stiffness in comparison with other shape voided slabs, having the same volume of voids.
- The structural behaviour of biaxial voided slab subjected to flexure (one-way and two-way) and shear (one-way and punching) can be conveniently predicted by carrying out non-linear analysis in available finite element software like DIANA.

#### **6.3 Scope for Further Research**

- The effect of prestress (one-way and biaxial) on the structural behaviour of the biaxial voided slab may be carried out to minimise the reduction in flexural stiffness as well as to enhance the capacity.
- The change in the structural behaviour of biaxial voided slab subject to fire may be studied to understand the post-fire performance.
- The guidelines to estimate the shear (one-way) capacity of the biaxial voided slab may be developed.
- The structural behaviour of the biaxial voided slab with long term effects (creep and shrinkage) with and without prestress may be investigated.
- The beam-slab (biaxial voided slab) system may be investigated to verify the applicability of conventional yield line analysis.
- A parametric study with respect to the combined effect of shape and volume of voids on the flexural behaviour of the biaxial voided slab may be studied.
- A parametric study with respect to the position of the void from the face of the column and shape of void on the punching shear capacity of the biaxial voided slab may be studied.

- The applicability of methodologies, such as the inclusion of shear studs, drop panels, shear reinforcement, metal / fibre-reinforced plastic sheets, which are being adopted to increase the punching shear capacity of the solid slab needs to be verified for biaxial voided slab by experimental and numerical studies.

## REFERENCES

1. **ACI Committee 318.** (2011). *Building Code Requirements for Structural Concrete (ACI 318-11) and Commentary (ACI 318R-11)*. American Concrete Institute, USA.
2. **ACI Committee 318.** (2014). *Building Code Requirements for Structural Concrete (ACI 318-14) and Commentary (ACI 318R-14)*. American Concrete Institute, USA.
3. **ACI Committee 318.** (2019). *Building Code Requirements for Structural Concrete (ACI 318-19) and Commentary (ACI 318R-19)*. American Concrete Institute, USA.
4. **Bailey, C. G.** (2001). Membrane Action of Unrestrained Lightly Reinforced Concrete Slabs at Large Displacements. *Engineering Structures*, **23(5)**, 470–483. [https://doi.org/10.1016/S0141-0296\(00\)00064-X](https://doi.org/10.1016/S0141-0296(00)00064-X)
5. **Bailey, C. G., Toh, W. S., and Chan, B. M.** (2008). Simplified and Advanced Analysis of Membrane Action of Concrete Slabs. *ACI Structural Journal*, **105(1)**, 30–40. <https://doi.org/10.14359/19066>
6. **Bijily, B.** (2017). *Yield Line Analysis of Rectangular RC Beam-Slab Systems*. PhD Thesis, Indian Institute of Technology Madras, Chennai, India.
7. **Björnson, G.** (2003). *BubbleDeck - Two-way Hollow slab*. Denmark.
8. **Brotchie, J. F., and Holley, M. J.** (1971). Membrane Action in Slabs. *ACI Structural Journal - Special Publication*, **30(30-16)**, 345–377.
9. **BubbleDeck Technology.** (2008). *BubbleDeck Voided Flat Slab Solutions - Technical Manual and Documents*. UK.
10. **Burgess, I.** (2017). Yield-line Plasticity and Tensile Membrane Action in Lightly-Reinforced Rectangular Concrete Slabs. *Engineering Structures*, **138**, 195–214. <https://doi.org/10.1016/j.engstruct.2017.01.072>
11. **Chung, J. H., Park, J. H., Choi, H. K., Lee, S. C., and Choi, C. S.** (2010). An Analytical Study on the Impact of Hollow Shapes in Bi-axial Hollow Slabs. In *FraMCoS-7* (pp. 1729–1736). Korea Concrete Institute.
12. **Chung, Joo Hong, Bae, B. Il, Choi, H. K., Jung, H. S., and Choi, C. S.** (2018a). Evaluation of Punching Shear Strength of Voided Slabs Considering the Effect of the Ratio  $b_0/d$ . *Engineering Structures*, **164**, 70–81. <https://doi.org/10.1016/j.engstruct.2018.02.085>
13. **Chung, Joo Hong, Choi, H. K., Lee, S. C., and Choi, C. S.** (2011a). Punching Shear Strength of Biaxial Hollow Slab with Donut Type Hollow Sphere. *Key Engineering Materials*, **452–453**, 777–780. <https://doi.org/10.4028/www.scientific.net/KEM.452->

14. **Chung, Joo Hong, Choi, H. K., Lee, S. C., and Choi, C. S.** (2011b). Shear Capacity of Biaxial Hollow Slab with Donut Type Hollow Sphere. *Procedia Engineering*, **14**, 2219–2222. <https://doi.org/10.1016/j.proeng.2011.07.279>
15. **Chung, Joo Hong, Jung, H. S., Bae, B. il, Choi, C. S., and Choi, H. K.** (2018b). Two-Way Flexural Behavior of Donut-Type Voided Slabs. *International Journal of Concrete Structures and Materials*, **12(1)**. <https://doi.org/10.1186/s40069-018-0247-6>
16. **Churakov, A. G.** (2014). Biaxial Hollow Slab with Innovative Types of Voids. *Construction of Unique Buildings and Structures*, **6(21)**, 70–88.
17. **Cobix Technologies.** (2010). *Cobix Engineering Manual*. Switzerland.
18. **Cornellissen, H. A. W., Hordijk, D. A., and Reinhardt, H. W.** (1986). Experimental Determination of Crack Softening Characteristics of Normal Weight and Lightweight Concrete. *HERON*, **31(2)**, 45–56.
19. **Daliform Group.** (2012). *U-Boot Beton® Disposable Formworks for Lightened Structures in Reinforced Concrete Cast on Site*. Italy.
20. **Darwin, D., Dolan, C., and Nilson, A.** (2002). *Design of Concrete Structures* (15th ed.). McGraw-Hill.
21. **De Borst, R.** (1987). Smearred Cracking, Plasticity, Creep, and Thermal Loading - A Unified Approach. *Computer Methods in Applied Mechanics and Engineering*, **62**, 89–110. [https://doi.org/10.1016/0045-7825\(87\)90091-0](https://doi.org/10.1016/0045-7825(87)90091-0)
22. **DIANA FEA BV.** (2017a). *DIANA-10.2 User's Manual - Analysis Procedures*. The Netherlands.
23. **DIANA FEA BV.** (2017b). *DIANA-10.2 User's Manual - Element Library*. The Netherlands.
24. **DIANA FEA BV.** (2017c). *DIANA-10.2 User's Manual - Getting Started*. The Netherlands.
25. **DIANA FEA BV.** (2017d). *DIANA-10.2 User's Manual - Material Library*. The Netherlands.
26. **EN 1992-1-1.** (2004). *Eurocode 2: Design of Concrete Structures – Part 1-1: General Rules and Rules for Buildings*. BSI, London, UK.
27. **Eyre, J. R.** (1997). Direct Assessment of Safe Strengths of RC Slabs under Membrane Action. *Journal of Structural Engineering*, **123(10)**, 1331–1338.
28. **Ezhilan, M.** (2011). *Numerical Study on Capacity of Biaxial Hollow Slabs*. MTech Thesis,

Indian Institute of Technology Madras, Chennai, India.

29. **Ferreira, D. C. S.** (2013). *A Model for the Nonlinear, Time-Dependent and Strengthening Analysis of Shear Critical Frame Concrete Structures*. PhD Thesis, Universitat Politècnica de Catalunya, Barcelona Tech.
30. **Han, S. W., and Lee, C. S.** (2014). Evaluation of Punching Shear Strength of Voided Transfer Slabs. *Magazine of Concrete Research*, **66(21)**, 1116–1128. <https://doi.org/10.1680/mac.14.00080>
31. **Harding, P.** (2004). BubbleDeck<sup>TM</sup>–Advanced Structure Engineering. *BubbleDeck Article*, 15–16.
32. **Hayes, B.** (1968). Allowing for Membrane Action in the Plastic Analysis of Rectangular Reinforced Concrete Slabs. *Magazine of Concrete Research*, **20(65)**, 205–212. <https://doi.org/10.1680/mac.1968.20.65.205>
33. **Hedley, R. G.** (n.d.). *Private Communication on Work Carried out on Behalf of the Home Office*. Foulness, UK.
34. **Held, M. S., and Pfeffer, K.** (2002). Punching Behavior of Biaxial Hollow Slabs. *Cement and Concrete Composites*, **24**, 551–556. [https://doi.org/10.1016/S0958-9465\(01\)00071-3](https://doi.org/10.1016/S0958-9465(01)00071-3)
35. **Herraiz, B., and Vogel, T.** (2016). Novel Design Approach for the Analysis of Laterally Unrestrained Reinforced Concrete Slabs Considering Membrane Action. *Engineering Structures*, **123**, 313–329. <https://doi.org/10.1016/j.engstruct.2016.05.033>
36. **Hognestad, E.** (1953). Yield-line Theory for the Ultimate Flexural Strength of Reinforced Concrete Slabs. In *Proceedings, Journal of the American Concrete Institute* (Vol. **24**, pp. 637–656). Boston, Massachusetts. <https://doi.org/10.14359/11842>
37. **Hognestad, E., Hanson, N. W., and Mchenry, D.** (1955). Concrete Stress Distribution in Ultimate Strength Design. *Journal of the American Concrete Institute*, **52(28)**, 455–480. <https://doi.org/10.14359/11609>
38. **Hordijk, D. A., and Reinhardt, H. W.** (1990). Fracture of Concrete in Uniaxial Tensile Experiments as Influenced by Curing Conditions. *Engineering Fracture Mechanics*, **35(4–5)**, 819–826. [https://doi.org/10.1016/0013-7944\(90\)90166-E](https://doi.org/10.1016/0013-7944(90)90166-E)
39. **Hordijk, Dirk Arend.** (1991). *Local Approach to Fatigue of Concrete*. PhD Thesis, Delft University of Technology.
40. **Hsueh, P. K.** (1966). *The Yield-Line Theory for Concrete Slabs*. PhD Thesis, Kansas State University, Manhattan.
41. **Ibrahim, A. M., Ali, N. K., and Salman, W. D.** (2013a). Finite Element Analysis of

- Reinforced Concrete Slabs with Spherical Voids. *Diyala Journal of Engineering Sciences*, **6(4)**, 15–37.
42. **Ibrahim, A. M., Ali, N. K., and Salman, W. D.** (2013b). Flexural Capacities of Reinforced Concrete Two-Way Bubbledeck Slabs of Plastic Spherical Voids. *Diyala Journal of Engineering Sciences*, **06(02)**, 9–20.
  43. **IS 1608.** (2018). *Metallic Materials - Tensile Testing. Part 1: Method of Test at Room Temperature*. Bureau of Indian Standards, New Delhi.
  44. **IS 1786.** (2008). *High Strength Deformed Steel Bars and Wires for Concrete Reinforcement - Specification*. Bureau of Indian Standards, New Delhi.
  45. **IS 456.** (2000). *Plain and Reinforced Concrete - Code of Practice*. Bureau of Indian Standards, New Delhi.
  46. **Kankeri, P., Prakash, S. S., and Sarma Pachalla, S. K.** (2018). Analytical and Numerical Studies on Hollow Core Slabs Strengthened with Hybrid FRP and Overlay Techniques. *Structural Engineering and Mechanics*, **65(5)**, 535–546. <https://doi.org/10.12989/sem.2018.65.5.535>
  47. **Kemp, K. O.** (1967). Yield of A Square Reinforced Concrete Slab. *The Structural Engineer*, **45(7)**, 235–240.
  48. **Kim, B. H., Chung, J. H., Choi, H. K., Lee, S. C., and Choi, C. S.** (2011). Flexural Capacities of One-Way Hollow Slab with Donut Type Hollow Sphere. *Key Engineering Materials*, **452–453**, 773–776. <https://doi.org/10.4028/www.scientific.net/KEM.452-453.773>
  49. **Kim, S. H.** (2011). Flexural Behavior of Void RC and PC Slab with Polystyrene Forms. *Key Engineering Materials*, **452–453**, 61–64. <https://doi.org/10.4028/www.scientific.net/KEM.452-453.61>
  50. **Matešan, D., Radnić, J., Grgić, N., and Čamber, V.** (2012). Strength Capacity of Square Reinforced Concrete Slabs. *Materials Science and Engineering*, **43(5)**, 399–404. <https://doi.org/10.1002/mawe.201200972>
  51. **Midkiff, C. J.** (2013). *Plastic Voided Slab Systems: Applications and Design*. MS Thesis, Kansas State University, Manhattan.
  52. **Mohammadi, S.** (2008). *Extended Finite Element Method: for Fracture Analysis of Structures*. Wiley-Blackwell.
  53. **Mota, M.** (2013). *Innovative Structural Slab Practices – Voided Slabs*. Minneapolis.
  54. **Muttoni, A.** (2003). *Shear and Punching Strength of Slabs without Shear Reinforcement*.

- Concrete and Reinforced Concrete*, 98(2), 74–84.
55. **Muttoni, A.** (2008). Punching Shear Strength of Reinforced Concrete Slabs without Transverse Reinforcement. *ACI Structural Journal*, **105(4)**, 440–450. <https://doi.org/10.14359/19858>
  56. **Muttoni, A., & Schwartz, J.** (1991). Behaviour of Beams and Punching in Slabs without Shear Reinforcement. In *IABSE Colloquium* (pp. 703–708). Zurich, Switzerland.
  57. **Oukaili, N. K. A., and Husain, L. F.** (2017). Punching Shear in Reinforced Concrete Bubbled Slabs: Experimental Investigation. In *Smart Monitoring, Assessment and Rehabilitation of Civil Structures*. Zurich, Switzerland.
  58. **Pillai, S. U., and Menon, D.** (2012). *Reinforced Concrete Design* (3rd ed.). Tata McGraw Hill, New Delhi.
  59. **Roesler, J., Paulino, G. H., Park, K., and Gaedicke, C.** (2007). Concrete Fracture Prediction using Bilinear Softening. *Cement and Concrete Composites*, **29(4)**, 300–312. <https://doi.org/10.1016/j.cemconcomp.2006.12.002>
  60. **Sawczuk, A., and Winnicki, L.** (1965). Plastic Behavior of Simply Supported Reinforced Concrete Plates at Moderately Large Deflections. *International Journal of Solids and Structures*, **1**, 97–111. [https://doi.org/10.1016/0020-7683\(65\)90019-3](https://doi.org/10.1016/0020-7683(65)90019-3)
  61. **Taskin, K., and Peker, K.** (2014). Design Factors and the Economical Application of Spherical Type Voids in RC Slabs. In *International Scientific Conference People, Buildings and Environment 2014, An International Scientific Conference* (pp. 448–458). Kroměříž, Czech Republic.
  62. **Taylor, R.** (1965). A Note on A Possible Basis for A New Method of Ultimate Load Design of Reinforced Concrete Slabs. *Magazine of Concrete Research*, **17(53)**, 183–186. <https://doi.org/10.1680/mac.1965.17.53.183>
  63. **Taylor, R., Maher, D. R. H., and Hayes, B.** (1966). Effect of the Arrangement of Reinforcement on the Behaviour of Reinforced Concrete Slabs. *Magazine of Concrete Research*, **18(55)**, 85–94. <https://doi.org/10.1680/mac.1967.19.58.58>
  64. **Valivonis, J., Jonaitis, B., Zavalis, R., Skuturna, T., and Šneideris, A.** (2014). Flexural Capacity and Stiffness of Monolithic Biaxial Hollow Slabs. *Journal of Civil Engineering and Management*, **20(5)**, 693–701. <https://doi.org/10.3846/13923730.2014.917122>
  65. **Valivonis, J., Skuturna, T., Daugevičius, M., and Šneideris, A.** (2017a). Punching Shear Strength of Reinforced Concrete Slabs with Plastic Void Formers. *Construction and Building Materials*, **145**, 518–527. <https://doi.org/10.1016/j.conbuildmat.2017.04.057>

66. **Valivonis, J., Šneideris, A., Šalna, R., Popov, V., Daugevičius, M., and Jonaitis, B.** (2017b). Punching Strength of Biaxial Voided Slabs. *ACI Structural Journal*, **114(6)**, 1373–1383. <https://doi.org/10.14359/51700912>
67. **Wang, Y. Z., Sun, Y. Y., Wang, L. N., and Chen, Y.** (2008). Punching Shear Behavior of Reinforced Concrete Hollow Slab. In *11th ASCE Aerospace Division International Conference (Earth and Space 2008)* (pp. 1–7). California, USA: American Society of Civil Engineers. [https://doi.org/10.1061/40988\(323\)62](https://doi.org/10.1061/40988(323)62)
68. **Wood, R. H.** (1961). *Plastic and Elastic Design of Slabs and Plates*. Thames and Hudson, London.



**LIST OF PAPERS**  
**SUBMITTED ON THE BASIS OF THIS THESIS**

**I. PAPERS IN REFEREED JOURNALS**

1. **Sagadevan, R., and Rao, B. N.** (2020). Flexural Behaviour of Reinforced Concrete Biaxial Voided Square Slabs. *ACI Structural Journal*. (Accepted).
2. **Sagadevan, R., and Rao, B. N.** (2019). Experimental and Analytical Investigation of Punching Shear Capacity of Biaxial Voided Slabs. *Structures*, **20**, 340–352.
3. **Sagadevan, R., and Rao, B. N.** (2019). Effect of void former shapes on one-way flexural behaviour of biaxial hollow slabs. *International Journal of Advanced Structural Engineering*, **11(3)**, 297–307.
4. **Sagadevan, R., and Rao, B. N.** (2020). Effect of Reinforcement Orientation on Ultimate Flexural Capacity of Reinforced Concrete Slabs. *The Indian Concrete Journal*. (Accepted).
5. **Sagadevan, R., and Rao, B. N.** (2019). Investigations on One-way Flexural Behaviour of Biaxial Voided Slab with Cuboid Shape Void Formers.” *Journal of Structural Engineering (Madras)*, **64(4)**, 287-297.
6. **Sagadevan, R., and Rao, B. N.** (2019). Evaluation of One-Way Flexural Behaviour of Biaxial Voided Slab. *The Indian Concrete Journal*, **98(5)**, 7–16.
7. **Sagadevan, R., and Rao, B. N.** (2019). Prediction of Punching Shear Capacity of Biaxial Voided Slab. *Journal of Structural Engineering and Management*, **6(2)**, 24–33.

**II. CONFERENCE PROCEEDINGS**

1. **Sagadevan, R., and Rao, B. N.** (2019). Experimental Study on the Flexural and Shear Behaviour of Precast Prestressed Hollow Core Slab. *10<sup>th</sup> International Conference on Structural Engineering and Construction Management*, Kandy, Sri Lanka.
2. **Sagadevan, R., and Rao, B. N.** (2019). Experimental and Analytical Investigations on Two-way Flexural Capacity of Biaxial Voided Slab. In *Proceedings, National Conference on Advances in Structural Technologies* (pp.

- 635–648), Silchar, India. – *Received Best Session Paper Award.*
3. **Sagadevan, R., and Rao, B. N.** (2014). Numerical Study on Punching Shear Capacity of Biaxial Hollow Slabs. In *Proceedings, 5th International Congress on Computational Mechanics and Simulation* (pp. 1881–1890). Singapore.
  4. **Sagadevan, R., and Rao, B. N.** (2017). Analytical Studies on Flexural Capacity of Biaxial Hollow Slab. In *Proceedings, International Conference on Composite Materials and Structures*. Hyderabad, India.
  5. **Sagadevan, R., and Rao, B. N.** (2019). Numerical Study on Flexural Capacity of Biaxial Hollow Slab. In A. R. M. Rao and K. Ramanjaneyulu (Eds.), *Recent Advances in Structural Engineering, Volume 1. Select Proceedings of SEC 2016* (pp. 97–105). Singapore: Springer.

## CURRICULUM VITAE

1. **Name:** Sagadevan R
2. **Date of Birth:** 08-04-1990
3. **Educational Qualifications**

### **Bachelor of Engineering (B.E.) – 2011**

Institution: College of Engineering Guindy, Anna University, Chennai, India

Specialisation: Civil Engineering

### **Master of Technology (M.Tech.) – 2013**

Institution: Indian Institute of Technology Madras, Chennai, India

Specialisation: Civil Engineering (Structural Engineering)

### **Doctor of Philosophy (Ph.D.)**

Institution: Indian Institute of Technology Madras, Chennai, India

Registration Date: 15-07-2013

Viva-voce Exam Date: 28-02-2020

This page is intentionally left blank.

## DOCTORAL COMMITTEE

- Chairperson** : **Prof. Manu Santhanam**  
Head of the Department  
Department of Civil Engineering
- Guide** : **Prof. B. Nageswara Rao**  
Department of Civil Engineering
- Members** : **Prof. P. Alagusundaramoorthy**  
Department of Civil Engineering
- Prof. Amlan Kumar Sengupta**  
Department of Civil Engineering
- Prof. C. Lakshmana Rao**  
Department of Applied Mechanics

This page is intentionally left blank.